Studies on Lattice Reduction Aided Detection and Its Application in MIMO Systems

Wei Hou

Department of Information and Communication Engineering

The University of Electro-Communications

A dissertation submitted for the degree of

Doctor of Philosophy

March 2014

Studies on Lattice Reduction Aided Detection and Its Application in MIMO Systems

APPROVED BY SUPERVISORY COMMITTE

Chair person: Associate Professor Toshiharu KOJIMA

Member: Professor Tsutomu KAWABATA

Member: Professor Naoto KISHI

Member: Professor Eiji OKI

Member: Professor Tadashi FUJINO

Abstract

Multiple-input multiple-output (MIMO) technology has attracted attention in wireless communications, since it provides significant increases in data throughput and the high spectral efficiency. MIMO systems employ multiple antennas at both ends of the wireless link, and hence can increase the data rate by transmitting multiple data streams. To exploit the potential gains offered by MIMO, signal processing involved in a MIMO receiver requires a large computational complexity in order to achieve the optimal performance. In MIMO systems, it is usually required to detect signals jointly as multiple signals are transmitted through multiple signal paths between the transmitter and the receiver. This joint detection becomes the MIMO detection.

The maximum likelihood (ML) detection (MLD) is known as the optimal detector in terms of minimizing bit error rate (BER). However, the complexity of MLD obstructs its practical implementation. The common linear detection such as zero-forcing (ZF) or minimum mean squared error (MMSE) offers a remarkable complexity reduction with performance loss. The non-linear detection, e.g. the successive interference cancellation (SIC), detects each symbol sequentially with the aid of cancellation operations which remove the interferences from the received signal. The BER performance is improved by using the SIC, but is still inferior to that of the ML detector with low complexity. Numerous suboptimal detection techniques have been proposed to approximately approach the ML performance with relatively lower complexity, such as sphere detection (SD) and QRM-MLD. To look for

suboptimal detection algorithm with near optimal performance and affordable complexity costs for MIMO gains faces a major challenge.

Lattice-reduction (LR) is a promising technique to improve the performance of MIMO detection. The LR makes the column vectors of the channel state information (CSI) matrix close to mutually orthogonal. The following signal estimation of the transmitted signal applies the reduced lattice basis instead of the original lattice basis. The most popular LR algorithm is the well-known LLL algorithm, introduced by Lenstra, Lenstra, and Lovász. Using this algorithm, the LR aided (LRA) detector achieves more reliable signal estimation and hence good BER performance. Combining the LLL algorithm with the conventional linear detection of ZF or MMSE can further improve the BER performance in MIMO systems, especially the LR-MMSE detection. The non-linear detection i.e. SIC based on LR (LR-SIC) is selected from many detection methods since it features the good BER performance. And ordering SIC based on LR (LR-OSIC) can further improve the BER performance with the costs of the implementation of the ordering but requires high computational complexity. In addition, list detection can also obtain much better performance but with a little high computational cost in terms of the list of candidates. However, the expected performance of the several detections is not satisfied directly like the ML detector, in particular for the high modulation order or the large size MIMO system.

This thesis presents our studies about lattice reduction aided detection and its application in MIMO system. Our studies focus on the evaluation of BER performance and the computational complexity. On the hand, we improve the detection algorithms to achieve the near-ML BER performance. On the other hand, we reduce the complexity of the useless computation, such as the exhaustive tree search. We mainly solve three problems existed in the conventional detection methods as

- The MLD based on QR decomposition and M-algorithm (QRM-MLD) is one solution to relatively reduce the complexity while retaining the ML performance. The number of M in the conventional QRM-MLD is defined as the number of the survived branches in each detection layer of the tree search, which is a tradeoff between complexity and performance. Furthermore, the value of M should be large enough to ensure that the correct symbols exist in the survived branches under the ill-conditioned channel, in particular for the large size MIMO system and the high modulation order. Hence the conventional QRM-MLD still has the problem of high complexity in the better-conditioned channel.
- For the LRA MIMO detection, the detection errors are mainly generated from the channel noise and the quantization errors in the signal estimation stage. The quantization step applies the simple rounding operation, which often leads to the quantization error. If this error occurs in a row of the transmit signal, it has to propagate to many symbols in the subsequent signal estimation and result in degrading the BER performance. The conventional LRA MIMO detection has the quantization problem, which obtains less reliable signal estimation and leads to the BER performance loss.
- Ordering the column vectors of the LR-reduced channel matrix brings large improvement on the BER performance of the LR-SIC due to decreasing the error propagation. However, the improvement of the LR-OSIC is not sufficient to approach the ML performance in the large size MIMO system, such as 8×8 MIMO system. Hence, the LR-OSIC detection cannot achieve the near-ML BER performance in the large size of MIMO system.

The aim of our researches focuses on the detection algorithm, which provides near-ML BER performance with very low additional complexity. Therefore, we have produced various new results on low

complexity MIMO detection with the ideas of lattice reduction aided detection and its application even for large size MIMO system and high modulation order. Our works are to solve the problems in the conventional MIMO detections and to improve the detection algorithms in the signal estimation. As for the future research, these detection schemes combined with the encoding technique lead to interesting and useful applications in the practical MIMO system or massive MIMO.

Acknowledgements

This dissertation is a summary of my doctoral study in Kojima laboratory at the Department of Electronic Engineering, The University of Electro-Communications (UEC) in Tokyo, Japan. I am grateful to a large number of people who have helped me to accomplish my work. Without the support, patience and guidance of these people, this study would not have been completed. It is to them that I owe my deepest gratitude.

First of all, I would like to express my grateful thanks to Professor Tadashi Fujino, who gave me a chance for my study. He has been a wonderful advisor, providing me with support, encouragement, understanding and an endless source of ideas. After he retired, he kindly continued to especially assist me.

Second, I thank Associate Professor Toshiharu Kojima, who took care of me after Professor Fujino retired. His encouragements immensely helped me throughout my research.

My life has been enriched professionally, intellectually and personally by working with them. It has been a great honor and privilege to work under their supervision.

I am deeply indebted to other members of this dissertation committee: Professor Tsutomu Kawabata, Professor Naoto Kishi, and Professor Eiji Oki. I would like to thank them for their valuable comments to improve my dissertation and being part of my judging committee.

Thanks also to all members of Fujino & Kojima laboratory for their helpful interaction and kindness. I would like to thank all of my

friends I made in Japan, for making my life in Japan wonderful and memorable.

Finally, I want to thank my wonderful husband Huifa Lin. After I decided to continue my study in Japan, he is always supporting me and followed me together. He kept me happy and shared my pain. I thank him for his patience when I was frustrated and stressed. Without his constant support and understanding, I would not have been completed my study. I also give thanks to my lovely parents-in-low and parents, for all their love, support and understanding.

Contents

List of Figures

LIST OF FIGURES

List of Tables

LIST OF TABLES

Acronyms

AWGN Additive white Gaussian noise

BER Bit error rate

CDF Cumulative distribution function

CSI Channel state information

ED Euclidean distance

flops Floating point operations

GS Gram-Schmidt

GSM-MLD ML detection based on GS orthogonalization and M-algorithm

GSO Gram-Schmidt orthogonalation

i.i.d. Independent and identically distributed

LR Lattice reduction

LRA Lattice reduction aided

LRAD Lattice reduction aided detection

LTE Long Term Evolution

MGS Modified Gram-Schmidt

MIMO Multiple-input multiple-output

ML Maximum likelihood

MLD Maximum likelihood detection

ACRONYMS

MMSE Minimum mean square error

OSIC Ordering successive interference cancellation

PED Partial Euclidean distance

PEP Pairwise error probability

QAM Quadrature amplitude modulation

QRM-MLD ML detection based on QR decomposition and M-algorithm

RE Reliability evaluation

SC Surviving candidates

SD Sphere detection

SIC Successive interference cancellation

SISO Single-input single-output

SNR Signal-to-noise ratio

ZF Zero-forcing

Chapter 1

Introduction

This thesis represents our studies about lattice reduction (LR) aided detections in multiple-input multiple-output (MIMO) systems. This chapter introduces the research background first. Then, based on MIMO system, we give the research motivation and objective. Finally, the organization of the thesis is concluded in the last section of chapter.

1.1 Background

Digital wireless communications using MIMO has emerged as one of the most remarkable scientific revolutions in modern communications [1]−[11]. Among the recent developments to relieve the bottleneck of wireless data transmission, MIMO techniques show tremendous potential. MIMO technology has attracted attention in wireless communications, because it offers significant increases in data throughput and link range without additional bandwidth or increased transmit power. It achieves this goal by spreading the same total transmit power over the antennas to achieve an array gain that improves the spectral efficiency (more bits per second per Hz of bandwidth) and/or to achieve a diversity gain that improves the link reliability (reduced fading). Because of these properties, MIMO is an important part of modern wireless communication standards such as IEEE 802.11n (Wi-Fi), 4G, 3GPP Long Term Evolution (LTE), WiMAX and HSPA+.

The idea behind MIMO is that these spatial subchannels can be combined in such a way as to improve the quality (bit error rate or BER) or data rate

(bits/sec/Hz) of communication. As the radio waves are transmitted over the air, these virtual spatial subchannels suffer from interference or leakage between themselves. Therefore, space-time processing is required to decouple these spatial subchannels. MIMO systems can be viewed as an extension of smart antenna systems, a popular technique, dating back several decades, for improving link reliability through the use of antenna array beamforming. Multipath propagation has long been a pitfall for wireless communications. The goal of wireless design has been to combat the multipath fading, by dynamic modulation and channel coding schemes, using Rayleigh fading as a worst-case scenario for design purposes. MIMO wireless systems, on the other hand, exploit this multipath to enhance the transmission over wireless links. MIMO systems provide a large increase in capacity without the cost of additional frequency bands, just requiring more complexity and hardware.

MIMO communication systems achieve higher data rates than single antenna systems by using multiple antennas to transmit and to receive multiple independent data streams simultaneously over a communication channel as seen in Fig. 1.1. Each receiving antenna acquires a superposition of these transmitted streams. The process of separating out each independent data stream is called MIMO detection. Although the optimal solution to the MIMO symbol detection problem, maximum likelihood (ML) detection, is known, a brute-force ML detector implementation involves an exhaustive search over all possible transmitted symbol vectors [11]. This approach is infeasible for hardware implementation when either a large signal constellation or large number of antennas is employed.

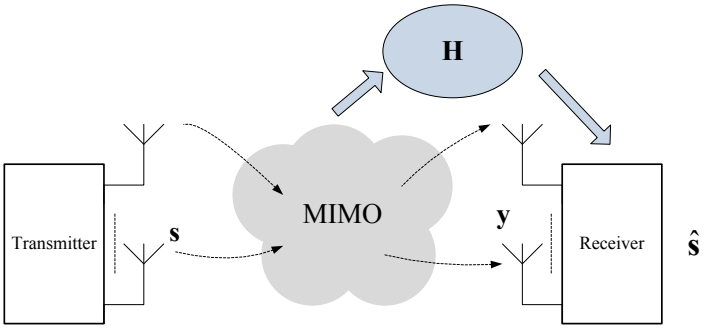

Figure 1.1: MIMO system

In many practical MIMO communication systems, detection is enabled by periodically characterizing the relative contribution of each signal transmitted on each antenna to the signal received on each antenna [9]. This process is referred to as the channel estimation and is accomplished by transmitting known training signals at the start of each packet. A variety of low complexity methods such as zero-forcing (ZF) and mean minimum square error (MMSE) and successive interference cancellation (SIC) detections involve a preprocessing step that transforms knowledge about the channel behavior into a form suitable for symbol detection [10]. However, the low complexity detection methods bring the worse performance. Hence, a good MIMO detection method is a tradeoff between the performance and the complexity, which could determine the performance of MIMO system.

1.2 MIMO system

There is ever growing demand of wireless services of higher data rates. Unfortunately, a conventional single-input single-output (SISO) system where the transmitter and the receiver are equipped with single antenna can have the limitations to support higher data services. The capacity grows logarithmically with the signal-to-noise ratio (SNR), in order to have a high transmission rate, it requires either high SNR or wide bandwidth. In wireless communications, since there are the limitation to increase SNR due to propagation loss, the bandwidth should be wide enough to support high data rate services. However, the scarce wireless spectrum has a big challenge on wireless communication systems with increasing data rate demands. To improve the spectral efficiency in wireless communications, multiple antennas are employed at both transmitter and receiver, where this system is called MIMO system. Thus, the channel matrix in MIMO system with N_t transmit and N_r receive antennas can be expressed as

$$\mathbf{H}^c = \begin{bmatrix} h^c_{11} & h^c_{12} & \dots & h^c_{1,N_t} \\ h^c_{21} & h^c_{22} & \dots & h^c_{2,N_t} \\ \vdots & \vdots & \ddots & \vdots \\ h^c_{N_r,1} & h^c_{N_r,2} & \dots & h^c_{N_r,N_t} \end{bmatrix} \tag{1.1}$$

The receive signal $\mathbf{y}^c$ can be expressed as

$$\mathbf{y}^c = \mathbf{H}^c\mathbf{s}^c + \mathbf{z}^c \tag{1.2}$$

where $\mathbf{H}^c$, $\mathbf{s}^c$ and $\mathbf{z}^c$ denote the channel matrix, the transmit signal vector and the noise vector, respectively. Note that the superscript c denotes the complex value. The channel capacity can be formulated as

$$\begin{aligned} C_{channel} &= E\left[\log_2\left(1+\frac{\sum_{i=1}^{N_t}|\mathbf{h}_i|^2 E_s}{N_0}\right)\right] \\ &\leq \log_2\left(1+\frac{\sum_{i=1}^{N_t}|\mathbf{h}_i|^2 E_s}{N_0}\right) \end{aligned} \tag{1.3}$$

where $E_s = \frac{E[||\mathbf{s}^c||^2]}{N_t}$ and $N_0 = E[||\mathbf{z}^c||^2]$.

It is well-known that the capacity of MIMO channels can linearly increase with the minimum number of transmit and receive antennas under the conditions, where the channel gains are independent complex Gaussian random vector. For a given bandwidth, the MIMO system has the more antennas, the higher transmission rates can be achieved without increasing the transmission power. To exploit the capacity, it requires the efficient signal modulation schemes for MIMO systems. Quadrature amplitude modulation (QAM) has been developed as the modulation order of digital signals in MIMO systems. In this thesis we consider the modulation order of QPSK, 16QAM and 64QAM.

1.3 Motivation and objective

MIMO detection is to detect the transmit signal from the receive signal under the knowledge of the channel state information (CSI). According to the performance, we divide the MIMO detections into four parts as seen in Fig. 1.2.

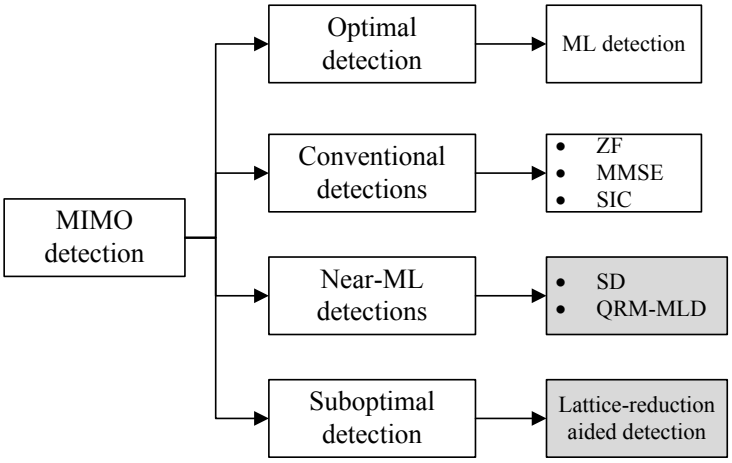

Figure 1.2: MIMO detections

The ML detection achieves the optimal performance in terms of minimizing the bit error rate (BER) among the existing detection schemes in the MIMO systems. However, the complexity of the ML detection exponentially increases with the number of the transmit antennas and thus obstructs its practical implementation. The conventional MIMO detections are linear ZF and MMSE detections, and non-linear SIC detection, which provide worse BER performance with low complexity. A near-ML scheme of the sphere-detection (SD) can be used to reduce the complexity which is still high in the low E_b/N_0 region or large size MIMO system or high modulation order [11]−[16]. The ML detection based on QR decomposition and M-algorithm (QRM-MLD) is one solution to relatively reduce the complexity while retaining the ML performance. However, the conventional QRM-MLD has the problem of high complexity in the high E_b/N_0 region or large size MIMO system or high modulation order [17]−[27]. These SD and QRM-MLD are called as near-ML detection.

Lattice-reduction (LR) aided (LRA) detection has been introduced into the MIMO detection to achieve the good tradeoff between the performance and the complexity [28]−[35]. The most popular LR algorithm is the well-known LLL algorithm, introduced by Lenstra, Lenstra and Lovász [36]. Combining the LLL algorithm with the linear detections such as ZF or MMSE can achieve the good

BER performance, especially the LR-MMSE detection which is close to the ML detector in the small size MIMO system. In contrast, the BER improvement in the large size MIMO system is not sufficient. The non-linear detection, i.e. SIC, is selected from many detection methods since it features the good BER performance. And ordering SIC (OSIC) based on LR (LR-OSIC) can further improve the BER performance with the costs of the implementation of the ordering but requires high computational complexity. In addition, the list detection can also obtain much better performance but a little high computational cost in terms of the list of candidates.

Our researches have been investigated in order to achieve the ultimate goal looking for a near-ML detection scheme on the performance together with low complexity. In this thesis, the objective is to solve three problems existed in MIMO detection methods marked with hatched boxes in Fig. 1.2 as

- The number of M in the conventional QRM-MLD is defined as the number of the survived branches in each detection layer of the tree search, which is a tradeoff between complexity and performance [23]. Furthermore, the value of M should be large enough to ensure that the correct symbols exist in the survived branches under the ill-conditioned channel, in particular for the large size MIMO system and the high modulation order. Hence the conventional QRM-MLD still has the problem of high complexity in the high E_b/N_0 region.

- For the LRA MIMO detection, the detection errors are mainly generated from the channel noise and the quantization errors in the signal estimation stage. The quantization step applies the simple rounding operation, which often leads to the quantization error. If this error occurs in a row of the transmit signal, it has to propagate to many symbols in the subsequent signal estimation and result in degrading the BER performance. The conventional LRA MIMO detection has the quantization problem, which obtains less reliable signal estimation and leads to the BER performance loss.

- Ordering the column vectors of the LR-reduced channel matrix brings large improvement on the BER performance of the LR-SIC due to decreasing

the error propagation. However, the improvement of the LR-OSIC is not sufficient to approach the ML performance in the large size MIMO system, such as 8×8 MIMO system. Hence, the LR-OSIC detection cannot achieve the near-ML BER performance in the large size of MIMO system.

1.4 Overview of the dissertation

This thesis summarizes our research works about lattice reduction aided detection in MIMO systems. The dissertation consists of seven chapters as follows.

Chapter 1 introduces the research background, the MIMO system, the motivation and objective of our researches.

Chapter 2 presents the system model and the conventional MIMO detections, such as zero-forcing, mean minimum square error, maximum likelihood detection, and the QRM-MLD.

Chapter 3 explains the LR algorithm first. Then, we describe several lattice reduction aided detection methods, which combine the LR technology with the linear detections, SIC detection or list detection. And these detection schemes employ some algorithms, including Gram-Schmidt orthogonalization algorithm.

Chapter 4 proposes a novel adaptive tree search detection with variable path expansion based on GSM-MLD. The adaptive tree search detection scheme retains the same breadth of the tree search as the GSM-MLD to achieve the near-ML performance, and however the number of the possible branches is adaptively controlled. The adaptive scheme avoids a large amount of the path metric evaluations and sorting to reduce the computational complexity.

Chapter 5 describes an improved quantization scheme based on LR-GS detection. The improved quantization scheme applies a simple tree search in order to obtain an optimum quantization results. We introduce a threshold function in order to survive the candidates for each entry of the signal vectors according to the path metric. This improved quantization scheme based on LR-GS detection can achieve near-ML performance and offer significant reduction in computational complexity compared to the QRM-MLD.

Chapter 6 introduces the conditional list detection based on the LR-OSIC detection. According to the mean squared error of the signal vector in the LR

domain, we use the conditional list generation to update the soft estimate of the LR-OSIC. Using this property, we decrease the complexity for computing the useless list candidates in the better-conditioned channel. This proposed detection can achieve the near-ML performance in the 8×8 MIMO system and require almost the same complexity of the LR-OSIC in the high E_b/N_0 region.

Chapter 7 summarizes the research contribution of the thesis and explores the future works. We compare the BER performance and complexity among three proposed detections and recommend the suitable applications according to the size of MIMO system, the modulation order and the type of fading channel.

Appendices are described after chapter 7. Weigh matrices of MMSE in chapter 2 is derived in appendix A. Appendix B shows the MMSE estimation of new signal vector using the LR technology in chapter 3.

Chapter 2

Background of MIMO Detection

In this chapter, we introduce a system model for MIMO detection. Then, we present several well-known MIMO detection methods, including the ML, linear detections.

2.1 System model

Consider a multiple antenna system with N_t transmit and N_r ($N_r \geqslant N_t$) receive antennas in Fig. 2.1.

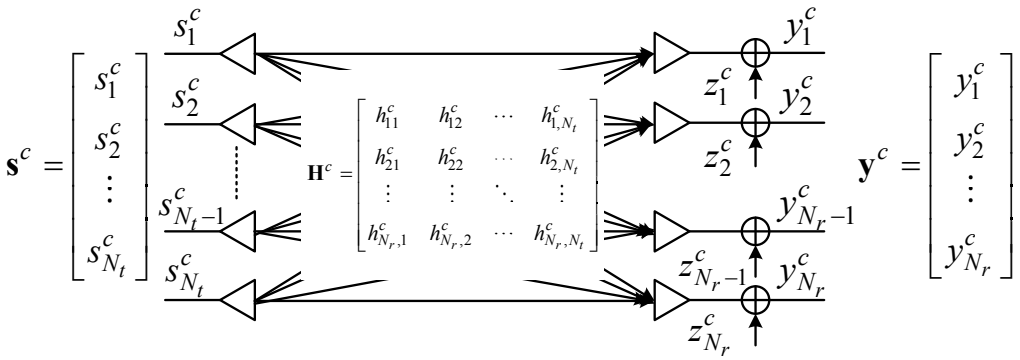

Figure 2.1: The model of MIMO system.

We assume that the signals are transmitted over a quasi-static flat Rayleigh fading channel such that the channel is non-time variant in the packet duration. In this thesis, we assume that the receiver has perfect knowledge of the

CSI. Let $\mathbf{H}^c = [\mathbf{h}_1^c, \mathbf{h}_2^c, ..., \mathbf{h}_{N_t}^c]$ denote the $N_r \times N_t$ channel matrix. The entries of $\mathbf{H}^c$ are of the independent and identically distributed (i.i.d.) complex Gaussian process with zero mean and unity variance. The receive signal vector $\mathbf{y}^c = [y_1^c, y_2^c, ..., y_{N_r}^c]^{\mathrm{T}} \in \mathbb{C}^{N_r \times 1}$ is expressed as

$$\mathbf{y}^c = \mathbf{H}^c \mathbf{s}^c + \mathbf{z}^c \tag{2.1}$$

where y_q^c is the receive signal at the q-th receive antenna. The transmit signal vector is denoted as $\mathbf{s}^c = [s_1^c, s_2^c, ..., s_{N_t}^c]^{\mathrm{T}} \in \mathbb{S}^{N_t \times 1}$, where each symbol s_p^c at the p-th transmit antenna is chosen from a finite subset of the complex-valued integer set $\mathbb{S}$. The noise vector $\mathbf{z}^c = [z_1^c, z_2^c, ..., z_{N_r}^c]^{\mathrm{T}} \in \mathbb{C}^{N_r \times 1}$ is the additive white Gaussian noise (AWGN) vector, of which each entry is assumed to be zero mean and variance of N_0, the one-sided noise power spectral density.

According to [1], the MIMO channel capacity grows linearly with $\min(N_t, N_r)$. Note that there is a fundamental trade-off between receive diversity gain and multiplexing gain [6]. Thus, we prefer that $N_t = N_r$ which results in the square channel matrix.

2.2 Symbol mapping and definition of E_b/N_0

In this thesis, we explain the symbol mapping, the definition of the average energy per one symbol E_s, the energy per one bit E_b, and E_b/N_0 for the mappings of QPSK, 16QAM and 64QAM. Let s_p^c be the complex amplitude of the mapped symbol transmitted from the p-th transmitter. One symbol consists of two bits for QPSK, of four bits for 16QAM, and of six bits for 64QAM. Let E_s be the average energy per one symbol, and E_b be the energy per one bit. We have $E_s = 2E_b$ for QPSK, $E_s = 4E_b$ for 16QAM, and $E_s = 6E_b$ for 64QAM, respectively.

2.2.1 QPSK

The complex symbol amplitude and the set of QPSK in the symbol constellation in Fig. 2.2 are defined, respectively, as

$$s_p^c = a + jb : \{a|b\} \in \{\pm 1\}, \text{ and } \mathbb{C}^{(s_p^c)} \in \{(00), (01), (11), (10)\} \tag{2.2}$$

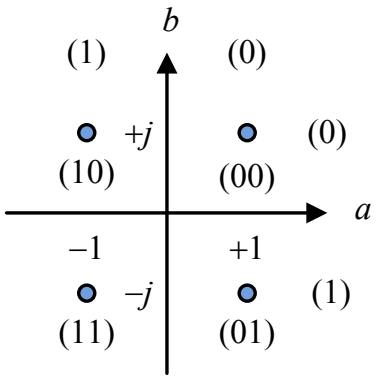

Figure 2.2: Constellation of QPSK

The average energy per one symbol for QPSK is expressed as

$$\begin{aligned} E_s = \mathrm{E}\left[|s_p^c|^2\right] &= \frac{|1+j|^2+|1-j|^2+|-1+j|^2+|-1-j|^2}{4} \\ &= \frac{2+2+2+2}{4} = 2 \end{aligned} \tag{2.3}$$

Since $E_s = 2E_b$ for QPSK, the energy per one bit E_b, E_b/N_0 and $E_s/N_0 (= \gamma)$ are expressed, respectively, as

$$E_b = \frac{E_s}{2} = \frac{2}{2} = 1 \tag{2.4}$$

$$\frac{E_b}{N_0} = \frac{1}{N_0} \ : \ i.e., \ N_0 = \frac{1}{(E_b/N_0)} = \mathrm{E}\left[|z_q^c|^2\right] \tag{2.5}$$

The noise amplitude z_q^c should be generated so that (2.5) is satisfied. Then, E_b/N_0 for QPSK is defined as

$$\gamma = \frac{E_s}{N_0} = \frac{2E_b}{N_0} \tag{2.6}$$

where γ will be used for the weight matrix of MMSE detection in the following subsection. Note that QPSK signal is a two-dimensional bi-orthogonal signal.

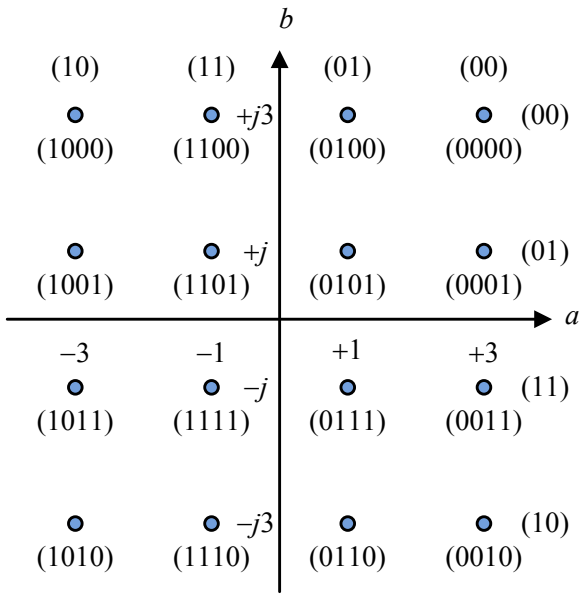

Figure 2.3: Constellation of 16QAM

2.2.2 16QAM

The complex symbol amplitude and the set of 16QAM in the symbol constellation in Fig. 2.3 are defined, respectively, as

$$s_p^c = a + jb : \tag{2.7}$$

$$\{a|b\} \in \{\pm 1,\ \pm 3\}, \text{and } \mathbb{C}^{(s_p^c)} \in \left\{ \begin{array}{cccc} (0000), & (0001), & (0011), & (0010) \\ (0100), & (0101), & (0111), & (0110) \\ (1100), & (1101), & (1111), & (1110) \\ (1000), & (1001), & (1011), & (1010) \end{array} \right\} \tag{2.8}$$

The average energy per one symbol for 16QAM is expressed as

$$\begin{aligned} E_s = \mathrm{E}\left[|s_p^c|^2\right] &= \frac{|1+j|^2 + |3+j|^2 + |1+j3|^2 + |3+j3|^2}{4} \\ &= \frac{2+10+10+18}{4} = \frac{40}{4} = 10 \end{aligned} \tag{2.9}$$

Since $E_s = 4E_b$ for 16QAM, the energy per one bit E_b, E_b/N_0 and $E_s/N_0 (= \gamma)$

are expressed, respectively, as

$$E_b = \frac{E_s}{4} = \frac{5}{2} \tag{2.10}$$

$$\frac{E_b}{N_0} = \frac{\frac{5}{2}}{N_0} = \frac{5}{2N_0} \ : \ i.e., \ N_0 = \frac{5}{2(E_b/N_0)} = \mathrm{E}\Big[|z_q^c|^2\Big] \tag{2.11}$$

The noise amplitude z_q^c should be generated so that (2.11) is satisfied. Then, E_b/N_0 for 16QAM is defined as

$$\gamma = \frac{E_s}{N_0} = \frac{4E_b}{N_0} \tag{2.12}$$

2.2.3 64QAM

The complex symbol amplitude and the set of 64QAM in the symbol constellation in Fig. 2.4 are defined, respectively, as

$$s_p^c = a + jb : \ \{a|b\} \in \{\pm 1, \ \pm 3 \ \pm 5, \ \pm 7\}, \tag{2.13}$$

$$\text{and } \mathbb{C}^{(s_p^c)} \in \begin{Bmatrix} (000000), & (000001), & ..., & (000100) \\ (001001), & (001001), & ..., & (001100) \\ \vdots & \vdots & \ddots & \vdots \\ (100000), & (100001), & ..., & (100100) \end{Bmatrix} \tag{2.14}$$

The average energy per one symbol for 64QAM is expressed as

$$\begin{aligned} E_s = \mathrm{E}\Big[|s_p^c|^2\Big] &= \frac{|1+j|^2 + |3+j3|^2 + |5+j5|^2 + |7+j7|^2}{16} \\ &\quad + 2\ \frac{|1+j3|^2 + |1+j5|^2 + |1+j7|^2 + |3+j5|^2 + |3+j7|^2 + |5+j7|^2}{16} \\ &= \frac{2+18+50+98}{16} + 2\ \frac{10+26+50+34+58+74}{16} = \frac{672}{16} = 42 \end{aligned} \tag{2.15}$$

Since $E_s = 6E_b$ for 64QAM, the energy per one bit E_b, E_b/N_0 and $E_s/N_0 (= \gamma)$

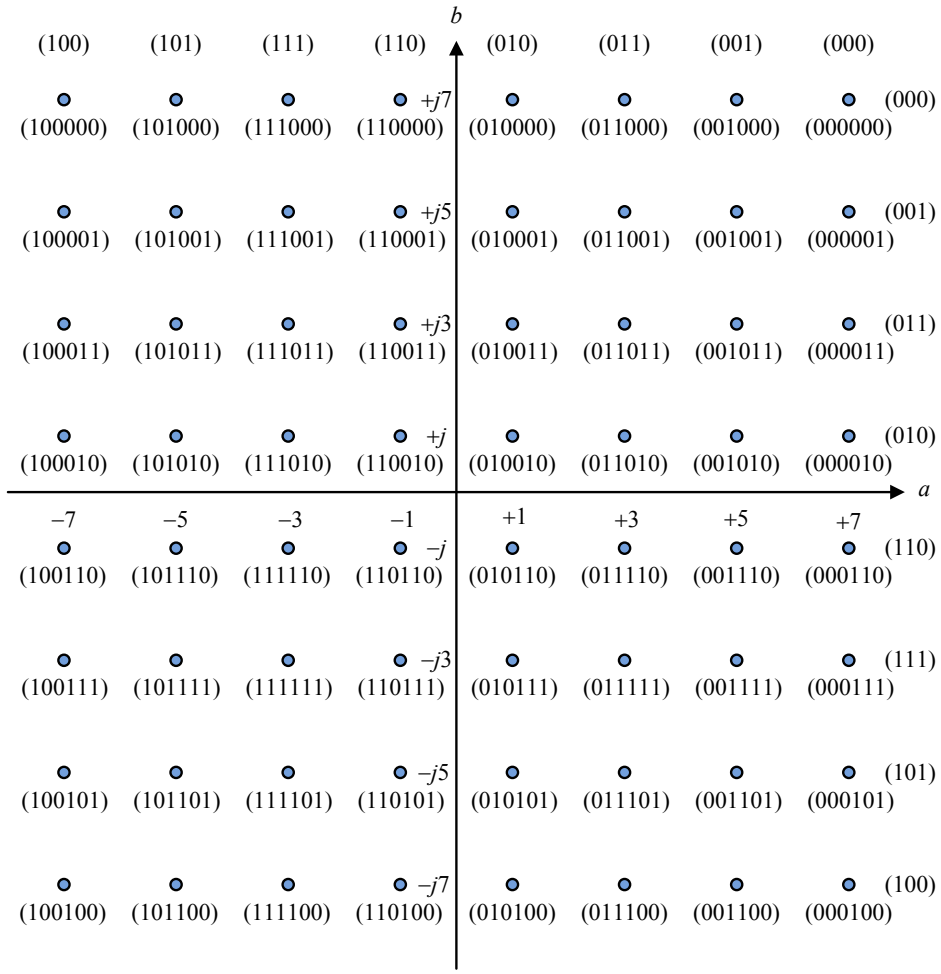

Figure 2.4: Constellation of 64QAM

are expressed, respectively, as

$$E_b = \frac{E_s}{6} = \frac{42}{6} = 7 \tag{2.16}$$

$$\frac{E_b}{N_0} = \frac{7}{N_0} \;:\; i.e.,\; N_0 = \frac{7}{(E_b/N_0)} = \mathrm{E}\left[|z_q^c|^2\right] \tag{2.17}$$

The noise amplitude z_q^c should be generated so that (2.17) is satisfied. Then,

E_b/N_0 for 64QAM is defined as

$$\gamma = \frac{E_s}{N_0} = \frac{6E_b}{N_0} \tag{2.18}$$

2.3 Conventional MIMO detections

2.3.1 Maximum likelihood detection

MIMO detection is to estimate the unknown transmit signal vector $\mathbf{s}^c$, using the given receive signal vector $\mathbf{y}^c$, and the channel matrix $\mathbf{H}^c$. Although we cannot predict the noise vector $\mathbf{z}^c$, we have the knowledge of all the possible combinations of $\mathbf{s}^c$. For N_t transmit antennas, with the signal alphabet $\mathbb{S}$, the number of candidate vectors is given by $\mathbb{S}^{N_t}$, where $\mathbb{S}$ denotes the constellation points and $\mathbb{S}^{N_t}$ denotes the N_t-dimensional product of $\mathbb{S}$. Hence, using a certain modulation order, we can show that the number of candidate vectors grows exponentially with N_t.

For example, when the modulation order of QPSK is employing for signaling over 2×2 MIMO system, we have $4^2 = 16$ possible candidates for the combination of $\mathbf{s}^c$ as following

Table 2.1: Possible candidates for the combination in 2×2 MIMO with QPSK

$\mathbf{s}^c$	s_1^c	s_2^c	$\mathbf{s}^c$	s_1^c	s_2^c
1	$1+j$	$1+j$	2	$1+j$	$1-j$
3	$1+j$	$-1+j$	4	$1+j$	$-1-j$
5	$1-j$	$1+j$	6	$1-j$	$1-j$
7	$1-j$	$-1+j$	8	$1-j$	$-1-j$
9	$-1+j$	$1+j$	10	$-1+j$	$1-j$
11	$-1+j$	$-1+j$	12	$-1+j$	$-1-j$
13	$-1-j$	$1+j$	14	$-1-j$	$1-j$
15	$-1-j$	$-1+j$	16	$-1-j$	$-1-j$

The ML detection can be carried out by exhaustively searching for all the candidate vectors and select the most likely one with the smallest error probability

[11]. Let $f(\mathbf{y}^c|\mathbf{s}^c)$ denote the likelihood function of $\mathbf{s}^c$ for a given signal vector $\mathbf{y}^c$. Then, the best symbol vector under the ML detection is given by

$$\begin{aligned}\hat{\mathbf{s}}^{c(\mathrm{ML})} &= \arg\min_{\mathbf{s}^c \in \mathbb{S}^{N_t}} f(\mathbf{y}^c|\mathbf{s}^c) \\ &= \arg\min_{\mathbf{s}^c \in \mathbb{S}^{N_t}} \|\mathbf{y}^c - \mathbf{H}^c\mathbf{s}^c\|^2\end{aligned} \tag{2.19}$$

Since the exhaustive search is carried out to find the ML vector and the number of candidate vectors for $\mathbf{s}^c$ is $\mathbb{S}^{N_t}$, the complexity grows exponentially with the number of the transmit antenna, N_t.

2.3.2 Zero-forcing detection

The ZF estimator and the estimated symbol vector are given by

$$\mathbf{W}_{ZF} = \mathbf{H}^c(\mathbf{H}^{c\mathrm{H}}\mathbf{H}^c)^{-1} \tag{2.20}$$

and

$$\begin{aligned}\tilde{\mathbf{s}}^{c(ZF)} &= \mathbf{W}_{ZF}^{\mathrm{H}}\mathbf{y}^c \\ &= (\mathbf{H}^{c\mathrm{H}}\mathbf{H}^c)^{-1}\mathbf{H}^{c\mathrm{H}}\mathbf{y}^c \\ &= \mathbf{s}^c + (\mathbf{H}^{c\mathrm{H}}\mathbf{H}^c)^{-1}\mathbf{H}^{c\mathrm{H}}\mathbf{z}^c\end{aligned} \tag{2.21}$$

It is shown that when $\mathbf{H}^c$ is near singular, the term of noise, i.e., $(\mathbf{H}^{c\mathrm{H}}\mathbf{H}^c)\mathbf{H}^{c\mathrm{H}}\mathbf{z}$ in (2.21), is enhanced. In this case, good performance cannot be guaranteed with an enhanced noise vector.

With $\tilde{\mathbf{s}}^{c(ZF)} = \left[\tilde{s}_1^{c(ZF)}, \tilde{s}_2^{c(ZF)}, \ldots, \tilde{s}_{N_t}^{c(ZF)}\right]^{\mathrm{T}}$ and $\mathbb{S}$ for K^2-ary QAM, the hard decision of $\mathbf{s}^c$ is carried out to the nearest constellation points as

$$\hat{\mathbf{s}}^c = \arg\min_{s_i^{c(k)} \in \mathbb{S}} \sum_{i=1}^{N_t} \left| s_i^{c(k)} - \tilde{s}_i^{c(ZF)} \right|^2, \; i \in [1, N_t] \text{ and } k \in [1, K^2] \tag{2.22}$$

Note that the final decision $\hat{\mathbf{s}}^c$ is forced to the nearest constellation points if they are lying outside the original signal constellation, defined as $\hat{\mathbf{s}}^c := \mathcal{C}\left[\tilde{\mathbf{s}}^{c(ZF)}\right]$, where the symbol $\mathcal{C}$ denotes this operation.

2.3.3 Minimum mean square error detection

To reduce the impact from the background noise, the MMSE detection employs a linear filter that can take into account the noise. The MMSE filter can be found by minimizing the mean square error (MSE) using (A.1) and (A.10) described in Appendix A as

$$\begin{aligned}\mathbf{W}_{MMSE} &= \arg\min_{\mathbf{W}} E\left[\left\|\mathbf{s}^c - \mathbf{W}_{MMSE}^{\mathrm{H}}\mathbf{y}^c\right\|^2\right] \\ &= \left(E\left[\mathbf{y}^c\mathbf{y}^{c\mathrm{H}}\right]\right)^{-1} E\left[\mathbf{y}^c\mathbf{s}^{c\mathrm{H}}\right] \\ &= \mathbf{H}^c\left(\mathbf{H}^{c\mathrm{H}}\mathbf{H}^c + \gamma^{-1}\mathbf{I}_{N_t}\right)^{-1}\end{aligned} \tag{2.23}$$

where E_s denotes the symbol energy and $\gamma = \frac{E_s}{N_0}$. After some derivation, the resulting estimated symbol vector of the MMSE detection is given by

$$\begin{aligned}\tilde{\mathbf{s}}^{c(MMSE)} &= \mathbf{W}_{MMSE}^{\mathrm{H}}\mathbf{y}^c \\ &= \left(\mathbf{H}^{c\mathrm{H}}\mathbf{H}^c + \gamma^{-1}\mathbf{I}_{N_t}\right)^{-1}\mathbf{H}^{c\mathrm{H}}\mathbf{y}^c\end{aligned} \tag{2.24}$$

and it follows that

$$\begin{aligned}A &= E\left[\left(\mathbf{s}^c - \mathbf{W}_{MMSE}^{\mathrm{H}}\mathbf{y}^c\right)\left(\mathbf{s}^c - \mathbf{W}_{MMSE}^{\mathrm{H}}\mathbf{y}^c\right)^{\mathrm{H}}\right] \\ &= E_s\left(E_s\mathbf{H}^c\mathbf{H}^{c\mathrm{H}} + N_0\mathbf{I}_{N_t}\right)^{-1}\mathbf{H}^c \\ &= \left(\mathbf{H}^c\mathbf{H}^{c\mathrm{H}} + \gamma^{-1}\mathbf{I}_{N_t}\right)^{-1}\mathbf{H}^c\end{aligned} \tag{2.25}$$

The MSE for each symbol estimate of the MMSE detection can be obtained from the corresponding diagonal element of A as described in Appendix A. Using the method in (2.22), the MMSE hard decision of $\hat{\mathbf{s}}^c$ can be obtained from $\tilde{\mathbf{s}}^{c(MMSE)}$ as $\hat{\mathbf{s}}^c := \mathcal{C}\left[\tilde{\mathbf{s}}^{c(MMSE)}\right]$.

2.3.4 Performance analysis

We have shown that the output of a linear detector becomes

$$\tilde{\mathbf{s}}^c = \mathbf{W}^{\mathrm{H}}\mathbf{y}^c \tag{2.26}$$

where $\mathbf{W} = \mathbf{H}^c(\mathbf{H}^{c\mathrm{H}}\mathbf{H}^c)^{-1}$ is used for the ZF detection and $\mathbf{W} = \mathbf{H}^c(\mathbf{H}^{c\mathrm{H}}\mathbf{H}^c + \gamma^{-1}\mathbf{I}_{N_t})^{-1}$ is used for the MMSE detection. With a high SNR, we have $\gamma^{-1} \to 0$ and the MMSE detection becomes the ZF detection. Denote s_i^c and $\tilde{s}_i^c$ to be the i-th element of $\mathbf{s}^c$ and $\tilde{\mathbf{s}}^c$, respectively, for $i = 1, 2, \ldots, N_t$. Let

$$\begin{aligned} \tilde{s}_i^c &= \mathbf{w}_i^{\mathrm{H}}\mathbf{y}^c \\ &= \mathbf{w}_i^{\mathrm{H}}\mathbf{h}_i^c s_i^c + \mathbf{w}_i^{\mathrm{H}}\left(\sum_{j=1, j\neq i}^{N_t} \mathbf{h}_j^c s_j^c + \mathbf{z}^c\right) \end{aligned} \tag{2.27}$$

where $\mathbf{w}_i$ denotes the linear filter for s_i^c that needs be clarified.

In the case of ZF detection, the interferences are completely suppressed: $\mathbf{w}_i^{\mathrm{H}} \sum_{j=1, j\neq i}^{N_t} \mathbf{h}_j^c s_j^c = 0$, $\mathbf{w}_i$ has to be orthogonal to the subspace of $\mathbf{H}_i^c = [\mathbf{h}_1^c, \ldots, \mathbf{h}_i^c, \mathbf{h}_{i+1}^c, \ldots, \mathbf{h}_{N_t}^c]$.

To this end, we have

$$\mathbf{w}_i = \mathbf{H}^c\mathbf{g}_i \tag{2.28}$$

where $\mathbf{g}_i$ denotes the i-th column vector of $\mathbf{G} = (\mathbf{H}^{c\mathrm{H}}\mathbf{H}^c)^{-1}$ is used for the ZF detection. Thus, Eq. (2.27) becomes

$$\tilde{s}_i^c = \mathbf{w}_i^{\mathrm{H}}\mathbf{h}_i^c s_i^c + \mathbf{w}_i^{\mathrm{H}}\mathbf{z}^c \tag{2.29}$$

It is not difficult to verify that the given $\mathbf{H}^c$, $\mathbf{z}^c$ is complex Gaussian distribution with zero mean and covariance matrix as

$$\begin{aligned} E\left[\mathbf{z}^c\mathbf{z}^{c\mathrm{H}}\right] &= N_0\mathbf{H}^{c\dagger}\left(\mathbf{H}^{c\dagger}\right)^{\mathrm{H}} \\ &= N_0\left(\mathbf{H}^{c\mathrm{H}}\mathbf{H}^c\right)^{-1} \\ &= N_0\mathbf{G} \end{aligned} \tag{2.30}$$

Supposing $\mathbf{s}^c$ is transmitted, while $\hat{\mathbf{s}}^c$ is erroneously detected as $\hat{\mathbf{s}}^c \neq \mathbf{s}^c$, the pairwise error probability (PEP) of the linear detection is given by

$$P(s_i^c \to \hat{s}_i^c) = \Pr\left(|\tilde{s}_i^c - \hat{s}_i^c|^2 < |\tilde{s}_i^c - s_i^c|^2\right) \tag{2.31}$$

If we define that $e_i = s_i^c - \hat{s}_i^c$, then the PEP can be further simplified as

$$\begin{aligned} P(s_i^c \to \hat{s}_i^c) &= \Pr\left(|\tilde{s}_i^c - \hat{s}_i^c|^2 < |\tilde{s}_i^c - s_i^c|^2\right) \\ &= \Pr\left(|e_i + z_i^c|^2 < |z_i^c|^2\right) \\ &= \Pr\left(-e_i z_i^{c*} - e_i^* z_i^c > |e_i|^2\right) \end{aligned} \tag{2.32}$$

where we define a variable $n_i = (-e_i z_i^{c*} - e_i^* z_i^c)$ and n_i is complex Gaussian distributed with zero mean and variance $2|e_i|^2 E[|n_i|^2] = 2|e_i|^2 N_0 g_{i,i}$, where $g_{i,i}$ is the (i,i)th element of $\mathbf{G}$. Thus, the PEP in (2.32) can be rewritten as

$$P(s_i^c \to \hat{s}_i^c) = Q\left(\sqrt{\frac{|e_i|^2}{2N_0 g_{i,i}}}\right) \tag{2.33}$$

2.4 QRM-MLD

2.4.1 QR decomposition

Here we first introduce the QR decomposition, giving an example for 2×2 MIMO system. Consider a 2×2 channel matrix of $\mathbf{H}^c = [\mathbf{h}_1^c \ \mathbf{h}_2^c]$, where $\mathbf{h}_i^c$ is the i-th column vector of $\mathbf{H}^c$. To find two orthogonal vectors that generates the same lattice as $\mathbf{H}^c$ does, we define

$$\begin{aligned} \mathbf{r}_1^c &= \mathbf{h}_1^c \\ \mathbf{r}_2^c &= \mathbf{h}_2^c - \mu_{p,q}\mathbf{h}_1^c \end{aligned} \tag{2.34}$$

where

$$\begin{aligned} \mu_{p,q} &= \frac{< \mathbf{h}_2^c, \mathbf{r}_1^c >}{\|\mathbf{r}_1^c\|^2} \\ &= \frac{< \mathbf{h}_2^c, \mathbf{h}_1^c >}{\|\mathbf{h}_1^c\|^2} \end{aligned} \tag{2.35}$$

in order to lead $< \mathbf{r}_1^c, \mathbf{r}_2^c >= \mathbf{r}_1^{c\mathrm{H}}\mathbf{r}_2^c = 0$.

With the linear relationship provided in (2.34), we can show that $(\mathbf{h}_1^c, \mathbf{h}_2^c)$ and $(\mathbf{r}_1^c, \mathbf{r}_2^c)$ can span the same subspace. Under the condition that $\mathbf{r}_i^c$ is a nonzero

vector for $i \in \{1, 2\}$, it is derived as

$$\begin{aligned}
[\mathbf{h}_1^c \ \mathbf{h}_2^c] &= [\mathbf{r}_1^c \ \mathbf{r}_2^c] \begin{bmatrix} 1 & \mu_{p,q} \\ 0 & 1 \end{bmatrix} \\
&= [\mathbf{q}_1^c \ \mathbf{q}_2^c] \begin{bmatrix} \|\mathbf{r}_1^c\| & 0 \\ 0 & \|\mathbf{r}_2^c\| \end{bmatrix} \begin{bmatrix} 1 & \mu_{p,q} \\ 0 & 1 \end{bmatrix} \\
&= [\mathbf{q}_1^c \ \mathbf{q}_2^c] \begin{bmatrix} \|\mathbf{r}_1^c\| & \mu_{p,q} \|\mathbf{r}_1^c\| \\ 0 & \|\mathbf{r}_2^c\| \end{bmatrix}
\end{aligned} \tag{2.36}$$

where $\mathbf{q}_i^c = \frac{\mathbf{r}_i^c}{\|\mathbf{r}_i^c\|}$. From (2.36) the QR decomposition is given by letting the orthogonal matrix $\mathbf{Q}^c = [\mathbf{q}_1^c \ \mathbf{q}_2^c]$ and the upper triangular matrix $\mathbf{R}^c = \begin{bmatrix} \|\mathbf{r}_1^c\| & \mu_{p,q} \|\mathbf{r}_1^c\| \\ 0 & \|\mathbf{r}_2^c\| \end{bmatrix}$. Note that with $\mathbf{r}_2^c = \mathbf{h}_2^c$ and $\mathbf{r}_1^c = \mathbf{h}_1^c - \mu_{p,q}\mathbf{h}_2^c$, the other QR decomposition of $\mathbf{H}^c$ can be obtained.

2.4.2 Scheme description

Since the expansion nodes in the QRM-MLD are the constellation points, the system model is modified using the real vectors. Eq. (2.1) can be rewritten using the real representation as

$$\mathbf{y} = \mathbf{H}\mathbf{s} + \mathbf{z} \tag{2.37}$$

where the equivalent real-valued channel matrix and vectors letting $n = 2N_r$ and $m = 2N_t$ are defined as

$$\begin{aligned}
&\mathbf{H} \triangleq \begin{bmatrix} \mathrm{Re}[\mathbf{H}^c] & -\mathrm{Im}[\mathbf{H}^c] \\ \mathrm{Im}[\mathbf{H}^c] & \mathrm{Re}[\mathbf{H}^c] \end{bmatrix} \in \mathbb{R}^{n \times m}, \ \mathbf{s} \triangleq \begin{bmatrix} \mathrm{Re}[\mathbf{s}^c] \\ \mathrm{Im}[\mathbf{s}^c] \end{bmatrix} \in \mathbb{Z}^{m \times 1}, \\
&\mathbf{y} \triangleq \begin{bmatrix} \mathrm{Re}[\mathbf{y}^c] \\ \mathrm{Im}[\mathbf{y}^c] \end{bmatrix} \in \mathbb{R}^{n \times 1}, \text{ and } \mathbf{z} \triangleq \begin{bmatrix} \mathrm{Re}[\mathbf{z}^c] \\ \mathrm{Im}[\mathbf{z}^c] \end{bmatrix} \in \mathbb{R}^{n \times 1}
\end{aligned} \tag{2.38}$$

We define the dimension of the real-valued channel matrix $\mathbf{H}$ to be $n \times m$. The dimensions of the vectors in (2.38) are given as $\mathbf{y} \in \mathbb{R}^{n \times 1}, \mathbf{z} \in \mathbb{R}^{n \times 1}$ and $\mathbf{s} \in \mathbb{Z}^{m \times 1}$, where $\mathbb{Z}$ denotes the finite set of the real-valued transmit signals. The set of the real-valued signals is given by $\mathbb{Z} = \{\pm 1, \pm 3, \ldots, \pm(K-1)\}$ for K^2-QAM. Since the data is binary in the digital telecommunication, the value of K in the constellation is usually a power of 2.

The channel matrix $\mathbf{H}$ applies the QR decomposition as $\mathbf{H}$=$\mathbf{QR}$, where $\mathbf{Q}$ is a

unitary matrix: i.e., $\mathbf{Q}^{\mathrm{T}}\mathbf{Q} = \mathbf{I}_m$, and $\mathbf{R}$ is an $m \times m$ upper triangular matrix. The QR decomposition is executed by the modified GS algorithm (MGS) in [56]. The matrix $\mathbf{R}$ retains the property of the channel matrix $\mathbf{H}$. Then, we pre-multiply both the hand sides of (2.37) by $\mathbf{Q}^{\mathrm{T}}$ as

$$\begin{aligned} \mathbf{y}' &\triangleq \mathbf{Q}^{\mathrm{T}}\mathbf{y} \\ &= \mathbf{Q}^{\mathrm{T}}(\mathbf{QRs} + \mathbf{z}) \\ &= \mathbf{Rs} + \mathbf{z}' \end{aligned} \tag{2.39}$$

with expressing $\mathbf{R}$ as

$$\mathbf{R} = \begin{bmatrix} r_{11} & r_{12} & \cdots & r_{1,m} \\ & r_{22} & \cdots & r_{2,m} \\ & & \ddots & \vdots \\ \mathbf{0} & & & r_{m,m} \end{bmatrix} \tag{2.40}$$

where $\mathbf{z}' \triangleq \mathbf{Q}^{\mathrm{T}}\mathbf{z}$. The ML detector searches over the whole set of transmit signals $\mathbf{s} \in \mathbb{Z}^m$, and decides the transmit signal $\mathbf{s}^{(\mathrm{ML})}$ in terms of the minimum Euclidean distance (ED) to the receive vector $\mathbf{y}$. The ML detection can be formulated as

$$\begin{aligned} \hat{\mathbf{s}}^{(\mathrm{ML})} &= \arg\min_{\mathbf{s}\in\mathbb{Z}^m} \left\| \mathbf{y} - \mathbf{Hs} \right\|^2 \\ &= \arg\min_{\mathbf{s}\in\mathbb{Z}^m} \left\| \mathbf{y}' - \mathbf{Rs} \right\|^2 \\ &= \arg\min_{\mathbf{s}\in\mathbb{Z}^m} \left[\sum_{i=1}^{m} \left| y_i' - \sum_{j=i}^{m} r_{i,j} s_j \right|^2 \right] \end{aligned} \tag{2.41}$$

where $\lambda_i \triangleq |y_i' - \sum_{j=i}^{m} r_{i,j}^c s_j|^2$ denotes the branch metric in the i-th layer. The accumulated branch metric $\Lambda_i \triangleq \sum_{j=i}^{m} \lambda_i$ is defined as the path metric from the m-th layer down to the i-th layer.

The concept of the QRM-MLD is to apply a tree search to detect the symbols in a sequential manner [17]−[20], which is one solution to reduce the complexity of the ML detection retaining the ML performance. As seen in Fig. 2.5, we give an example of tree search of the QRM-MLD in 2×2 MIMO system with $M = 2$, where M denotes the number of survived branch in each detection layer.

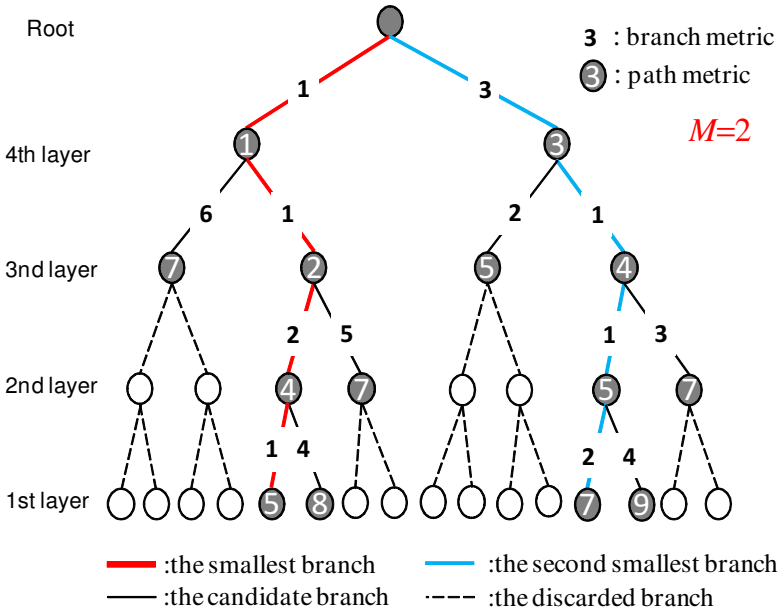

Figure 2.5: Example of tree search of the QRM-MLD in 2×2 MIMO system with $M = 2$.

The QRM-MLD is breadth-first algorithm that in each detection layer the same number of branches is survived. In order to retain the correct path, the value of M should be large enough to achieve the near-ML performance, especially in large size MIMO system or high modulation order.

For each detection layer of the tree search in the QRM-MLD, there are three major operations:

- Candidate Expansion: Expand the children nodes from each survived branch. The candidates for the children nodes consist of all the constellation points.
- Path metric evaluations: There are MK possible branches for K^2-QAM in each layer. Calculate the path metric for all the possible branches.
- Sorting and retaining: Sort the path metric and retain M branches with the smallest path metric from MK possible branches. The rest of branches are discarded.

Let $\Lambda_i^{(l)}$ denote the l-th smallest path metric of the survived path $\Pi_i^{(l)}$ after the operations of sorting and retaining, where $l \in [1, M]$ and $\Lambda_i^{(1)} \leq \Lambda_i^{(2)} \leq \cdots \leq$

$\Lambda_i^{(M)}$. Correspondingly, the partial transmit signal $\hat{\mathbf{s}}_i^{(l)}$ based $\Lambda_i^{(l)}$ is expressed as $\hat{\mathbf{s}}_i^{(l)} = [\hat{s}_i^{(l)}, \hat{s}_{i+1}^{(l)}, \cdots, \hat{s}_m^{(l)}]^{\mathrm{T}}$. The same operations are executed until the first layer. The output of the QRM-MLD is $\hat{\mathbf{s}} = [\hat{s}_1^{(1)}, \hat{s}_2^{(1)}, \cdots, \hat{s}_m^{(1)}]^{\mathrm{T}}$ as the final estimate of transmit signal.

Although the exhaustive tree search of the QRM-MLD should visit MK nodes in each detection layer instead of K^{m-i+1} nodes in the i-th layer for the full MLD. The conventional QRM-MLD reduces the exponentially growing complexity to a linear growing complexity while retaining the ML performance. However, the conventional QRM-MLD still requires high complexity in the high E_b/N_0 region.

Comparing to the ML detection that requires a number of $\mathbb{Z}^m$ matrix multiplications to detect one symbol vector, the linear detectors perform the hard decision with the matrix multiplication, which is once for detecting a vector. Hence, a significant complexity reduction is achieved. However, due to the impact of interference, the linear detection cannot provide good performance with a full receive diversity gain, which will be illustrated in next section.

Considering the complexity of the QRM-MLD [19], the exhaustive tree search of the QRM-MLD should visit $2M$, $4M$ and $8M$ nodes in each layer for QPSK, 16QAM and 64QAM, respectively. Next, we derive the complexity of QRM-MLD in the real-valued system model. Before the tree search of the QRM-MLD, the channel matrix is also QR-decomposed, which requires $(2mn - n)$ flops for computing of $\mathbf{y}'$. We calculate the path metric using $\|\mathbf{y}' - \mathbf{R}\mathbf{s}\|^2$ instead of $\|\mathbf{y} - \mathbf{H}\mathbf{s}\|^2$, expressed as

$$\|\mathbf{y}' - \mathbf{R}\mathbf{s}\|^2 = \sum_{i=1}^{m-1} \left(y_i' - r_{i,i}s_i - \sum_{j=i+1}^{m} r_{i,j}s_j \right)^2 + (y_m' - r_{m,m}s_m)^2 \tag{2.42}$$

There are K real-valued expansion candidates for K^2-QAM. Thus, it requires $3K$ flops for computing the path metric in the m-th entry. From the $(m-1)$-th entry down to the 1st entry, we survive M branches in each detection layer. The complexity of a surviving path for computing the path metric are $\sum_{i=1}^{m-1}(2m - 2i + 4K)(= m^2 - m + 4Km - 4K)$ flops. Hence, the total complexity for the QRM-MLD is expressed as $(2mn - m + 3K + M(m^2 - m + 4Km - 4K))$ flops. The computational complexity for QRM-MLD is shown in Table 2.2.

Table 2.2: The computational complexity for QRM-MLD [flops]

Modulation order	$N_t = N_r = 4$	$N_t = N_r = 8$
QPSK	$(M = 8)$ 1022	$(M = 16)$ 6262
16QAM	$(M = 16)$ 2820	$(M = 64)$ 31228
64QAM	$(M = 64)$ 18064	$(M = 128)$ 92680

From Table 2.2, the complexity significantly increases as the size of MIMO system and the modulation order. Hence, a low complexity MIMO detection scheme for large size MIMO has been attractive in our research.

2.5 Simulation results

The computer simulations were carried out for QPSK, 16QAM and 64QAM in the 4×4 and 8×8 MIMO systems, respectively. Each channel was assumed to be non-frequency selective slow-varying fading channel. In the simulations, the channel gains were generated using the i.i.d. Gaussian random variables with zero mean and variance of $1/2$ for each dimension. Additive noise at each receive antenna was generated using the i.i.d. Gaussian random variables with zero mean and variance of $N_0/2$ for each dimension.

The BER characteristics vs. E_b/N_0 are shown in Figs. 2.6 - 2.11. The near-ML performance can be achieved by the QRM-MLD with M=8, 16, and 64 for QPSK, 16QAM and 64QAM in the 4×4 MIMO system, M=16, 64, and 128 for QPSK, 16QAM and 64QAM in the 8×8 MIMO system, respectively.

The MMSE detection has the better BER performance than the ZF detection. As the modulation order increases, the BER curve of the ZF detection approaches that of the MMSE detection, such as 64QAM. The simulation results show that the BER performance of the MMSE is about 28dB, 30dB and 30dB worse than that of the ML at a BER of 10^{-5} for QPSK, 16QAM and 64QAM in the 4×4 MIMO system as seen in Figs. 2.6, 2.8 and 2.10, respectively, and about 32dB, 36dB and 36dB worse than that of the ML at a BER of 10^{-5} for QPSK, 16QAM and 64QAM in the 8×8 MIMO system in Figs. 2.7, 2.9 and 2.11, respectively.

Unfortunately, the expected performance for the linear detections is not satisfied directly like the ML detector.

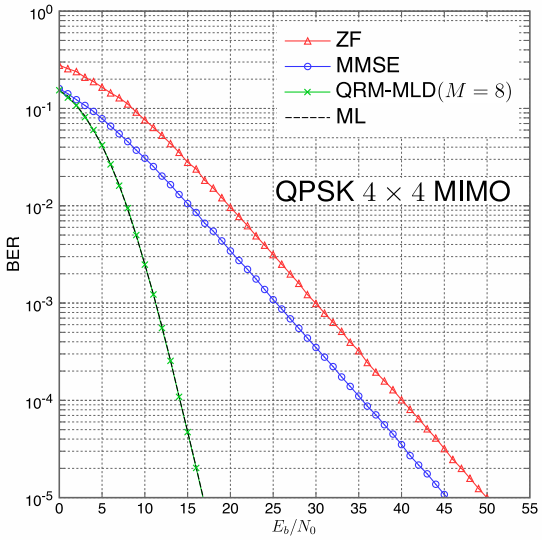

Figure 2.6: The BER vs. E_b/N_0 for the conventional detections over 4×4 MIMO: QPSK

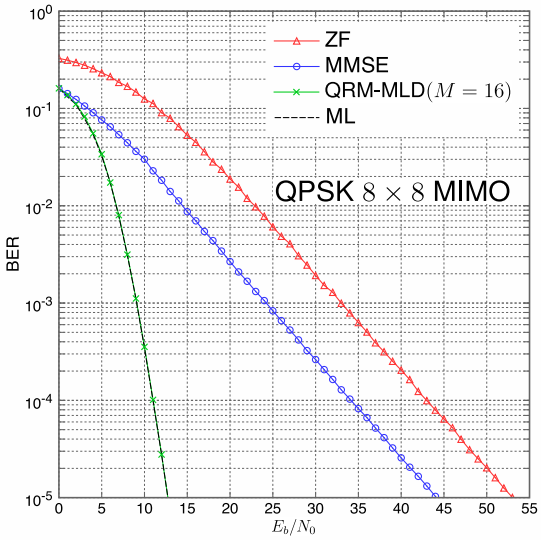

Figure 2.7: The BER vs. E_b/N_0 for the conventional detections over 8×8 MIMO: QPSK

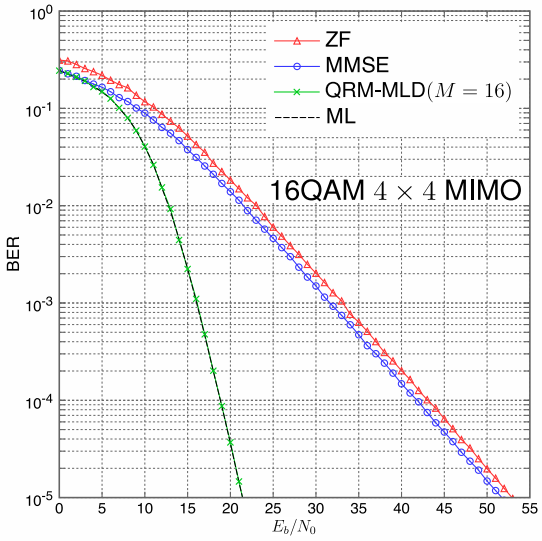

Figure 2.8: The BER vs. E_b/N_0 for the conventional detections over 4×4 MIMO: 16QAM

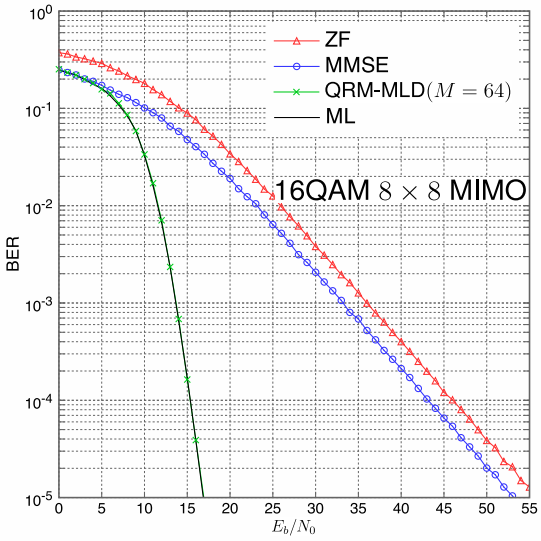

Figure 2.9: The BER vs. E_b/N_0 for the conventional detections over 8×8 MIMO: 16QAM

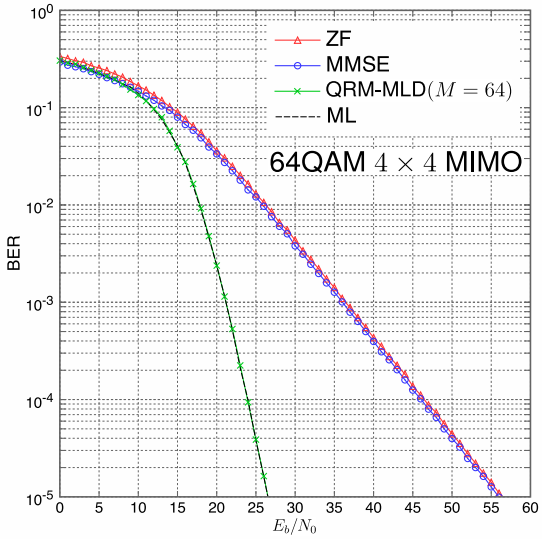

Figure 2.10: The BER vs. E_b/N_0 for the conventional detections over 4×4 MIMO: 64QAM

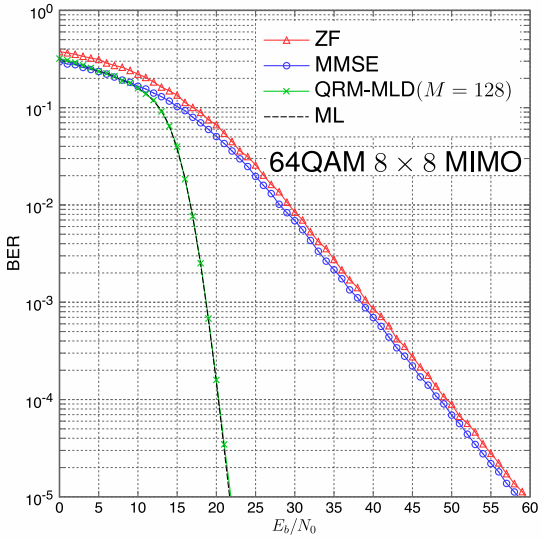

Figure 2.11: The BER vs. E_b/N_0 for the conventional detections over 8×8 MIMO: 64QAM

2.6 Chapter summary

In this chapter, we presented three well-known approaches for MIMO detections. While exhaustive search can be used for optimal performance of the ML detection, the prohibitively high complexity makes it unrealistic to be employed. We described the QRM-MLD with low complexity compared to the ML detection, which can provide the near-ML performance. However, the complexity of QRM-MLD is fixed and determined by the value of survived branches in each detection layer even in the better-conditioned channel. Hence, the QRM-MLD still has the problem of complexity. There are some linear detections with low complexity, such as ZF and MMSE detections. However, these performances are not comparable with that of the ML detection, in particular, in the high E_b/N_0 region. Therefore, it is necessary to find additional techniques for conventional approaches to improve the performance of these conventional methods. In the following chapter, we explain the other detection methods based on lattice reduction.

Chapter 3

Lattice Reduction Aided MIMO Detection Methods

3.1 Introduction

Lattice-reduction aided detection has been introduced into the MIMO detection to achieve the good tradeoff between the performance and the complexity [28]−[44]. The most popular LR algorithm is the well-known LLL algorithm, introduced by Lenstra, Lenstra, and Lovász. Combining the LR algorithm with the linear detections such as ZF or MMSE can achieve good BER performance, especially the LR-MMSE detection which is close to the ML detector in the small size MIMO system [30]. In contrast, the BER improvement in the large size MIMO system is not sufficient. The non-linear detection, i.e. SIC, is selected from many detection methods since it features the good BER performance. However, SIC has the property of error propagation, which degrades the system performance. Ordering SIC (OSIC) based on LR (LR-OSIC) can further improve the BER performance at the cost of the implementation of the ordering but requires high computational complexity [45]. In addition, the list detection can also obtain much better performance but with a little high computational cost in terms of the list of candidates [47]−[49].

3.2 Lattice reduction algorithm

The LR algorithm makes the column vectors of the channel state information matrix to be nearly orthogonal. The following estimation of the transmit signal applies the reduced lattice basis instead of the original lattice basis based on the Gram-Schmidt (GS) orthogonalization (GSO). In this chapter, we first introduce the GSO algorithm.

3.2.1 Gram-Schmidt orthgonalization algorithm

Let $\mathbf{h}_1^c, \mathbf{h}_2^c, \ldots, \mathbf{h}_{N_t}^c$ be the spatial vectors which are not mutually orthogonal. We first reduce the vector $\mathbf{h}_2^c$ to create the new vector $\hat{\mathbf{h}}_2^c$, which is orthogonal to the vector $\mathbf{h}_1^c$.

Let $\mathbf{i}_1^c$ denote the unit vector of $\mathbf{h}_1^c$ as

$$\mathbf{i}_1^c = \frac{\mathbf{h}_1^c}{\|\mathbf{h}_1^c\|} \tag{3.1}$$

Denote the inner product of two vectors $\mathbf{a}$ and $\mathbf{b}$ as $\mathbf{a} \cdot \mathbf{b} \equiv < \mathbf{a}, \mathbf{b} >= \mathbf{a}^{\mathrm{H}}\mathbf{b}$. The length of the $\mathbf{i}_1^c$-component of $\mathbf{h}_2^c$, i.e., the projection of $\mathbf{h}_2^c$ on $\mathbf{i}_1^c$, is given by the inner product of $\mathbf{i}_1^c$ and $\mathbf{h}_2^c$ as

$$\mathbf{i}_1^c \cdot \mathbf{h}_2^c = \frac{< \mathbf{h}_1^c, \mathbf{h}_2^c >}{\|\mathbf{h}_1^c\|} = \frac{\mathbf{h}_1^{c\mathrm{H}}\mathbf{h}_2^c}{\|\mathbf{h}_1^c\|} \tag{3.2}$$

Then, the $\mathbf{i}_1^c$-component of $\mathbf{h}_2^c$ is expressed as

$$\begin{aligned}\left(\mathbf{i}_1^c \cdot \mathbf{h}_2^c\right)\mathbf{i}_1^c = \left(\frac{\mathbf{h}_1^{c\mathrm{H}}\mathbf{h}_2^c}{\|\mathbf{h}_1^c\|}\right)\mathbf{i}_1^c = \left(\frac{\mathbf{h}_1^{c\mathrm{H}}\mathbf{h}_2^c}{\|\mathbf{h}_1^c\|}\right)\frac{\mathbf{h}_1^c}{\|\mathbf{h}_1^c\|} = \left(\frac{\mathbf{h}_1^{c\mathrm{H}}\mathbf{h}_2^c}{\|\mathbf{h}_1^c\|^2}\right)\mathbf{h}_1^c \\ = \mu_{21}\mathbf{h}_1^c\end{aligned} \tag{3.3}$$

with

$$\mu_{21} \triangleq \frac{\mathbf{h}_1^{c\mathrm{H}}\mathbf{h}_2^c}{\|\mathbf{h}_1^c\|^2} \tag{3.4}$$

Subtracting $\mu_{21}\mathbf{h}_1^c$ from $\mathbf{h}_2^c$, we obtain the new vector $\hat{\mathbf{h}}_2^c$, which is orthogonal to $\mathbf{h}_1^c$ as

$$\hat{\mathbf{h}}_2^c = \mathbf{h}_2^c - \mu_{21}\mathbf{h}_1^c \tag{3.5}$$

Note that it is clear that $\left\|\hat{\mathbf{h}}_2^c\right\| \leq \|\mathbf{h}_2^c\|$.

Next, we reduce the vector $\mathbf{h}_3^c$ to create the new vector $\hat{\mathbf{h}}_3^c$, which is orthogonal to the vectors $\mathbf{h}_1^c$ and $\hat{\mathbf{h}}_2^c$. Let $\mathbf{i}_2^c$ denote the unit vector of $\mathbf{h}_2^c$ as

$$\mathbf{i}_2^c = \frac{\mathbf{h}_2^c}{\|\mathbf{h}_2^c\|} \tag{3.6}$$

Since $\mathbf{i}_1^c$ and $\mathbf{i}_2^c$ are mutually orthogonal, their inner product is zero, i.e., $< \mathbf{i}_1^c, \mathbf{i}_2^c >= 0$. The $\mathbf{i}_1^c$-component of $\mathbf{h}_3^c$ and $\mathbf{i}_2^c$-component of $\mathbf{h}_3^c$ are expressed, respectively, as

$$\begin{aligned}\left(\mathbf{i}_1^c \cdot \mathbf{h}_3^c\right)\mathbf{i}_1^c &= \left(\frac{\mathbf{h}_1^{c\mathrm{H}}\mathbf{h}_3^c}{\|\mathbf{h}_1^c\|}\right)\mathbf{i}_1^c = \left(\frac{\mathbf{h}_1^{c\mathrm{H}}\mathbf{h}_3^c}{\|\mathbf{h}_1^c\|}\right)\frac{\mathbf{h}_1^c}{\|\mathbf{h}_1^c\|} = \left(\frac{\mathbf{h}_1^{c\mathrm{H}}\mathbf{h}_3^c}{\|\mathbf{h}_1^c\|^2}\right)\mathbf{h}_1^c \\ &= \mu_{31}\mathbf{h}_1^c\end{aligned} \tag{3.7}$$

$$\begin{aligned}\left(\mathbf{i}_2^c \cdot \mathbf{h}_3^c\right)\mathbf{i}_2^c &= \left(\frac{\mathbf{h}_2^{c\mathrm{H}}\mathbf{h}_3^c}{\|\mathbf{h}_2^c\|}\right)\mathbf{i}_2^c = \left(\frac{\mathbf{h}_2^{c\mathrm{H}}\mathbf{h}_3^c}{\|\mathbf{h}_2^c\|}\right)\frac{\mathbf{h}_2^c}{\|\mathbf{h}_2^c\|} = \left(\frac{\mathbf{h}_2^{c\mathrm{H}}\mathbf{h}_3^c}{\|\mathbf{h}_2^c\|^2}\right)\mathbf{h}_2^c \\ &= \mu_{32}\mathbf{h}_2^c\end{aligned} \tag{3.8}$$

with

$$\mu_{31} \triangleq \frac{\mathbf{h}_1^{c\mathrm{H}}\mathbf{h}_3^c}{\|\mathbf{h}_1^c\|^2} \text{ and } \mu_{32} \triangleq \frac{\mathbf{h}_2^{c\mathrm{H}}\mathbf{h}_3^c}{\|\mathbf{h}_2^c\|^2} \tag{3.9}$$

Subtracting $\mu_{31}\mathbf{h}_1^c$ and $\mu_{32}\mathbf{h}_2^c$ from $\mathbf{h}_3^c$, we obtain the new vector $\hat{\mathbf{h}}_3^c$, which is orthogonal to $\mathbf{h}_1^c$ and to $\hat{\mathbf{h}}_2^c$ as

$$\hat{\mathbf{h}}_3^c = \mathbf{h}_3^c - \left(\mu_{31}\mathbf{h}_1^c + \mu_{32}\hat{\mathbf{h}}_2^c\right) = \mathbf{h}_3^c - \sum_{q=1}^{3-1}\mu_{3,q}\hat{\mathbf{h}}_q^c,\ \hat{\mathbf{h}}_1^c = \mathbf{h}_1^c \tag{3.10}$$

It is clear that $\left\|\hat{\mathbf{h}}_3^c\right\| \leq \|\mathbf{h}_3^c\|$.

In the similar manner, we reduce the vector $\mathbf{h}_p^c : p \in [2, N_t]$, to create the new vector $\hat{\mathbf{h}}_p^c$ which is orthogonal to the vectors $\mathbf{h}_q^c : q \in [1, p-1]$ as

$$\hat{\mathbf{h}}_p^c = \mathbf{h}_p^c - \sum_{q=1}^{p-1}\mu_{p,q}\hat{\mathbf{h}}_q^c, p \in [2, N_t] \tag{3.11}$$

where $\hat{\mathbf{h}}_1^c = \mathbf{h}_1^c, \left\|\hat{\mathbf{h}}_p^c\right\| \leq \left\|\mathbf{h}_p^c\right\|$ and

$$\mu_{p,q} \triangleq \frac{\mathbf{h}_q^{c\mathrm{H}} \mathbf{h}_p^c}{\left\|\mathbf{h}_q^c\right\|^2} \tag{3.12}$$

The new vector $\hat{\mathbf{h}}_p^c$ is created by subtracting the $\hat{\mathbf{h}}_q^c$-components of $\mathbf{h}_q^c, q \in [1, p-1]$, from $\mathbf{h}_p^c, p \in [2, N_t]$. Thus, $\hat{\mathbf{h}}_p^c$ with the larger p is the shorter than $\hat{\mathbf{h}}_p^c$ with the smaller p such that

$$E\left[\left\|\hat{\mathbf{h}}_{N_t}^c\right\|\right] \leq E\left[\left\|\hat{\mathbf{h}}_{N_t-1}^c\right\|\right] \leq \cdots \leq E\left[\left\|\hat{\mathbf{h}}_2^c\right\|\right] \leq E\left[\left\|\hat{\mathbf{h}}_1^c\right\|\right] \tag{3.13}$$

where $E[\cdot]$ denotes the ensemble average operator.

Therefore, if $\left\|\mathbf{h}_1^c\right\| \geq \left\|\mathbf{h}_2^c\right\| \geq \cdots \geq \left\|\mathbf{h}_{N_t}^c\right\|$, it might hold with high probability that all of the new vectors $\hat{\mathbf{h}}_p^c$'s, $p \in [1, N_t]$, are almost of the equal length. It is remarkable that the coefficients of $\mu_{p,q}$ are important scalar factors for the LRA detection. Thus, we summarize the GSO algorithm as seen in Table 3.1. This algorithm is to transform the lattice basis of $\mathbf{H}^c$ into the purely orthogonal lattice basis of $\hat{\mathbf{H}}^c$ and create the transformation matrix $\hat{\mathbf{T}}^c$ with $\det\{\hat{\mathbf{T}}^c\}$=1. The upper triangular matrix $\hat{\mathbf{T}}^c$ with unity diagonal entries and the non-diagonal entries is invertible.

Table 3.1: Complex Gram-Schmidt orthogonalization algorithm

(1)	**Begin** Input $\mathbf{H}^c = [\mathbf{h}_1^c, ..., \mathbf{h}_{N_t}^c]$, $\hat{\mathbf{T}}^c = [\hat{\mathbf{t}}_1^c, ..., \hat{\mathbf{t}}_{N_t}^c]$
	set $\hat{\mathbf{h}}_p^c = \mathbf{h}_p^c$, $\hat{\mathbf{t}}_p^c = \mathbf{t}_p^c : p \in [1, N_t]$
(2)	**for** $p := 2, ..., N_t$
(3)	**for** $q := p-1, ..., 1$
(4)	$\mu_{p,q} = \dfrac{\hat{\mathbf{h}}_q^{c\mathrm{H}} \hat{\mathbf{h}}_p^c}{\|\hat{\mathbf{h}}_q^c\|^2}$
(5)	$\hat{\mathbf{h}}_p^c := \hat{\mathbf{h}}_p^c - \mu_{p,q} \hat{\mathbf{h}}_q^c$
(6)	$\hat{\mathbf{t}}_p^c := \hat{\mathbf{t}}_p^c - \mu_{p,q} \hat{\mathbf{t}}_q^c$
(7)	**end**
(8)	**end**
(9)	$\hat{\mathbf{H}}^c = [\hat{\mathbf{h}}_1^c, ..., \hat{\mathbf{h}}_{N_t}^c]$, $\hat{\mathbf{T}}^c = [\hat{\mathbf{t}}_1^c, ..., \hat{\mathbf{t}}_{N_t}^c]$
(10)	**End**

3.2.2 LLL algorithm

The set of column vectors $\mathbf{H}^c = [\mathbf{h}_1^c, \mathbf{h}_2^c, \ldots, \mathbf{h}_{N_t}^c]$ is called a basis of the lattice $\mathcal{L}$. A lattice has infinitely many bases but some are more useful than others. The goal of the LR algorithm is to find an optimal basis among many possible lattice bases such as the basis consisting of the reasonably short and nearly orthogonal vectors. Thus, it is called lattice reduction. The popular algorithm for LR is the LLL algorithm in Table 3.2. The main concept of the LR algorithm is similar to the GSO algorithm. First, we shall reduce the column $\mathbf{h}_p^c, p \in [1, N_t]$, to be mutually orthogonal using the GSO. After that, we extend the GS be the lattice reduction.

Table 3.2: Complex LLL algorithm

(1)	**Begin** Input $\mathbf{H}^c = [\mathbf{h}_1^c, ..., \mathbf{h}_{N_t}^c]$, $\mathbf{T}^c = [\mathbf{t}_1^c, ..., \mathbf{t}_{N_t}^c]$, set $\delta = 3/4$
(2)	**for** $p := 2, ..., N_t$
(3)	**for** $q := p-1, ..., 1$
(4)	$\mu_{p,q} = \dfrac{\hat{\mathbf{h}}_q^{c\mathrm{H}} \mathbf{h}_p^c}{\|\mathbf{h}_q^c\|^2}$
(5)	$\mathbf{h}_p^c := \mathbf{h}_p^c - \lceil \mu_{p,q} \rfloor \mathbf{h}_q^c$
(6)	$\mathbf{t}_p^c := \mathbf{t}_p^c - \lceil \mu_{p,q} \rfloor \mathbf{t}_q^c$
(7)	**end**
(8)	**let** $\hat{\mathbf{h}}_p^c = \mathbf{h}_p^c$
(9)	**for** $q := p-1, ..., 1$
(10)	$\mu_{p,q} = \dfrac{\hat{\mathbf{h}}_q^{cH} \mathbf{h}_p^c}{\|\|\mathbf{h}_q^c\|\|^2}$
(11)	$\hat{\mathbf{h}}_p^c := \hat{\mathbf{h}}_p^c - \mu_{p,q} \hat{\mathbf{h}}_q^c$
(13)	**end**
(14)	**if** $\delta \|\hat{\mathbf{h}}_{p-1}^c\|^2 > \|\hat{\mathbf{h}}_p^c + \mu_{p,p-1} \hat{\mathbf{h}}_{p-1}^c\|^2$
(15)	swap the $(p-1)$-th and p-th columns in $\mathbf{H}^c$ and $\mathbf{T}^c$
(16)	$p := \max\{p-1, 2\}$
(17)	**else** $p := p + 1$
(18)	**end**
(19)	**end**
(20)	$\mathbf{H}^{c\prime} = [\mathbf{h}_1^c, ..., \mathbf{h}_{N_t}^c], \mathbf{T}^c = [\mathbf{t}_1^c, ..., \mathbf{t}_{N_t}^c]$
(21)	**End**

Note that $\lceil \cdot \rfloor$ denotes the rounding operation.

A complex lattice is discrete subgroup in $\mathbb{C}^{N_r}$ which consists of all integer linear combinations of the set of the linearly independent basis column vectors $\mathbf{h}_i^c$ $(1 \leq i \leq N_t)$ of the basis matrix $\mathbf{H}^c \in \mathbb{C}^{N_r \times N_t}$, $N_t \leq N_r$. Any basis $\mathbf{H}^{c\prime} = \mathbf{H}^c\mathbf{T}^c$ forms the same lattice $\mathcal{L}(\mathbf{H}^{c\prime}) = \mathcal{L}(\mathbf{H}^c)$, when the transmation matrix $\mathbf{T}^c$ is unimodular with integral elements, i.e., $\det\{\mathbf{T}^c\} = \pm 1$. Lattice reduction is based on the concept of transforming a given basis of a lattice into another basis of the same lattice whose characteristics are appropriate for certain defined purposes such as having shorter basis vectors or getting nearer towards orthogonal basis vectors, where two vectors are orthogonal if the inner product equals to zero. There are two conditions to be satisfied as

$$\left|\mathrm{Re}[h_{q,p}^c]\right| \leq \frac{1}{2}\left|\mathrm{Re}[h_{q,q}^c]\right| \text{ and } \left|\mathrm{Im}[h_{q,p}^c]\right| \leq \frac{1}{2}\left|\mathrm{Im}[h_{q,q}^c]\right| \tag{3.14}$$

for all $1 \leq q < p \leq N_t$ and

$$\delta\|\hat{\mathbf{h}}_{p-1}^c\|^2 > \|\hat{\mathbf{h}}_p^c + \mu_{p,p-1}\hat{\mathbf{h}}_{p-1}^c\|^2 \tag{3.15}$$

for all $2 \leq p \leq N_t$.

As seen in Table 3.2, a basis fulfilling (3.14) is said to be size-reduction. The parameter $\delta(\frac{1}{4} < \delta < 1)$ trades off the quality of the lattice reduction for large δ, and a faster termination for small δ. We set $\delta = \frac{3}{4}$ as a common choice.

The LLL algorithm successively performs a size reduction steps (3) - (7), and then possibly performs a column exchange steps (14) - (18) to swap two basis vectors in order to fulfill (3.15). In the case of an exchange, the altered columns are size-reduced again. All the changes operations are tracked by the transformation matrix $\mathbf{T}^c$.

3.3 Lattice reduction aided detection

Since a lattice can be generated by different bases or channel matrices, in order to mitigate the noise and the interferences between the multiple signals, we can find a matrix whose column vectors are nearly orthogonal to generate the same lattice. LR can be applied to MIMO systems to improve the BER performance of

suboptimal MIMO detection, where the resulting detection methods are regarded as the LR-based detection. In this chapter, we present the LR aided detection for MIMO systems.

3.3.1 LR-ZF detection

In the ZF detector, the interference is completely suppressed by multiplying the receive signal vector $\mathbf{y}^c$ with the pseudo-inverse of the channel matrix $\mathbf{H}^{c\dagger} = (\mathbf{H}^{c\mathrm{H}}\mathbf{H}^c)^{-1}\mathbf{H}^{c\mathrm{H}}$. For an orthogonal channel matrix, ZF detection is identical to ML. However, the general ZF detection leads to the noise enhancement. First, recall the system model in (2.1) and the estimation of ZF detection in (2.21), respectively, as

$$\mathbf{y}^c = \mathbf{H}^c\mathbf{s}^c + \mathbf{z}^c$$

and

$$\tilde{\mathbf{s}}^{c(ZF)} = (\mathbf{H}^{c\mathrm{H}}\mathbf{H}^c)^{-1}\mathbf{H}^{c\mathrm{H}}\mathbf{y}^c$$

As above mentioned, linear detection is optimal for an orthogonal channel matrix. The LLL algorithm is to transform a given lattice basis $\mathbf{H}^c$ into a new reduced basis $\mathbf{H}^{c\prime}$, of which column vectors are nearly orthogonal as $\mathbf{H}^{c\prime} = \mathbf{H}^c\mathbf{T}^c$. Due to a finite QAM constellation $\mathbb{S}$ with odd lattice points, it results in the boundary problem. Hence we assume that $\mathbf{s}^c$ is drawn from $\mathcal{A}^{N_t}$, of which $\mathcal{A}$ is a shifted and scaled set of the signals as $\mathcal{A} = \frac{1}{2}\mathbb{S} + \frac{K-1}{2}(1+j)\mathbf{1}_{N_t}$. First, scale $\mathbf{y}^c$ as $\frac{\mathbf{y}^c}{2} = \mathbf{H}^c\frac{\mathbf{s}^c}{2} + \frac{\mathbf{z}^c}{2}$. Then, shift the above as $\mathbf{y}^{c\mathcal{S}} \triangleq \frac{\mathbf{y}^c}{2} + \frac{K-1}{2}(1+j)\mathbf{H}^c\mathbf{1}_{N_t} = \mathbf{H}^c\left(\frac{\mathbf{s}^c}{2} + \frac{K-1}{2}(1+j)\mathbf{1}_{N_t}\right) + \frac{\mathbf{z}^c}{2}$. Using $\mathbf{H}^{c\prime}$ and $\mathbf{T}^c$, the system model in (2.1) can be rewritten as

$$\begin{aligned}
\mathbf{y}^{c\mathcal{S}} &= \mathbf{H}^c\left(\frac{\mathbf{s}^c}{2} + \frac{K-1}{2}(1+j)\mathbf{1}_{N_t}\right) + \frac{\mathbf{z}^c}{2} \\
&= (\mathbf{H}^c\mathbf{T}^c)\left(\mathbf{T}^{c-1}\left(\frac{\mathbf{s}^c}{2} + \frac{K-1}{2}(1+j)\mathbf{1}_{N_t}\right)\right) + \frac{\mathbf{z}^c}{2} \\
&= \mathbf{H}^{c\prime}\left(\mathbf{T}^{c-1}\left(\frac{\mathbf{s}^c}{2} + \frac{K-1}{2}(1+j)\mathbf{1}_{N_t}\right)\right) + \frac{\mathbf{z}^c}{2} \\
&= \mathbf{H}^{c\prime}\mathbf{v}^c + \frac{\mathbf{z}^c}{2}
\end{aligned} \tag{3.16}$$

where $\mathbf{H}^{c\prime} \triangleq \mathbf{H}^c\mathbf{T}^c$, and $\mathbf{1}_{N_t}$ denotes the $N_t \times 1$ vector with all the unity entries. The new signal vector $\mathbf{v}^c$ is defined as $\mathbf{v}^c \triangleq \mathbf{T}^{c-1}\left(\frac{\mathbf{s}^c}{2} + \frac{K-1}{2}(1+j)\mathbf{1}_{N_t}\right)$. The scaled and shifted vector of $\mathbf{s}^c$ is defined as $\mathbf{s}^{c\mathcal{S}} = \mathcal{S}[\mathbf{s}^c] \triangleq \frac{\mathbf{s}^c}{2} + \frac{K-1}{2}(1+j)\mathbf{1}_{N_t}$ with $\mathcal{S}[\mathbf{s}^c]$ denoting the scaling and shifting operator of $\mathbf{s}^c$.

The idea behind LR-ZF detection is to consider the system model in (2.1) as the equivalent system model in (3.16). The soft estimate $\tilde{\mathbf{v}}^c$ using the LR-ZF detection in [30] can be derived by

$$\begin{aligned}\tilde{\mathbf{v}}^{c(LR-ZF)} &= \mathbf{H}^{c\prime\dagger}\mathbf{y}^{c\mathcal{S}} \\ &= \left(\mathbf{H}^{c\prime\mathrm{H}}\mathbf{H}^{c\prime}\right)^{-1}\mathbf{H}^{c\prime\mathrm{H}}\mathbf{y}^{c\mathcal{S}}\end{aligned} \tag{3.17}$$

Since all the elements of $\mathbf{T}^c$ are integers, we perform the simple rounding quantization operations as $\hat{v}_i^c = \mathcal{Q}\{\tilde{v}_i^c\}$, $i \in [1, N_t]$. The new transmit signal vector $\hat{\mathbf{v}}^c$ is transformed back as $\hat{\mathbf{s}}^{c\mathcal{S}} = \mathbf{T}^c\hat{\mathbf{v}}^c$. Then, $\hat{\mathbf{s}}^{c\mathcal{S}}$ is shifted back and scaled back, expressing as $\hat{\mathbf{s}}^c = \mathcal{S}^{-1}[\hat{\mathbf{s}}^{c\mathcal{S}}] = 2\hat{\mathbf{s}}^{c\mathcal{S}} - (K-1)(1+j)\mathbf{1}_{N_t}$. Note that the distance of the adjacent symbols of $\hat{\mathbf{s}}^{c\mathcal{S}}$ and that of $\mathbf{v}^c$ are both 1. The final decision $\hat{\mathbf{s}}^c$ is forced to the nearest constellation points if they are lying outside the original signal constellation as $\hat{\mathbf{s}^c} := \mathcal{C}[\hat{\mathbf{s}}^c]$.

3.3.2 LR-MMSE detection

Similarly to LR-ZF detection, the LR-MMSE detection gets an estimate for noise vector. Recall the estimation of MMSE detection in (2.24):

$$\tilde{\mathbf{s}}^{c(MMSE)} = \left(\mathbf{H}^{c\mathrm{H}}\mathbf{H}^c + \gamma^{-1}\mathbf{I}_{N_t}\right)^{-1}\mathbf{H}^{c\mathrm{H}}\mathbf{y}^c$$

Thus, based on the system model in (3.16), the soft estimate $\tilde{\mathbf{v}}^c$ using the LR-MMSE detection in [30] can be derived by

$$\begin{aligned}\tilde{\mathbf{v}}^{c(LR-MMSE)} &= \mathbf{T}^{c-1}\tilde{\mathbf{s}}^{c(MMSE)} \\ &= \left(\mathbf{H}^{c\prime\mathrm{H}}\mathbf{H}^{c\prime} + \gamma^{-1}\mathbf{T}^{c\mathrm{H}}\mathbf{T}^c\right)^{-1}\mathbf{H}^{c\prime\mathrm{H}}\mathbf{y}^{c\mathcal{S}}\end{aligned} \tag{3.18}$$

In [34], Hassibi proposed an MMSE detector with the extended matrix form

as

$$\bar{\mathbf{y}}^c \triangleq \begin{bmatrix} \mathbf{y}^c \\ \mathbf{0}_{N_t} \end{bmatrix},\ \bar{\mathbf{H}}^c \triangleq \begin{bmatrix} \mathbf{H}^c \\ \sqrt{\gamma^{-1}}\mathbf{I}_{N_t} \end{bmatrix},\ \bar{\mathbf{z}}^c \triangleq \begin{bmatrix} \mathbf{z}^c \\ -\sqrt{\gamma^{-1}}\mathbf{s}^c \end{bmatrix} \tag{3.19}$$

where $\gamma = E_s/N_0$ with $E_s = E[\|\mathbf{s}^c\|^2]/N_t$. Then it holds instead of (2.1) that

$$\bar{\mathbf{y}}^c = \bar{\mathbf{H}}^c\mathbf{s}^c + \bar{\mathbf{z}}^c \tag{3.20}$$

The LLL algorithm in Table 3.2 is to transform a given lattice basis $\bar{\mathbf{H}}^c$ into a new reduced basis $\bar{\mathbf{H}}^{c\prime}$, of which column vectors are nearly orthogonal. The scaled and shifted receive signal $\bar{\mathbf{y}}^{c\mathcal{S}}$ is given as

$$\begin{aligned} \bar{\mathbf{y}}^{c\mathcal{S}} &\triangleq \frac{\bar{\mathbf{y}}^c}{2} + \frac{K-1}{2}(1+j)\bar{\mathbf{H}}^c\mathbf{1}_{N_t} \\ &= \bar{\mathbf{H}}^c\left(\frac{\mathbf{s}^c}{2} + \frac{K-1}{2}(1+j)\mathbf{1}_{N_t}\right) + \frac{\bar{\mathbf{z}}^c}{2} \end{aligned} \tag{3.21}$$

Using $\bar{\mathbf{H}}^{c\prime}$ and $\mathbf{T}^c$, the system model in (3.21) is rewritten as

$$\begin{aligned} \bar{\mathbf{y}}^{c\mathcal{S}} &= \bar{\mathbf{H}}^c\left(\frac{\mathbf{s}^c}{2} + \frac{K-1}{2}(1+j)\mathbf{1}_{N_t}\right) + \frac{\bar{\mathbf{z}}^c}{2} \\ &= \left(\bar{\mathbf{H}}\mathbf{T}^c\right)\left(\mathbf{T}^{c-1}\left(\frac{\mathbf{s}^c}{2} + \frac{K-1}{2}(1+j)\mathbf{1}_{N_t}\right)\right) + \frac{\bar{\mathbf{z}}^c}{2} \\ &\equiv \bar{\mathbf{H}}^{c\prime}\mathbf{v}^c + \frac{\bar{\mathbf{z}}^c}{2} \end{aligned} \tag{3.22}$$

where $\bar{\mathbf{H}}^{c\prime} = \bar{\mathbf{H}}\mathbf{T}^c$, and the new signal vector in the LR domain $\mathbf{v}^c$ is defined as $\mathbf{v}^c \triangleq \mathbf{T}^{c-1}\left(\frac{\mathbf{s}^c}{2} + \frac{K-1}{2}(1+j)\mathbf{1}_{N_t}\right)$. The scaled and shifted vector of $\mathbf{s}^c$ is defined as

$$\mathbf{s}^{c\mathcal{S}} = \mathcal{S}[\mathbf{s}^c] \triangleq \frac{\mathbf{s}^c}{2} + \frac{K-1}{2}(1+j)\mathbf{1}_{N_t} \tag{3.23}$$

The soft estimate $\tilde{\mathbf{v}}^c$ using the LR-MMSE detection instead of (3.18) can be derived by

$$\begin{aligned} \tilde{\mathbf{v}}^{c(LR-MMSE)} &= \bar{\mathbf{H}}^{c\prime\dagger}\bar{\mathbf{y}}^{c\mathcal{S}} \\ &\equiv \left(\bar{\mathbf{H}}^{c\prime\mathrm{H}}\bar{\mathbf{H}}^{c\prime}\right)^{-1}\bar{\mathbf{H}}^{c\prime\mathrm{H}}\bar{\mathbf{y}}^{c\mathcal{S}} \\ &= \left(\mathbf{H}^{c\prime\mathrm{H}}\mathbf{H}^{c\prime} + \gamma^{-1}\mathbf{T}^{c\mathrm{H}}\mathbf{T}^c\right)^{-1}\mathbf{H}^{c\prime\mathrm{H}}\mathbf{y}^{c\mathcal{S}} \end{aligned} \tag{3.24}$$

where $\mathbf{y}^{c\mathcal{S}}$ denotes the shifting and scaling of the original receive signal. The detailed derivation is described in Appendix B.

After that, the following estimation of the LR-MMSE detection is derived as

$$\begin{aligned} \hat{v}_i^c &= \mathcal{Q}\left\{\tilde{v}_i^{c(LR-MMSE)}\right\},\ i \in [1, N_t] \\ \hat{\mathbf{s}}^{c\mathcal{S}} &= \mathbf{T}^c \hat{\mathbf{v}}^c \\ \hat{\mathbf{s}}^c &= \mathcal{S}^{-1}[\hat{\mathbf{s}}^{c\mathcal{S}}] = 2\hat{\mathbf{s}}^{c\mathcal{S}} - (K-1)(1+j)\mathbf{1}_{N_t} \end{aligned} \tag{3.25}$$

In the same method, the final decision $\hat{\mathbf{s}}^c$ is forced to the nearest constellation points if they are lying outside the original signal constellation as $\hat{\mathbf{s}}^c := \mathcal{C}[\hat{\mathbf{s}}^c]$.

3.3.3 Performance and simulation results

The computer simulations were carried out for QPSK, 16QAM and 64QAM in the 4×4 and the 8×8 MIMO systems, respectively. We compare the LR-ZF detection and the LR-MMSE detection with the conventional detection methods, such as the ZF detection and the MMSE detection and the ML detection described in Chapter 2.

The BER characteristics vs. E_b/N_0 are shown in Figs. 3.1 - 3.6. The LR aided MIMO detection has large improvement of the BER performance compared to the ZF or MMSE detection. The LR-MMSE detection is also better BER performance than that of the LR-ZF detection. For the 4×4 MIMO system, the LR-MMSE detection is about 27dB, 28dB and 28dB improvement of BER performance at a BER of 10^{-5} over the MMSE detection for QPSK, 16QAM and 64QAM, respectively. And the curve of the LR-MMSE detection approaches that of the ML detection. On the contrary, for the 8×8 MIMO system, the LR-MMSE detection is about 24dB, 28dB and 28dB improvement of BER performance at a BER of 10^{-5} over the MMSE detection for QPSK, 16QAM and 64QAM, respectively. And the curve of the LR-MMSE detection is still far to that of the ML detection.

Therefore, the LR aided detection achieves the suboptimal BER performance for the 4×4 MIMO system. However, the LR aided detection in the 8×8 MIMO system cannot achieve so good BER as that in the 4×4 MIMO does, compared to the BER of the ML detection.

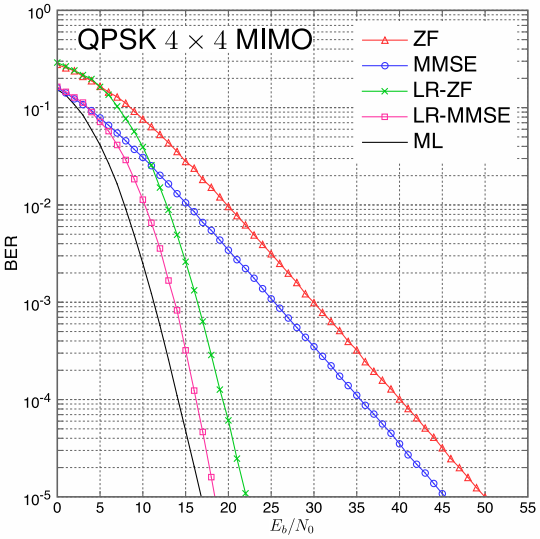

Figure 3.1: The BER vs. E_b/N_0 for the LRA detection over 4×4 MIMO: QPSK

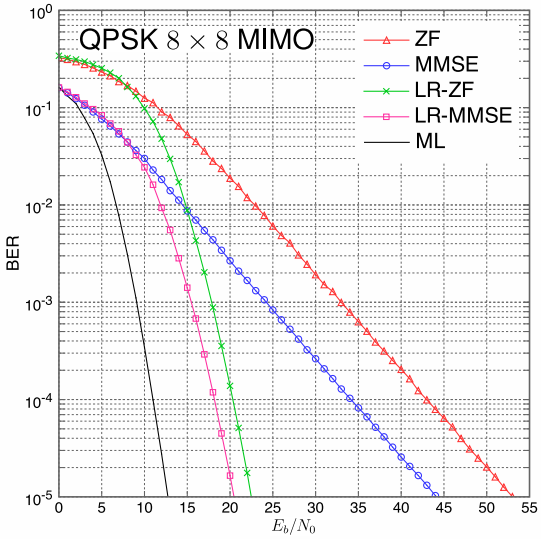

Figure 3.2: The BER vs. E_b/N_0 for the LRA detection over 8×8 MIMO: QPSK

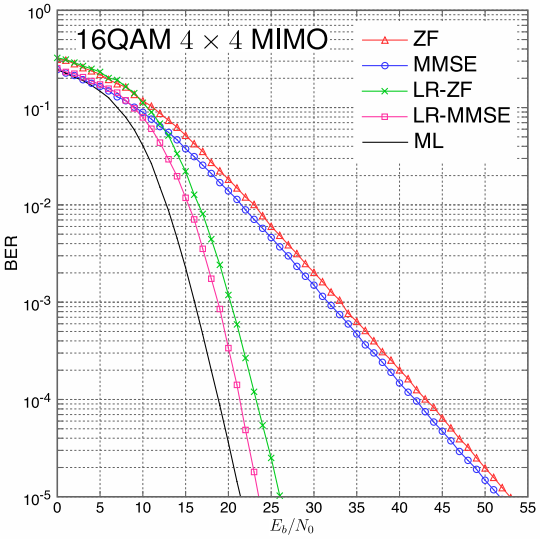

Figure 3.3: The BER vs. E_b/N_0 for the LRA detection over 4×4 MIMO: 16QAM

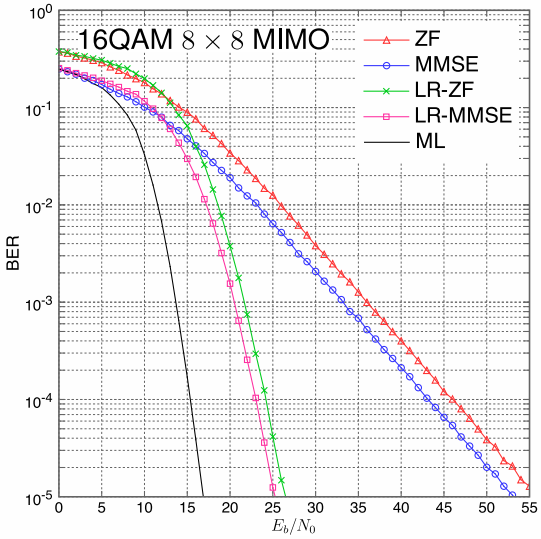

Figure 3.4: The BER vs. E_b/N_0 for the LRA detection over 8×8 MIMO: 16QAM

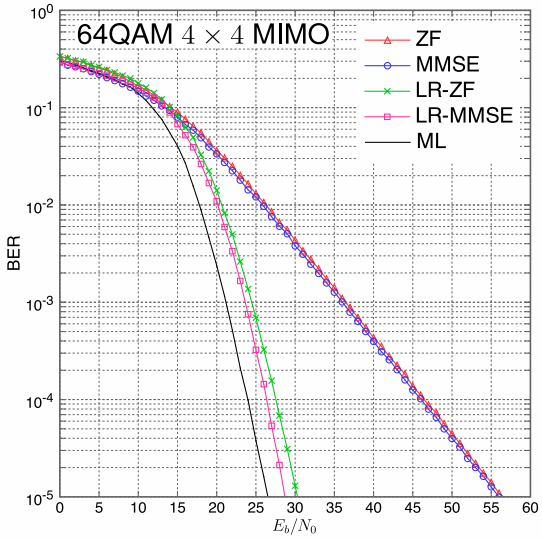

Figure 3.5: The BER vs. E_b/N_0 for the LRA detection over 4×4 MIMO: 64QAM

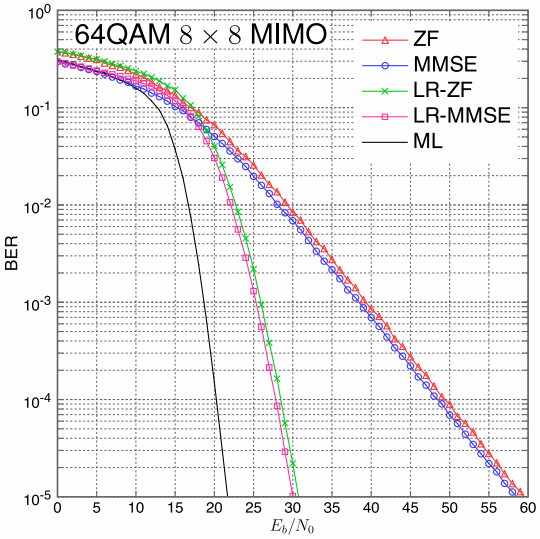

Figure 3.6: The BER vs. E_b/N_0 for the LRA detection over 8×8 MIMO: 64QAM

3.4 Gram-Schmidt based lattice reduction aided detection

After the LLL algorithm, the column vectors of the LLL-reduced channel matrix are nearly orthogonal, but not purely orthogonal. Then, we input the LLL-reduced channel matrix into the GSO algorithm in Table 3.1, and hence the decision boundary becomes purely orthogonal in order to achieve the better BER performance.

3.4.1 LR-GS detection

The LR-GS detection is based on the LR-MMSE detection [39]−[41]. The GSO algorithm is to transform the nearly orthogonal lattice basis of $\bar{\mathbf{H}}^{c\prime}$ into the purely orthogonal lattice basis of $\hat{\bar{\mathbf{H}}}^{c}$ and create the transformation matrix $\hat{\mathbf{T}}^{c}$ with $\det\{\hat{\mathbf{T}}^{c}\}$=1. The upper triangular matrix $\hat{\mathbf{T}}^{c}$ with unity diagonal entries and the non-diagonal entries is invertible. The column vectors of the channel matrix $\hat{\bar{\mathbf{H}}}^{c} = \bar{\mathbf{H}}^{c\prime}\hat{\mathbf{T}}^{c}$ are mutually orthogonal and span the same subspace as that of

the original channel matrix $\bar{\mathbf{H}}^c$. Using $\hat{\bar{\mathbf{H}}}^c$ called the GS-orthogonalized channel matrix and $\hat{\mathbf{T}}^c$, Eq. (3.22) can be expressed as

$$\begin{aligned}\bar{\mathbf{y}}^{c\mathcal{S}} &= \bar{\mathbf{H}}^{c\prime}\mathbf{v}^c + \frac{\bar{\mathbf{z}}^c}{2} \\ &= \left(\bar{\mathbf{H}}^{c\prime}\hat{\mathbf{T}}^c\right)\left(\hat{\mathbf{T}}^{c-1}\mathbf{v}^c\right) + \frac{\bar{\mathbf{z}}^c}{2} \\ &\equiv \hat{\bar{\mathbf{H}}}^c\mathbf{u}^c + \frac{\bar{\mathbf{z}}^c}{2}\end{aligned} \tag{3.26}$$

where $\hat{\bar{\mathbf{H}}}^c \triangleq \bar{\mathbf{H}}^{c\prime}\hat{\mathbf{T}}^c$ and $\mathbf{u}^c \triangleq \hat{\mathbf{T}}^{c-1}\mathbf{v}^c \equiv (\hat{\mathbf{T}}^{c-1}\mathbf{T}^{c-1})\mathbf{s}^{c\mathcal{S}} = (\mathbf{T}^c\hat{\mathbf{T}}^c)^{-1}\mathbf{s}^{c\mathcal{S}}$ with expressing $\hat{\mathbf{T}}^{c-1}$ as

$$\hat{\mathbf{T}}^{c-1} = \begin{bmatrix} 1 & \tau_{12} & \dots & \tau_{1,N_t-1} & \tau_{1,N_t} \\ & 1 & \dots & \tau_{2,N_t-1} & \tau_{2,N_t} \\ & & \ddots & \vdots & \vdots \\ & & & 1 & \tau_{N_t-1,N_t} \\ \mathbf{0} & & & & 1 \end{bmatrix} \tag{3.27}$$

where the transformation matrix $\hat{\mathbf{T}}^c$ is upper triangular matrix with unity of diagonal elements and non-integers of other elements. Note that the property of the noise vector still obeys Gaussian distribution if the channel matrix is performed by using LR and GSO operations. These operations are just to look for a better lattice basis in the following signal estimation.

We first assume that the receiver has perfect knowledge of the transmit signal $\mathbf{s}^c$. Here we call $\mathbf{s}^c$ as the pilot signal. The scaled and shifted transmit signal is obtained as $\mathbf{s}^{c\mathcal{S}} = \mathcal{S}[\mathbf{s}^c] \triangleq \frac{\mathbf{s}^c}{2} + \frac{K-1}{2}(1+j)\mathbf{1}_{N_t}$. From (3.26), the signal $\mathbf{s}^c$ is transformed to the u-domain as

$$\begin{aligned}\mathbf{u}^c &= \left[u_1^c, \dots, u_p^c, \dots, u_{N_t}^c\right]^{\mathrm{T}} \\ &= (\mathbf{T}^c\hat{\mathbf{T}}^c)^{-1}\mathbf{s}^{c\mathcal{S}}\end{aligned} \tag{3.28}$$

Since the entries of $\mathbf{u}^c$ are not integers, we cannot use the rounding operations as the conventional LR-MMSE. Then we first measure the distance between $\mathbf{u}^c$

and the original $\mathbf{0}$ as

$$\begin{aligned}\Delta\mathbf{u}^c &= \left[\Delta u_1^c, \ldots, \Delta u_p^c, \ldots, \Delta u_{N_t}^c\right]^{\mathrm{T}} \\ &= \mathbf{0} - \mathbf{u}^c \\ &= \left[-u_1^c, \ldots, -u_p^c, \ldots, -u_{N_t}^c\right]^{\mathrm{T}} \\ &= -(\mathbf{T}^c\hat{\mathbf{T}}^c)^{-1}\mathbf{s}^{c\mathcal{S}}\end{aligned} \tag{3.29}$$

The p-th entry Δu_p^c of $\Delta\mathbf{u}^c$ is expressed as

$$\Delta u_p^c = -u_p^c \tag{3.30}$$

The soft estimate of $\mathbf{u}^c$ is derived using (3.26) as

$$\begin{aligned}\tilde{\mathbf{u}}^c &= \left(\hat{\bar{\mathbf{H}}}^{c\mathrm{H}}\hat{\bar{\mathbf{H}}}^c\right)^{-1}\hat{\bar{\mathbf{H}}}^{c\mathrm{H}}\bar{\mathbf{y}}^{c\mathcal{S}} \\ &= \mathbf{u}^c + \left(\hat{\bar{\mathbf{H}}}^{c\mathrm{H}}\hat{\bar{\mathbf{H}}}^c\right)^{-1}\hat{\bar{\mathbf{H}}}^{c\mathrm{H}}\frac{\bar{\mathbf{z}}^c}{2}\end{aligned} \tag{3.31}$$

where

$$\begin{aligned}\hat{\bar{\mathbf{H}}}^{c\mathrm{H}}\hat{\bar{\mathbf{H}}}^c &= \begin{bmatrix} \hat{\bar{\mathbf{h}}}_1^{c\mathrm{H}} \\ \vdots \\ \hat{\bar{\mathbf{h}}}_p^{c\mathrm{H}} \\ \vdots \\ \hat{\bar{\mathbf{h}}}_{N_t}^{c\mathrm{H}} \end{bmatrix} \begin{bmatrix} \hat{\bar{\mathbf{h}}}_1^c & \ldots & \hat{\bar{\mathbf{h}}}_p^c & \ldots & \hat{\bar{\mathbf{h}}}_{N_t}^c \end{bmatrix} \\ &= \begin{bmatrix} \left\|\hat{\bar{\mathbf{h}}}_1^c\right\|^2 & \ldots & \hat{\bar{\mathbf{h}}}_1^{c\mathrm{H}}\hat{\bar{\mathbf{h}}}_p^c & \ldots & \hat{\bar{\mathbf{h}}}_1^{c\mathrm{H}}\hat{\bar{\mathbf{h}}}_{N_t}^c \\ \vdots & \ddots & \vdots & \ddots & \vdots \\ \hat{\bar{\mathbf{h}}}_p^{c\mathrm{H}}\hat{\bar{\mathbf{h}}}_1^c & \ldots & \left\|\hat{\bar{\mathbf{h}}}_p^c\right\|^2 & \ldots & \hat{\bar{\mathbf{h}}}_p^{c\mathrm{H}}\hat{\bar{\mathbf{h}}}_{N_t}^c \\ \vdots & \ddots & \vdots & \ddots & \vdots \\ \hat{\bar{\mathbf{h}}}_{N_t}^{c\mathrm{H}}\hat{\bar{\mathbf{h}}}_1^c & \ldots & \hat{\bar{\mathbf{h}}}_{N_t}^{c\mathrm{H}}\hat{\bar{\mathbf{h}}}_p^c & \ldots & \left\|\hat{\bar{\mathbf{h}}}_{N_t}^c\right\|^2 \end{bmatrix}\end{aligned} \tag{3.32}$$

Since $\hat{\tilde{\mathbf{h}}}_p^{c\mathrm{H}}\hat{\tilde{\mathbf{h}}}_{p'}^{c} = 0$ for $p \neq p'$, we have

$$\left(\hat{\tilde{\mathbf{H}}}^{c\mathrm{H}}\hat{\tilde{\mathbf{H}}}^{c}\right)^{-1} = \begin{bmatrix} \frac{1}{\left\|\hat{\tilde{\mathbf{h}}}_1^c\right\|^2} & & & \mathbf{0} \\ & \ddots & & \\ & & \frac{1}{\left\|\hat{\tilde{\mathbf{h}}}_p^c\right\|^2} & \\ & & & \ddots \\ \mathbf{0} & & & \frac{1}{\left\|\hat{\tilde{\mathbf{h}}}_{N_t}^c\right\|^2} \end{bmatrix} \tag{3.33}$$

Therefore, the p-th entry of $\tilde{\mathbf{u}}^c$ in (3.31) is expressed as

$$\tilde{u}_p^c = u_p^c + \frac{\hat{\tilde{\mathbf{h}}}_p^{c\mathrm{H}}\mathbf{z}^c}{2\left\|\hat{\tilde{\mathbf{h}}}_p^c\right\|^2}, p \in [1, N_t] \tag{3.34}$$

Note that the LR-GS has less noise enhancement.

We have obtained the correct point of u_p^c: $p \in [1, N_t]$, in (3.28) and its soft estimate $\tilde{u}_p^c$ in (3.31) for LR-MMSE. Next, shift u_p^c and $\tilde{u}_p^c$ by Δu_p^c such that u_p^c should be shifted to the origin (or some integer point). Then, the shifted u_p^c and $\tilde{u}_p^c$ are expressed, respectively, as

$$u_p^{c\prime} \triangleq u_p^c + \Delta u_p^c = u_p^c - u_p^c = 0 \tag{3.35}$$

$$\tilde{u}_p^{c\prime} \triangleq \tilde{u}_p^c + \Delta u_p^c = \tilde{u}_p^c - u_p^c = 0 \tag{3.36}$$

where $\Delta u_p^c = -u_p^c$.

Figure 3.7 (a) illustrates the shifting u_p^c and $\tilde{u}_p^c$ by Δu_p^c. Since $\tilde{u}_p^{c\prime}$ is integer (zero), $\tilde{u}_p^{c\prime}(\tilde{u}_p^{c\prime} \triangleq \tilde{u}_p^c + \Delta u_p^c)$ can be quantized such that
$\hat{u}_p^{c\prime} = \mathcal{Q}\left[\tilde{u}_p^{c\prime}\right] = \mathcal{Q}\left[\tilde{u}_p^c + \Delta u_p^c\right] = \mathcal{Q}\left[\tilde{u}_p^c - u_p^c\right]$.

After that, $\hat{u}_p^{c\prime}$ is shifted back by $-\Delta u_p^c$ to obtain the quantized $\hat{u}_p^c$ as

$$\begin{aligned} \hat{u}_p^c &= \hat{u}_p^{c\prime} - \Delta u_p^c = \mathcal{Q}\left[\tilde{u}_p^{c\prime}\right] - \Delta u_p^c \\ &= \mathcal{Q}\left[\tilde{u}_p^c + \Delta u_p^c\right] - \Delta u_p^c = \mathcal{Q}\left[\tilde{u}_p^c - u_p^c\right] + u_p^c \end{aligned} \tag{3.37}$$

As seen in Fig. 3.7 (b), this is the quantization of $\tilde{u}_p^{c\prime}(\triangleq \tilde{u}_p^c + \Delta u_p^c)$ to create $\hat{u}_p^{c\prime}(= \mathcal{Q}\left[\tilde{u}_p^c + \Delta u_p^c\right])$, and shifting back of $\tilde{u}_p^{c\prime}$ by $-\Delta u_p^c(= u_p^c)$ to create $\hat{u}_p^c =$

$\hat{u}_p^{c\prime} - \Delta u_p^c = \mathcal{Q}\left[\tilde{u}_p^c + \Delta u_p^c\right] - \Delta u_p^c = \mathcal{Q}\left[\tilde{u}_p^c - u_p^c\right] + u_p^c$, which is the quantized signal of $\tilde{u}_p$. Figure 3.7 (c) shows an example that $\hat{u}_p^{c\prime}$ is the erroneously quantized to be -1 and not the origin. To avoid the errors quantization, the quantization method described in Chapter 5 is very important and useful.

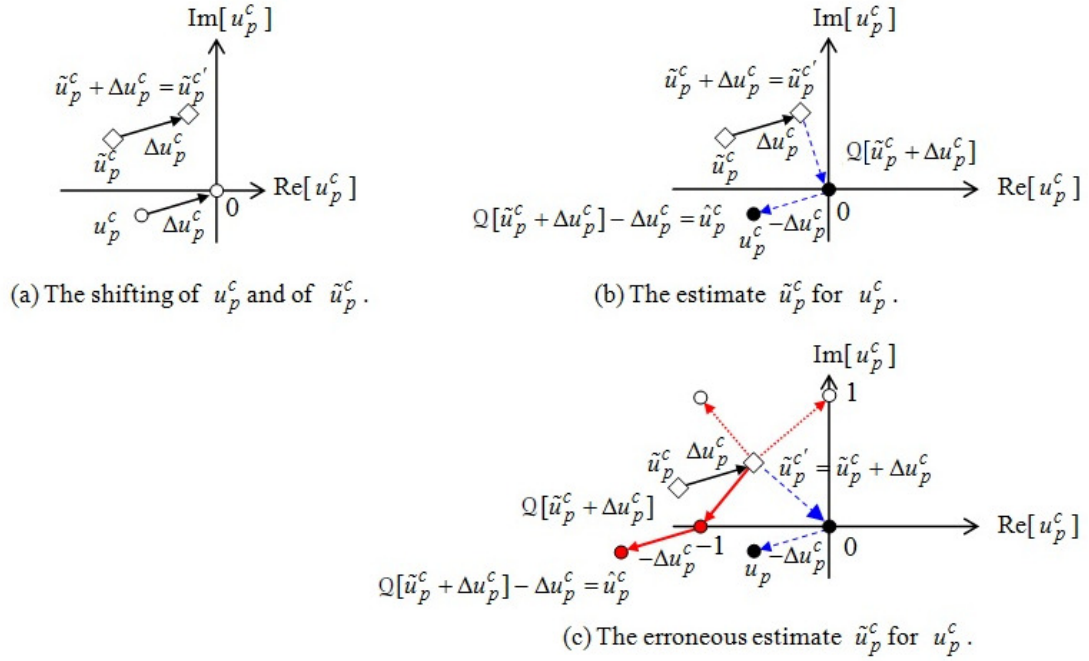

Figure 3.7: Quantization flow of the soft estimate $\tilde{\mathbf{u}}^c$.

The following estimation of the LR-GS detection is derived as

$$\begin{aligned}
&\hat{v}_i^c = \mathcal{Q}\left\{\tilde{v}_i^{c(LR-MMSE)}\right\},\ i \in [1, N_t] \\
&\hat{\mathbf{u}}^c = \mathcal{Q}\left\{\tilde{\mathbf{u}}^c - \hat{\mathbf{T}}^{c-1}\hat{\mathbf{v}}^c\right\} + \hat{\mathbf{T}}^{c-1}\hat{\mathbf{v}}^c \\
&\hat{\mathbf{s}}^{c\mathcal{S}} = \mathcal{Q}\left\{\mathbf{T}^c\hat{\mathbf{T}}^c\hat{\mathbf{u}}^c\right\} \\
&\hat{\mathbf{s}}^c = \mathcal{S}^{-1}[\hat{\mathbf{s}}^{c\mathcal{S}}] = 2\hat{\mathbf{s}}^{c\mathcal{S}} - (K-1)(1+j)\mathbf{1}_{N_t}
\end{aligned} \tag{3.38}$$

In the same method, the final decision $\hat{\mathbf{s}}^c$ is forced to the nearest constellation points if they are lying outside the original signal constellation as $\hat{\mathbf{s}}^c := \mathcal{C}[\hat{\mathbf{s}}^c]$.

3.4.2 Performance and simulation results

The computer simulations were carried out for QPSK, 16QAM and 64QAM in the 4×4 and the 8×8 MIMO systems, respectively. We compare the LR-GS detection with the LR-ZF detection, the LR-MMSE detection and the conventional detection methods, such as the ZF detection and the MMSE detection and the ML detection described in Chapter 2.

The BER characteristics vs. E_b/N_0 are shown in Figs. 3.8 - 3.13. The LR-GS detection has large improvement of the BER performance compared to the LR-MMSE detection due to the less noise enhancement. For the 4×4 MIMO system, the LR-GS detection is about 1dB, 0.8dB and 0.7dB improvement of BER performance at a BER of 10^{-5} over the LR-MMSE detection for QPSK, 16QAM and 64QAM, respectively. And the curves of the LR-GS detection approach that of the ML detection at a BER of 10^{-5}, in particular for QPSK. On the contrary, for the 8×8 MIMO system, the LR-GS detection is about 2dB, 1.8dB and 1.7dB improvement of BER performance at a BER of 10^{-5} over the MMSE detection for QPSK, 16QAM and 64QAM, respectively. And the curves of the LR-GS detection are still far to that of the ML detection.

Therefore, compared to the LR aided detection, the LR-GS detection achieves the better BER performance and approaches the BER of the ML detection in the 4×4 MIMO system. However, the LR-GS detection in the 8×8 MIMO system cannot achieve so good BER as that in the 4×4 MIMO does, compared to the BER of the ML detection. The LR-GS detection is more suitable in the small size MIMO system and low modulation order.

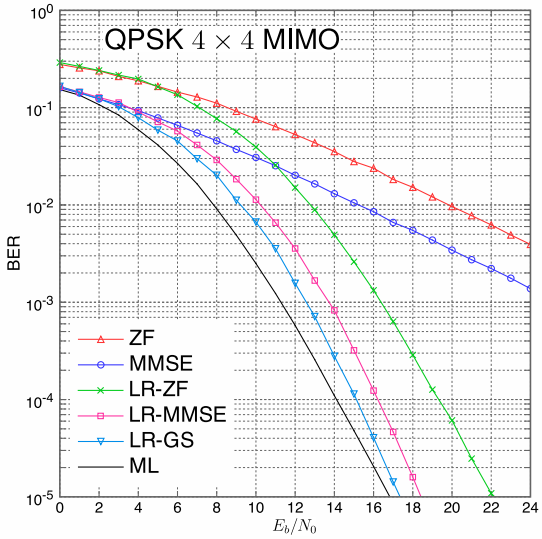

Figure 3.8: The BER vs. E_b/N_0 for the LR-GS over 4×4 MIMO: QPSK

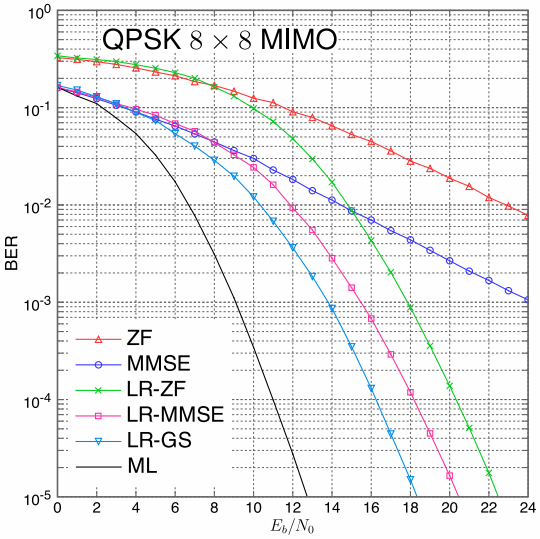

Figure 3.9: The BER vs. E_b/N_0 for the LR-GS over 8×8 MIMO: QPSK

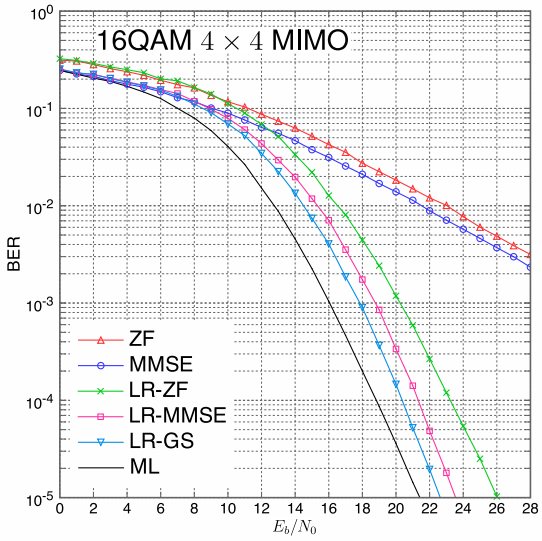

Figure 3.10: The BER vs. E_b/N_0 for the LR-GS over 4×4 MIMO: 16QAM

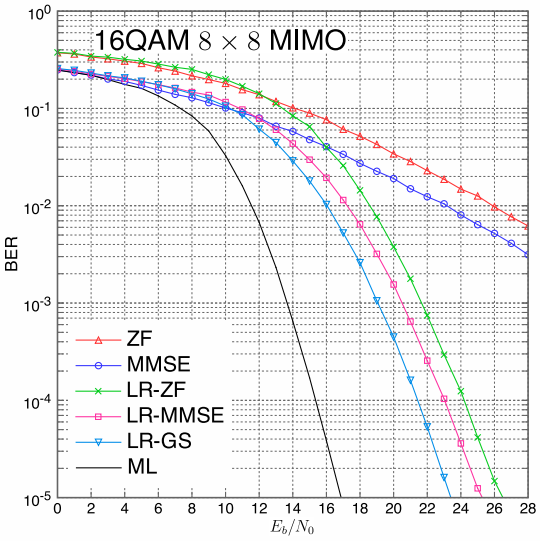

Figure 3.11: The BER vs. E_b/N_0 for the LR-GS over 8×8 MIMO: 16QAM

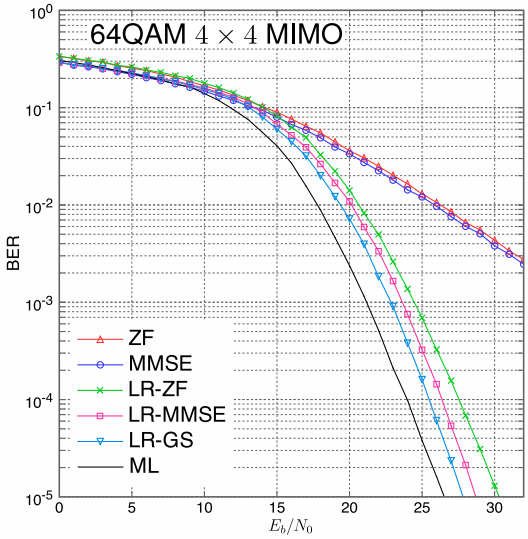

Figure 3.12: The BER vs. E_b/N_0 for the LR-GS over 4×4 MIMO: 64QAM

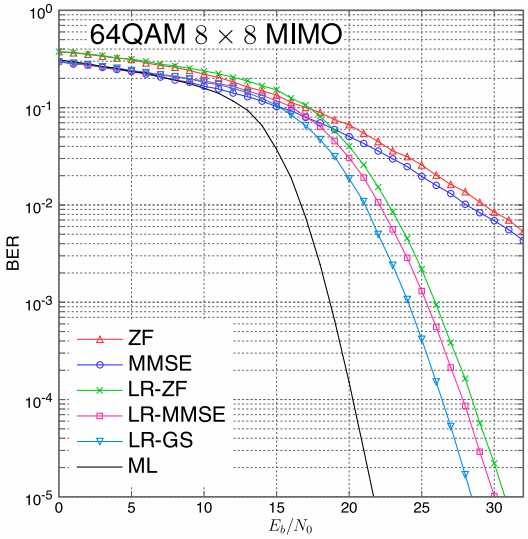

Figure 3.13: The BER vs. E_b/N_0 for the LR-GS over 8×8 MIMO: 64QAM

3.5 Lattice reduction based SIC detection

3.5.1 LR-SIC detection

The SIC detection estimates the symbols layer by layer. The channel matrix is usually QR-decomposed [56]. Therefore, the QR decomposition plays a key role in the SIC detection. Based on the QR decomposition of the channel matrix $\bar{\mathbf{H}}^c$, the channel matrix $\bar{\mathbf{H}}^c$ is QR-decomposed as

$$\begin{aligned}\bar{\mathbf{H}}^c &= \mathbf{Q}^c\mathbf{R}^c \\ &= \begin{bmatrix} q^c_{11} & q^c_{12} & \cdots & q^c_{1,N_t} \\ q^c_{21} & q^c_{22} & \cdots & q^c_{1,N_t} \\ \vdots & \vdots & \ddots & \vdots \\ q^c_{N_t+N_r,1} & q^c_{N_t+N_r,2} & \cdots & r^c_{N_t+N_r,N_t} \end{bmatrix} \begin{bmatrix} r^c_{11} & r^c_{12} & \cdots & r^c_{1,N_t} \\ 0 & r^c_{22} & \cdots & r^c_{1,N_t} \\ \vdots & \vdots & \ddots & \vdots \\ 0 & 0 & \cdots & r^c_{N_r,N_t} \end{bmatrix}\end{aligned} \tag{3.39}$$

where $\mathbf{Q}^c$ of size $(N_r + N_t) \times N_t$ is a unitary matrix with $\mathbf{Q}^{c\mathrm{H}}\mathbf{Q}^c = \mathbf{I}^c_{N_t \times N_t}$ and $\mathbf{R}^c$ of size $N_t \times N_t$ is an upper triangular matrix. Here $r^c_{i,j}$ denotes the (i,j)th entry of $\mathbf{R}^c$. Then the matrix $\mathbf{R}$ is LLL-reduced as $\tilde{\mathbf{R}}$ in Table 3.3, while creating the transformation matrix $\mathbf{T}^c$, which is the complex LLL algorithm based on QR

decomposition.

The LLL algorithm successively performs a size reduction at steps (4) - (10) in Table 3.3, which ensures that step (11) is fulfilled, and then possibly performs a column exchange steps (12) - (17) to swap two basis vectors in order to fulfill (3.15). Here we apply Givens rotation matrix $\mathbf{\Theta}$ to keep $\tilde{\mathbf{R}}^c$ to be upper triangular matrix. The matrix $\tilde{\mathbf{Q}}^c$ is also updated by multiplying $\mathbf{\Theta}^{\mathrm{H}}$. The output of the LLL algorithm is $\tilde{\mathbf{Q}}^c$, $\tilde{\mathbf{R}}^c$, and $\mathbf{T}^c$.

Table 3.3: Complex LLL algorithm based on QR decomposition

Input: $\mathbf{Q}^c$, $\mathbf{R}^c$, and $\mathbf{T}^c := \mathbf{I}^c_{N_t}$, set δ; Output: $\tilde{\mathbf{Q}}^c$, $\tilde{\mathbf{R}}^c$, $\mathbf{T}^c$

(1) **Initialization**: $\tilde{\mathbf{Q}}^c := \mathbf{Q}^c$ and $\tilde{\mathbf{R}}^c := \mathbf{R}^c$.
(2) $p = 2$
(3) **while** $p \leq N_t$
(4) **for** $q := p-1$ down to 1
(5) $\mu_{q,p} = \lceil \tilde{r}^c_{q,p} / \tilde{r}^c_{q,q} \rfloor$
(6) **if** $\mu_{q,p} \neq 0$
(7) $\tilde{\mathbf{R}}^c_{1:q,p} := \tilde{\mathbf{R}}^c_{1:q,p} - \mu_{q,p}\tilde{\mathbf{R}}^c_{1:q,q}$
(8) $\mathbf{T}^c_{:,p} := \mathbf{T}^c_{:,p} - \mu_{q,p}\mathbf{T}^c_{:,q}$
(9) **end**
(10) **end**
(11) **if** $\delta \left\|\tilde{r}^c_{p-1,p-1}\right\|^2 > \left\|\tilde{r}^c_{p,p}\right\|^2 + \left\|\tilde{r}^c_{p-1,p}\right\|^2$
(12) Swap columns $p-1$ and p in $\tilde{\mathbf{R}}^c$ and $\mathbf{T}^c$
(13) $\mathbf{\Theta} = \begin{bmatrix} \alpha & \beta \\ -\beta & \alpha \end{bmatrix}$ with $\alpha = \dfrac{\tilde{r}^c_{p-1,p-1}}{\|\tilde{\mathbf{R}}^c_{p-1:p,p-1}\|^2}$, $\beta = \dfrac{\tilde{\mathbf{R}}^c_{p,p-1}}{\|\tilde{\mathbf{R}}^c_{p-1:p,p-1}\|^2}$
(14) $\tilde{\mathbf{R}}^c_{p-1:p,p-1:N_t} := \mathbf{\Theta}\tilde{\mathbf{R}}^c_{p-1:p,p-1:N_t}$
(15) $\tilde{\mathbf{Q}}^c_{:,p-1:p} := \tilde{\mathbf{Q}}^c_{:,p-1:p}\mathbf{\Theta}^{\mathrm{H}}$
(16) $p := \max\{p-1, 2\}$
(17) **else** $p := p+1$
(18) **End**

Note that $\mathbf{A}^c_{a:b,c}$ denotes the entries from rows a to b in the c-th column. $\mathbf{A}^c_{a:b,:}$ is the submatrix of $\mathbf{A}^c$ from rows a to b across the whole columns.

The LLL-reduced matrix $\tilde{\mathbf{R}}^c$ is expressed as

$$\tilde{\mathbf{R}}^c = \begin{bmatrix} \tilde{r}^c_{11} & \tilde{r}^c_{12} & \cdots & \tilde{r}^c_{1,N_t} \\ 0 & \tilde{r}^c_{22} & \cdots & \tilde{r}^c_{1,N_t} \\ \vdots & \vdots & \ddots & \vdots \\ 0 & 0 & \cdots & \tilde{r}^c_{N_r,N_t} \end{bmatrix} \tag{3.40}$$

By pre-multiplying $\tilde{\mathbf{Q}}^{c\mathrm{H}}$, the model system in (3.22) is rewritten as

$$\begin{aligned} \mathbf{y}^{c\prime} &= \tilde{\mathbf{Q}}^{c\mathrm{H}} \bar{\mathbf{y}}^{c\mathcal{S}} \\ &= \tilde{\mathbf{R}}^c \mathbf{v}^c + \mathbf{Q}^{c\mathrm{H}} \frac{\bar{\mathbf{z}}^c}{2} \\ &= \tilde{\mathbf{R}}^c \mathbf{v}^c + \mathbf{z}^{c\prime} \end{aligned} \tag{3.41}$$

where $\mathbf{z}^{c\prime} \triangleq \tilde{\mathbf{Q}}^{c\mathrm{H}} \frac{\bar{\mathbf{z}}^c}{2}$ is a zero-mean Gaussian random vector.

Since $\mathbf{z}^{c\prime}$ and $\bar{\mathbf{z}}^c$ have the same statistical properties, $\mathbf{z}^{c\prime}$ can be used to denote $\bar{\mathbf{z}}^c$. We have

$$\mathbf{y}^{c\prime} = \tilde{\mathbf{R}}^c \mathbf{v}^c + \mathbf{z}^{c\prime} \tag{3.42}$$

$$\begin{bmatrix} y^{c\prime}_1 \\ y^{c\prime}_2 \\ \vdots \\ y^{c\prime}_{N_t} \end{bmatrix} = \begin{bmatrix} \tilde{r}_{11} & \tilde{r}_{12} & \cdots & \tilde{r}_{1,N_t} \\ 0 & \tilde{r}_{22} & \cdots & \tilde{r}_{1,N_t} \\ \vdots & \vdots & \ddots & \vdots \\ 0 & 0 & \cdots & \tilde{r}_{N_t,N_t} \end{bmatrix} \begin{bmatrix} v^c_1 \\ v^c_2 \\ \vdots \\ v^c_{N_t} \end{bmatrix} + \begin{bmatrix} z^{c\prime}_1 \\ z^{c\prime}_2 \\ \vdots \\ z^{c\prime}_{N_t} \end{bmatrix} \tag{3.43}$$

where the vectors of $y^{c\prime}_k$ and $z^{c\prime}_k$ denote the k-th element of $\mathbf{y}^{c\prime}$ and $\mathbf{z}^{c\prime}$, respectively. Thus, we have

$$\begin{aligned} y^{c\prime}_{N_t} &= \tilde{r}^c_{N_t,N_t} v^c_{N_t} + z^{c\prime}_{N_t} \\ y^{c\prime}_{N_t-1} &= \tilde{r}^c_{N_t-1,N_t-1} v^c_{N_t-1} + \tilde{r}^c_{N_t-1,N_t} v^c_{N_t} + z^{c\prime}_{N_t-1} \\ &\vdots \\ y^{c\prime}_1 &= \tilde{r}^c_{1,1} v^c_1 + \tilde{r}^c_{1,2} v^c_2 + \cdots + \tilde{r}^c_{1,N_t-1} v^c_{N_t-1} + \tilde{r}^c_{1,N_t} v^c_{N_t} + z^{c\prime}_1 \end{aligned} \tag{3.44}$$

Thus, in the LR-SIC detection, the last entry of signal $v^c_{N_t}$ is first derived as $\hat{v}^c_{N_t} = \mathcal{Q}\{y^{c\prime}_{N_t} / \tilde{r}^c_{N_t,N_t}\}$. Assuming that the previous decisions are correct, the interferences can be cancelled in each step. The rest of the transmit signals are

derived in the following recursion as

$$\hat{v}_i^c = \mathcal{Q}\left\{\frac{y_i^{c\prime} - \sum_{j=i+1}^{N_t} \tilde{r}_{i,j}^c \hat{v}_j^c}{\tilde{r}_{i,i}^c}\right\}, i = N_t - 1, \ldots, 1. \tag{3.45}$$

As the same method as the LR-MMSE detection, the signal vector in the LR domain should be transformed back into the s-domain as

$$\begin{aligned} \hat{\mathbf{s}}^{c\mathcal{S}} &= \mathbf{T}^c \hat{\mathbf{v}}^c \\ \hat{\mathbf{s}}^c &= \mathcal{S}^{-1}[\hat{\mathbf{s}}^{c\mathcal{S}}] = 2\hat{\mathbf{s}}^{c\mathcal{S}} - (K-1)(1+j)\mathbf{1}_{N_t} \end{aligned} \tag{3.46}$$

Using the same method, the final decision $\hat{\mathbf{s}}^c$ is forced to the nearest constellation points if they are lying outside the original signal constellation as $\hat{\mathbf{s}}^c := \mathcal{C}[\hat{\mathbf{s}}^c]$.

3.5.2 Performance and simulation results

The computer simulations were carried out for QPSK, 16QAM and 64QAM in the 4×4 and the 8×8 MIMO systems, respectively. We compare the LR-SIC detection with the LR-ZF detection, the LR-MMSE detection and the conventional detection methods, such as the ZF detection and the MMSE detection and the ML detection described in Chapter 2.

The BER characteristics vs. E_b/N_0 are shown in Figs. 3.14 - 3.19. The LR-SIC detection has large improvement of the BER performance compared to the LR-MMSE detection due to the less noise enhancement. For the 4×4 MIMO system, the LR-SIC detection is about 1.2dB, 1.1dB and 0.9dB improvement of BER performance at a BER of 10^{-5} over the LR-MMSE detection for QPSK, 16QAM and 64QAM, respectively. And the curve of the LR-OSIC detection almost agrees with that of the LR-SIC detection and closely approaches that of the ML detection at a BER of 10^{-5}. On the contrary, for the 8×8 MIMO system, the LR-SIC detection is about 4.0dB, 3.7dB and 3.5dB improvement of BER performance at a BER of 10^{-5} over the MMSE detection for QPSK, 16QAM and 64QAM, respectively.

Therefore, compared to the LR aided detection, the LR-SIC detection achieves the better BER performance in the 4×4 MIMO system and closely approaches the BER of the ML detection only for QPSK. However, the LR-SIC detection

in the 8×8 MIMO system is still about 5dB worse than the BER of the ML detection at a BER of 10^{-5}.

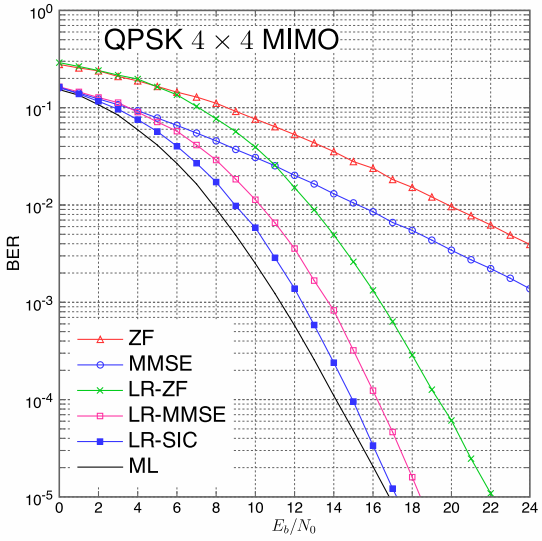

Figure 3.14: The BER vs. E_b/N_0 for the LR-SIC over 4×4 MIMO: QPSK

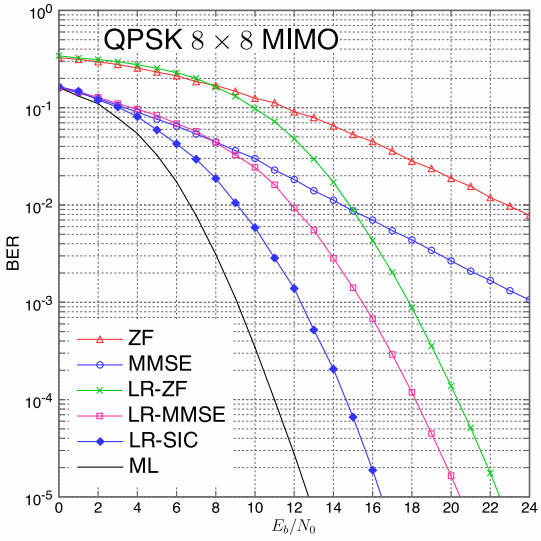

Figure 3.15: The BER vs. E_b/N_0 for the LR-SIC over 8×8 MIMO: QPSK

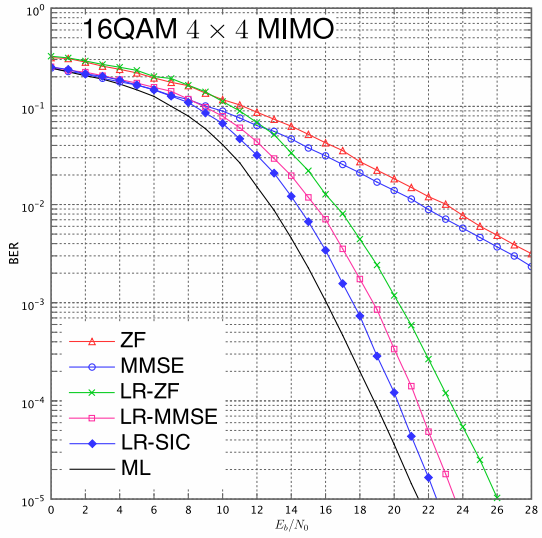

Figure 3.16: The BER vs. E_b/N_0 for the LR-SIC over 4×4 MIMO: 16QAM

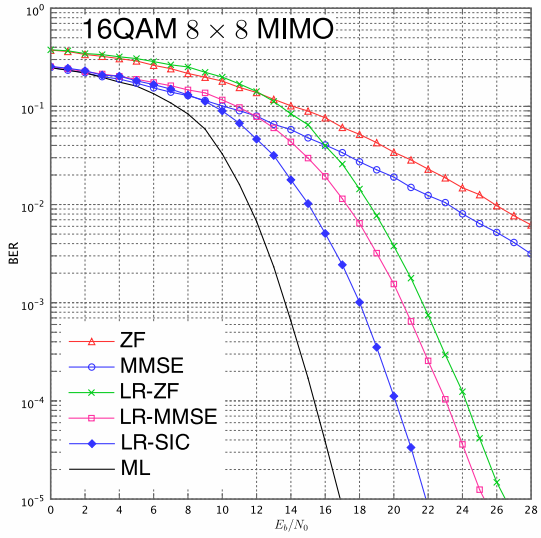

Figure 3.17: The BER vs. E_b/N_0 for the LR-SIC over 8×8 MIMO: 16QAM

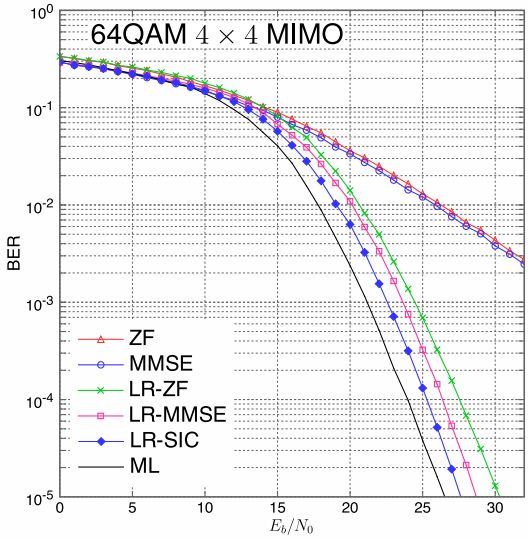

Figure 3.18: The BER vs. E_b/N_0 for the LR-SIC over 4×4 MIMO: 64QAM

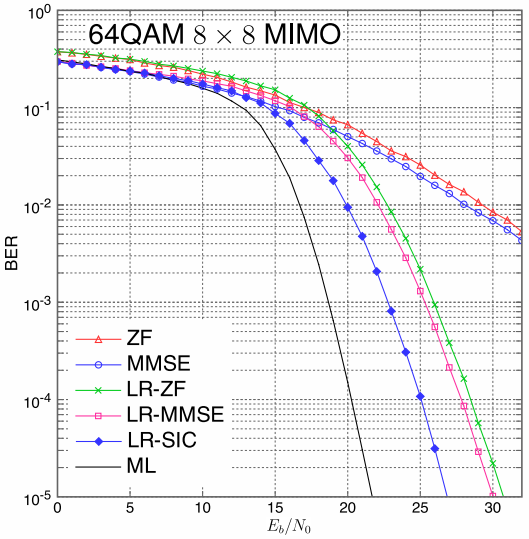

Figure 3.19: The BER vs. E_b/N_0 for the LR-SIC over 8×8 MIMO: 64QAM

3.6 Lattice reduction based List detection

In the MIMO detection, the signals transmitted from multiple antennas can be detected jointly using the ML metric for the optimal performance. However, the complexity is prohibitively high for a large number of the candidate vectors for the transmit signal and a higher order modulation method. Therefore, it is desirable to find some new detection methods that can provide near ML performance with low complexity, which is comparable to that of linear detection.

3.6.1 LR-List detection

Since the sequential decision and cancellation are carried out, the SIC detection suffers from the error propagation. List-based approaches [47]−[49] can be employed to mitigate error propagation by selection of an optimal signal vector from multiple candidate vectors for the hard decision. For the LR-MMSE detection, the simplest quantization in (3.25) is the rounding operation. However, the good BER is not achieved by quantizing of $\tilde{v}_i^c, i \in [1, N_t]$. Hence we present two list scheme methods based on LR-MMSE detection, which are referred to as the

linear-list detection. First, recall the signal estimation using LR-MMSE:

$$\begin{aligned}\tilde{\mathbf{v}}^{c(LR-MMSE)} &= \bar{\mathbf{H}}^{c\prime\dagger}\bar{\mathbf{y}}^{c\mathcal{S}} \\ &\equiv \left(\bar{\mathbf{H}}^{c\prime\mathrm{H}}\bar{\mathbf{H}}^{c\prime}\right)^{-1}\bar{\mathbf{H}}^{c\prime\mathrm{H}}\bar{\mathbf{y}}^{c\mathcal{S}} \\ &= \left(\mathbf{H}^{c\prime\mathrm{H}}\mathbf{H}^{c\prime}+\gamma^{-1}\mathbf{T}^{c\mathrm{H}}\mathbf{T}^{c}\right)^{-1}\mathbf{H}^{c\prime\mathrm{H}}\mathbf{y}^{c\mathcal{S}}\end{aligned} \tag{3.47}$$

After that, the following estimation of the LR-MMSE detection is derived as

$$\begin{aligned}&\hat{v}_i^c = \mathcal{Q}\left\{\tilde{v}_i^{c(LR-MMSE)}\right\},\ i\in[1,N_t] \\ &\hat{\mathbf{s}}^{c\mathcal{S}} = \mathbf{T}^c\hat{\mathbf{v}}^c \\ &\hat{\mathbf{s}}^c = \mathcal{S}^{-1}[\hat{\mathbf{s}}^{c\mathcal{S}}] = 2\hat{\mathbf{s}}^{c\mathcal{S}} - (K-1)(1+j)\mathbf{1}_{N_t}\end{aligned} \tag{3.48}$$

The final decision $\hat{\mathbf{s}}^c$ is forced to the nearest constellation points if they are lying outside the original signal constellation as $\hat{\mathbf{s}}^c := \mathcal{C}[\hat{\mathbf{s}}^c]$.

The performance strongly depends on the accuracy of the estimation and quantization of $\tilde{\mathbf{v}}^c$, which is obtained by LR-MMSE detection. However, since the entries of $\mathbf{v}^c$ are not independent, the simple rounding quantization of $\tilde{\mathbf{v}}^c$ is only a suboptimal process and sometimes may cause erroneously decided entries, compared to the optimal one. In the high E_b/N_0 region, the reduced channel $\bar{\mathbf{H}}^{c\prime}$ has nearly orthogonal column vectors, and thus the quantization error trends to become the main reason for the detection error.

Considering the high E_b/N_0 region, we aim at correcting the quantization errors in a limited case that the rounded $\hat{\mathbf{v}}^c$ contains at most one erroneously decided entry, such as $\hat{\mathbf{v}}_i^c$, which entry is some complex integers away from the optimally decided entry. Since the estimation with the reduced channel matrix is very accurate in the high E_b/N_0 region, the limited case seems to be the major case of quantization errors. Based on this limitation, we attempt to achieve the near-optimal quantization by generating a list of $\hat{\mathbf{v}}^c$ from the estimated one and search for the best estimate using the ML metric. The list quantization method called **Method 1** is explained below.

Method 1

For each entry $\hat{v}_i^c, i\in[1,N_t]$, we create the list of the quantization candidates based on $\tilde{\mathbf{v}}^c$. There are (N_t+1) candidates of $\hat{\mathbf{v}}^c$ with N_t transmit antenna, including the rounded estimate $\hat{\mathbf{v}}^c$.

Step 1):

(1) Input $\tilde{\mathbf{v}}^c = [\tilde{v}_1^c, \ldots, \tilde{v}_{N_t}^c]^{\mathrm{T}}$, $\mathbf{H}^c$ and $\mathbf{T}^c$.

(2) Let $\hat{v}_i^{c(0)} = \lceil \tilde{v}_i^c \rfloor, i \in [1, N_t]$, and create $\hat{\mathbf{v}}^{c(0)} = [\tilde{v}_1^{c(0)}, \ldots, \tilde{v}_{N_t}^{c(0)}]^{\mathrm{T}}$.

(3) Calculate $\hat{\mathbf{s}}^{c(0)\mathcal{S}} = \mathbf{T}^c \hat{\mathbf{v}}^{c(0)}$ and $\hat{\mathbf{s}}^{c(0)} = \mathcal{S}^{-1}[\hat{\mathbf{s}}^{c(0)\mathcal{S}}] = 2\hat{\mathbf{s}}^{c(0)\mathcal{S}} - (K-1)\mathbf{1}_{N_t}^c$.

(4) The final decision $\hat{\mathbf{s}}^{c(0)}$ is forced to the nearest constellation points if they are lying outside the original signal constellation as $\hat{\mathbf{s}}^{c(0)} := \mathcal{C}[\hat{\mathbf{s}}^{c(0)}]$.

Step 2):

(1) for $l := 1$ to N_t

(2) If $\left|\mathrm{Re}\left[\tilde{v}_l^{c(0)} - \hat{v}_l^{c(0)}\right]\right| > \left|\mathrm{Im}\left[\tilde{v}_l^{c(0)} - \hat{v}_l^{c(0)}\right]\right|$, then $\hat{v}_l^{c(1)} \triangleq \hat{v}_l^{c(0)} + j\mathrm{sgn}\left\{\mathrm{Re}\left[\tilde{v}_l^{c(0)} - \hat{v}_l^{c(0)}\right]\right\}$.

(3) Else, $\hat{v}_l^{c(1)} \triangleq \hat{v}_l^{c(0)} + j\mathrm{sgn}\left\{\mathrm{Im}\left[\tilde{v}_l^{c(0)} - \hat{v}_l^{c(0)}\right]\right\}$.

(4) Create $\hat{\mathbf{v}}^{c(l)} = \left[\hat{v}_1^{c(0)}, \ldots, \hat{v}_{l-1}^{c(0)}, \hat{v}_l^{c(1)}, \hat{v}_{l+1}^{c(0)}, \ldots, \hat{v}_{N_t}^{c(0)}\right]^{\mathrm{T}}$.

(5) As (4) in *Step* 1), we also obtain the candidates of $\hat{\mathbf{s}}^{c(l)}, l \in [1, N_t]$.

(6) end

(7) The ML metric is employed as $\hat{\mathbf{s}}^c = \arg\min_{l \in [0, N_t]} \left\|\mathbf{y}^c - \mathbf{H}^c \hat{\mathbf{s}}^{c(l)}\right\|^2$.

There are $(N_t + 1)$ candidates in the list of the transmit signal vectors as

$$\begin{aligned}
\hat{\mathbf{v}}^{c(0)} &= [\hat{v}_1^{c(0)}, \hat{v}_2^{c(0)}, \ldots, \hat{v}_{N_t}^{c(0)}]^{\mathrm{T}} \\
\hat{\mathbf{v}}^{c(1)} &= [\hat{v}_1^{c(1)}, \hat{v}_2^{c(0)}, \ldots, \hat{v}_{N_t}^{c(0)}]^{\mathrm{T}} \\
\hat{\mathbf{v}}^{c(2)} &= [\hat{v}_1^{c(0)}, \hat{v}_2^{c(1)}, \hat{v}_3^{c(0)}, \ldots, \hat{v}_{N_t}^{c(0)}]^{\mathrm{T}} \\
&\vdots \\
\hat{\mathbf{v}}^{c(l)} &= [\hat{v}_1^{c(0)}, \ldots, \hat{v}_{l-1}^{c(0)}, \hat{v}_l^{c(1)}, \hat{v}_{l+1}^{c(0)}, \ldots, \hat{v}_{N_t}^{c(0)}]^{\mathrm{T}} \\
&\vdots \\
\hat{\mathbf{v}}^{c(N_t)} &= [\hat{v}_1^{c(0)}, \ldots, \hat{v}_{N_t}^{c(1)}]^{\mathrm{T}}
\end{aligned} \tag{3.49}$$

Based on the difference between the estimated symbol and the rounded integer, we also introduce another list scheme method which requires the half size of list candidates in the **Method 1**. This list quantization method called **Method 2** is explained below.

Method 2

For each entry $\hat{v}_i^c, i \in [1, N_t]$, we create the list of the quantization candidates based on $\tilde{\mathbf{v}}^c$. There are $(\frac{N_t}{2} + 1)$ candidates of $\hat{\mathbf{v}}^c$ with N_t transmit antenna,

including the rounded estimate $\hat{\mathbf{v}}^c$.

Step 1):

(1) Input $\tilde{\mathbf{v}}^c = [\tilde{v}_1^c, \ldots, \tilde{v}_{N_t}^c]^{\mathrm{T}}$, $\mathbf{H}^c$ and $\mathbf{T}^c$.

(2) Let $\hat{v}_i^{c(0)} = \lceil \tilde{v}_i^c \rfloor, i \in [1, N_t]$, and create $\hat{\mathbf{v}}^{c(0)} = [\tilde{v}_1^{c(0)}, \ldots, \tilde{v}_{N_t}^{c(0)}]^{\mathrm{T}}$.

(3) Calculate $\hat{\mathbf{s}}^{c(0)\mathcal{S}} = \mathbf{T}^c \hat{\mathbf{v}}^{c(0)}$ and $\hat{\mathbf{s}}^{c(0)} = \mathcal{S}^{-1}[\hat{\mathbf{s}}^{c(0)\mathcal{S}}] = 2\hat{\mathbf{s}}^{c(0)\mathcal{S}} - (K-1)\mathbf{1}_{N_t}^c$.

(4) The final decision $\hat{\mathbf{s}}^{c(0)}$ is forced to the nearest constellation points if they are lying outside the original signal constellation as $\hat{\mathbf{s}}^{c(0)} := \mathcal{C}[\hat{\mathbf{s}}^{c(0)}]$.

Step 2):

(1) Define $\delta\tilde{\mathbf{v}}_j^c \triangleq \max\Big\{|\mathrm{Re}[\tilde{v}_l^{c(0)} - \hat{v}_l^{c(0)}]|, |\mathrm{Im}[\tilde{v}_l^{c(0)} - \hat{v}_l^{c(0)}]|\Big\}, j \in [1, N_t]$.

(2) Define $\Delta\tilde{v}_{j_p}^c \triangleq \tilde{v}_{j_p}^c - \hat{v}_{j_p}^{c(0)}$.

(3) Let $\delta\tilde{v}_{j_p}^c \equiv \max\Big\{|\mathrm{Re}[\Delta\tilde{v}_{j_p}^c|, |\mathrm{Im}[\Delta\tilde{v}_{j_p}^c|\Big\}$ be the p-th longest among all $\delta\tilde{v}_j^c$'s, $j \in [1, N_t]$.

(4) Let $\tilde{v}_{j_p}^c$ be the j_p-th entry of $\tilde{\mathbf{v}}^c$ and $\tilde{v}_{j_p}^{c(0)}$ be the j_p-th entry of $\tilde{\mathbf{v}}^{c(0)}$, where the entry number j_p is from 1 to N_t.

(5) for $p := 1$ to $\frac{N_t}{2}$

(6) If $|\mathrm{Re}[\Delta\tilde{v}_{j_p}^c]| > |\mathrm{Im}[\Delta\tilde{v}_{j_p}^c]|$, then $\hat{v}_{j_p}^{c(1)} \triangleq \hat{v}_{j_p}^{c(0)} + j\mathrm{sgn}\{\mathrm{Re}[\Delta\tilde{v}_{j_p}^c]\}$.

(7) Else, $\hat{v}_{j_p}^{c(1)} \triangleq \hat{v}_{j_p}^{c(0)} + j\mathrm{sgn}\{\mathrm{Im}[\Delta\tilde{v}_{j_p}^c]\}$.

(8) Create $\hat{\mathbf{v}}^{c(p)} = [\hat{v}_1^{c(0)}, \ldots, \hat{v}_{j_p-1}^{c(0)}, \hat{v}_{j_p}^{c(1)}, \hat{v}_{j_p+1}^{c(0)}, \ldots, \hat{v}_{N_t}^{c(0)}]^{\mathrm{T}}$.

(9) As (4) in *Step* 1), we also obtain the candidates of $\hat{\mathbf{s}}^{c(p)}, p \in [1, \frac{N_t}{2}]$.

(10) end

(11) The ML metric is employed as $\hat{\mathbf{s}}^c = \arg\min_{p \in [0, \frac{N_t}{2}]} \left\|\mathbf{y}^c - \mathbf{H}^c \hat{\mathbf{s}}^{c(p)}\right\|^2$.

Based on **Method 1** , we choose the most reliable $(\frac{N_t}{2} + 1)$ candidates in the list of the transmit signal vectors. We order the difference between the estimated symbol and the rounded integer, separating the real part and imaginary part, respectively. Thus, the complexity of **Method 2** for the list candidates should be reduced half compared to **Method 1**, and the final soft estimation of transmit signal becomes reliable.

3.6.2 Performance and simulation results

The computer simulations were carried out for QPSK, 16QAM and 64QAM in the 4×4 and the 8×8 MIMO systems, respectively. We compare the LR-List detections (**Method 1** and **Method 2**) with the LR-ZF detection, the LR-MMSE

detection and the conventional detection methods, such as the ZF detection and the MMSE detection and the ML detection described in Chapter 2.

The BER characteristics vs. E_b/N_0 are shown in Figs. 3.20 - 3.25. The LR-List detection has large improvement of the BER performance compared to the LR-MMSE detection due to reducing the quantization error. For the 4×4 MIMO system, the curve of the LR-List detections of **Method 1** and **Method 2** closely approaches that of the ML detection at a BER of 10^{-5}. On the contrary, for the 8×8 MIMO system, the LR-List of **Method 2** has a little improvement of BER compared to that of **Method 1** with nearly half complexity. The BER performance of the LR-List detection for the **Method 2** is about 5.5dB, 6.0dB and 6.0dB worst than that of the ML detection at a BER of 10^{-5} for QPSK, 16QAM and 64QAM, respectively.

Compared to the LR aided detection, the LR-SIC detection achieves the better BER performance in the 4×4 MIMO system and closely approaches the BER of the ML detection. However, the LR-List detection in the 8×8 MIMO system is still about 4dB worse than the BER of the ML detection at a BER of 10^{-5}.

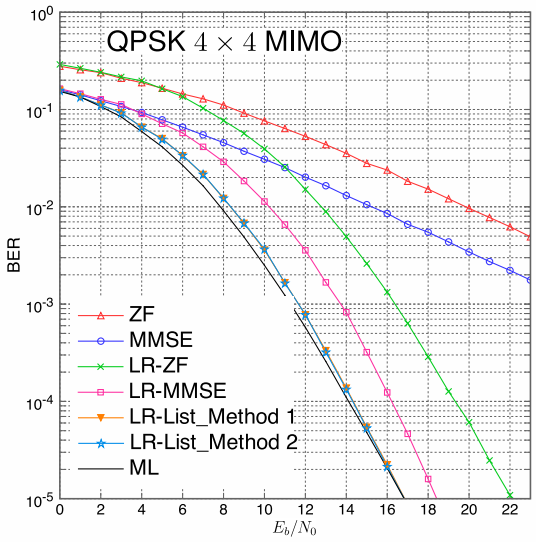

Figure 3.20: The BER vs. E_b/N_0 for the LR-List over 4×4 MIMO: QPSK

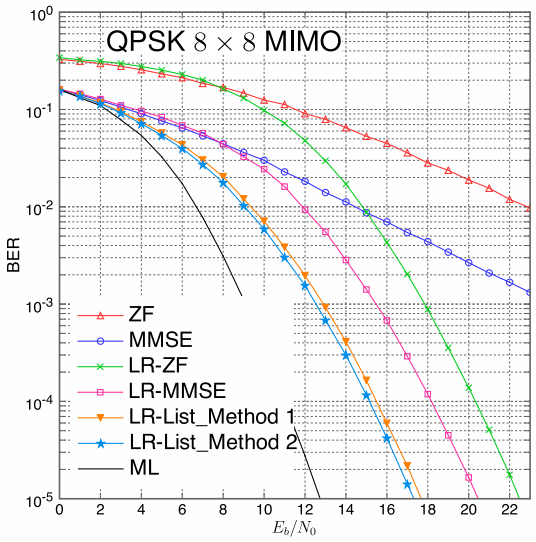

Figure 3.21: The BER vs. E_b/N_0 for the LR-List over 8×8 MIMO: QPSK

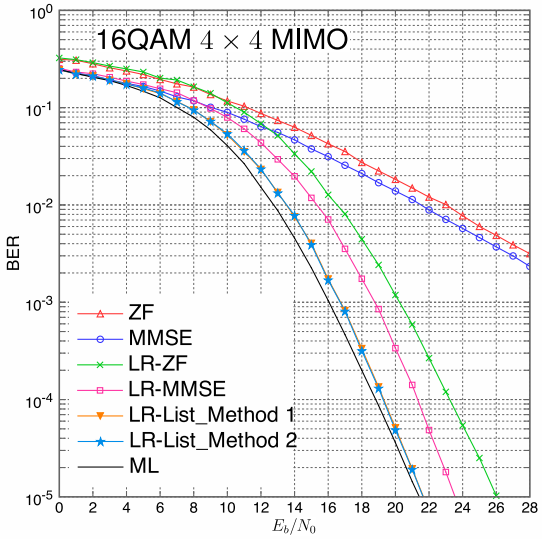

Figure 3.22: The BER vs. E_b/N_0 for the LR-List over 4×4 MIMO: 16QAM

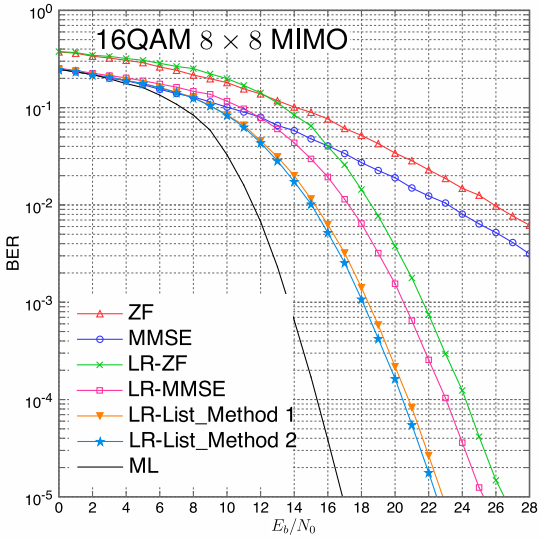

Figure 3.23: The BER vs. E_b/N_0 for the LR-List over 8×8 MIMO: 16QAM

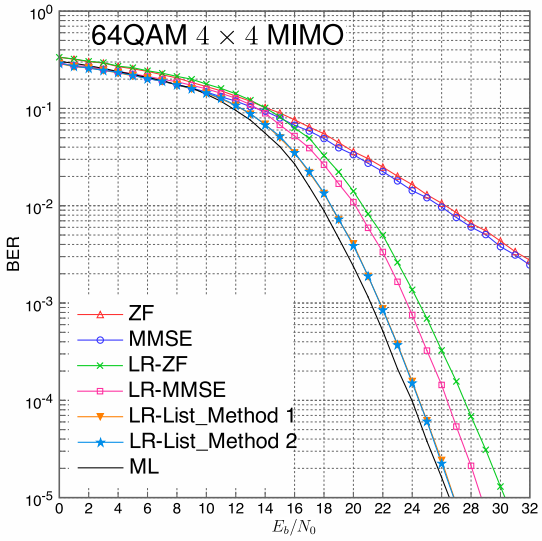

Figure 3.24: The BER vs. E_b/N_0 for the LR-List over 4×4 MIMO: 64QAM

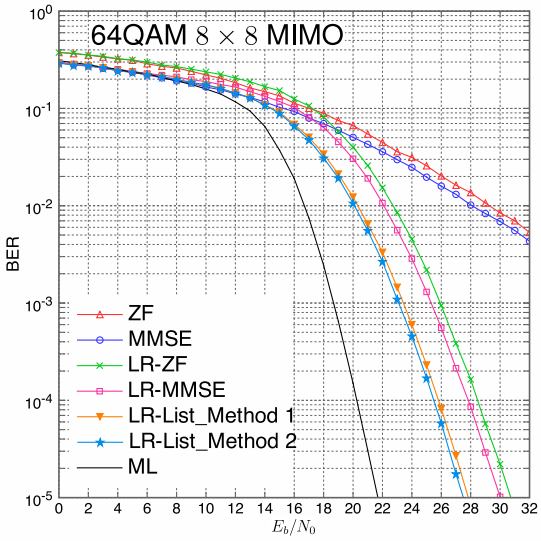

Figure 3.25: The BER vs. E_b/N_0 for the LR-List over 8×8 MIMO: 64QAM

3.7 Chapter summary

In this chapter, we first introduced the LR algorithm, i.e., the GSO algorithm and the LLL algorithm. The LR algorithm is applied into the MIMO detection, which

results in better decision boundary and obtains more reliable estimation. For the conventional LR-ZF or LR-MMSE detections, they have low complexity but worse BER performance, especially in the 8×8 MIMO system. Hence we combined the LR algorithm with the conventional linear detections, the SIC detection and the list detection. These detection schemes brought good improvement of BER performance, and achieved suboptimal BER performance for the 4×4 MIMO system. For the 8×8 MIMO system, the BER curves of these detections were still far to that of ML detection.

To further improve the performance with low complexity, different schemes and components are adopted, which will be introduced in the following chapters.

Chapter 4

Adaptive Tree Search Detection with Variable Path Expansion Based on Gram-Schmidt Orthogonalization

4.1 Introduction

In this chapter, we first present a detection scheme combined the Gram-Schmidt orthogonalization reduction with the M-algorithm, which we call the GSM-MLD. This scheme has such features that it achieves near-ML BER performance like the QRM-MLD with relatively low computational complexity. The channel matrix is reduced using the GSO procedure, and meanwhile a transform matrix is created. In contrast to the QR decomposition of the channel matrix in the QRM-MLD, the column vectors of the GS-reduced channel matrix are purely orthogonal for the GSM-MLD. The GS-reduced channel matrix spans the same subspace as the columns of the original channel matrix. The transform matrix is an upper triangular matrix with unity diagonal entries.

Based on the GSM-MLD, we propose novel adaptive tree search detection with variable path expansion based on GSO in the MIMO systems. The proposed algorithm in this chapter retains the same breadth of the tree search as the GSM-MLD to achieve the near-ML performance, and however the number of the

possible branches is adaptively controlled. The adaptive scheme avoids a large amount of the path metric evaluations and sorting to reduce the computational complexity. We also analyze the complexity of the proposed detection. The proposed detection in this chapter can considerably decrease the complexity in the high E_b/N_0 region.

4.2 Model system

In this thesis, we describe some MIMO detection schemes based on lattice reduction. These detection schemes estimate the transmit signals by the real-valued channel matrix and vectors. Hence, Eq. (2.1) can be rewritten using the real representation as

$$\mathbf{y} = \mathbf{H}\mathbf{s} + \mathbf{z} \tag{4.1}$$

where the equivalent real-valued channel matrix and vectors letting $n = 2N_r$ and $m = 2N_t$ are defined as

$$\begin{aligned} &\mathbf{H} \triangleq \begin{bmatrix} \mathrm{Re}[\mathbf{H}^c] & -\mathrm{Im}[\mathbf{H}^c] \\ \mathrm{Im}[\mathbf{H}^c] & \mathrm{Re}[\mathbf{H}^c] \end{bmatrix} \in \mathbb{R}^{n\times m},\ \mathbf{s} \triangleq \begin{bmatrix} \mathrm{Re}[\mathbf{s}^c] \\ \mathrm{Im}[\mathbf{s}^c] \end{bmatrix} \in \mathbb{Z}^{m\times 1}, \\ &\mathbf{y} \triangleq \begin{bmatrix} \mathrm{Re}[\mathbf{y}^c] \\ \mathrm{Im}[\mathbf{y}^c] \end{bmatrix} \in \mathbb{R}^{n\times 1},\ \text{and}\ \mathbf{z} \triangleq \begin{bmatrix} \mathrm{Re}[\mathbf{z}^c] \\ \mathrm{Im}[\mathbf{z}^c] \end{bmatrix} \in \mathbb{R}^{n\times 1} \end{aligned} \tag{4.2}$$

We define the dimension of the real-valued channel matrix $\mathbf{H}$ to be $n \times m$. The dimensions of the vectors in (4.2) are given as $\mathbf{y} \in \mathbb{R}^{n\times 1}, \mathbf{z} \in \mathbb{R}^{n\times 1}$ and $\mathbf{s} \in \mathbb{Z}^{m\times 1}$, where $\mathbb{Z}$ denotes the finite set of the real-valued transmit signals. The set of the real-valued signals is given by $\mathbb{Z} = \{\pm 1, \pm 3, \ldots, \pm(K-1)\}$ for K^2-QAM (Quadrature Amplitude Modulation). Since the data is binary in the digital telecommunication, the value of K in the constellation is usually a power of 2.

Given $\mathbf{y}$ and the channel matrix $\mathbf{H}$, the ZF soft estimate of the transmit signals is expressed as

$$\begin{aligned} \tilde{\mathbf{s}}^{(\mathrm{ZF})} &= \mathbf{H}^{\dagger}\mathbf{y} \\ &\equiv \left(\mathbf{H}^{\mathrm{T}}\mathbf{H}\right)^{-1}\mathbf{H}^{\mathrm{T}}\mathbf{y} \end{aligned} \tag{4.3}$$

4.3 GSM-MLD

We first introduce the GSM-MLD algorithm. The column vectors of channel matrix $\mathbf{H}$ are first sorted in the ascending order in length. Then, they are weakly reduced using the GSO procedure shown in Table 4.1. This algorithm transforms the channel matrix $\mathbf{H}$ to create the GS-reduced channel matrix $\hat{\mathbf{H}}$ and the transform matrix $\hat{\mathbf{T}}$. The column vectors of $\hat{\mathbf{H}}$ are mutually orthogonal, and the transform matrix $\hat{\mathbf{T}}$ is an upper triangular matrix with unity diagonal entries and $\det\{\hat{\mathbf{T}}\} = 1$. Note that this algorithm in Table 4.1 is computationally-simple since it weakly reduces the column vectors of $\mathbf{H}$ without the size reduction in the LLL algorithm [39].

Table 4.1: Real Gram-Schmidt orthogonalization algorithm

(1) **Begin** Input: $\mathbf{H} = [\mathbf{h}_1, \cdots, \mathbf{h}_m]$, and $\hat{\mathbf{T}} := \mathbf{I}_m = [\mathbf{t}_1, \cdots, \mathbf{t}_m]$.
Set $\hat{\mathbf{h}}_p = \mathbf{h}_p, p \in [1, m]$.
(2) **for** p:=2 to m
(3) **for** $q := p - 1$ down to 1
(4) $\mu_{p,q} = \frac{\hat{\mathbf{h}}_q^{\mathrm{T}} \hat{\mathbf{h}}_p}{||\hat{\mathbf{h}}_q||^2}$
(5) $\hat{\mathbf{h}}_p := \hat{\mathbf{h}}_p - \mu_{p,q} \hat{\mathbf{h}}_q$
(6) $\hat{\mathbf{t}}_p := \hat{\mathbf{t}}_p - \mu_{p,q} \hat{\mathbf{t}}_q$
(7) **end**
(8) **end**
(9) **End**

The upper triangular matrix $\hat{\mathbf{T}}$ with unity diagonal entries is invertible. The column vectors of the matrix $\hat{\mathbf{H}} = \mathbf{H}\hat{\mathbf{T}}$ are orthogonal and span the same subspace as the columns of the original matrix $\mathbf{H}$. Using the GS-reduced channel matrix $\hat{\mathbf{H}}$ and $\hat{\mathbf{T}}$, we have

$$\begin{aligned} \mathbf{y} &= \mathbf{H}\mathbf{s} + \mathbf{z} \\ &= \left(\mathbf{H}\hat{\mathbf{T}}\right)(\hat{\mathbf{T}}^{-1}\mathbf{s}) + \mathbf{z} \\ &= \hat{\mathbf{H}}\mathbf{v} + \mathbf{z} \end{aligned} \tag{4.4}$$

where $\hat{\mathbf{H}} \triangleq \mathbf{H}\hat{\mathbf{T}}$ and $\mathbf{v} \triangleq \hat{\mathbf{T}}^{-1}\mathbf{s}$ with expressing $\hat{\mathbf{T}}^{-1}$ as

$$\hat{\mathbf{T}}^{-1} = \begin{bmatrix} 1 & \tau_{12} & \dots & \tau_{1,m-1} & \tau_{1,m} \\ & 1 & \dots & \tau_{2,m-1} & \tau_{2,m} \\ & & \ddots & \vdots & \vdots \\ & & & 1 & \tau_{m-1,m} \\ \mathbf{0} & & & & 1 \end{bmatrix} \tag{4.5}$$

The soft estimate of $\mathbf{v}$ is derived as

$$\begin{aligned} \tilde{\mathbf{v}} &= \hat{\mathbf{T}}^{-1}\tilde{\mathbf{s}} \\ \begin{bmatrix} \tilde{v}_1 \\ \tilde{v}_2 \\ \vdots \\ \tilde{v}_{m-1} \\ \tilde{v}_m \end{bmatrix} &= \begin{bmatrix} 1 & \tau_{12} & \dots & \tau_{1,m-1} & \tau_{1,m} \\ & 1 & \dots & \tau_{2,m-1} & \tau_{2,m} \\ & & \ddots & \vdots & \vdots \\ & & & 1 & \tau_{m-1,m} \\ \mathbf{0} & & & & 1 \end{bmatrix} \begin{bmatrix} \tilde{s}_1 \\ \tilde{s}_2 \\ \vdots \\ \tilde{s}_{m-1} \\ \tilde{s}_m \end{bmatrix} \end{aligned} \tag{4.6}$$

where

$$\begin{aligned} \tilde{v}_m &= \tilde{s}_m \\ \tilde{v}_{m-1} &= \tilde{s}_{m-1} + \tau_{m-1,m}\tilde{s}_m \\ &\vdots \\ \tilde{v}_2 &= \tilde{s}_2 + \tau_{2,3}\tilde{s}_3 + \cdots + \tau_{2,m-1}\tilde{s}_{m-1} + \tau_{2,m}\tilde{s}_m \\ \tilde{v}_1 &= \tilde{s}_1 + \tau_{1,2}\tilde{s}_2 + \cdots + \tau_{1,m-1}\tilde{s}_{m-1} + \tau_{1,m}\tilde{s}_m \end{aligned} \tag{4.7}$$

The soft estimate of $\hat{\mathbf{s}}$ is obtained by performing the following recursion as

$$\hat{s}_i = \begin{cases} \mathcal{Q}\left\{\tilde{s}_i\right\} = \mathcal{Q}\left\{\tilde{v}_i\right\}, i = m \\ \mathcal{Q}\left\{\tilde{s}_i\right\} = \mathcal{Q}\left\{\tilde{v}_i - \sum_{j=i+1}^{m} \tau_{i,j}\hat{s}_j\right\}, i = m-1, \cdots, 1 \end{cases} \tag{4.8}$$

where $\tilde{s}_i \triangleq \tilde{v}_i, i = m$ and $\tilde{s}_i \triangleq \tilde{v}_i - \sum_{j=i+1}^{m} \tau_{i,j}\hat{s}_j, i = m-1, \cdots, 1$.

4.3.1 Definition of metric in GSM-MLD

The GSM-MLD applies a fixed number of M in each detection layer as the QRM-MLD, starting from the last entry of $\mathbf{s}$. Since $\hat{\mathbf{T}}^{-1}$ is a upper triangular matrix,

the entry s_i depends on the decided estimates $\hat{s}_j$'s where $j \in [i+1, m]$. We define the branch metric λ_i: $i \in [1, m]$ in GSM-MLD as

$$\lambda_i = \begin{cases} \left|\hat{\mathbf{h}}_i\right|^2 \left|\tilde{v}_i - \hat{s}_i\right|^2, i = m \\ \left|\hat{\mathbf{h}}_i\right|^2 \left|\tilde{v}_i - \hat{s}_i - \sum_{j=i+1}^{m} \tau_{i,j} \hat{s}_j\right|^2 = \left|\hat{\mathbf{h}}_i\right|^2 \left|\tilde{s}_i - \hat{s}_i\right|^2, i = m-1, \cdots, 1 \end{cases} \tag{4.9}$$

where $\tilde{s}_m \triangleq \tilde{v}_m$ and $\tilde{s}_i \triangleq \sum_{j=i+1}^{m} \tau_{i,j} \hat{s}_j$ for $i = m-1, \cdots, 1$. The path metric $\Lambda_i : i \in [1, m]$ is the accumulated branch metric, which is defined as

$$\begin{aligned} \Lambda_i &= \sum_{j=i}^{m} \lambda_j \\ &= \sum_{j=i}^{m} \left|\hat{\mathbf{h}}_j\right|^2 \left|\tilde{s}_j - \hat{s}_j\right|^2 \\ &= \begin{cases} \lambda_i, i = m \\ \lambda_i + \Lambda_{i+1}, i = m-1, \cdots, 1 \end{cases} \end{aligned} \tag{4.10}$$

where the path metric denotes the partial Euclidean distance (PED). In the GSM-MLD, $\Lambda_i^{(l)}$ denotes the l-th smallest path metric. Correspondingly, the partial transmit signal $\hat{\mathbf{s}}_i^{(l)}$ based on $\Lambda_i^{(l)}$ should be expressed as $\hat{\mathbf{s}}_i^{(l)} = \left[\hat{s}_i^{(l)}, \hat{s}_{i+1}^{(l)}, \cdots, \hat{s}_m^{(l)}\right]^{\mathrm{T}}$. Three major operations are the same as the conventional QRM-MLD. The output of the GSM-MLD is $\hat{\mathbf{s}}^{(1)} = [\hat{s}_1^{(1)}, \hat{s}_2^{(1)}, \cdots, \hat{s}_m^{(1)}]^{\mathrm{T}}$ as the final estimate of the transmit signal.

4.3.2 Computational complexity

We here use the floating point operations (flops) for the measure of the complexity, which defines one addition, one subtraction, one multiplication, and one division for real-valued number to take one flop. For the m-th layer, expanding K branches, λ_m in (4.9) requires two multiplications and one subtraction, and it consumes 3 flops expressed by $\mathcal{N}(\lambda_m) = 3$. For the $(m-1)$-th layer down to the first layer, M branches are retained from MK possible branches in the i-th layer, where $i \in [1, m-1]$. For a survived branch, $\tilde{s}_i$ in (4.8) requires $(m-i)$ multiplications and $(m-i)$ subtractions. Hence, the complexity for the computing of $\tilde{s}_i$ is expressed as $\mathcal{N}(\tilde{s}_i) = 2(m-i)$. For a possible branch, Λ_i

in (4.10) requires one addition, which we express the complexity as $\mathcal{N}(\Lambda_i) = 1$. $\mathcal{N}(\lambda_i, \Lambda_i) = \mathcal{N}(\lambda_i) + \mathcal{N}(\Lambda_i) = 4$ denotes the total complexity for the computations of the branch metric λ_i in (4.9) and the path metric Λ_i in (4.10).

The complexity of the GSM-MLD $\mathcal{N}_{GSM-MLD}$ which excludes the complexity of the GSO reduction can be derived as

$$\begin{aligned}\mathcal{N}_{GSM-MLD} &= 2mn - m + \underbrace{K\mathcal{N}(\lambda_m)}_{m\text{-th layer}} + \sum_{i=1}^{m-1}\left[\underbrace{M\mathcal{N}(\tilde{s}_i)}_{\text{Survived Branches}} + \underbrace{MK\mathcal{N}(\lambda_i, \Lambda_i)}_{\text{Path Expansion}}\right] \\ &= 2mn - m + 3K + \sum_{i=1}^{m-1}[2M(m-i) + 4MK] \\ &= 2mn - m + 3K + M(m^2 - m) + 4MK(m-1)\end{aligned} \tag{4.11}$$

4.4 Proposed adaptive tree search in GSM-MLD

In this section, we propose an adaptive tree search scheme in the GSM-MLD. The proposed algorithm retains the same breadth of the tree search as the GSM-MLD to achieve the near-ML performance. On the other hand, we perform adaptive tree search scheme to reduce the complexity, and to overcome the drawback which the fixed number of tree search algorithm requires high complexity in the high E_b/N_0 region. In the adaptive tree search scheme, we introduce a path metric ratio without the necessity to accurately and dynamically measure SNR. According to the reliability of each survived branch, assign a suitable candidates expansion from a parent node. To decrease the number of lower reliable possible branch, thereby avoid a large amount of the path metric evaluations and sorting.

4.4.1 Reliability evaluation

In this subsection, we derive the reliability evaluation (RE) for all the survived branches in each layer. As above mentioned, the estimate of entry s_i depends on the decided estimates $\hat{s}_j$'s where $j \in [i+1, m]$. Hence, the wrong estimate existing in the decided estimates may cause more erroneous estimates of the transmit signal in the following recursion detection. According to MLD, the final

estimate of transmit signal is determined by the path with the smallest path metric. To a certain degree, we can apply the PED to evaluate the reliability of all the survived paths in a detection layer of the tree search. In that sense, we introduce a ratio function among the path metrics in the i-th layer, where $i \in [1, m]$, defined as

$$\beta_i(l) = \frac{\Lambda_i^{(l)}}{\Lambda_i^{(1)}}, l \in [1, M] \tag{4.12}$$

where $\Lambda_i^{(1)}$ denotes the smallest path metric after sorting the survived branch in the i-th layer. Note that the layer number i is decreased such that $i := m$ down to 1 successively. In general, the survived path $\Pi_i^{(1)}$ with the high probability should be the correct path if the channel is better-conditioned. Hence, we assume that the survived path $\Pi_i^{(1)}$ has the most possible to be correct path. In terms of the path metric ratio $\beta_i(l)$ in (4.12), we indirectly evaluate the reliability of the l-th branch in the i-th layer. That is, if $\Lambda_i^{(l)}$ is much larger than $\Lambda_i^{(1)}$ and thus $\beta_i(l)$ is larger, it is unlikely that the correct path is the l-th path. The ratio function $\beta_i(l)$ can be the measure of evaluating the reliability for the l-th branch.

In order to adaptively control the candidates expansion according to $\beta_i(l)$, we assume that the number of the candidates should be an integer between 1 and K in the $(i-1)$-th layer. That means the candidates from a parent node is determined by the path metric ratio in the previous layer. We define the number of the candidates as $\rho_{i-1}(l)$ for the l-th survived branch in the $(i-1)$-th layer. In order to find a proper rule to adaptively assign the candidates for a survived branch, we consider a decision function of the i-th layer as

$$\alpha(i) = \frac{i}{m} \cdot C, i \in [1, m] \tag{4.13}$$

where C is a constant to be predetermined, which is the tradeoff between the BER performance and the computational complexity.

The parameter $\alpha(i)$ is depended on the detection layer i. Since the tree search starts with the last entry of $\mathbf{s}$, the path metric at first in the larger numbered layer is insufficient to reflect the whole channel condition. To retain the correct path, the parameter $\alpha(i)$ is defined to be proportional to the value of the detection layer i. Using the variable decision function, the value $\alpha(m)$ is maximum as

C. Correspondingly, the value $\alpha(1)$ is minimum as C/m. The decision value becomes strict as the detected layers increase. The various decision based on the layer number significantly reduces the number of candidates in the smaller numbered layer seen in the numerical results. For K^2-QAM, the number of the finite set for the real-valued transmit signals is K. We compare $\beta_i(l)$ with $\{\alpha(i), 2\alpha(i), ..., (K-1)\cdot\alpha(i)\}$. Then we have

$$\rho_{i-1}(l) = \begin{cases} K, & \text{for } \beta_i(l) \in [0, \alpha(i)] \\ K-x, & \text{for } \beta_i(l) \in (x\cdot\alpha(i), (x+1)\cdot\alpha(i)] \\ 1, & \text{for } \beta_i(l) > (K-1)\cdot\alpha(i) \end{cases} \tag{4.14}$$

where $i \in [2, m]$ and $x \in [1, K-2]$.

Let $\alpha(i)$ denote the basic unit to divide $\beta_i(l)$ into K regions. Then, according to $\beta_i(l)$ in which region resolves the number of candidates $\rho_{i-1}(l)$. Ranking the constellation points with the nearest distance to $\tilde{s}_{i-1}^{(l)}$ obtained in (4.8), the candidates in the $(i-1)$-th layer consist of the nearest constellation point up to the $\rho_{i-1}(l)$-th nearest constellation point. In the case of 16QAM, if $\tilde{s}_{i-1}^{(l)} = 2.5$, the order of candidates is $\{3,1,-1,-3\}$. If $\rho_{i-1}(l) = 2$, the candidate selection from the constellation points is $\{3, 1\}$.

Due to the definitions of the branch metric and the path metric in the GSM-MLD, the ED can be expressed as

$$\|\mathbf{y} - \mathbf{H}\mathbf{s}\|^2 = \sum_{i=1}^{m} \left|\hat{\mathbf{h}}_i\right|^2 \left|\tilde{s}_i - \hat{s}_i\right|^2 \tag{4.15}$$

The maximum likelihood detection is very simple to implement since the decision criterion depends on the ED. This detection scheme minimizes the probability of bit error if the transmitted messages are equally likely. Since the proposed detection expects to achieve the near-ML performance as GSM-MLD, we first investigate the cumulative distribution function (CDF) of the minimum path metric. Giving examples in Figs. 4.1 and 4.2, we plot the CDF of the minimum path metric compared the GSM-MLD with the proposed detection with $C = \{2, 4, 8\}$ for 16QAM and 64QAM, respectively. The results illustrate that the CDF curve of the proposed detection closely approaches the that of GSM-MLD as the value

of constant C increases. The constant $C = 4$ is almost optimal value between the BER performance and the complexity.

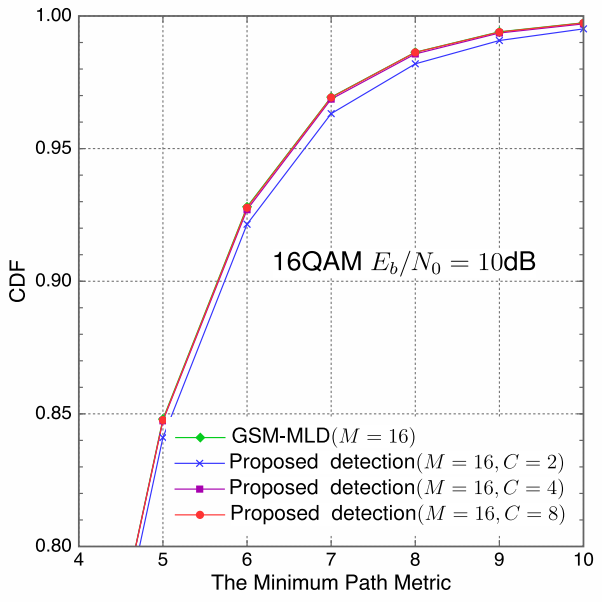

Figure 4.1: The CDF of the minimum path metric at E_b/N_0=10dB for 16QAM.

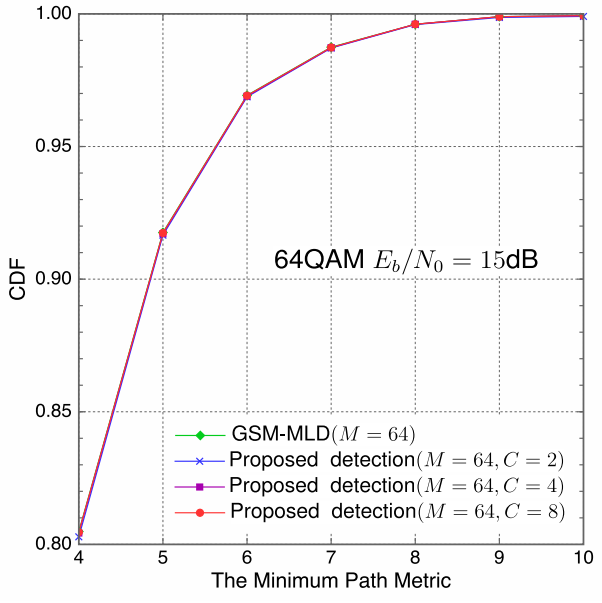

Figure 4.2: The CDF of the minimum path metric at E_b/N_0=15dB for 64QAM.

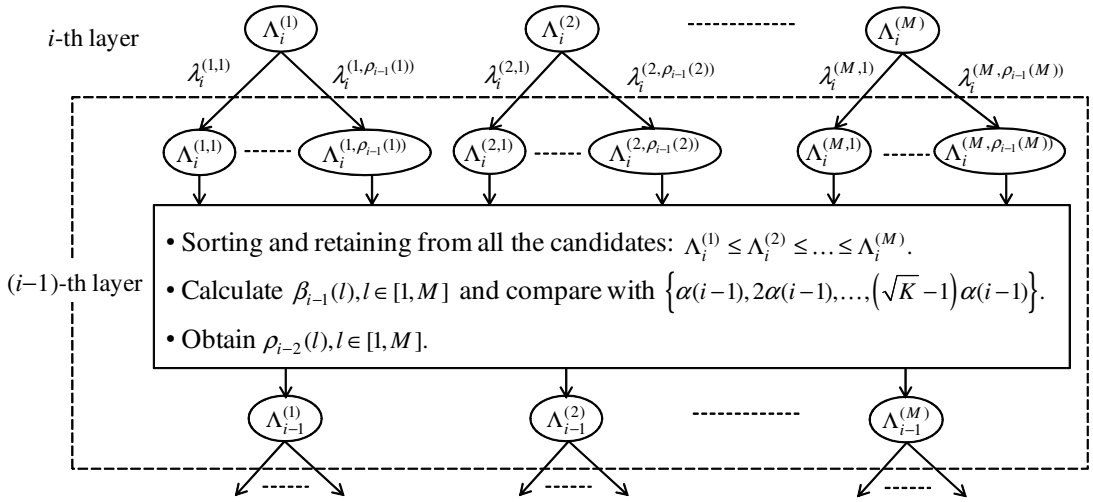

Figure 4.3: Example of the adaptive tree search scheme from the i-th layer to the $(i-1)$-th layer.

4.4.2 Proposed detection scheme

As an example, Fig. 4.3 illustrates an adaptive tree search scheme from the i-th layer to the $(i-1)$-th layer. In the $(i-1)$-th layer, we first perform the path expansion from M survived branches in the i-th layer. Since the adaptive tree search scheme is executed, the branch metric and the path metric can be expressed as $\lambda_{i-1}^{(1,1)}, \ldots, \lambda_{i-1}^{(1,\rho_{i-1}(1))}, \lambda_{i-1}^{(2,1)}, \ldots, \lambda_{i-1}^{(2,\rho_{i-1}(2))}, \lambda_{i-1}^{(M,1)}, \ldots, \lambda_{i-1}^{(M,\rho_{i-1}(M))}$ and $\Lambda_{i-1}^{(1,1)}, \ldots, \Lambda_{i-1}^{(1,\rho_{i-1}(1))}, \Lambda_{i-1}^{(2,1)}, \ldots, \Lambda_{i-1}^{(2,\rho_{i-1}(2))}, \Lambda_{i-1}^{(M,1)}, \ldots, \Lambda_{i-1}^{(M,\rho_{i-1}(M))}$, respectively. Note that $\lambda_{i-1}^{(l,k)}$ represents the branch metric expanded from the l-th branch in the $(i-1)$-th layer. We calculate the path metric for the possible branches as $\Lambda_{i-1}^{(l,k)} = \lambda_{i-1}^{(l,k)} + \Lambda_i^{(l)}$. Hence, $\sum_{l=1}^{M} \rho_{i-1}(l)$ denotes the total number of all the children nodes in the $(i-1)$-th layer, which should be equal to or less than MK. Next, sort $\sum_{l=1}^{M} \rho_{i-1}(l)$ path metrics and select M with the smallest path metric. Based on the sorted $\Lambda_{i-1}^{(l)}$, calculate the number of candidates expansion $\rho_{i-2}(l), l \in [1, M]$, for the next layer. The proposed adaptive tree search scheme is summarized as follows:

- *Step* 1: Set a fixed value of M. For K^2-QAM, if $K < M$, define a layer number q such that K^{m-q+1} should be equal to or more than M in order to select M branches with the smallest path metric among all of the possible

branches. Then, the candidates from the m-th layer down to the q-th layer are all the constellation points.

- *Step* 2: Start the adaptive candidate selection scheme from the q-th layer. According to $\beta_q(l)$ and $\alpha(q)$, the number of the candidates $\rho_{q-1}(l)$ for the l-th survived branch in the $(q-1)$-th layer is obtained in (4.14). Hence, the number of the possible branches in the $(q-1)$-th layer is from M to MK.

- *Step* 3: Proceed to the next stage of the $(q-1)$-th layer. Rank the constellation points for the l-th survived branches with the nearest distance to $\tilde{s}_{q-1}^{(l)}$ in (4.8). According to $\rho_{q-1}(l)$, we select the candidates from the constellation points and calculate the path metric for the possible branches. M branches are retained with the smallest path metric to the next layer. The same operations are executed until the first layer.

- *Step* 4: Obtain the detection result of the estimate $\hat{\mathbf{s}}^{(1)} = \left[\hat{s}_1^{(1)}, \hat{s}_2^{(1)}, \cdots, \hat{s}_m^{(1)}\right]^{\mathrm{T}}$.

4.4.3 Complexity analysis

The proposed detection reduces the complexity of the path metric evaluations with less possible branches. The additional complexity $\mathcal{N}_A$ is the computations for the path metric ratio in (4.12), which require a complexity of $(M-1)(q-1)$ flops. If we fix the value of the constant C, $\alpha(i)$ in (4.13) is predetermined. Hence, the computational complexity of $\alpha(i)$ is neglect. The complexity of the proposed detection consists of three parts: the fixed complexity from the m-th layer down to the q-th layer, the various complexity from the $(q-1)$-th layer down to the first layer, and the above additional complexity. The fixed complexity of the proposed detection $\mathcal{N}_F$ including the computation of $\tilde{\mathbf{s}}$ in (4.8) can be derived as

$$\begin{aligned}\mathcal{N}_F &= 2mn - m + K\mathcal{N}(\lambda_m) + \sum_{i=q}^{m-1}\left[K^{m-i}\mathcal{N}(\tilde{s}_i) + K^{m-i+1}\mathcal{N}(\lambda_i, \Lambda_i)\right] \\ &= 2mn - m + 3K + \sum_{i=q}^{m-1}\left[2(m-i)K^{m-i} + 4K^{m-i+1}\right]\end{aligned} \tag{4.16}$$

The various complexity of the proposed detection $\mathcal{N}_V$ is varied with the number of the children nodes, derived as

$$\begin{aligned}\mathcal{N}_V &= \sum_{i=1}^{q-1}\left\{M\mathcal{N}(\tilde{s}_i) + \left[\sum_{l=1}^{M}\rho_i(l)\right]\mathcal{N}(\lambda_i,\Lambda_i)\right\} \\ &= \sum_{i=1}^{q-1}\left[2M(m-i) + 4\sum_{l=1}^{M}\rho_i(l)\right]\end{aligned} \tag{4.17}$$

where $\sum_{l=1}^{M}\rho_i(l)$ denotes the total number of the children nodes in the i-th layer. As a result, the complexity of the proposed detection $\mathcal{N}_{Prop.}$ which excludes the complexity of the GSO reduction can be derived as

$$\begin{aligned}\mathcal{N}_{Prop.} &= \mathcal{N}_A + \mathcal{N}_V + \mathcal{N}_F \\ &= (M-1)(q-1) + \sum_{i=1}^{q-1}\left[2M(m-i) + 4\sum_{l=1}^{M}\rho_i(l)\right] \\ &+ 2mn - m + 3K + \sum_{i=q}^{m-1}\left[2(m-i)K^{m-i} + 4K^{m-i+1}\right]\end{aligned} \tag{4.18}$$

4.5 Numerical results

The computer simulations were carried out for QPSK, 16QAM and 64QAM in the 4×4 and 8×8 MIMO system, respectively. We assume the channel is the typical flat Rayleigh fading. The performances of the different detection algorithms are measured by the BER characteristics and the complexity. The complexity of the tree search detection is determined by the amount of the path metric evaluations.

4.5.1 BER characteristics

Figures. 4.4 - 4.9 show the BER characteristics versus E_b/N_0 using the full MLD, the conventional QRM-MLD, the GSM-MLD and the proposed detection, respectively. The value of M in the proposed detection is the same as that in the QRM-MLD and the GSM-MLD, i.e. $M = 8$ for QPSK, $M = 16$ for 16QAM and $M = 64$ for 64QAM in the 4×4 MIMO system, and $M = 16$ for QPSK, $M = 64$ for 16QAM and $M = 128$ for 64QAM in the 8×8 MIMO system, respectively. For

the proposed detection, the constant C in the decision function is predetermined and assigned as the suitable value to approach the near-ML performance.

As seen in Fig. 4.4, we chose $M = 8$, which is large enough for the QPSK in the 4×4 MIMO system, and hence the BER curves of the GSM-MLD and the QRM-MLD totally achieve the ML performance. For the proposed detection, the BER curve with $C = 8$ is almost equivalent to the BER characteristics of the GSM-MLD or the QRM-MLD. The proposed detection with $C = 4$ has less possible branches in each layer, and hence the BER curve is about 1dB worse than the BER of the QRM-MLD at a BER of 10^{-5}. In Fig. 4.6, the value of $M = 16$ is assigned for the 16QAM in the 4×4 MIMO system. For the proposed detection, the BER curve with $C = 8$ is almost equivalent to the BER characteristics of the GSM-MLD or the QRM-MLD. The proposed detection with $C = 2$ has less possible branches in each layer, and the BER curve is about 1dB worse than the BER of the QRM-MLD at a BER of 10^{-5}. The BER curves of the QRM-MLD and the GSM-MLD with $M = 64$ for 64QAM are equivalent to the BER characteristics of the full MLD in Fig. 4.8. For the proposed detection, the BER curves with $C = \{4, 8\}$ achieve a near-ML performance. The proposed detection with $C = 2$ remarkably reduces the possible branches in each layer, and hence the BER curve is about 0.5dB worse than that of the QRM-MLD at a BER of 10^{-5}.

In the 8×8 MIMO system, we compare the BER characteristics of the proposed detection with $C = \{4, 8, 16\}$ for QPSK, $C = \{16, 32, 64\}$ for 16QAM and $C = \{16, 32, 64\}$ for 64QAM, respectively. The proposed detection achieves better BER performance as the value of C increases. In order to achieve the near-ML performance, the value of C in the proposed detection is 16 for QPSK, 32 for 16QAM and 64 for 64QAM as the suitable choice, respectively. From the BER characteristics, the proposed scheme is more efficient in the high modulation order. In the large size MIMO, the value of C requires a large number. The factor of C is a tradeoff parameter between the BER performance and the complexity described in the following subsection.

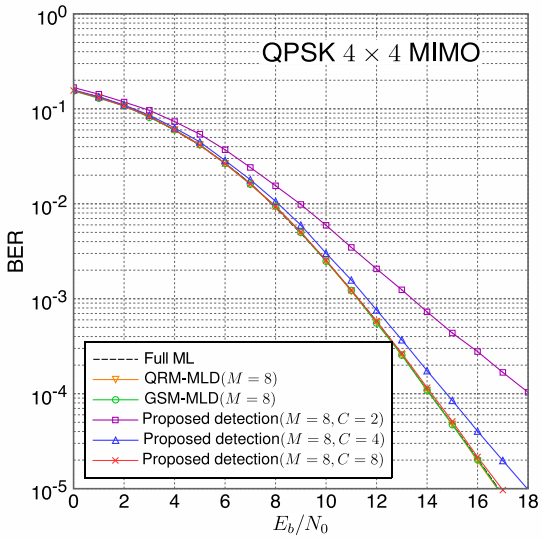

Figure 4.4: The E_b/N_0 vs. BER characteristics in the 4×4 MIMO system: QPSK.

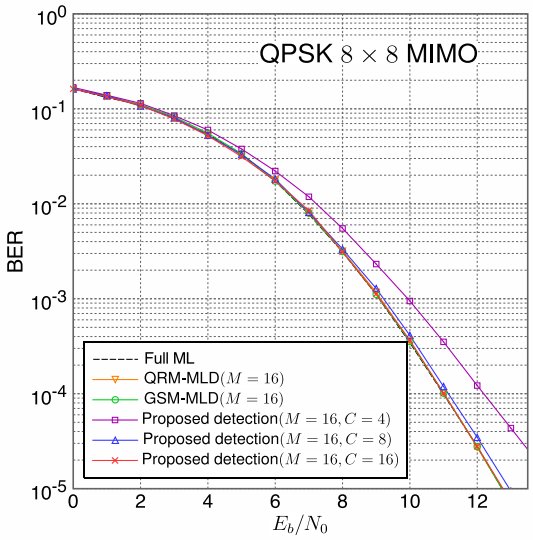

Figure 4.5: The E_b/N_0 vs. BER characteristics in the 8×8 MIMO system: QPSK.

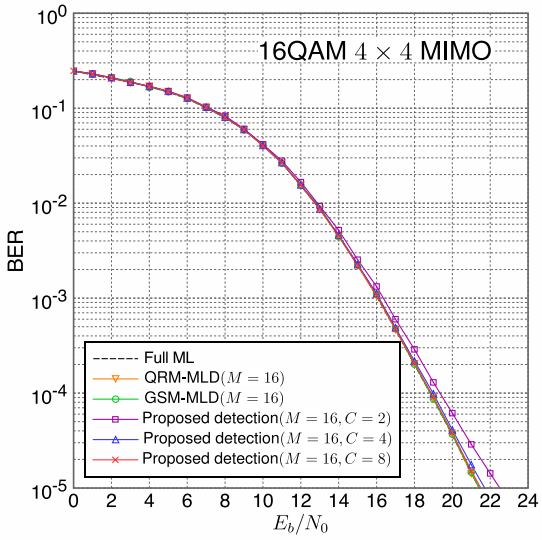

Figure 4.6: The E_b/N_0 vs. BER characteristics in the 4×4 MIMO system: 16QAM.

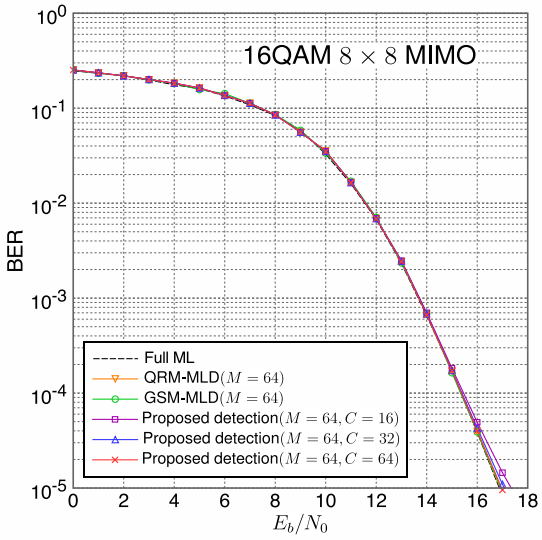

Figure 4.7: The E_b/N_0 vs. BER characteristics in the 8×8 MIMO system: 16QAM.

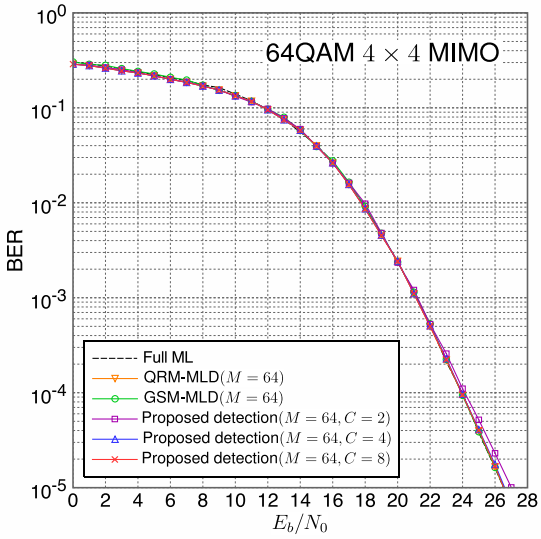

Figure 4.8: The E_b/N_0 vs. BER characteristics in the 4×4 MIMO system: 64QAM.

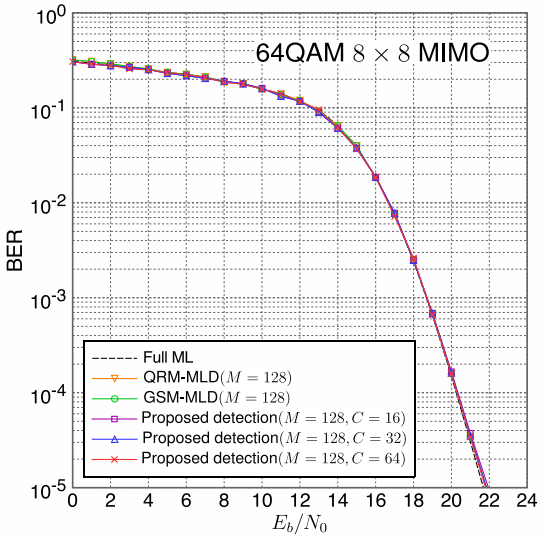

Figure 4.9: The E_b/N_0 vs. BER characteristics in the 8×8 MIMO system: 64QAM.

4.5.2 Computational complexity

We firstly evaluated the average number of possible branches in each layer for the proposed detection with the different values of C, seen in Figs. 4.10 - 4.15. For the QRM-MLD or GSM-MLD, the number of the possible branches in each layer is fixed. On the contrary, the proposed detection in the adaptive stage is varied within a certain range. We observed the average number of possible branches in each layer in the various E_b/N_0.

For the QRM-MLD or GSM-MLD, the number of the possible branches in each layer is fixed to 16 if $M = 8$ for QPSK, 64 if $M = 16$ for 16QAM and 512 if $M = 64$ for 64QAM in the 4×4 MIMO system, respectively. In Fig. 4.10, the average number of the possible branches in the adaptive stage is varied within a certain range from 8 to 16 for QPSK. In particular, for the curve with $C = 2$ in Fig. 4.10 (a), the average number of the possible branches is 8 in any E_b/N_0. However, the BER characteristics are degraded in the high E_b/N_0 region. It should be noticed that the number of the low reliable possible branches in the proposed detection with $C = 4$ in Fig. 4.10 (b) is almost halved, compared to the fixed number of 16. Furthermore, the BER curve of the proposed detection

with $C = 4$ is about 1dB worse than that of the full MLD at a BER of 10^{-5}. In addition, the BER of the proposed detection with $C = 8$ shown in Fig. 4.4 can retain the near-ML performance. The number of the possible branches for QPSK is less reduced. As seen in Fig. 4.12, the average number of the possible branches in the adaptive stage is varied within a certain range from 16 to 64 for 16QAM. In particular, for the curve with $C = 2$ in Fig. 4.12 (a), the average number of the possible branches is close to 16 if the BER characteristics are less than 10^{-2}. Furthermore, the BER curve of the proposed detection with $C = 2$ is about 1dB worse than that of the full MLD at a BER of 10^{-5}. It should be noticed that the number of the low reliable possible branches in the proposed detection with $C = 4$ in Fig. 4.12 (b) is halved or more reduced, compared to the fixed number of 64. The BER curve of the proposed detection with $C = 4$ is about 0.2dB worse than that of the full MLD at a BER of 10^{-5}. In addition, the BER of the proposed detection with $C = 8$ shown in Fig. 4.6 can retain the near-ML performance. The number of the possible branches in Fig. 4.12 (c) can remarkably reduce in the high E_b/N_0 region. Figures. 4.14 shows the average number of possible branches in each layer for the proposed detection for 64QAM. The average number of the possible branches in the adaptive stage is varied within a certain range from 64 to 512. Similarly to 16QAM, the curves with $C = 2$ in Fig. 4.14 (a) are close to 64 if the BER characteristics are less than 10^{-2}, and correspondingly the BER curve with $C = 2$ as illustrated in Fig. 4.8 has about 0.5dB performance loss compared to the full MLD at a BER of 10^{-5}. If the channel is better-conditioned, the average numbers of the possible branches of the proposed detection with $C = \{4, 8\}$ in the adaptive stage are in the range from 64 to 128, which is much less than the fixed number of 512 compared to the conventional QRM-MLD. Meanwhile, the BER curves of the proposed detection with $C = \{4, 8\}$ achieve the ML performance corresponding to Fig. 4.8.

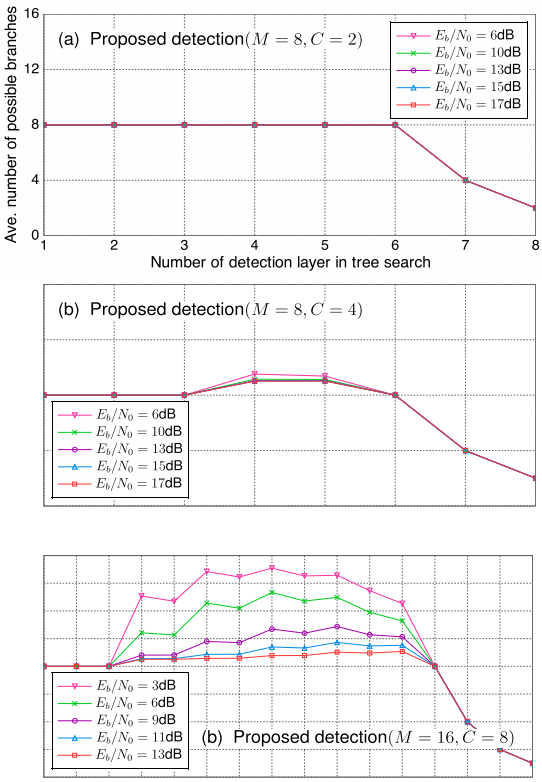

Figure 4.10: The average number of possible branches in each layer of tree search at various E_b/N_0 in the 4×4 MIMO system: QPSK.

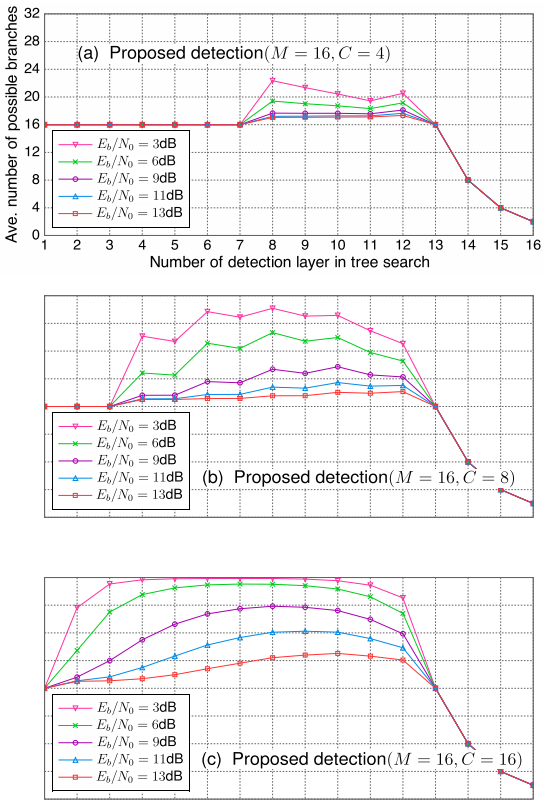

Figure 4.11: The average number of possible branches in each layer of tree search at various E_b/N_0 in the 8×8 MIMO system: QPSK.

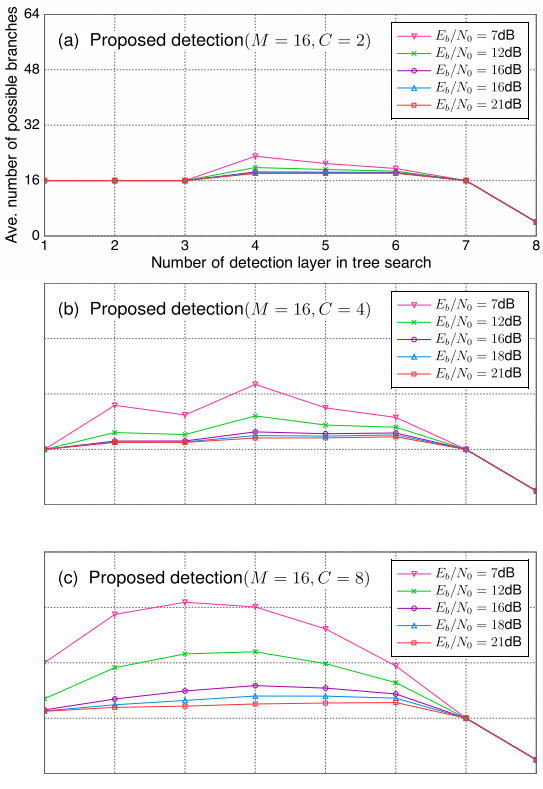

Figure 4.12: The average number of possible branches in each layer of tree search at various E_b/N_0 in the 4×4 MIMO system: 16QAM.

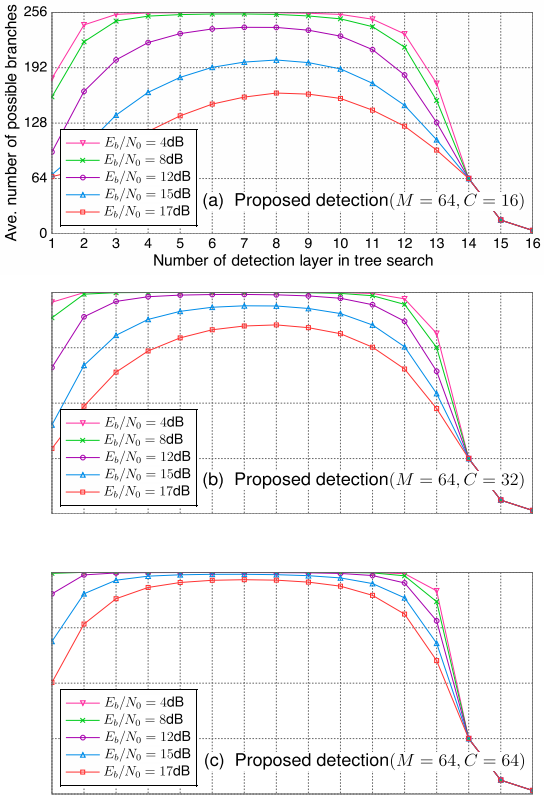

Figure 4.13: The average number of possible branches in each layer of tree search at various E_b/N_0 in the 8×8 MIMO system: 16QAM.

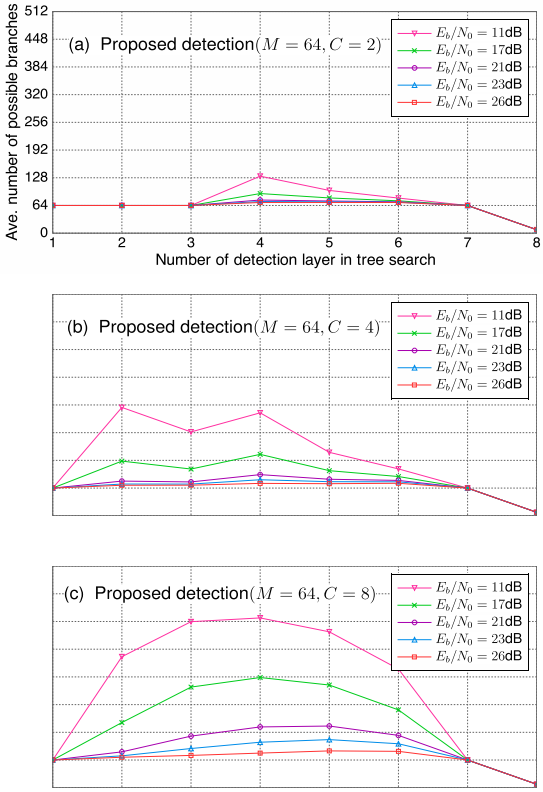

Figure 4.14: The average number of possible branches in each layer of tree search at various E_b/N_0 in the 4×4 MIMO system: 64QAM.

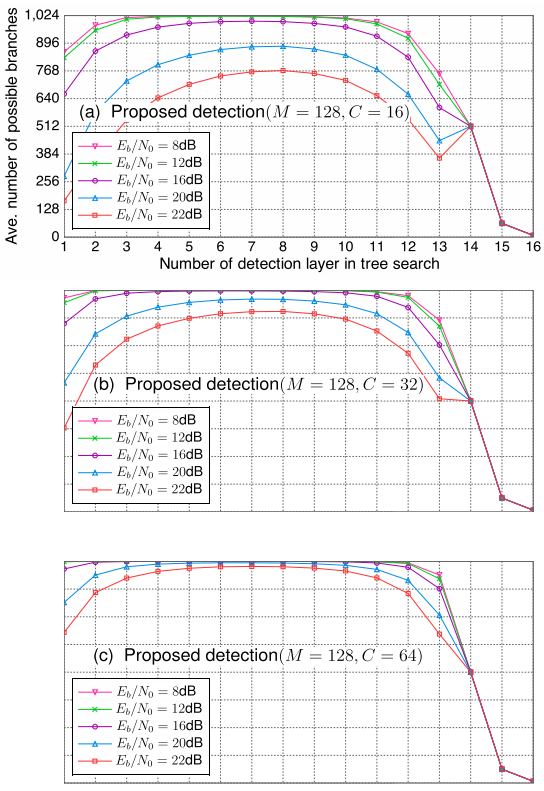

Figure 4.15: The average number of possible branches in each layer of tree search at various E_b/N_0 in the 8×8 MIMO system: 64QAM.

For the 8×8 MIMO system, the number of the possible branches in each layer is fixed to 32 if $M = 16$ for QPSK, 512 if $M = 64$ for 16QAM and 1024 if $M = 128$ for 64QAM, respectively. As seen in Fig. 4.11, 4.13 and 4.15, we observe that the proposed detection with a large value of C provides the near-ML BER performance. Hence, the number of the low reliable possible branches is less reduced. In Fig. 4.11(c), the average number of the possible branches in the adaptive stage is varied within a certain range from 16 to 22 for QPSK, compared to the fixed number of 32 for the QRM-MLD or the GSM-MLD. The proposed detection with $C = 32$ for 16QAM and 64QAM can achieve the near-ML BER performance. However, corresponding to Fig. 4.13 and Fig. 4.15, the number of the low reliable possible branches is less reduced even in the high E_b/N_0. Hence,

the complexity of the proposed detection should be less reduced.

From the simulation results of Figs. 4.10 - 4.15, the adaptive decision using the threshold in each detection layer is determined by the constant C, which is the tradeoff between the BER performance and the complexity.

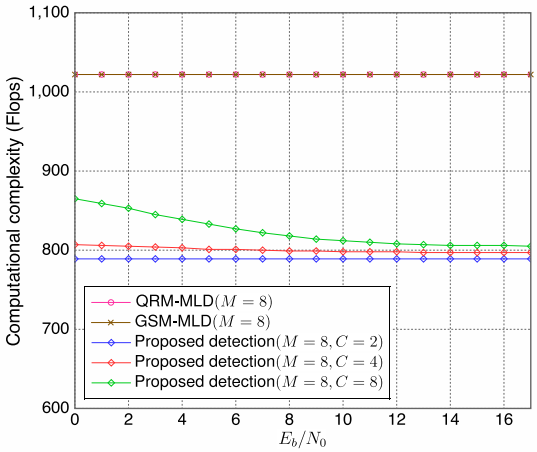

Figure 4.16: The average complexity comparison for three detection schemes in the 4×4 MIMO system: QPSK.

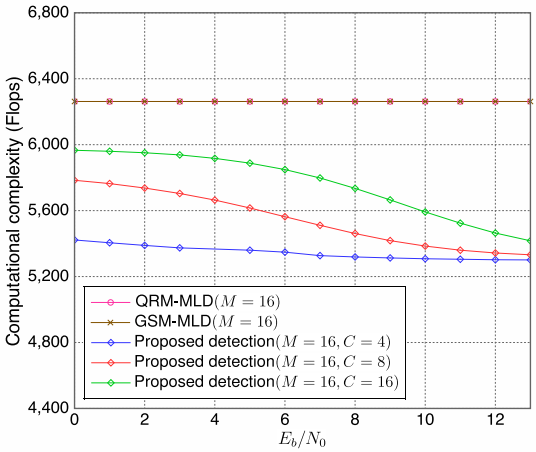

Figure 4.17: The average complexity comparison for three detection schemes in the 8×8 MIMO system: QPSK.

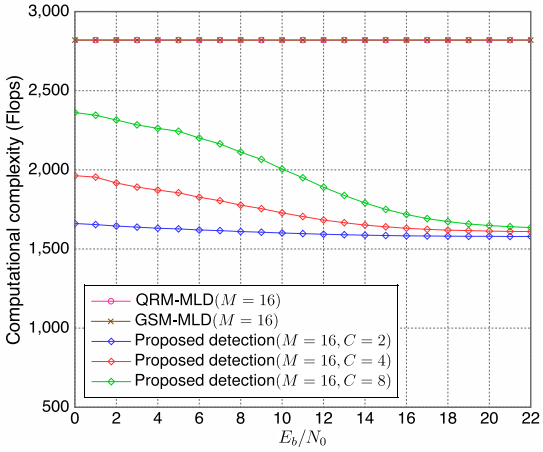

Figure 4.18: The average complexity comparison for three detection schemes in the 4×4 MIMO system: 16QAM.

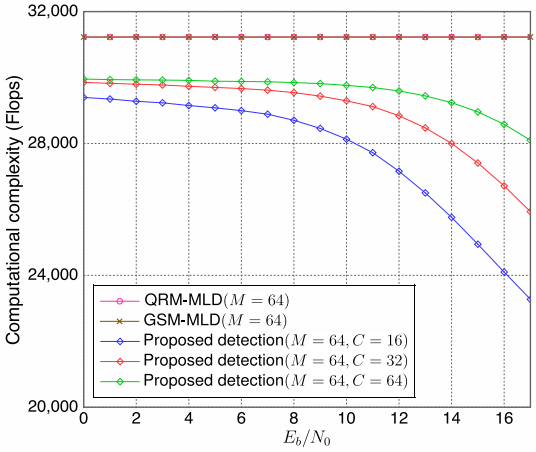

Figure 4.19: The average complexity comparison for three detection schemes in the 8×8 MIMO system: 16QAM.

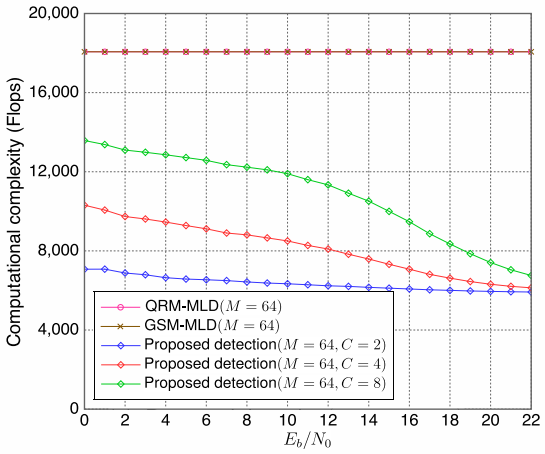

Figure 4.20: The average complexity comparison for three detection schemes in the 4×4 MIMO system: 64QAM.

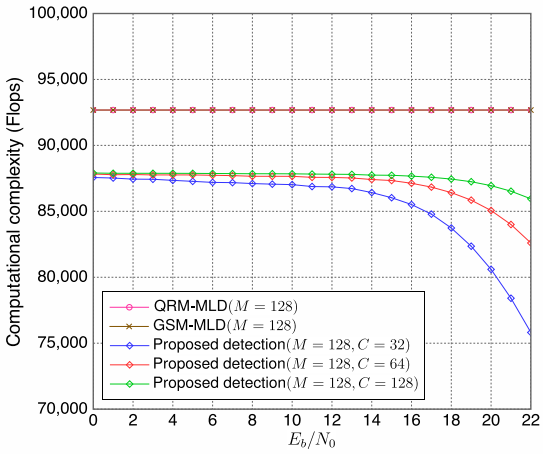

Figure 4.21: The average complexity comparison for three detection schemes in the 8×8 MIMO system: 64QAM.

According to the average number of possible branches, we present the computational complexity of the proposed detection in Figs. 4.16 - 4.21 for QPSK, 16QAM and 64QAM in the 4×4 and 8×8 MIMO systems, respectively. We compare the complexity of the proposed detection with the complexity of QRM-MLD as seen in Chapter 2.4.

In the 4×4 MIMO system, we set the layer number q in (4.16) - (4.18) as $q = m - 2$ for QPSK. Due to $M = 16$ for 16QAM and $M = 64$ for 64QAM, the layer number q in (4.16) - (4.18) is set as $q = m - 1$. From the numerical results, the GSM-MLD has the same complexity with the conventional QRM-MLD. Since the GSO reduction is computationally-simple and the transform matrix is with unity diagonal entries, the soft estimate of $\tilde{\mathbf{s}}$ is directly obtained in (4.8) with no division operation. It is convenient to rank the constellation points according to $\tilde{\mathbf{s}}$ in the adaptive stage. The adaptive tree search scheme is performed using the path metric ratio function, and thus the number of the possible branches in each layer of adaptive stage is remarkably reduced. Hence, the computational complexity of the proposed detection is much lower than the conventional QRM-MLD, especially in the high E_b/N_0 region. From Figs. 4.16, 4.18 and 4.20, the complexity of the proposed detection at a BER of 10^{-5} is about 21%, 40% and 64% smaller than that of the QRM-MLD for QPSK, 16QAM and 64QAM, respectively.

In the 8×8 MIMO system, we set the layer number q in (4.16) - (4.18) as $q = m - 3$ for QPSK. Due to $M = 64$ for 16QAM and $M = 128$ for 64QAM, the layer number q in (4.16) - (4.18) is set as $q = m - 2$. From the numerical results, the GSM-MLD has the same complexity with the conventional QRM-MLD. From Figs. 4.17, 4.19 and 4.21, the complexity of the proposed detection at a BER of 10^{-5} is about 14%, 17% and 18% smaller than that of the QRM-MLD for QPSK, 16QAM and 64QAM, respectively.

4.6 Chapter summary

In this chapter, introducing the Gram-Schmidt Orthogonalization procedure to reduce the channel matrix, we proposed a MIMO detection scheme using the adaptive tree search with variable path expansion in the GSM-MLD algorithm. The adaptive tree search scheme was to adaptively control the candidates for each survived branch in the tree search. We adopted a path metric ratio function to evaluate the reliability for all the survived branches. To decrease the number of the low reliable candidates in each layer, a large amount of the computation for the path metric was avoided. Hence, the complexity of the proposed detection should be reduced.

Since the GSO reduction was computationally-simple, it required very low complexity for the LR operations. In the 4×4 MIMO system, the proposed adaptive scheme was very efficient, especially for the high modulation. In particular in the high E_b/N_0 region, the complexity of the proposed detection in the 4×4 MIMO system was about 79%, 60% and 36% of that of the QRM-MLD for QPSK, 16QAM and 64QAM, respectively. The proposed detection can provide the near-ML performance with relatively lower complexity. For the large size MIMO system, in order to achieve the near-ML performance, the number of the low reliable possible branches was less reduced. Hence, the proposed detection required a little lower complexity than the complexity of the QRM-MLD.

As a result, it was worthy for applying even to the high modulation order in the small size MIMO system.

Chapter 5

An Improved Quantization Scheme for Lattice-Reduction Aided MIMO Detection Based on Gram-Schmidt Orthogonalization

In the previous chapter, we observed that the exhaustive tree search of MIMO detection required high complexity especially in the high modulation and the large size MIMO system. Hence combining the LR technology, we further reduce the complexity compared to the proposed scheme in Chapter 4. Meanwhile, the new scheme can achieve the near-ML performance in terms of deceasing the quantization errors, which are the problem of the conventional LRA detection.

5.1 Introduction

For the LRA MIMO detection, the detection errors are mainly generated from the channel noise and the quantization errors in the signal estimation stage. The quantization step applies the simple rounding operation, which often leads to the quantization error. If this error occurs in a row of the transmit signal, it has to propagate to many symbols in the subsequent signal estimation and result in degrading the BER performance. Therefore, the objective of the proposed detection pays attention on solving this problem in the quantization step.

In this chapter, we introduce the Gram-Schmidt orthogonalization after the LLL algorithm. Using the orthogonal column vectors of the channel matrix, the interferences affected from other antennas are diminished. Based on the LR and GS aided detection, we investigate that the rounding quantization errors occasionally occur in such a case that the decimal fraction of the estimate symbols should be close to 0.5. Therefore, the proposed quantization scheme applies a simple tree search in order to obtain an optimum quantization results. There are two expansion candidates from each parent branch, which are the rounding integer and the adjacent integer. Then, we introduce a threshold function in order to survive at most two candidates for each entry of the signal vectors according to the path metric, in order to retain the quantization candidate with the branch metric close to 0.25 and rarely correct the quantization error. The simulations show that the propose detection can achieve near-ML performance and offers significant reduction in computational complexity compared to the QRM-MLD.

5.2 System model and conventional LRA detection

5.2.1 System model

The system model is employed the real-valued channel matrix and vectors as same as Chapter 4. Recall (4.1) as

$$\mathbf{y} = \mathbf{H}\mathbf{s} + \mathbf{z} \tag{5.1}$$

where the equivalent real-valued channel matrix and vectors letting $n = 2N_r$ and $m = 2N_t$ are defined as

$$\begin{aligned} \mathbf{H} &\triangleq \begin{bmatrix} \mathrm{Re}[\mathbf{H}^c] & -\mathrm{Im}[\mathbf{H}^c] \\ \mathrm{Im}[\mathbf{H}^c] & \mathrm{Re}[\mathbf{H}^c] \end{bmatrix} \in \mathbb{R}^{n \times m}, \\ \mathbf{s} &\triangleq \begin{bmatrix} \mathrm{Re}[\mathbf{s}^c] \\ \mathrm{Im}[\mathbf{s}^c] \end{bmatrix}, \ \mathbf{y} \triangleq \begin{bmatrix} \mathrm{Re}[\mathbf{y}^c] \\ \mathrm{Im}[\mathbf{y}^c] \end{bmatrix}, \text{ and } \mathbf{z} \triangleq \begin{bmatrix} \mathrm{Re}[\mathbf{z}^c] \\ \mathrm{Im}[\mathbf{z}^c] \end{bmatrix} \end{aligned} \tag{5.2}$$

We define the dimension of the real-valued channel matrix $\mathbf{H}$ to be $n \times m$.

The dimensions of the vectors in (5.2) are given as $\mathbf{y} \in \mathbb{R}^{n\times 1}, \mathbf{z} \in \mathbb{R}^{n\times 1}$ and $\mathbf{s} \in \mathbb{Z}^{m\times 1}$, where $\mathbb{Z}$ denotes the finite set of the real-valued transmitted signals. Hassibi proposed a MMSE detector with the extended matrix form as

$$\bar{\mathbf{y}} \triangleq \begin{bmatrix} \mathbf{y} \\ \mathbf{0}_m \end{bmatrix}, \ \bar{\mathbf{H}} \triangleq \begin{bmatrix} \mathbf{H} \\ \sqrt{\gamma^{-1}}\mathbf{I}_m \end{bmatrix}, \ \bar{\mathbf{z}} \triangleq \begin{bmatrix} \mathbf{z} \\ -\sqrt{\gamma^{-1}}\mathbf{s} \end{bmatrix} \tag{5.3}$$

where $\gamma = E_s/N_0$ with $E_s = E[\|\mathbf{s}\|^2]/m$. Then it holds instead of (5.1) that

$$\bar{\mathbf{y}} = \bar{\mathbf{H}}\mathbf{s} + \bar{\mathbf{z}} \tag{5.4}$$

5.2.2 Conventional LRA detection

The channel matrix can be QR-decomposed as $\bar{\mathbf{H}}$=$\mathbf{QR}$, where $\mathbf{Q}$ is a unitary matrix, having the orthogonal column vectors with the unit norm. The channel matrix $\mathbf{R}$=$[\mathbf{r}_1, \mathbf{r}_2, \ldots, \mathbf{r}_m]$ is an $m \times m$ upper triangular matrix, which retains the property of the channel matrix. The real LLL algorithm in Table 5.1 is to transform a given lattice basis $\mathbf{R}$ into a new reduced basis $\tilde{\mathbf{R}}$, of which column vectors are nearly orthogonal. In the same method as (3.16), the scaled and shifted receive signal vector can be expressed as

$$\bar{\mathbf{y}}^{\mathcal{S}} \triangleq \frac{\bar{\mathbf{y}}}{2} + \frac{K-1}{2}\bar{\mathbf{H}}\mathbf{1}_m = \bar{\mathbf{H}}\left(\frac{\mathbf{s}}{2} + \frac{K-1}{2}\mathbf{1}_m\right) + \frac{\bar{\mathbf{z}}}{2} \tag{5.5}$$

Using $\tilde{\mathbf{R}}$, $\tilde{\mathbf{Q}}$ and $\mathbf{T}$, the system model in (5.5) is rewritten as

$$\begin{aligned} \bar{\mathbf{y}}^{\mathcal{S}} &= \bar{\mathbf{H}}\left(\frac{\mathbf{s}}{2} + \frac{K-1}{2}\mathbf{1}_m\right) + \frac{\bar{\mathbf{z}}}{2} \\ &= \mathbf{QR}\left(\frac{\mathbf{s}}{2} + \frac{K-1}{2}\mathbf{1}_m\right) + \frac{\bar{\mathbf{z}}}{2} \\ &= \bar{\mathbf{H}}'\left(\mathbf{T}^{-1}\left(\frac{\mathbf{s}}{2} + \frac{K-1}{2}\mathbf{1}_m\right)\right) + \frac{\bar{\mathbf{z}}}{2} \\ &= \tilde{\mathbf{Q}}\tilde{\mathbf{R}}\left(\mathbf{T}^{-1}\left(\frac{\mathbf{s}}{2} + \frac{K-1}{2}\mathbf{1}_m\right)\right) + \frac{\bar{\mathbf{z}}}{2} \\ &\equiv \tilde{\mathbf{Q}}\tilde{\mathbf{R}}\mathbf{v} + \frac{\bar{\mathbf{z}}}{2} \end{aligned} \tag{5.6}$$

where $\bar{\mathbf{H}}' = \tilde{\mathbf{Q}}\tilde{\mathbf{R}} = \mathbf{QRT}$ and the new signal vector $\mathbf{v}$ is defined as $\mathbf{v} \triangleq \mathbf{T}^{-1}\left(\frac{\mathbf{s}}{2} + \frac{K-1}{2}\mathbf{1}_m\right)$. The scaled and shifted vector of $\mathbf{s}$ is defined as $\mathbf{s}^{\mathcal{S}} = \mathcal{S}[\mathbf{s}] \triangleq \frac{\mathbf{s}}{2} + \frac{K-1}{2}\mathbf{1}_m$. The soft estimate $\tilde{\mathbf{v}}$ using the LR-MMSE detection can be derived by

$$\begin{aligned}\tilde{\mathbf{v}}^{(LR-MMSE)} &= \bar{\mathbf{H}}'^{\dagger}\bar{\mathbf{y}}^{\mathcal{S}} \equiv \left(\bar{\mathbf{H}}'^{\mathrm{T}}\bar{\mathbf{H}}'\right)^{-1}\bar{\mathbf{H}}'^{\mathrm{T}}\bar{\mathbf{y}}^{\mathcal{S}} \\ &= \tilde{\mathbf{R}}^{-1}\tilde{\mathbf{Q}}^{\mathrm{T}}\bar{\mathbf{y}}^{\mathcal{S}} = \tilde{\mathbf{R}}^{-1}\mathbf{y}'\end{aligned} \tag{5.7}$$

where $\mathbf{y}' \triangleq \tilde{\mathbf{Q}}^{\mathrm{T}}\bar{\mathbf{y}}^{\mathcal{S}}$ and $\bar{\mathbf{H}}'^{\dagger} = (\tilde{\mathbf{Q}}\tilde{\mathbf{R}})^{\dagger}$.

Table 5.1: Real LLL algorithm

Input: $\mathbf{Q}$, $\mathbf{R}$, and $\mathbf{T} := \mathbf{I}_m$, set δ; Output: $\tilde{\mathbf{Q}}$, $\tilde{\mathbf{R}}$, $\mathbf{T}$

(1) **Initialization**: $\tilde{\mathbf{Q}} := \mathbf{Q}$ and $\tilde{\mathbf{R}} := \mathbf{R}$.
(2) $p = 2$
(3) **while** $p \le m$
(4) **for** $q := p-1$ down to 1
(5) $\mu_{q,p} = \lceil \tilde{r}_{q,p}/\tilde{r}_{q,q} \rfloor$
(6) **if** $\mu_{q,p} \neq 0$
(7) $\tilde{\mathbf{R}}_{1:q,p} := \tilde{\mathbf{R}}_{1:q,p} - \mu_{q,p}\tilde{\mathbf{R}}_{1:q,q}$
(8) $\mathbf{T}_{:,p} := \mathbf{T}_{:,p} - \mu_{q,p}\mathbf{T}_{:,q}$
(9) **end**
(10) **end**
(11) **If** $\delta\tilde{r}^2_{p-1,p-1} > \tilde{r}^2_{p,p} + \tilde{r}^2_{p-1,p}$
(12) Swap columns $p-1$ and p in $\tilde{\mathbf{R}}$ and $\mathbf{T}$
(13) $\boldsymbol{\Theta} = \begin{bmatrix} \alpha & \beta \\ -\beta & \alpha \end{bmatrix}$ with $\alpha = \dfrac{\tilde{\mathbf{R}}_{p-1,p-1}}{\|\tilde{\mathbf{R}}_{p-1:p,p-1}\|^2}$, $\beta = \dfrac{\tilde{\mathbf{R}}_{p,p-1}}{\|\tilde{\mathbf{R}}_{p-1:p,p-1}\|^2}$
(14) $\tilde{\mathbf{R}}_{p-1:p,p-1:m} := \boldsymbol{\Theta}\tilde{\mathbf{R}}_{p-1:p,p-1:m}$
(15) $\tilde{\mathbf{Q}}_{:,p-1:p} := \tilde{\mathbf{Q}}_{:,p-1:p}\boldsymbol{\Theta}^{\mathrm{T}}$
(16) $p := \max\{p-1, 2\}$
(17) **Else** $p := p+1$
(18) **End**

Note that $\mathbf{A}^c_{a:b,c}$ denotes the entries from rows a to b in the c-th column. $\mathbf{A}^c_{a:b,:}$ is the submatrix of $\mathbf{A}^c$ from rows a to b across the whole columns.

The same method is performed as the complex-valued channel matrix and vectors in Chapter 3. We perform the simple rounding quantization operations as $\hat{v}_i = Q\{\tilde{v}_i^{(LR-MMSE)}\}$, $i \in [1, m]$. The new transmit signal vector $\hat{\mathbf{v}}$ in the LR domain is transformed back as $\hat{\mathbf{s}}^{\mathcal{S}} = \mathbf{T}\hat{\mathbf{v}}$. Then, $\hat{\mathbf{s}}$ is shifted back and scaled back, expressing as $\hat{\mathbf{s}} := \mathcal{S}^{-1}[\hat{\mathbf{s}}^{\mathcal{S}}] = 2\hat{\mathbf{s}}^{\mathcal{S}} - (K-1)\mathbf{1}_m$. The final decision $\hat{\mathbf{s}}$ is forced to the nearest constellation points if they are lying outside the original signal constellation as $\hat{\mathbf{s}} := \mathcal{C}[\hat{\mathbf{s}}]$.

5.3 Gram-Schmidt procedure based LRA detection

The real GS orthogonalization algorithm is performed after the real LLL algorithm shown in Table 5.2. This algorithm is to transform the nearly orthogonal lattice basis of $\tilde{\mathbf{R}}$ into the purely orthogonal lattice basis of $\hat{\mathbf{R}}$ and create the transformation matrix $\hat{\mathbf{T}}$ with $\det\{\hat{\mathbf{T}}\}$=1. The upper triangular matrix $\hat{\mathbf{T}}$ with unity diagonal entries and the non-diagonal entries is invertible. The column vectors of the channel matrix $\hat{\mathbf{R}} = \tilde{\mathbf{R}}\hat{\mathbf{T}}$ are mutually orthogonal and span the same subspace as that of the original channel matrix $\bar{\mathbf{H}}$.

Table 5.2: Real Gram-Schmidt orthogonalization algorithm

Input: $\tilde{\mathbf{R}}$, and $\hat{\mathbf{T}} := \mathbf{I}_m$; Output: $\hat{\mathbf{R}}$, $\hat{\mathbf{T}}$	
(1)	**Initialization**: $\hat{\mathbf{R}} := \tilde{\mathbf{R}}$
(2)	**for** p:=2 to m
(3)	**for** q:=$p-1$ down to 1
(4)	$\mu_{q,p} = \hat{r}_{q,p}/\hat{r}_{q,q}$
(5)	$\hat{\mathbf{R}}_{1:q,p} := \hat{\mathbf{R}}_{1:q,p} - \mu_{q,p}\hat{\mathbf{R}}_{1:q,q}$
(6)	$\hat{\mathbf{T}}_{:,p} := \hat{\mathbf{T}}_{:,p} - \mu_{q,p}\hat{\mathbf{T}}_{:,q}$
(7)	**end**
(8)	**end**
(9)	**End**

Using $\hat{\mathbf{R}}$ called the GS-orthogonalized channel matrix and $\hat{\mathbf{T}}$, we have

$$\mathbf{y}' = \tilde{\mathbf{R}}\mathbf{v} + \mathbf{z}' = (\tilde{\mathbf{R}}\hat{\mathbf{T}})(\hat{\mathbf{T}}^{-1}\mathbf{v}) + \mathbf{z}' \equiv \hat{\mathbf{R}}\mathbf{u} + \mathbf{z}' \tag{5.8}$$

where $\mathbf{z}' \triangleq \frac{\tilde{\mathbf{Q}}^{\mathrm{T}}\tilde{\mathbf{z}}}{2}$ and $\mathbf{u} \triangleq \hat{\mathbf{T}}^{-1}\mathbf{v} \equiv (\hat{\mathbf{T}}^{-1}\mathbf{T}^{-1})\mathbf{s} = (\mathbf{T}\hat{\mathbf{T}})^{-1}\mathbf{s}$ with expressing $\hat{\mathbf{T}}^{-1}$ as

$$\hat{\mathbf{T}}^{-1} = \begin{bmatrix} 1 & \tau_{12} & \dots & \tau_{1,m-1} & \tau_{1,m} \\ & 1 & \dots & \tau_{2,m-1} & \tau_{2,m} \\ & & \ddots & \vdots & \vdots \\ & & & 1 & \tau_{m-1,m} \\ \mathbf{0} & & & & 1 \end{bmatrix} \tag{5.9}$$

The LLL algorithm does not guarantee to find out the shortest lattice vector. Hence the LRA detection degrades the performance compared to the ML detection. The GSO procedure is performed after the LLL algorithm, which results in $\hat{\mathbf{R}}$ to be a diagonal matrix with its orthogonal column vectors to be almost of equal length. The highly reliable soft estimate $\tilde{\mathbf{u}}$ can be simply derived as

$$\tilde{\mathbf{u}} = \hat{\mathbf{R}}^{-1}\mathbf{y}' \quad \text{or} \quad \tilde{u}_i = y'_i/\hat{r}_{i,i},\ i \in [1, m] \tag{5.10}$$

The entries of $\mathbf{u}$ are non-integers. Those of $\tilde{\mathbf{u}}$ cannot be quantized only using the rounding operations like the LRA detection. $\hat{\mathbf{u}}$ is obtained using the decision method described in Chapter 3. After that, the soft estimate of $\hat{\mathbf{s}}$ is obtained as

$$\begin{aligned} \hat{v}_i &= \mathcal{Q}\left\{\tilde{v}_i^{(LR-MMSE)}\right\},\ i \in [1, m] \\ \hat{\mathbf{u}} &= \mathcal{Q}\left\{\tilde{\mathbf{u}} - \hat{\mathbf{T}}^{-1}\hat{\mathbf{v}}\right\} + \hat{\mathbf{T}}^{-1}\hat{\mathbf{v}} \\ \hat{\mathbf{s}}^{\mathcal{S}} &= \mathcal{Q}\left\{\mathbf{T}\hat{\mathbf{T}}\hat{\mathbf{u}}\right\} \\ \hat{\mathbf{s}} &= \mathcal{S}^{-1}[\hat{\mathbf{s}}^{\mathcal{S}}] = 2\hat{\mathbf{s}}^{\mathcal{S}} - (K-1)\mathbf{1}_m \end{aligned} \tag{5.11}$$

5.4 Proposed improved quantization scheme

5.4.1 Motivation

In the LRA detection, after the rounding operations of $\hat{\mathbf{v}} = \lceil \tilde{\mathbf{v}} \rfloor$, the symbols are transformed to s-domain. In the case that the soft estimate $\hat{\mathbf{s}}$ is outside

the original signal constellation, i.e., $\hat{s}_i \notin \mathbb{Z}, i \in [1, m]$, we assume that the quantization error occurs when performing $\hat{v}_i = \mathcal{Q}\{\tilde{v}_i\}$. This quantization error in the v-domain may result in the detection error in the s-domain. If this error occurs in the i-th row of the transmit signal, it has to propagate to as many symbols as non-zero entries of the i-th column of $\mathbf{T}$.

As a result, there are two cases for the difference of $(\tilde{v}_i - \hat{v}_i)$ as shown in Fig. 5.1. If the quantization error occurs in such a case that the difference of $(\tilde{v}_i - \hat{v}_i)$ is close to zero as shown in Fig. 5.1 (a), the final estimate of the transmit signal may be corrected even if the quantization error happens in the v-domain. However, the quantization error often generates in the case that the difference of $(\tilde{v}_i - \hat{v}_i)$ is around ± 0.5 as shown in Fig. 5.1 (b). Therefore, the quantization scheme is much important for improving the BER characteristics in the LRA detection.

In this chapter, we propose a new quantization scheme to improve the BER characteristics for quantizing the new signal vector $\tilde{\mathbf{v}}$ instead of the rounding operations in the conventional LRA detection. Hence we introduce the Gram-Schmidt orthogonalization procedure after the LLL algorithm. Using the purely orthogonal lattice basis, the proposed detection has much better decision boundary and less noise enhancement compared to the signal estimation in the conventional LRA detection. This property is the motivation to be applied in the proposed quantization scheme.

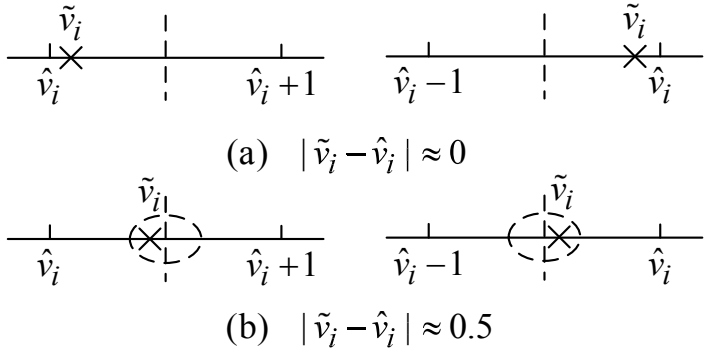

Figure 5.1: The difference between the soft estimate symbol and the rounding integer: $i \in [1, m]$.

5.4.2 Proposed quantization scheme

In this section, the quantization scheme is proposed for the new signal $\mathbf{v}$ in the v-domain. Considering the decision boundary, more reliable estimate $\tilde{\mathbf{u}}$ is first obtained in (5.10). Since the decision method for $\tilde{\mathbf{u}}$ is more complicated in (5.11) [39], the proposed scheme has no quantization for $\tilde{\mathbf{u}}$ and is totally different from the LR-GS detection with low complexity. According to the information of $\hat{\mathbf{T}}^{-1}$, interference-free operations are achieved if the following equation holds:

$$\tilde{\mathbf{v}} \triangleq \hat{\mathbf{T}}^{-1}\tilde{\mathbf{u}}, \text{ i.e.,} \tag{5.12}$$

$$\begin{bmatrix} \tilde{v}_1 \\ \tilde{v}_2 \\ \vdots \\ \tilde{v}_{m-1} \\ \tilde{v}_m \end{bmatrix} = \begin{bmatrix} 1 & \tau_{12} & \dots & \tau_{1,m-1} & \tau_{1,m} \\ & 1 & \dots & \tau_{2,m-1} & \tau_{2,m} \\ & & \ddots & \vdots & \vdots \\ & & & 1 & \tau_{m-1,m} \\ \mathbf{0} & & & & 1 \end{bmatrix} \begin{bmatrix} \tilde{u}_1 \\ \tilde{u}_2 \\ \vdots \\ \tilde{u}_{m-1} \\ \tilde{u}_m \end{bmatrix}$$

Due to the triangular structure of the matrix $\hat{\mathbf{T}}^{-1}$, the equations for $\hat{\mathbf{v}}$ lead to the following recursions as

$$\begin{aligned} \hat{v}_m &= \mathcal{Q}\{\tilde{v}_m\} = \mathcal{Q}\{\tilde{u}_m\} \triangleq \hat{u}_m \\ \hat{v}_{m-1} &= \mathcal{Q}\{\tilde{v}_{m-1}\} = \mathcal{Q}\{\tilde{u}_{m-1} - \tau_{m-1,m}\hat{v}_m\} \triangleq \hat{u}_{m-1} - \tau_{m-1,m}\hat{v}_m \\ &\vdots \\ \hat{v}_i &= \mathcal{Q}\{\tilde{v}_i\} = \mathcal{Q}\left\{\tilde{u}_i - \sum_{j=i+1}^{m} \tau_{i,j}\hat{v}_j\right\} \triangleq \hat{u}_i - \sum_{j=i+1}^{m} \tau_{i,j}\hat{v}_j \\ &\vdots \\ \hat{v}_1 &= \mathcal{Q}\{\tilde{v}_1\} = \mathcal{Q}\left\{\tilde{u}_1 - \sum_{j=2}^{m} \tau_{1,j}\hat{v}_j\right\} \triangleq \hat{u}_1 - \sum_{j=2}^{m} \tau_{1,j}\hat{v}_j \end{aligned} \tag{5.13}$$

where $\hat{u}_i$ is defined as the decided symbol of $\tilde{u}_i$, $i \in [1, m]$. Note that $\hat{u}_i$ is a non-integer. We introduce $\hat{\mathbf{u}}$ in order to explain the quantization operation for $\mathbf{v}$ as illustrated in Fig. 5.2. Using the GSO algorithm, $\hat{v}_i$ is a function of $\hat{u}_j$, $j \in [i+1, m]$. This $\tilde{\mathbf{v}}$ in (5.13) is different from the estimate of $\tilde{\mathbf{v}}^{(LR-MMSE)}$ obtained directly in (5.7).

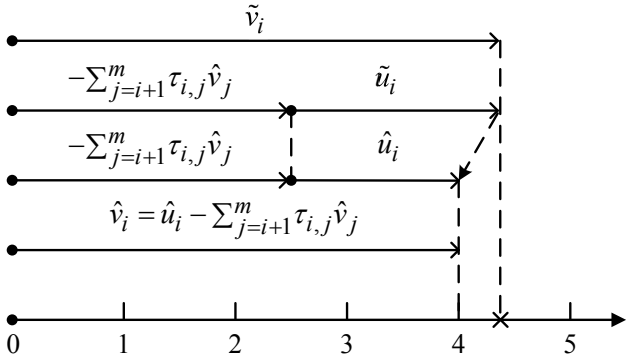

Figure 5.2: The decision flow of the soft estimate $\hat{u}_i$: $i \in [1, m]$.

As mentioned above, the quantization errors often happen in the case that the difference between the estimate symbol and the rounding integer is around ± 0.5. Hence we give another quantization candidate after rounding off the soft estimate symbol, which candidate is usually obtained by adding or subtracting 1 based on the rounding integer as

$$\hat{v}_i^{(k)} \triangleq \begin{cases} \hat{v}_i^{(1)} = \hat{v}_i \equiv \lceil \tilde{v}_i \rfloor \\ \hat{v}_i^{(2)} \triangleq \hat{v}_i + \mathrm{sgn}(\tilde{v}_i - \hat{v}_i) \end{cases} \tag{5.14}$$

where $i \in [1, m]$ and $\mathrm{sgn}(\cdot)$ represents the signum function, which is a sign of the real number, i.e. $\mathrm{sgn}(\tilde{v}_i - \hat{v}_i > 0) = +1$ and $\mathrm{sgn}(\tilde{v}_i - \hat{v}_i < 0) = -1$. The superscript k is defined as the index of the quantization candidates, $k \in \{1,2\}$.

Following the structure of the ML detection, the tree search of $\hat{\mathbf{v}}$ consists of m entries and 2^m combination candidates, which requires high complexity for the useless exhaustive search. The proposed detection applies a simple tree search, which is different from the QRM-MLD with the fixed number of the surviving candidates in each detection layer [17]−[23]. For each detection layer of the tree search in the proposed scheme, there are three major operations:

- Candidates expansion: Expand the children candidates from each surviving path, which are obtained in [22].
- Path metric evaluations: Calculate the path metric for all the possible branches.

- Sorting and surviving: Sort the path metric and survive the branches with the smallest path metric from the possible branches. The rest of branches should be discarded.

In the proposed quantization scheme, we define that the number of the surviving candidates (SC) in the i-th layer is expressed as $\mathcal{N}_{\mathrm{SC}}(i)$, and specify the maximum number of the surviving candidates in each layer as $\mathcal{N}_{\max}$, where $\mathcal{N}_{\mathrm{SC}}(i) \leq \mathcal{N}_{\max}$ and the value of $\mathcal{N}_{\max}$ is predetermined. For $\tilde{v}_m$, there are two quantization candidates $\hat{v}_m^{(k)}$, $k \in \{1,2\}$. For the candidates expansion between the current and the previous layers, the quantization candidates for $\hat{v}_i$, $i = m-1, m-2, \ldots, 1$, are expressed as

$$\hat{v}_i^{(k,l')} = \begin{cases} \hat{v}_i^{(1,l')} = \mathcal{Q}\left\{\tilde{v}_i^{(l')}\right\} = \mathcal{Q}\left\{\tilde{u}_i^{(l')} - \sum_{j=i+1}^{m} \tau_{i,j}\hat{v}_i^{(l')}\right\} \\ \hat{v}_i^{(2,l')} = \hat{v}_i^{(1,l')} + \mathrm{sgn}\left(\tilde{v}_i^{(l')} - \hat{v}_i^{(1,l')}\right) \end{cases} \tag{5.15}$$

where the superscript k denotes the index of the candidates from the same path $\Pi_{i+1}^{(l')}$, $k \in \{1,2\}$, and the superscript l' is the index of the surviving path from the previous layer, $l' \in [1, \mathcal{N}_{\mathrm{SC}}(i+1)]$. The surviving candidates of the partial decided vector in the previous layer are expressed in sequence as $\hat{\mathbf{v}}_{i+1}^{(l')} = \left[\hat{v}_{i+1}^{(l')}, \ldots, \hat{v}_m^{(l')}\right]^{\mathrm{T}}$. Hence there are $2\mathcal{N}_{\mathrm{SC}}(i+1)$ possible candidates for the partial vectors in the i-th layer, which can be expressed as

$$\hat{\mathbf{v}}_i^{(k,l')} = \left[\hat{v}_i^{(k,l')}, \hat{v}_{i+1}^{(l')}, \ldots, \hat{v}_m^{(l')}\right]^{\mathrm{T}} \tag{5.16}$$

In order to obtain an optimum quantization result, we define the branch metric in the i-th detection layer as

$$\begin{aligned} \lambda_m^{(k)} &\triangleq \left|\tilde{v}_m - \hat{v}_m^{(k)}\right|^2 \\ \lambda_i^{(k,l')} &\triangleq \left|\tilde{v}_i^{(l')} - \hat{v}_i^{(k,l')}\right|^2, i = m-1, \ldots, 1 \end{aligned} \tag{5.17}$$

and the accumulated branch metric called the path metric as

$$\begin{aligned}
&\Lambda_m^{(k)} \triangleq \lambda_m^{(k)} \\
&\Lambda_{m-1}^{(k,l')} \triangleq \lambda_{m-1}^{(k,l')} + \Lambda_m^{(l'=k)} \\
&\text{Let the } l'\text{-}th \min_k \Lambda_{m-1}^{(k,l')} \triangleq \Lambda_{m-1}^{(l')}, \text{then } \Lambda_{m-2}^{(k,l')} \triangleq \lambda_{m-2}^{(k,l')} + \Lambda_{m-1}^{(l')} \\
&\quad \vdots \\
&\text{Let the } l'\text{-}th \min_k \Lambda_{i+1}^{(k,l')} \triangleq \Lambda_{i+1}^{(l')}, \text{then } \Lambda_i^{(k,l')} \triangleq \lambda_i^{(k,l')} + \Lambda_{i+1}^{(l')} \\
&\quad \vdots \\
&\text{Let the } l'\text{-}th \min_k \Lambda_2^{(k,l')} \triangleq \Lambda_2^{(l')}, \text{then } \Lambda_1^{(k,l')} \triangleq \lambda_1^{(k,l')} + \Lambda_2^{(l')}
\end{aligned} \tag{5.18}$$

where $\Lambda_{i+1}^{(l')}$ denotes the l'-th smallest path metric of the surviving path $\Pi_{i+1}^{(l')}$ in the previous layer, corresponding to $\hat{\mathbf{v}}_{i+1}^{(l')} = \left[\hat{v}_{i+1}^{(l')}, \hat{v}_{i+2}^{(l')}, \ldots, \hat{v}_m^{(l')}\right]^{\mathrm{T}}$. In the i-th layer, we rank the path metric of the possible candidates in the ascending order. Let $\Lambda_i^{(l)}$ denote the l-th smallest path metric of the surviving path $\Pi_i^{(l)}$ after the surviving operations, where $l \in [1, \mathcal{N}_{\mathrm{SC}}(i)]$ and $\Lambda_i^{(1)} \leq \Lambda_i^{(2)} \leq \cdots \leq \Lambda_i^{(\mathcal{N}_{\mathrm{SC}}(i))}$. Correspondingly, the partial decided signals $\hat{\mathbf{v}}_i^{(l)}$ are expressed as $\hat{\mathbf{v}}_i^{(l)} = \left[\hat{v}_i^{(l)}, \hat{v}_{i+1}^{(l)}, \ldots, \hat{v}_m^{(l)}\right]^{\mathrm{T}}$.

According to the ML detection, the final estimate of the transmit signal is determined by the path with the smallest path metric. In general, we can express the Euclidean distance as

$$E\left[\|\mathbf{y} - \mathbf{H}\mathbf{s}\|^2\right] = dN_0 \tag{5.19}$$

where d is a fuzzy factor and N_0 is one-sided noise power spectral density. To a certain degree, we can apply the partial path metric to evaluate the reliability of the surviving paths in each detection layer. Since $\hat{\mathbf{R}}$ is a diagonal matrix, $\hat{\mathbf{R}}^{\mathrm{T}}\hat{\mathbf{R}}$ is also a diagonal matrix, expressed as

$$\hat{\mathbf{R}}^{\mathrm{T}}\hat{\mathbf{R}} = \mathrm{diag}\left\{|\hat{r}_{11}|^2, |\hat{r}_{22}|^2, \ldots, |\hat{r}_{m,m}|^2\right\} \tag{5.20}$$

It is obvious that the smaller eigenvalue of $\hat{\mathbf{R}}^{\mathrm{T}}\hat{\mathbf{R}}$ will cause more errors due to noise enhancement. Hence the norm of $|\hat{r}_{i,i}|^2$ can denote the channel condition

for the i-th entry of the transmit signal. Using the property of the channel, we set the threshold function for the i-th layer, which is a function of the minimum partial path metric and the norm of $|\hat{r}_{i,i}|^2$, defined as

$$o_i \triangleq \min \Lambda_i^{(k,l')} \left(1 + R_D/|\hat{r}_{i,i}|^2\right) \tag{5.21}$$

where i is from m down to 1 and $|\hat{r}_{i,i}|^2$ is normalized as $R_D \triangleq (\sum_{i=1}^{m} |\hat{r}_{i,i}|^2)/m$. R_D is used to measure the relative channel power gain with respect to the channel power gain across all the detection layers. Note that $R_D/|\hat{r}_{i,i}|^2$ is fluctuated up and down centering around 1.

According to (5.19), the partial path metric $\Lambda_i^{(k,l')}$ is instead of N_0 and the factor d is replaced by $(1 + R_D/|\hat{r}_{i,i}|^2)$. Hence the threshold o_i denotes the search radius in each detection layer. Combined with the property of the channel gain, the threshold function is updated by the minimum partial path metric in each detection layer in order to retain the quantization candidate with the branch metric close to 0.25.

Table 5.3: Proposed quantization scheme

Input: $\hat{\mathbf{T}}^{-1}$, and $\tilde{\mathbf{u}}$; Output: $\mathcal{N}_{\mathrm{SC}}(1)$, and $\hat{\mathbf{v}}^{(l)}$, $l \in [1, \mathcal{N}_{\mathrm{SC}}(1)]$
(1) **Initialization**: set $\mathcal{N}_{\mathrm{SC}}(i) = 0, i \in [1, m]$, $\mathcal{N}_{\max}$, and$R_D = (\sum_{i=1}^{m} \lvert\hat{r}_{i,i}\rvert^2)/m$
(2) $i = m$
(3) $\tilde{v}_m = \tilde{u}_m$
Obtain $\hat{v}_m^{(k)}$ and $\Lambda_m^{(k)}$;
Survive the candidates: $\mathcal{N}_{\mathrm{SC}}(m)$.
(4) $i = m - 1$
(5) while $i \geq 1$
(6) Obtain $\hat{v}_i^{(k,l')}$ in (5.15) and $\Lambda_i^{(k,l')}$ in (5.18);
(7) Sort $\Lambda_i^{(k,l')}$ in the ascending order: $\Lambda_i^{(l'')}, l'' \in [1, 2\mathcal{N}_{\mathrm{SC}}(i+1)]$;
(8) $o_i \triangleq \Lambda_i^{(1)} (1 + R_D/\lvert\hat{r}_{i,i}\rvert^2)$;
(9) Compare the path metric and the threshold:
for $l'' = 1$ to $2\mathcal{N}_{\mathrm{SC}}(i+1)$
if $\Lambda_i^{(l'')} \leq o_i$, $\mathcal{N}_{\mathrm{SC}}(i) := \mathcal{N}_{\mathrm{SC}}(i) + 1$;
else break;
end for
(10) Survive the paths: $\mathcal{N}_{\mathrm{SC}}(i) := \min\{\mathcal{N}_{\mathrm{SC}}(i), \mathcal{N}_{\max}\}$ and $\hat{\mathbf{v}}_i^{(l)} = \left[\hat{v}_i^{(l)}, \ldots, \hat{v}_m^{(l)}\right]^{\mathrm{T}}, l \in [1, \mathcal{N}_{\mathrm{SC}}(i)]$;
(11) $i := i - 1$;
(12) end while
(13)**End**

The proposed quantization scheme is summarized in Table 5.3. The superscript l'' in step (7) of Table 5.3 denotes the index of the sorted path metric in the ascending order among all the possible candidates, $l'' \in [1, 2\mathcal{N}_{\mathrm{SC}}(i+1)]$. And through l''-loop in step (9), we survive the candidates with the path metric under the threshold in this layer. The iteration operation from steps (5) to (12) is illustrated in Fig. 5.3. At last, it is the key parameter for the output of $\mathcal{N}_{\mathrm{SC}}(1)$.

- If $\mathcal{N}_{\mathrm{SC}}(1) = 1$, then let $\hat{\mathbf{s}}^{\mathcal{S}} = \mathbf{T}\hat{\mathbf{v}}$ and $\hat{\mathbf{s}} := \mathcal{C}[\mathcal{S}^{-1}[\hat{\mathbf{s}}^{\mathcal{S}}]]$.

- Else, let $\mathcal{N}_{\mathrm{SC}}(1) \neq 1$. There are two candidates: $\hat{\mathbf{v}}^{(l)}$, $l \in [1, \mathcal{N}_{max}]$. Then let $\hat{\mathbf{s}}^{\mathcal{S}(l)} = \mathbf{T}\hat{\mathbf{v}}^{(l)}$ and $\hat{\mathbf{s}}^{(l)} := \mathcal{C}[\mathcal{S}^{-1}[\hat{\mathbf{s}}^{\mathcal{S}(l)}]]$. After that, perform the ML metric:

5. AN IMPROVED QUANTIZATION SCHEME FOR LATTICE-REDUCTION AIDED MIMO DETECTION BASED ON GRAM-SCHMIDT ORTHOGONALIZATION

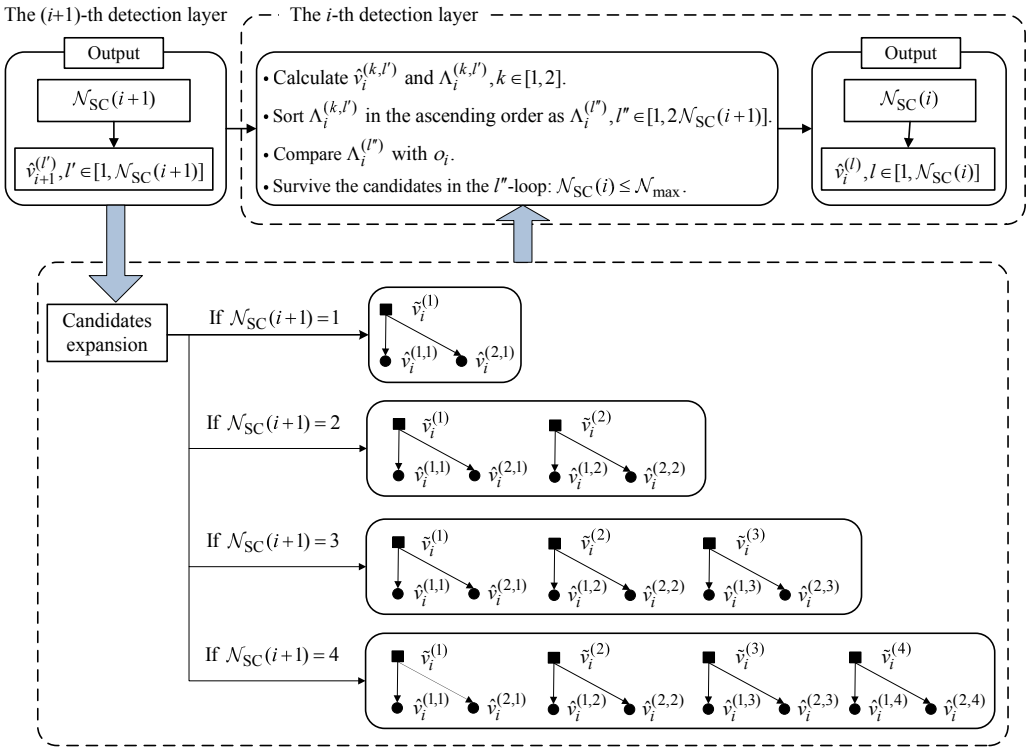

Figure 5.3: The iteration operation of the proposed quantization scheme in the i-th entry, $i \in [1, m-1]$: steps (5) - (12) in Table 5.3.

$$\hat{\mathbf{s}} = \underset{l \in [1, \mathcal{N}_{max}]}{\arg\min} \left\| \mathbf{y} - \mathbf{H}\hat{\mathbf{s}}^{(l)} \right\|^2 \tag{5.22}$$

According to the value of $\mathcal{N}_{\mathrm{SC}}(1)$, we search over at most $\mathcal{N}_{max}$ candidates of $\hat{\mathbf{s}}$ to decide the final estimate of the transmit signal. However, the ML metric should be performed only if $\mathcal{N}_{\mathrm{SC}}(1) \neq 1$. The proposed detection is to use a function of path metric ratio. The magnification factor of the minimum path metric is determined by the norm of the diagonal element of $\hat{\mathbf{R}}$, which tightens the threshold with the less noise enhancement or looses the threshold due to the rounding integer with less reliability. It illustrates that the quantization errors may rarely happen if the threshold approaches the minimum partial path metric. Although the additional computational complexity is required in order to correct the quantization error, the improvement of the BER performance is expected as

shown in numerical results.

5.4.3 Effort for quantization error reduction

To evaluate the effort for the quantization error reduction, we observe the percentage of the decided estimate of $\hat{s}_i$ lying out the original signal constellation points, i.e. $\hat{s}_i \notin \mathbb{Z}$, any $i \in [1, m]$, which is defined as the probability of the quantization error.

In this section, we investigate the probability of the quantization error in minus logarithmic scale for the quantization schemes of the proposed detection, the conventional LR-MMSE detection and the LR-GS detection, respectively. The probability of the quantization errors in minus logarithmic scale is higher, then the quantization errors are fewer.

Figures 5.4 - 5.9 show E_b/N_0 versus the probability of the quantization error in minus logarithmic scale for QPSK,16QAM and 64QAM in the 4×4 and 8×8 MIMO systems, respectively. Compared to the LR-MMSE detection, the quantization error of the LR-GS detection is reduced due to using the GSO algorithm. For the proposed detection, the effort for the quantization error reduction is valid. The quantized error remarkably reduced as the value of $\mathcal{N}_{max}$ increased in particular in the high E_b/N_0 region in the 8×8 MIMO system.

5. AN IMPROVED QUANTIZATION SCHEME FOR LATTICE-REDUCTION AIDED MIMO DETECTION BASED ON GRAM-SCHMIDT ORTHOGONALIZATION

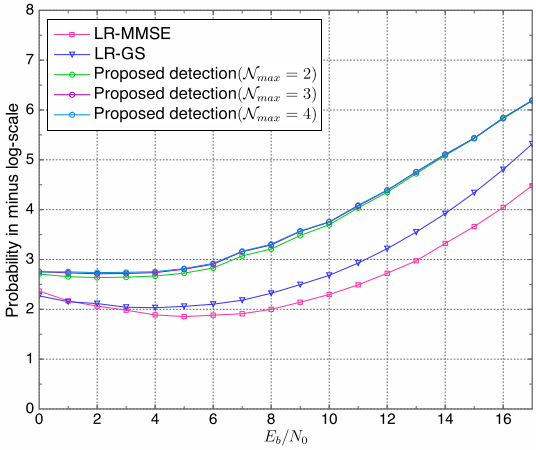

Figure 5.4: The E_b/N_0 vs. the probability of the quantization error in minus log-scale in 4×4 MIMO: QPSK.

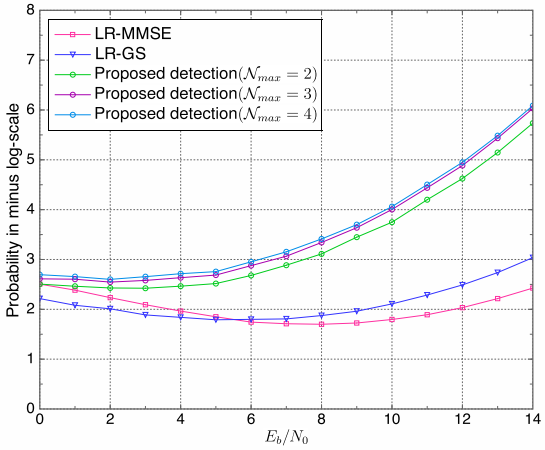

Figure 5.5: The E_b/N_0 vs. the probability of the quantization error in minus log-scale in 8×8 MIMO: QPSK.

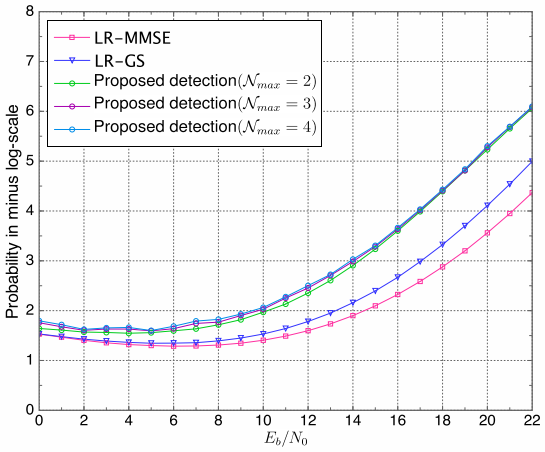

Figure 5.6: The E_b/N_0 vs. the probability of the quantization error in minus log-scale in 4×4 MIMO: 16QAM.

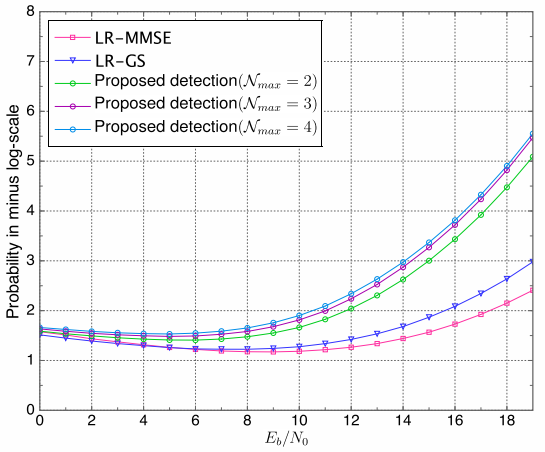

Figure 5.7: The E_b/N_0 vs. the probability of the quantization error in minus log-scale in 8×8 MIMO: 16QAM.

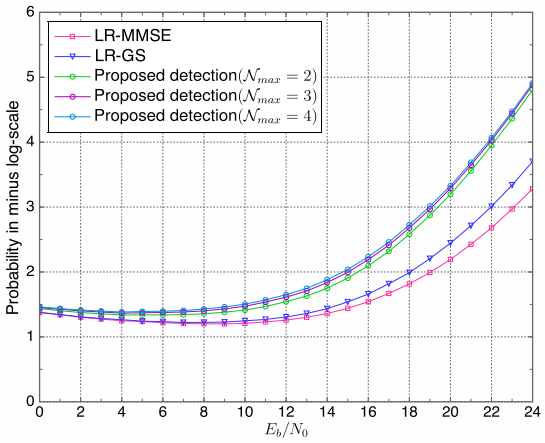

Figure 5.8: The E_b/N_0 vs. the probability of the quantization error in minus log-scale in 4×4 MIMO: 64QAM.

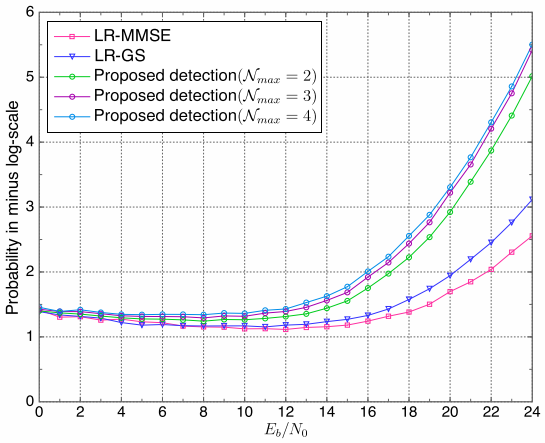

Figure 5.9: The E_b/N_0 vs. the probability of the quantization error in minus log-scale in 8×8 MIMO: 64QAM.

5.5 Numerical results

The computer simulations were carried out for QPSK, 16QAM and 64QAM in the 4×4 and 8×8 MIMO systems, respectively. In the simulations, the channel gains were generated using the i.i.d. Gaussian random variables with zero mean and variance of $1/2$ for each dimension. Additive noise at each receive antenna was generated using the i.i.d. Gaussian random variables with zero mean and variance of $N_0/2$ for each dimension. The performances of the different detections were measured by the BER performance and the complexity.

5.5.1 Suitable values of factor δ and $\mathcal{N}_{max}$

In the LLL algorithm, δ is chosen as $\delta \in (0.25,1]$. The value of δ close to 1 is preferred for approximating the shortest lattice vector at the cost of the high complexity for the swapping condition. The value of δ is the tradeoff between the BER performance and the complexity. Hence we observe that the various value of δ has a great influence on the BER performance, and look for a suitable value of δ for the LR-MMSE, LR-GS and the proposed detection with $\mathcal{N}_{max} = \{2, 3, 4\}$, respectively.

The various value of δ vs. the BER characteristics for QPSK, 16QAM and 64QAM in the 4×4 MIMO system are shown in Figs. 5.10, 5.12 and 5.14, respectively. In Fig. 5.10, the BER curves for QPSK are compared at the fixed E_b/N_0 of 16dB. The BER characteristics of the proposed detection with $\mathcal{N}_{max} = \{2, 3, 4\}$ have a little variation as δ is more than 0.5, in particular at a BER between 10^{-4} and 10^{-5}. For the conventional detections, the BER characteristics achieve the great performance with δ more than 0.75. Figure 5.12 shows the BER curves for 16QAM at the fixed E_b/N_0 of 21dB. The proposed detections with $\mathcal{N}_{max} = \{2, 3, 4\}$ have almost same BER performance and provide the great BER performance at $\delta \geq 0.75$. As seen in Fig. 5.12, the BER curves for 64QAM are compared at the fixed E_b/N_0 of 26dB. The trends of the proposed detections are as same as that of the BER curves for 16QAM in Fig. 5.12. The proposed detections with $\mathcal{N}_{max} = \{2, 3, 4\}$ provide the great BER performance at $\delta \geq 0.75$.

Figures 5.11, 5.13 and 5.15 shows the various value of δ vs. the BER characteristics for QPSK, 16QAM and 64QAM in the 8×8 MIMO system, respectively. We observe the BER characteristics for the proposed detection at the fixed E_b/N_0 of 13dB, 18dB and 23dB for QPSK, 16QAM and 64QAM, respectively. For the conventional detections, the value of δ is assigned as 0.75 for the LR-MMSE and LR-GS as the suitable choice. For the proposed detections with $\mathcal{N}_{max} = \{2, 3, 4\}$ regardless of the modulation order achieve better BER performance as the value of δ or $\mathcal{N}_{max}$ increases. Hence, the values of δ and $\mathcal{N}_{max}$ are the tradeoff factors between the complexity and the BER performance. We summarize the suitable values of both factors for the proposed detection in Table 5.4. Note that the value of δ is assigned as 0.75 for the LR-MMSE and LR-GS as the common choice.

Table 5.4: The suitable values of factor δ and $\mathcal{N}_{max}$ for the proposed detection

Modulation order	$N_t = N_r = 4$	$N_t = N_r = 8$
QPSK	$\delta = 0.55$, $\mathcal{N}_{max} = 2$	$\delta = 0.95$, $\mathcal{N}_{max} = 3$
16QAM	$\delta = 0.75$, $\mathcal{N}_{max} = 2$	$\delta = 0.95$, $\mathcal{N}_{max} = 3$
64QAM	$\delta = 0.75$, $\mathcal{N}_{max} = 2$	$\delta = 0.95$, $\mathcal{N}_{max} = 3$

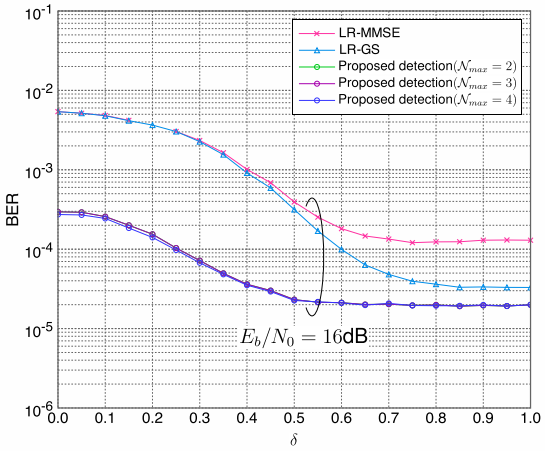

Figure 5.10: The δ vs. BER characteristics in the 4×4 MIMO system: QPSK.

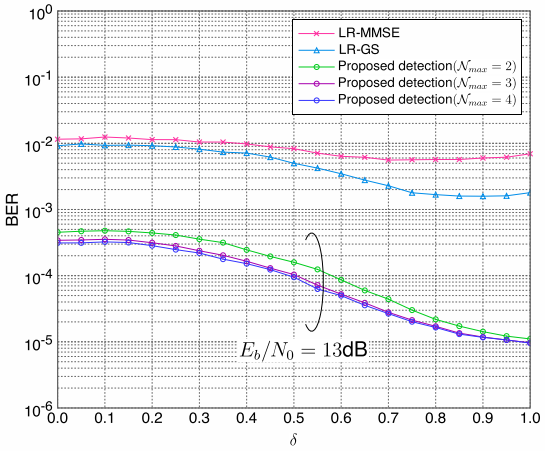

Figure 5.11: The δ vs. BER characteristics in the 8×8 MIMO system: QPSK.

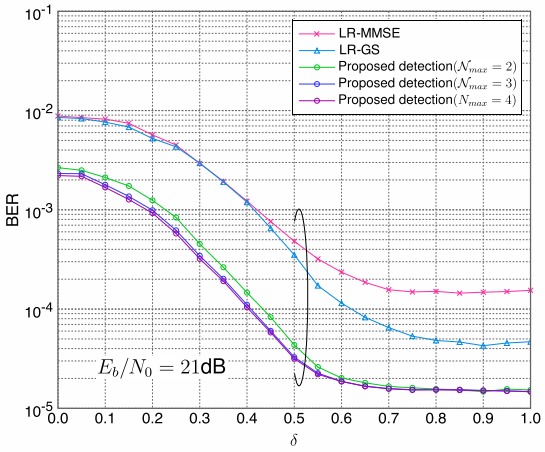

Figure 5.12: The δ vs. BER characteristics in the 4×4 MIMO system: 16QAM.

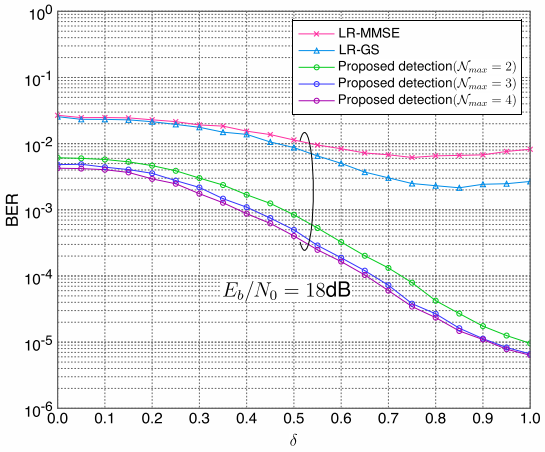

Figure 5.13: The δ vs. BER characteristics in the 8×8 MIMO system: 16QAM.

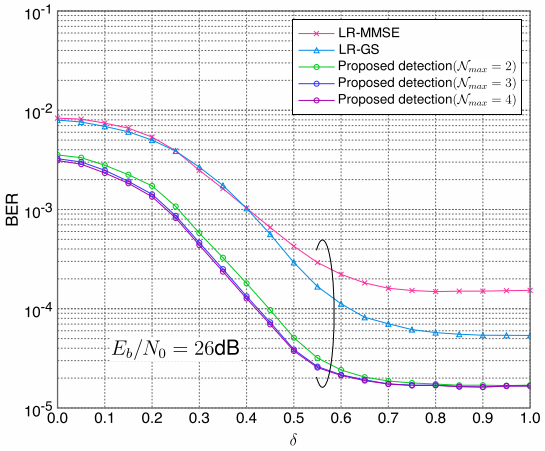

Figure 5.14: The δ vs. BER characteristics in the 4×4 MIMO system: 64QAM.

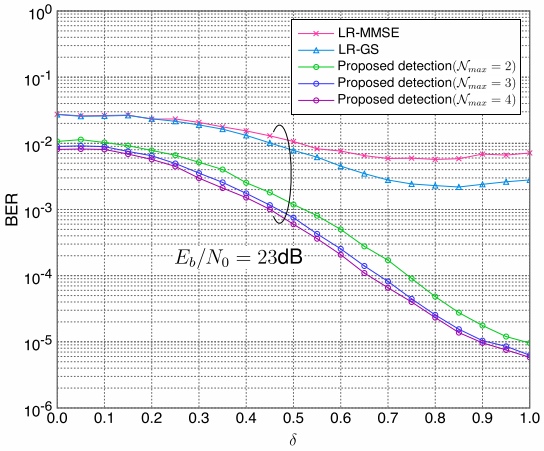

Figure 5.15: The δ vs. BER characteristics in the 8×8 MIMO system: 64QAM.

5.5.2 BER characteristics

We made computer simulations of the BER characteristics versus E_b/N_0 using the conventional LR-MMSE, the LR-GS, the proposed detection, and the QRM-MLD, respectively. The QRM-MLD based on QR decomposition and M-algorithm is one solution to relatively reduce the complexity of the ML detection while retaining the ML performance described in [17]−[23]. M is defined as the number of the surviving branches in each detection layer of the tree search, which is a tradeoff between the complexity and the BER performance. The QRM-MLD totally achieves the ML performance with M=8, 16, and 64 for QPSK, 16QAM and 64QAM in the 4×4 MIMO system, M=16, 64, and 128 for QPSK, 16QAM and 64QAM in the 8×8 MIMO system, respectively. The proposed detection applies the suitable values of factors as seen in Table 5.4.

Figure 5.16 shows the BER characteristics versus E_b/N_0 for QPSK in the 4×4 MIMO system. The BER performance of LR-GS further improves about 1 dB at a BER of 10^{-5} compared to that of the LR-MMSE detection. The BER curve of the proposed detection almost agrees with that of the ML performance. In Fig. 5.18, the BER curve of the LR-MMSE for 16QAM achieves the sub-optimal performance with about 2dB worse than that of the ML detection at

a BER of 10^{-5}. Furthermore, the LR-GS can further gain 1dB over the LR-MMSE. However, the BER curve of the proposed detection totally approaches the ML curve at a BER below 10^{-4}. This fact also verified that the effort for the quantization error reduction as shown in Fig. 5.6 was corresponding to the BER improvement in Fig. 5.18 for 16QAM. As seen in Fig. 5.20, the gain of the proposed detection for 64QAM is almost the same as that for 16QAM over the LR-MMSE. The BER curve of the proposed detection is also equivalent to that of the ML detection at a BER below 10^{-4}. Thus, the proposed quantization error reduction scheme is effective even for the high modulation order.

Figures 5.17, 5.19 and 5.21 show the BER characteristics versus E_b/N_0 for QPSK, 16QAM and 64QAM in the 8×8 MIMO system, respectively. For the conventional detection methods, the BER performances of LR-MMSE and LR-GS are still far away to that of the ML detection. The proposed detection for QPSK approaches the ML curve at a BER of 10^{-5}. And the BER curve of the proposed detection is more steeper than that of the ML curve. Therefore, they may coincide below the BER of 10^{-5}. The BER performance of the proposed detection for 16QAM further improves 5dB compared to the LR-GS detection and is still 1dB worse than that of the ML detection at a BER of 10^{-5}. As the same trend for 64QAM, the BER performance of the proposed detection further improves 5.5dB compared to the LR-GS detection and is still 1dB worse than that of the ML detection at a BER of 10^{-5}.

Therefore, the proposed detection can provide the near-ML performance in the 4×4 MIMO system even for the high modulation order such as 64QAM. However, the proposed detection has the great improvement of BER performance and achieves the suboptimal BER performance in the 8×8 MIMO system.

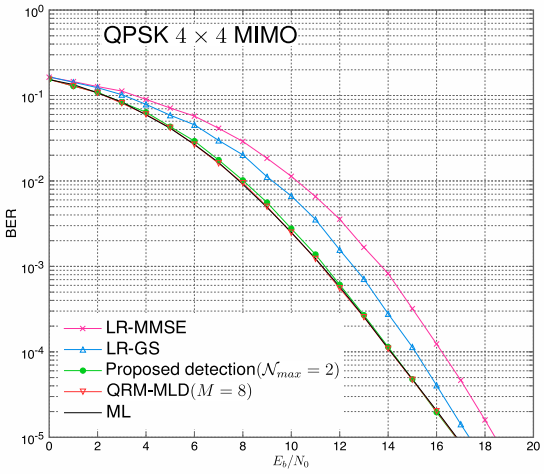

Figure 5.16: The E_b/N_0 vs. BER characteristics in the 4×4 MIMO: QPSK.

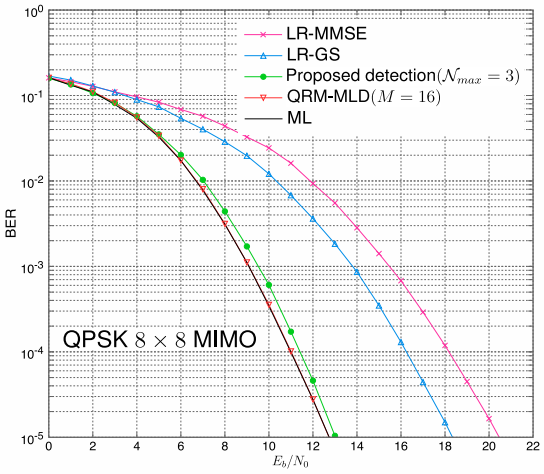

Figure 5.17: The E_b/N_0 vs. BER characteristics in the 8×8 MIMO: QPSK.

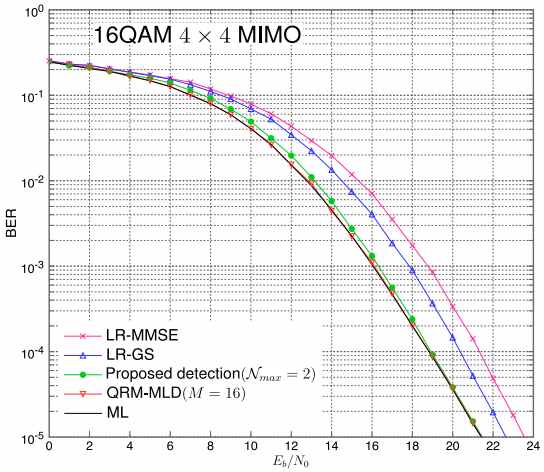

Figure 5.18: The E_b/N_0 vs. BER characteristics in the 4×4 MIMO: 16QAM.

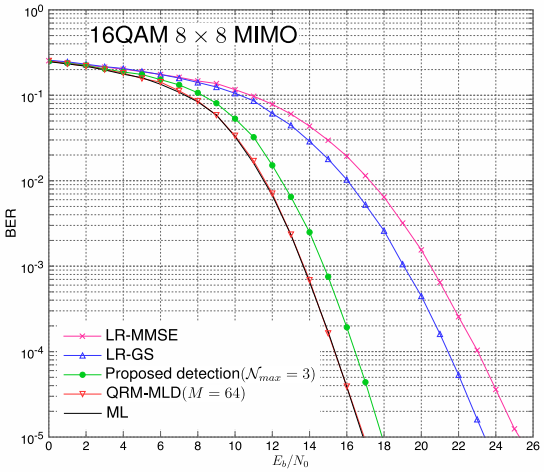

Figure 5.19: The E_b/N_0 vs. BER characteristics in the 8×8 MIMO: 16QAM.

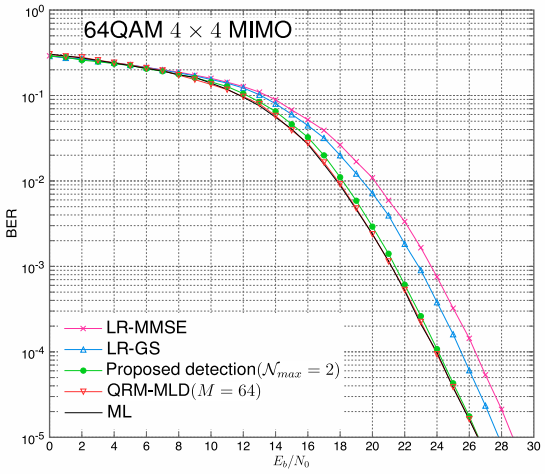

Figure 5.20: The E_b/N_0 vs. BER characteristics in the 4×4 MIMO: 64QAM.

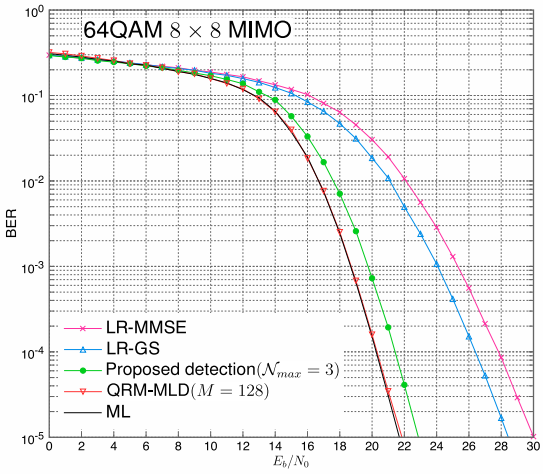

Figure 5.21: The E_b/N_0 vs. BER characteristics in the 8×8 MIMO: 64QAM.

5.5.3 Computational complexity

The flat fading channel is assumed that the data packet length is much shorter than the coherence time of the channel. Hence we can treat the channel to be non-time varying during the packet duration. If the LLL reduction and GSO procedure are performed at the beginning of the packet, we can apply them all over the packet. Therefore, the above complexity can be negligible. In this chapter, we focus on the analysis of the computational complexity in the signal estimation stage.

We evaluated the number of the surviving candidates in the i-th layer as $\mathcal{N}_{\mathrm{SC}}(i)$ in Figs. 5.22 - 5.27 for QPSK, 16QAM and 64QAM in the 4×4 and 8×8 MIMO systems, respectively. In this chapter, we assigned $\mathcal{N}_{\mathrm{SC}}(8) = 2$ in the 4×4 MIMO system. From the 7th entry down to the 2nd entry, the same iteration operations were done six times. Therefore, we counted up the average number of the surviving candidates. It was important for the value of $\mathcal{N}_{\mathrm{SC}}(1)$ to determine whether or not to perform the ML metric in (5.22). As similar in the 8×8 MIMO system, we assigned $\mathcal{N}_{\mathrm{SC}}(16) = 2$ for QPSK, $\mathcal{N}_{\mathrm{SC}}(16) = 3$ for 16QAM and 64QAM, respectively. From the 15th entry down to the 2nd entry, the same iteration operations were done fourteen times. Therefore, we also counted up

the average number of the surviving candidates. The value of $\mathcal{N}_{\mathrm{SC}}(1)$ is also to determine whether or not to perform the ML metric.

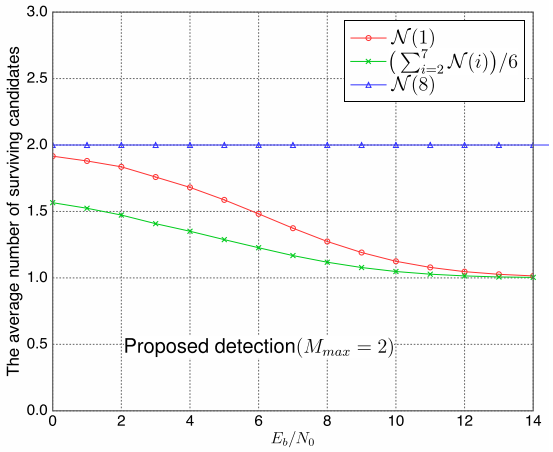

Figure 5.22: The E_b/N_0 vs. the average number of surviving candidates for each layer in the 4×4 MIMO: QPSK.

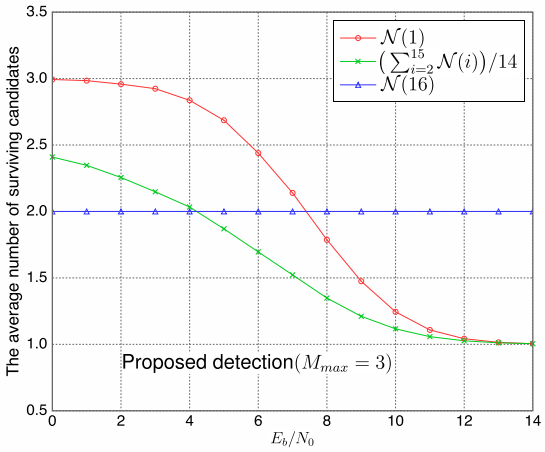

Figure 5.23: The E_b/N_0 vs. the average number of surviving candidates for each layer in the 8×8 MIMO: QPSK.

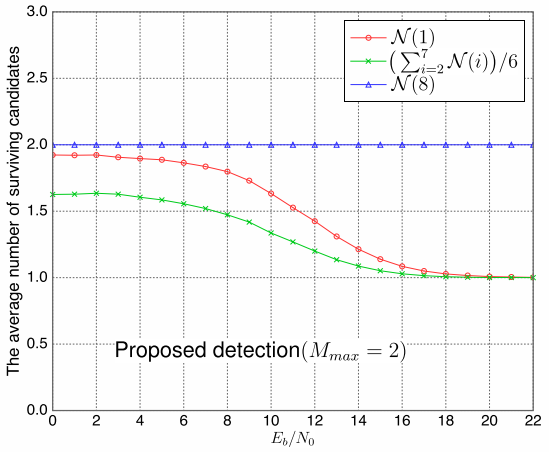

Figure 5.24: The E_b/N_0 vs. the average number of surviving candidates for each layer in the 4×4 MIMO: 16QAM.

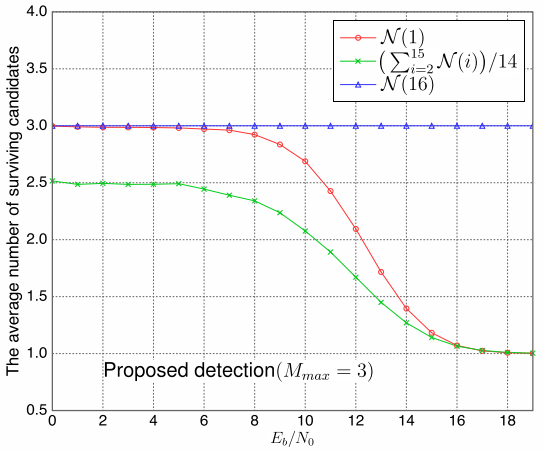

Figure 5.25: The E_b/N_0 vs. the average number of surviving candidates for each layer in the 8×8 MIMO: 16QAM.

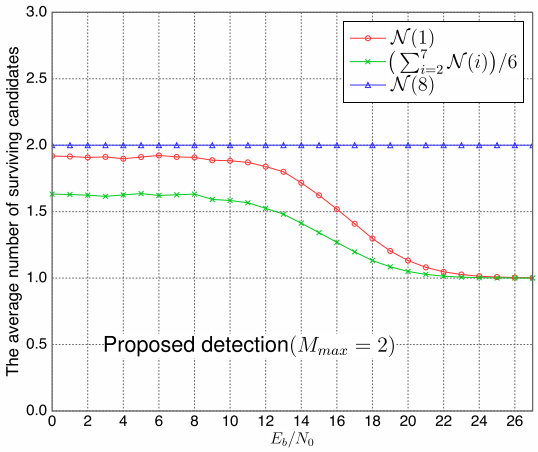

Figure 5.26: The E_b/N_0 vs. the average number of surviving candidates for each layer in the 4×4 MIMO: 64QAM.

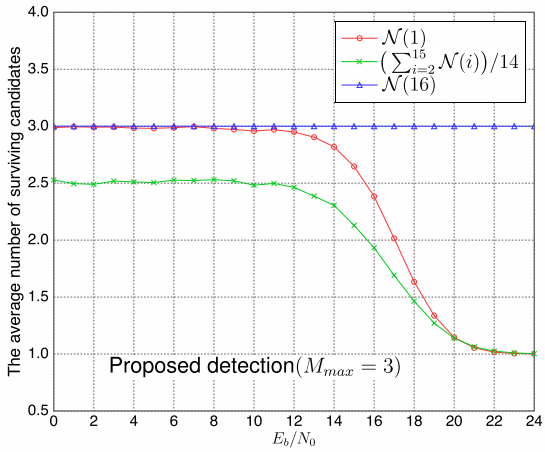

Figure 5.27: The E_b/N_0 vs. the average number of surviving candidates for each layer in the 8×8 MIMO: 64QAM.

Table 5.5: The computational complexity of the proposed detection

The real operations	The computational complexity (flops)
Scaled and shifted receive signal: $\bar{\mathbf{y}}^{\mathcal{S}}$	$2m+2n$
$\mathbf{y}' \triangleq \tilde{\mathbf{Q}}^{\mathrm{T}}\bar{\mathbf{y}}^{\mathcal{S}}$	$2m^2+2mn-2m$
Signal vector $\tilde{\mathbf{u}}$ in (5.10)	m
Expansion candidates for $\hat{\mathbf{v}}$ in (5.15)	$2+\sum_{i=1}^{m-1}\mathcal{N}_{\mathrm{SC}}(i+1)(2m-2i+2)$
Path metric in (5.17) and (5.18)	$4+\sum_{i=1}^{m-1}6\mathcal{N}_{\mathrm{SC}}(i+1)$
Threshold in (5.21)	m
Estimate of transmit signal: $\hat{\mathbf{s}}^{\mathcal{S}}=\mathbf{T}\hat{\mathbf{v}}$	$(2m^2-m)\mathcal{N}_{\mathrm{SC}}(1)$
Scaled back and shifted back signal: $\hat{\mathbf{s}}$	$2m\mathcal{N}_{\mathrm{SC}}(1)$
ML metric in (5.22): only if $\mathcal{N}_{\mathrm{SC}}(1)\neq 1$	$(2mn+2n)\mathcal{N}_{\mathrm{SC}}(1)$

Note that $i\in[1,m]$ and $\mathcal{N}_{\mathrm{SC}}(i)\leq\mathcal{N}_{\max}$.

In the 4×4 MIMO system, $\mathcal{N}_{\mathrm{SC}}(1)$ is around 1 at E_b/N_0 of 10dB, 15dB and 20dB with the BER of 10^{-2} for QPSK, 16QAM and 64QAM, respectively. Hence the complexity of the proposed detection may neglect the computing for performing the ML metric in (5.22). The trends of the average number of the surviving candidates from the 7th layer down to the 2nd layer for QPSK, 16QAM and 64QAM are almost equivalent to 1 in the high E_b/N_0 region, respectively.

As a result, the iteration operations for the quantization candidates require much lower complexity.

A similar observation for the 8×8 MIMO system, $\mathcal{N}_{\mathrm{SC}}(1)$ is around 1 at E_b/N_0 of 11dB, 15dB and 19dB with the BER of 10^{-3} for QPSK, 16QAM and 64QAM, respectively. The average number of the surviving candidates from the 15th layer down to the 2nd layer for QPSK, 16QAM and 64QAM are almost equivalent to 1 in the high E_b/N_0 region, respectively. Hence, the iteration operations for the quantization candidates require a little additional complexity.

According to the average number of the surviving candidates, we presented the complexity of the proposed detection in the signal estimation stage in Table 5.5. In the proposed quantization scheme, a simple tree search requires the computing for expanding candidates in (5.15), the evaluations of path metric in (5.17) and (5.18), and updating the threshold in (5.21). From a surviving path $\Pi_{i+1}^{(l')}, l' \in [1, \mathcal{N}_{\mathrm{SC}}(i+1)]$, $\tilde{v}_i^{(l')}$ is first derived, which requires $(2m-2i)$ flops. Then, there are 2 flops for computing the rounding operation and generating the quantization candidate. Hence the total complexity in (5.15) is counted up as $(2+\sum_{i=1}^{m-1}\mathcal{N}_{\mathrm{SC}}(i+1)(2m-2i+2))$ flops. For the computing of o_i, the value $(1+R_D/|\hat{r}_{i,i}|^2)$ is predetermined at the beginning of the packet. Hence only one multiplication is required in each detection layer in (5.21).

In the high E_b/N_0 region, the simulation results exhibited that $\mathcal{N}_{\mathrm{SC}}(i) \approx 1$. The proposed detection in the signal estimation requires $(5m^2+2mn+11m+2n-2)$ flops. The complexity is about 550 flops and 1998 flops in the 4×4 and 8×8 MIMO system, regardless of the modulation order, respectively. However, if we estimate the transmit signal using the conventional LR-MMSE detection, the complexity for computing $\mathbf{y}'$ and $\tilde{\mathbf{v}}$ in (5.6) and (5.7) is counted up as $(3m^2+2mn-m)$ flops. Then the new transmit signal is transformed back to s-domain, which requires $(2m^2-m)$ flops. The total complexity of the LR-MMSE including the scaling and shifting operations is $(5m^2+2mn+2m+2n)$ flops, which requires about 480 flops for $m=n=8$. Therefore, the extra complexity for the proposed detection is $(9m-2)$ flops compared to the conventional LR-MMSE.

Considering the complexity of the QRM-MLD described in Chapter 2, the QRM-MLD requires 574, 2820 and 18064 flops for QPSK, 16QAM and 64QAM

in the 4×4 MIMO system, respectively. Meanwhile, the complexity of the proposed detection at the BER below 10^{-2} only requires 550 flops regardless of the modulation order. As a consequence, the proposed detection scheme can achieve the near-ML performance with only a little additional complexity, which is about 96%, 20% and 3% of the complexity of the QRM-MLD for QPSK, 16QAM and 64QAM, respectively. In the 8×8 MIMO system, the QRM-MLD requires 6262, 31228 and 92680 flops for QPSK, 16QAM and 64QAM, respectively. Then, the complexity of the proposed detection at the BER below 10^{-3} only requires 1998 flops regardless of the modulation order. As a consequence, the proposed detection scheme can achieve the near-ML performance with only a little additional complexity, which is about 32%, 6% and 2% of the complexity of the QRM-MLD for QPSK, 16QAM and 64QAM, respectively.

5.6 Chapter summary

In this chapter, we proposed an improved quantization scheme for LRA MIMO detection using the GSO procedure. The new signal $\tilde{\mathbf{u}}$ in the u-domain was first detected, which was obtained by the receive signal and the GS-orthogonalized channel matrix. Then we led it to the new signal estimate of $\hat{\mathbf{v}}$ in the v-domain accompanying with the information of $\hat{\mathbf{T}}^{-1}$. By applying the signals in the u- and the v-domains, we successfully extracted much reliable estimate of the transmit signal in the s-domain.

In order to decrease the quantization errors in the quantization step in the v-domain, we gave another quantization candidate according to the rounding integer. We used a simple tree search in order to rarely correct some quantization errors. The threshold function was defined using the orthogonal lattice basis of the channel matrix and updated by the minimum partial path metric for each entry of the signal vectors. Hence the BER performance of the proposed detection was improved by decreasing the quantization errors. The numerical results exhibited that the proposed detection achieved the near-ML performance only with a little additional complexity compared to the LR-MMSE. The complexity of the proposed detection at the BER in the high E_b/N_0 region was about 20% and 3% of that of the QRM-MLD in the 4×4 MIMO system, and about 6%

and 2% of that of the QRM-MLD in the 8×8 MIMO system, for 16QAM and 64QAM, respectively. In addition, the proposed quantization scheme was efficient even for the high modulation order.

Chapter 6

Ordering SIC with Conditional List Generation for Lattice-Reduction Aided MIMO Detection

From the previous chapter, the proposed detection achieves the optimal BER performance with very low complexity in the small size MIMO system. The BER performance is remarkably improved in the large size MIMO system with high costs in the LLL algorithm ($\delta = 0.95$). In this chapter, we focus on improving the BER performance in the large size MIMO system and requiring relatively low complexity in the LR operations and the signal estimation.

6.1 Introduction

Many detection methods have been proposed in order to achieve the near-ML performance. In [45], the optimal OSIC based on LR has been proposed by updating the mean and variance of the effective symbols in the LR domain at each SIC detection stage to achieve the near-ML performance in the 4×4 MIMO system. In [46], the channel matrix is forward and backward reduced by the LLL algorithm, respectively. Using two reduced channel matrices in the signal estimation stage can decrease the difference of BERs among all the receive antennas. Meanwhile,

the detection scheme also applies the list detection in order to improve the BER performance. However, it requires somewhat high complexity for the ML metric. The detection scheme in [47] combines the SIC detection with the list detection. In the signal estimation, the partial symbols are first detected by the list detection to avoid the error propagation. After that, the rest of the symbols is obtained by the SIC operations, whose complexity is determined by the length of candidates. These detection scheme using the SIC or/and the list detection have the improvement of the BER performance in the 4×4 MIMO system accompanying with the complexity costs. Hence, most of the low complexity detection methods are effect in the small size MIMO system and the BER improvement is not good in the large size MIMO system.

In this chapter, we first apply the OSIC based on LR, called LR-OSIC, which can obtain more reliable estimation of the transmit signal compared to the LR-SIC. The improvement of the LR-OSIC is not sufficient to approach the ML performance in the large size MIMO. Therefore, we introduce the list detection. In the LR-OSIC, the estimate symbol in the LR domain is also quantized using the rounding operation. Through the observation of the probability distribution of the difference between the estimate symbol and the rounding integer, we evaluate the channel condition. According to the mean squared error of the signal vector in the LR domain, we use the conditional list generation to update the soft estimate of the LR-OSIC under the ill-conditioned channel. Using this property, we decrease the complexity for computing the useless list candidates in the better-conditioned channel. The simulation results also verify that the proposed detection can achieve the near-ML performance in the 8×8 MIMO system and require almost the same complexity of the LR-OSIC in the high E_b/N_0 region.

6.2 System model

The system model employes the real-valued channel matrix and vectors as same as Chapter 5. Recall (5.1) as

$$\mathbf{y} = \mathbf{H}\mathbf{s} + \mathbf{z} \tag{6.1}$$

where the equivalent real-valued channel matrix and vectors letting $n = 2N_r$ and $m = 2N_t$ are defined as

$$\mathbf{H} \triangleq \begin{bmatrix} \mathrm{Re}[\mathbf{H}^c] & -\mathrm{Im}[\mathbf{H}^c] \\ \mathrm{Im}[\mathbf{H}^c] & \mathrm{Re}[\mathbf{H}^c] \end{bmatrix} \in \mathbb{R}^{n \times m}, \ \mathbf{s} \triangleq \begin{bmatrix} \mathrm{Re}[\mathbf{s}^c] \\ \mathrm{Im}[\mathbf{s}^c] \end{bmatrix} \in \mathbb{Z}^{m \times 1},$$
$$\mathbf{y} \triangleq \begin{bmatrix} \mathrm{Re}[\mathbf{y}^c] \\ \mathrm{Im}[\mathbf{y}^c] \end{bmatrix} \in \mathbb{R}^{n \times 1}, \text{ and } \mathbf{z} \triangleq \begin{bmatrix} \mathrm{Re}[\mathbf{z}^c] \\ \mathrm{Im}[\mathbf{z}^c] \end{bmatrix} \in \mathbb{R}^{n \times 1} \tag{6.2}$$

We employ the extended matrix form of the channel matrix and vectors as

$$\bar{\mathbf{y}} \triangleq \begin{bmatrix} \mathbf{y} \\ \mathbf{0}_m \end{bmatrix}, \ \bar{\mathbf{H}} \triangleq \begin{bmatrix} \mathbf{H} \\ \sqrt{\gamma^{-1}}\mathbf{I}_m \end{bmatrix}, \ \bar{\mathbf{z}} \triangleq \begin{bmatrix} \mathbf{z} \\ -\sqrt{\gamma^{-1}}\mathbf{s} \end{bmatrix} \tag{6.3}$$

where $\gamma = E_s/N_0$ with $E_s = \frac{E[\|\mathbf{s}\|^2]}{m}$. Then it holds instead of (6.1) using the QR-decomposition of the channel matrix $\bar{\mathbf{H}}$=$\mathbf{QR}$ as that

$$\bar{\mathbf{y}} = \bar{\mathbf{H}}\mathbf{s} + \bar{\mathbf{z}} \equiv \mathbf{QR}\mathbf{s} + \bar{\mathbf{z}} \tag{6.4}$$

The real LLL algorithm is firstly performed in Table 5.1 to transform $\mathbf{R}$ as $\tilde{\mathbf{R}}$. By pre-multiplying $\tilde{\mathbf{Q}}^{\mathrm{T}}$, the model system using (5.6) is rewritten as

$$\begin{aligned} \mathbf{y}' &= \tilde{\mathbf{Q}}^{\mathrm{T}}\bar{\mathbf{y}}^{\mathcal{S}} \\ &= \tilde{\mathbf{R}}\mathbf{v} + \mathbf{Q}^{\mathrm{T}}\frac{\bar{\mathbf{z}}}{2} \\ &= \tilde{\mathbf{R}}\mathbf{v} + \mathbf{z}' \end{aligned} \tag{6.5}$$

where $\mathbf{z}' \triangleq \tilde{\mathbf{Q}}^{\mathrm{T}}\frac{\bar{\mathbf{z}}}{2}$.

In the case that the entries of $\mathbf{s}$ are of the commonly used QAM mapping, proper shifting and scaling of $\mathbf{s}$ is necessary in order to derive $\tilde{\mathbf{v}}$. The detailed explanation on shifting and scaling operations is given in Chapter 5. Thus, LR-SIC detection scheme starts from the last entry of the signal vector. The last entry of signal v_m is first derived as $\hat{v}_m = \mathcal{Q}\{y'_m/\tilde{r}_{m,m}\}$. Assuming that the previous decisions are correct, the interferences can be cancelled in each step. The rest of

the transmit signals are derived in the following recursion as

$$\hat{v}_i = \mathcal{Q}\left\{\frac{y_i' - \sum_{j=i+1}^{m} \tilde{r}_{i,j}\hat{v}_j}{\tilde{r}_{i,i}}\right\}, i = m-1, \ldots, 1. \tag{6.6}$$

As the same method as the LR-MMSE detection, the signal vector in the LR domain should be transformed back into the s-domain as

$$\hat{\mathbf{s}}^{\mathcal{S}} = \mathbf{T}\hat{\mathbf{v}} \tag{6.7}$$

$$\hat{\mathbf{s}} = \mathcal{S}^{-1}[\hat{\mathbf{s}}^{\mathcal{S}}] = 2\hat{\mathbf{s}}^{\mathcal{S}} - (K-1)\mathbf{1}_m \tag{6.8}$$

Using the same method, the final decision $\hat{\mathbf{s}}$ is forced to the nearest constellation points if they are lying outside the original signal constellation as $\hat{\mathbf{s}} := \mathcal{C}[\hat{\mathbf{s}}]$.

6.3 Proposed LR-OSIC with conditional list generation

The LRA detection can achieve full diversity gain like the ML detector. However, the LLL algorithm does not guarantee to find out the shortest lattice vector. Hence the LRA detection degrades the performance compared to the ML detection, especially in the large size MIMO. We first present the LR-SIC detection, and next the more reliable symbols are prior to being detected in the LR-OSIC. After that, we introduce the conditional list generation based on the soft estimate of the LR-OSIC to rarely correct the estimate errors, leading to better BER performance. Since the proposed detection is based on the LR-OSIC, first the ordering method will be briefly described as follows.

6.3.1 Ordering the real lattice basis of channel matrix

Ordering the column vectors of the LLL-reduced channel matrix brings large improvement on the BER performance of the LR-SIC due to decreasing the error propagation. The estimate errors of the new signal vector in the LR domain correspond to the main diagonal entries of the error covariance matrix $\mathbf{\Phi}$, defined

as

$$\begin{aligned}\mathbf{\Phi} &= E\Big[(\tilde{\mathbf{v}}-\mathbf{v})(\tilde{\mathbf{v}}-\mathbf{v})^{\mathrm{T}}\Big] = E\Big[\tilde{\mathbf{R}}^{-1}\mathbf{z}'\mathbf{z}'^{\mathrm{T}}(\tilde{\mathbf{R}}^{-1})^{\mathrm{T}}\Big] \\ &= \tilde{\mathbf{R}}^{-1}E\Big[\mathbf{z}'\mathbf{z}'^{\mathrm{T}}\Big](\tilde{\mathbf{R}}^{-1})^{\mathrm{T}} = (\tilde{\mathbf{R}})^{-1}\frac{N_0}{8}\mathbf{I}_m(\tilde{\mathbf{R}}^{-1})^{\mathrm{T}} \\ &= \frac{N_0}{8}\Big(\tilde{\mathbf{R}}^{\mathrm{T}}\tilde{\mathbf{R}}\Big)^{-1} \end{aligned} \tag{6.9}$$

It is obvious that the small eigenvalue of $\tilde{\mathbf{R}}^{\mathrm{T}}\tilde{\mathbf{R}}$ will lead to large errors due to noise amplification. According to (6.9), let $\mathbf{\Psi} = (\tilde{\mathbf{R}}^{\mathrm{T}}\tilde{\mathbf{R}})^{-1}$. In this chapter, we propose a simplified ordering method using the output of the LLL algorithm in the following procedures.

Algorithm: Ordering the real lattice basis.

Input: $\tilde{\mathbf{Q}}, \tilde{\mathbf{R}}$, and $\mathbf{T}$.

Output: The updated $\tilde{\mathbf{Q}}$, the updated $\tilde{\mathbf{R}}$, and the ordered $\mathbf{T}$.

- *Step* 1) Calculate $\mathbf{\Psi}_m = (\tilde{\mathbf{R}}_m^{\mathrm{T}}\tilde{\mathbf{R}}_m)^{-1}$, where the subscript m denotes the dimensions of the square matrix. Note that since $\tilde{\mathbf{R}}$ is the upper triangular matrix, the partial square matrix $\tilde{\mathbf{R}}_l$ denotes the partial columns(rows) of $\tilde{\mathbf{R}}$ from the first column(row) to the l-th column(row), $l \in [2, m]$.

- *Step* 2) Find out the minimum diagonal element of $\mathbf{\Psi}_m$. Then the specific transmit signal having the lowest detection error variance is first detected. Swapping this specific column to the last column in $\tilde{\mathbf{R}}$ and $\mathbf{T}$ by turns, we apply the Givens rotation matrix $\mathbf{\Theta}$ seen in Table 5.1 to keep the upper triangular matrix for $\tilde{\mathbf{R}}$. And $\tilde{\mathbf{Q}}$ is also updated by multiplying $\mathbf{\Theta}^{\mathrm{T}}$.

- *Step* 3) The iterations including *Step* 1) and *Step* 2) are performed. In each stage, $\mathbf{\Psi}_i = (\tilde{\mathbf{R}}_i^{\mathrm{T}}\tilde{\mathbf{R}}_i)^{-1}$ is first obtained, where $i = m-1, \ldots, 2$. Then the column of $\tilde{\mathbf{R}}_i$ corresponding to the minimum diagonal element of $\mathbf{\Psi}_i$ should be swapped to the i-th column of $\tilde{\mathbf{R}}_i$ by turns. Until the iteration with $i = 2$ is finished, finally obtain the output the updated $\tilde{\mathbf{Q}}$, the updated $\tilde{\mathbf{R}}$ and $\mathbf{T}$.

The ordering operations requires the polynomial complexity including the computation of the error covariance matrix $\mathbf{\Psi}_i$, $i \in [1, m]$, and the Givens rotation

matrix. Since the updated $\tilde{\mathbf{R}}$ has the information of the detection error variance, more reliable symbol is prior to being estimated by the SIC operations in (6.6). The ordered $\mathbf{T}$ records the whole operations of the updated $\tilde{\mathbf{R}}$, which is a unitary matrix. At last, align back the estimate signals to the original order as $\hat{\mathbf{s}} := \mathcal{C}[\mathcal{S}^{-1}[\mathbf{T}^{-1}\hat{\mathbf{v}}]]$.

6.3.2 Proposed LR-OSIC with conditional list generation

For the SIC operations, the simplest quantization in (6.6) is the rounding operation as $\hat{\mathbf{v}} = \mathcal{Q}\{\tilde{\mathbf{v}}\}$. However, the superior BER cannot be achieved only by rounding off the estimate symbol. First, we observe the probability distribution of $\tilde{\mathbf{v}} - \hat{\mathbf{v}}$ with all the antennas' signals using the LR-OSIC for QPSK, 16QAM and 64QAM in the 4×4 and 8×8 MIMO systems as shown in Figs. 6.1 - 6.6, respectively.

As illustrated in Figs. 6.1 - 6.6, the probability distribution of $\tilde{\mathbf{v}} - \hat{\mathbf{v}}$ is close to the average distribution in the low E_b/N_0 region. The quantization error often happens in case that the difference of $(\tilde{v}_i - \hat{v}_i)$ is around ± 0.5, $i \in [1, m]$. On the contrary, the probability distribution of $\tilde{\mathbf{v}} - \hat{\mathbf{v}}$ approaches to the Gaussian distribution as E_b/N_0 increases. The quantization errors should rarely occur since the difference is concentrated to zero.

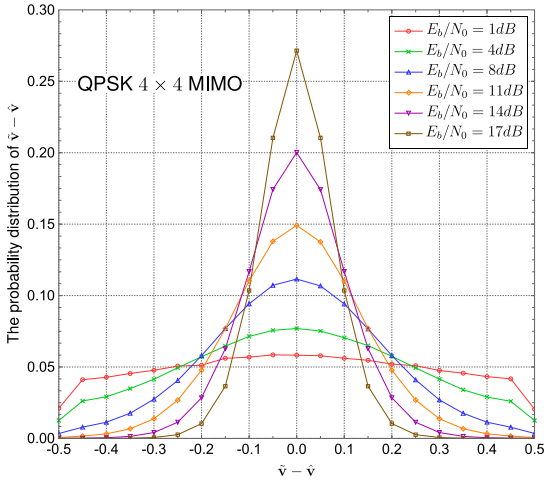

Figure 6.1: The probability distribution of $\tilde{\mathbf{v}} - \hat{\mathbf{v}}$ for LR-OSIC in the 4×4 MIMO: QPSK.

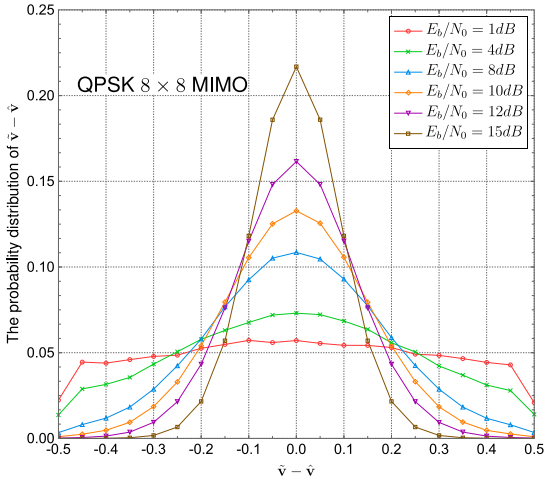

Figure 6.2: The probability distribution of $\tilde{\mathbf{v}} - \hat{\mathbf{v}}$ for LR-OSIC in the 8×8 MIMO: QPSK.

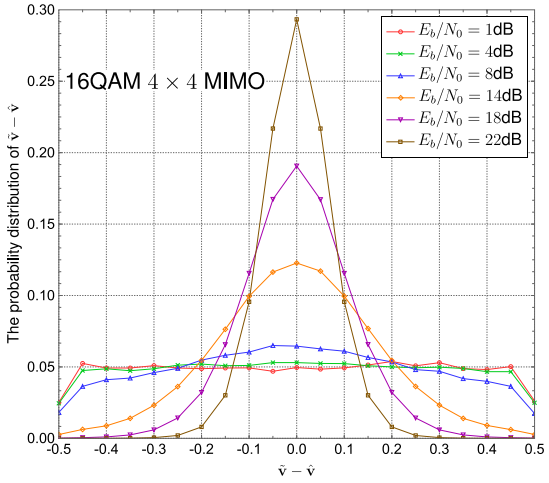

Figure 6.3: The probability distribution of $\tilde{\mathbf{v}} - \hat{\mathbf{v}}$ for LR-OSIC in the 4×4 MIMO: 16QAM.

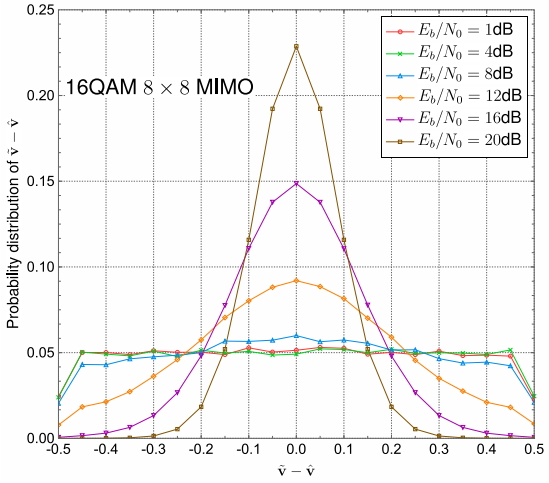

Figure 6.4: The probability distribution of $\tilde{\mathbf{v}} - \hat{\mathbf{v}}$ for LR-OSIC in the 8×8 MIMO: 16QAM.

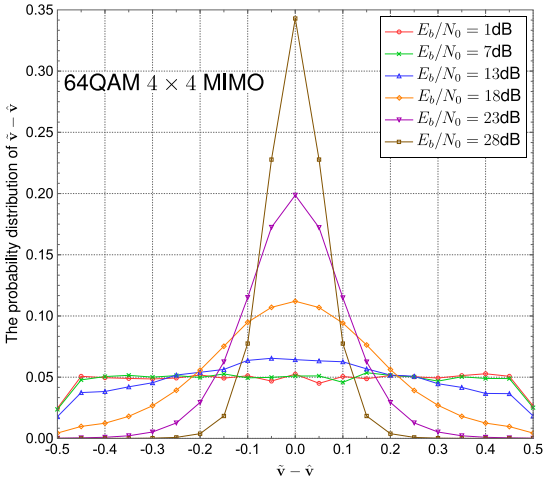

Figure 6.5: The probability distribution of $\tilde{\mathbf{v}} - \hat{\mathbf{v}}$ for LR-OSIC in the 4×4 MIMO: 64QAM.

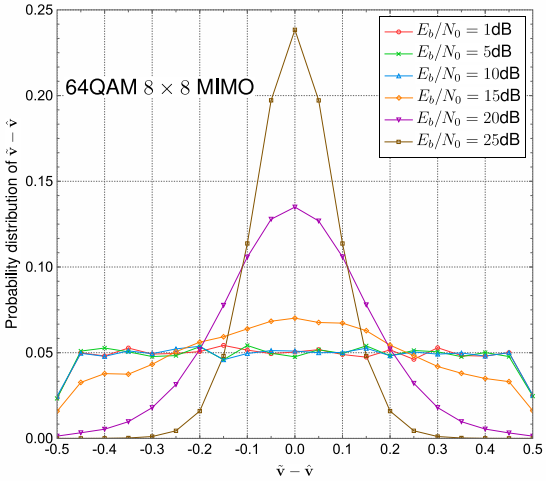

Figure 6.6: The probability distribution of $\tilde{\mathbf{v}} - \hat{\mathbf{v}}$ for LR-OSIC in the 8×8 MIMO: 64QAM.

Hence we define the mean squared error of the new signal vector in LR domain as $\varepsilon_v \triangleq \sum_{i=1}^{m} |\tilde{v}_i - \hat{v}_i|^2$. And define a threshold of the mean squared error ε_{TH} as

$$\varepsilon_{TH} \triangleq \Delta^2 \cdot m \tag{6.10}$$

with

$$\Delta^2 \triangleq \frac{\sum_{i=1}^{m} |\tilde{v}_i - \hat{v}_i|^2}{m} \tag{6.11}$$

where ε_{TH} is predetermined by the MIMO size and Δ^2 denotes the average mean squared error of the new signal vector, of which the difference of $(\tilde{v}_i - \hat{v}_i)$ is $\pm\Delta$ to zero in Figs. 6.1 - 6.6. The value $|\Delta|$ is chosen from $|\Delta| = \{0.1, 0.15, 0.2\}$ and $|\Delta| \leq 0.5$. Therefore, if $\varepsilon_v \leq \varepsilon_{TH}$, let the estimate symbols of the LR-OSIC be the final decision. Else, we propose the conditional list detection to update the estimate of the LR-OSIC. This proposed detection is called LR-OSIC with conditional list generation.

The list detection is proposed based on the soft estimate of the LR-OSIC. The list tree is generated in Fig. 6.7, where l denotes the list number, $l \in [0, m]$. The estimated symbols in the list 0 are detected by the LR-OSIC, expressing as $\hat{\mathbf{v}}^{(0)} = \left[\hat{v}_1^{(0)}, \hat{v}_2^{(0)}, \ldots, \hat{v}_m^{(0)}\right]^{\mathrm{T}}$. The quantization error often happens in case that the difference of $(\tilde{v}_i - \hat{v}_i)$ is around ± 0.5, $i \in [1, m]$. We give another

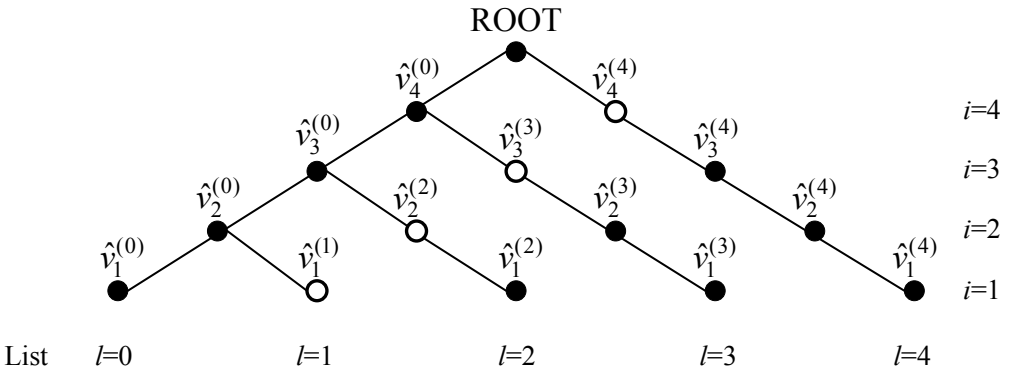

Figure 6.7: The example of list tree in 2×2 MIMO.

candidate for each entry of the soft estimate of the LR-OSIC. Thus, the symbols $\hat{v}_i^{(l)}$ with $l = i$ marked white nodes in Fig. 6.7 are obtained by $+1$ or -1 on the rounding integer obtained by the estimate of LR-OSIC. The symbols in the l-th list $\hat{\mathbf{v}}^{(l)} = \left[\hat{v}_1^{(l)}, \hat{v}_2^{(l)}, \ldots, \hat{v}_m^{(l)}\right]^{\mathrm{T}}$ are defined as

$$\hat{v}_i^{(l)} = \begin{cases} \hat{v}_i^{(0)} & l > i \\ \hat{v}_i^{(0)} + \mathrm{sgn}\left(\tilde{v}_i^{(0)} - \hat{v}_i^{(0)}\right) & l = i \\ \mathcal{Q}\left\{\tilde{v}_i^{(l)}\right\} = \mathcal{Q}\left\{\frac{y_i' - \sum_{j=i+1}^{m} \tilde{r}_{i,j}\hat{v}_j^{(l)}}{\tilde{r}_{i,i}}\right\} & l < i \end{cases} \tag{6.12}$$

Then, all the list candidates can be expressed as

$$\begin{aligned} \hat{\mathbf{v}}^{(1)} &= \left[\hat{v}_1^{(1)}, \hat{v}_2^{(1)}, \ldots, \hat{v}_m^{(1)}\right]^{\mathrm{T}} = \left[\hat{v}_1^{(1)}, \hat{v}_2^{(0)}, \ldots, \hat{v}_m^{(0)}\right]^{\mathrm{T}} \\ \hat{\mathbf{v}}^{(2)} &= \left[\hat{v}_1^{(2)}, \hat{v}_2^{(2)}, \ldots, \hat{v}_m^{(2)}\right]^{\mathrm{T}} = \left[\hat{v}_1^{(2)}, \hat{v}_2^{(2)}, \hat{v}_3^{(0)}, \ldots, \hat{v}_m^{(0)}\right]^{\mathrm{T}} \\ &\vdots \\ \hat{\mathbf{v}}^{(l)} &= \left[\hat{v}_1^{(l)}, \hat{v}_2^{(l)}, \ldots, \hat{v}_m^{(l)}\right]^{\mathrm{T}} = \left[\hat{v}_1^{(l)}, \ldots, \hat{v}_l^{(l)}, \hat{v}_{l+1}^{(0)}, \ldots, \hat{v}_m^{(0)}\right]^{\mathrm{T}} \\ &\vdots \\ \hat{\mathbf{v}}^{(m)} &= \left[\hat{v}_1^{(m)}, \hat{v}_2^{(m)}, \ldots, \hat{v}_m^{(m)}\right]^{\mathrm{T}} = \left[\hat{v}_1^{(m)}, \hat{v}_2^{(m)}, \ldots, \hat{v}_m^{(m)}\right]^{\mathrm{T}} \end{aligned} \tag{6.13}$$

In Fig. 6.7, the number under the nodes denotes the partial path metric for

each list candidate. If $\varepsilon_v > \varepsilon_{TH}$ in this example, the estimate symbols in list 2 should update the final new vector with smallest path metric. Thus, the ML metric ignoring a scaling factor for constructing the list becomes

$$\|\mathbf{y} - \mathbf{H}\mathbf{s}\|^2 \sim \left\|\mathbf{y}' - \tilde{\mathbf{R}}\mathbf{v}\right\|^2 \tag{6.14}$$

The probability function of the transmit signal can be expressed as $P(\mathbf{y}|\mathbf{s}) = \frac{1}{\sqrt{2\pi N_0}} \exp\left(-\frac{\|\mathbf{y}-\mathbf{H}\mathbf{s}\|^2}{2N_0}\right) \sim \frac{1}{\sqrt{2\pi N_0}} \exp\left(-\frac{\left\|\mathbf{y}'-\tilde{\mathbf{R}}\mathbf{v}\right\|^2}{2N_0}\right)$. According to (6.5), the new signal vector can be expressed as

$$\begin{aligned}
\tilde{\mathbf{v}} =& \tilde{\mathbf{R}}^{-1}\mathbf{y}' \\
=& \tilde{\mathbf{R}}^{-1}(\tilde{\mathbf{R}}\mathbf{v} + \mathbf{z}') \\
=& \mathbf{v} + \tilde{\mathbf{R}}^{-1}\mathbf{z}' \\
=& \mathbf{v} + \tilde{\mathbf{R}}^{-1}\frac{\mathbf{Q}^{\mathrm{T}}\mathbf{z}}{2} \\
=& \mathbf{v} + \tilde{\mathbf{z}}
\end{aligned} \tag{6.15}$$

where $\tilde{\mathbf{z}} \triangleq \tilde{\mathbf{R}}^{-1}\frac{\mathbf{Q}^{\mathrm{T}}\mathbf{z}}{2}$. Since the elements of $\mathbf{z}$ are i.i.d. Gaussian, $\tilde{\mathbf{z}}$ is jointly Gaussian with zero mean and covariance matrix given by $\mathbf{G} = \frac{N_0}{2}\frac{\tilde{\mathbf{R}}^{-1}\mathbf{Q}^{\mathrm{T}}}{2}\left(\frac{\tilde{\mathbf{R}}^{-1}\mathbf{Q}^{\mathrm{T}}}{2}\right)^{\mathrm{T}} = \frac{N_0}{8}\left(\tilde{\mathbf{R}}^{\mathrm{T}}\tilde{\mathbf{R}}\right)^{-1}$. Using the list candidates of the new signal vector, we have

$$\begin{aligned}
P(\mathbf{y}'|\hat{\mathbf{v}}^{(l)}) &= P(\mathbf{z}' = \tilde{\mathbf{v}}^{(l)} - \hat{\mathbf{v}}^{(l)}) \\
&= \frac{1}{((2\pi)^m \det \mathbf{G})^{\frac{1}{2}}} \exp\left(-\frac{1}{2}\left[\tilde{\mathbf{v}}^{(l)} - \hat{\mathbf{v}}^{(l)}\right]^{\mathrm{T}} \mathbf{G} \left[\tilde{\mathbf{v}}^{(l)} - \hat{\mathbf{v}}^{(l)}\right]\right)
\end{aligned} \tag{6.16}$$

Therefore the optimal estimate of new signal vector $\hat{\mathbf{v}}$ is chosen from $\hat{\mathbf{v}} = \{\hat{\mathbf{v}}^{(0)}, \hat{\mathbf{v}}^{(1)}, \ldots, \hat{\mathbf{v}}^{(m)}\}$, determined using the ED as

$$\begin{aligned}
\hat{\mathbf{v}}^{<\mathrm{opt}>} &= \arg\min_{l\in[0,m]} \sum_{i=1}^{m} \left| y'_i - \tilde{r}_{i,i}\hat{v}_i^{(l)} - \sum_{j=i+1}^{m} \tilde{r}_{i,j}\hat{v}_j^{(l)} \right|^2 \\
&= \arg\min_{l\in[0,m]} \sum_{i=1}^{m} \left| y_i''^{(l)} - \tilde{r}_{i,i}\hat{v}_i^{(l)} \right|^2
\end{aligned} \tag{6.17}$$

where the receive signal subtracted the interferences is defined as $y_i''^{(l)} \triangleq y'_i -$

$\sum_{j=i+1}^{m} \tilde{r}_{i,j}\hat{v}_j^{(l)}$.

The proposed LR-OSIC with conditional list detection is summarized in Table 6.1. The value of ε_{TH} is a tradeoff between the BER performance and the complexity. In the proposed detection, we apply the ML metric in the LR domain to obtain the optimal estimate of the new signal vector with the smallest path metric. In some cases that the quantization errors may occur, the list detection is used to update the soft estimate of the LR-OSIC in the condition of $\varepsilon_v > \varepsilon_{TH}$. Hence the path metric of the updated estimate of the new signal vector should be smaller than that of the estimate signal of the LR-OSIC, which results in the superior BER performance.

Table 6.1: LR-OSIC with conditional list detection

Input: $\mathbf{y}'$, the updated $\tilde{\mathbf{R}}$, the ordered $\mathbf{T}$ and $\hat{\mathbf{v}}^{(0)}$; Output: $\hat{\mathbf{s}}$
(1) **Initialization**: ε_{TH} and $\mathbf{y}'^{(l)} = \mathbf{y}'$.
(2) $\varepsilon_v \triangleq \sum_{i=1}^{m} \lvert\tilde{v}_i^{(0)} - \hat{v}_i^{(0)}\rvert^2$
(3) **if** $\varepsilon_v \leq \varepsilon_{TH}$
(4) $\quad\hat{\mathbf{v}}^{(\mathrm{Opt})} = \hat{\mathbf{v}}^{(0)}$.
(5) **end if**
(6) **else**
(7) $\quad$List candidates are generated in (6.12): $\hat{\mathbf{v}}^{(l)}, l \in [1, m]$.
(8) $\quad\hat{\mathbf{v}}^{(\mathrm{Opt})} = \arg\min_{l\in[0,m]} \sum_{i=1}^{m} \left\lvert y_i'^{(l)} - \tilde{r}_{i,i}\hat{v}_i^{(l)} - \sum_{j=i+1}^{m} \tilde{r}_{i,j}\hat{v}_j^{(l)} \right\rvert^2$.
(9) **end else**
(10) $\hat{\mathbf{s}}^{\mathcal{S}} = \mathcal{S}^{-1}[\mathbf{T}^{-1}\hat{\mathbf{v}}^{(\mathrm{Opt})}]$.
(11) $\hat{\mathbf{s}} := \mathcal{C}[\mathcal{S}^{-1}[\hat{\mathbf{s}}^{\mathcal{S}}]]$.
(12) **End**

6.4 Numerical results

The computer simulations were carried out for QPSK, 16QAM and 64QAM in the 4×4 and 8×8 MIMO systems, respectively. In the simulations, the channel gains were generated using the i.i.d. Gaussian random variables with zero mean and variance of 1/2 for each dimension. Additive noise at each receive antenna was generated using the i.i.d. Gaussian random variables with zero mean and variance

of $N_0/2$ for each dimension. The performances of the different detections were measured by the BER performance and the complexity.

6.4.1 Suitable values of factor δ and ε_{TH}

We observe that the various value of δ has a great influence on the BER performance, and look for a suitable value of δ for the proposed detection with $\varepsilon_{TH} = \{0.16, 0.36, 0.64\}$.

The various value of δ vs. the BER characteristics for QPSK, 16QAM and 64QAM in the 4×4 MIMO system are shown in Figs. 6.8, 6.10 and 6.12, respectively. In Fig. 6.8, the BER curves for QPSK are compared at the fixed E_b/N_0 of 16dB. The the proposed detection with $\varepsilon_{TH} = \{0.16, 0.36, 0.64\}$ has almost same BER characteristics as the various δ. For the LR-SIC detections, the BER characteristics achieve the great performance with δ more than 0.75. The LR-OSIC detection has same trend as the proposed detection. Figure 6.10 shows the BER curves for 16QAM at the fixed E_b/N_0 of 21dB. The proposed detections with $\varepsilon_{TH} = \{0.16, 0.36, 0.64\}$ have almost same BER performance and provide the great BER performance at $\delta \geq 0.4$. As seen in Fig. 6.12, the BER curves for 64QAM are compared at the fixed E_b/N_0 of 26dB. The trends of the proposed detections are as same as that of the BER curves for 16QAM in Fig. 6.10. The proposed detections with $\varepsilon_{TH} = \{0.16, 0.36, 0.64\}$ provide the great BER performance at $\delta \geq 0.5$.

Figures 6.9, 6.11 and 6.13 show the various value of δ vs. the BER characteristics for QPSK, 16QAM and 64QAM in the 8×8 MIMO system, respectively. We observe the BER characteristics for the proposed detection at the fixed E_b/N_0 of 12dB, 18dB and 21dB for QPSK, 16QAM and 64QAM, respectively. For the conventional detections, the value of δ is assigned as 0.75 for the LR-SIC and LR-OSIC as the common choice. For the proposed detections with $\varepsilon_{TH} = \{0.16, 0.36, 0.64\}$ regardless of the modulation order achieve better BER performance as the value of δ increases or the value of ε_{TH} decreases. Hence the conditional list detection remarkably reduces the error propagation.

The values of δ and ε_{TH} are the tradeoff factors between the complexity and the BER performance. In the large size MIMO system, the value of δ has less

influence to the BER performance. However, if the decision boundary is not good, the condition list detection is performed to correct the error estimation. Hence, if we choose a suitable value of δ, we can obtain the better decision boundary. And the smaller percentage of $\varepsilon_{TH} > \varepsilon_v$ also reduces the complexity of the proposed detection.

We summarize the suitable value for both factors for the proposed detection in Table 6.2.

Table 6.2: The suitable values of factor δ and ε_{TH} for the proposed detection

Modulation order	$N_t = N_r = 4$	$N_t = N_r = 8$
QPSK	$\delta = 0.0$, $\varepsilon_{TH} = 0.36$	$\delta = 0.5$, $\varepsilon_{TH} = 0.36$
16QAM	$\delta = 0.4$, $\varepsilon_{TH} = 0.36$	$\delta = 0.6$, $\varepsilon_{TH} = 0.36$
64QAM	$\delta = 0.5$, $\varepsilon_{TH} = 0.36$	$\delta = 0.6$, $\varepsilon_{TH} = 0.36$

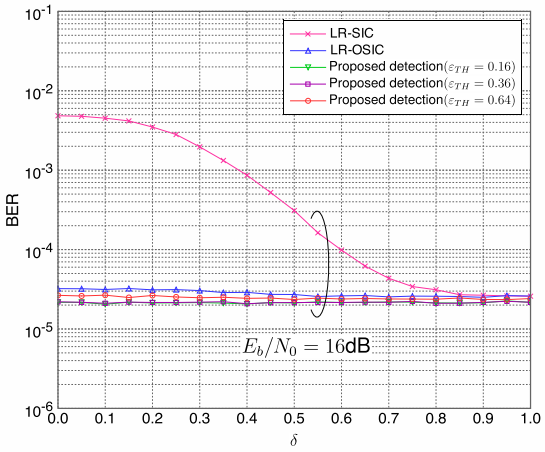

Figure 6.8: The δ vs. BER characteristics in the 4×4 MIMO system: QPSK.

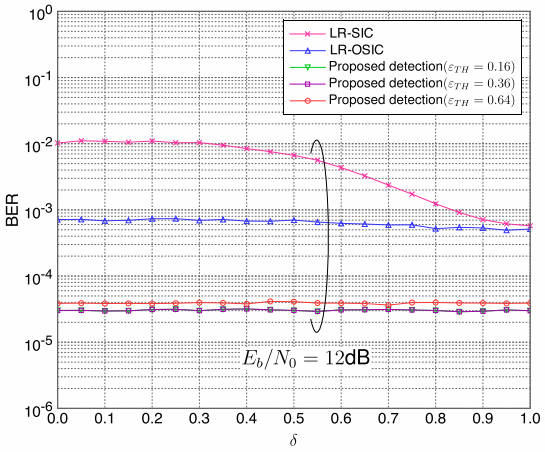

Figure 6.9: The δ vs. BER characteristics in the 8×8 MIMO system: QPSK.

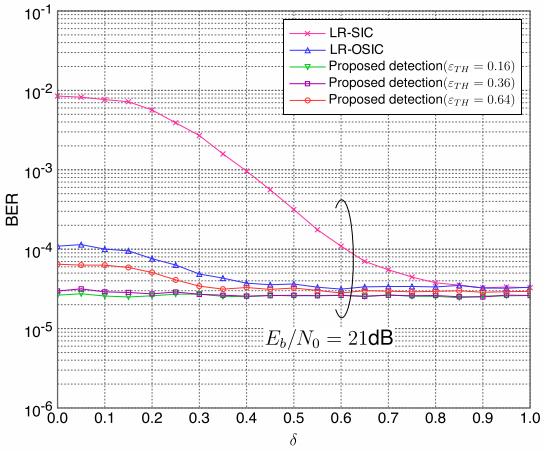

Figure 6.10: The δ vs. BER characteristics in the 4×4 MIMO system: 16QAM.

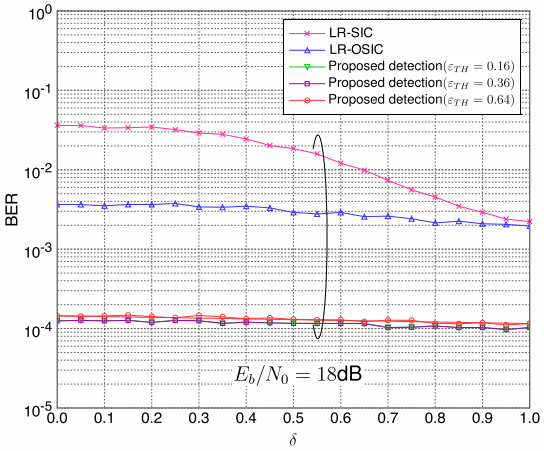

Figure 6.11: The δ vs. BER characteristics in the 8×8 MIMO system: 16QAM.

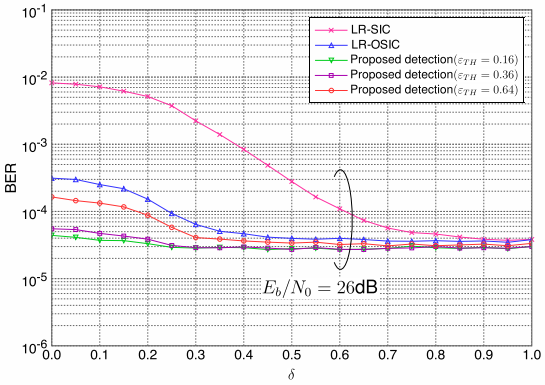

Figure 6.12: The δ vs. BER characteristics in the 4×4 MIMO system: 64QAM.

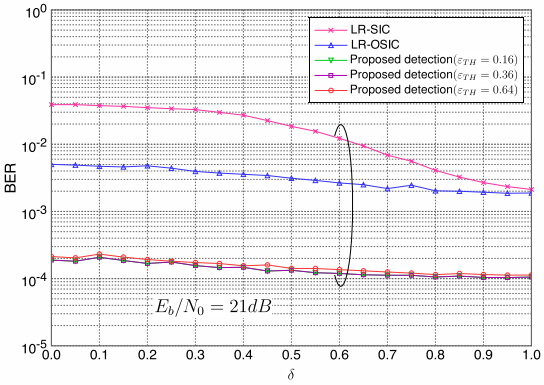

Figure 6.13: The δ vs. BER characteristics in the 8×8 MIMO system: 64QAM.

6.4.2 BER characteristics

We made computer simulations of the BER characteristics versus E_b/N_0 using the LR-SIC, the LR-OSIC, the proposed detection with $\varepsilon_{TH} = \{0.16, 0.36, 0.64\}$, respectively. Corresponding to $\varepsilon_{TH} = \{0.16, 0.36, 0.64\}$, the value Δ^2 is chosen from $\Delta^2 = \{0.1, 0.15, 0.2\}$.

Figure 6.14 shows the BER vs. E_b/N_0 for QPSK in the 4×4 MIMO system. The proposed detection with $\varepsilon_{TH} = \{0.16, 0.36, 0.64\}$ has a little improvement at a BER of 10^{-5} compared to LR-OSIC, respectively. Figure 6.15 shows the

BER vs. E_b/N_0 for QPSK in the 8×8 MIMO system. The curve of the LR-OSIC for QPSK improves 2dB gain compared with that of the LR-SIC and is still about 2dB worse than that of the ML at the BER of 10^{-5}. However, the proposed detection with $\varepsilon_{TH} \leq 0.36$ can achieve the near-ML BER performance, which almost coincides with the ML curve below the BER of 10^{-4}. It is noticed that the proposed detection with $\varepsilon_{TH} = 0.64$ has great improvement of the BER performance with lower complexity discussed in the following subsection.

As shown in Fig. 6.16, for 16QAM in the 4×4 MIMO system, the proposed detection with $\varepsilon_{TH} = \{0.16, 0.36, 0.64\}$ has a little improvement at a BER of 10^{-5} compared to LR-OSIC, respectively. In Fig. 6.17, the curve of the LR-OSIC for 16QAM in the 8×8 MIMO system improves 2dB gain compared with that of the LR-SIC and is still about 3.2dB worse than that of the ML at the BER of 10^{-5}. In addition, the curve of the proposed detection with $\varepsilon_{TH} \leq 0.36$ for 16QAM significantly improves 2.8dB gain compared with that of the LR-OSIC at the BER of 10^{-5}, which is about 0.4dB worse than that of the ML at the BER of 10^{-5}. However, the curve of the proposed detection is much steeper than that of ML detection. It illustrates that both of curves may coincide below the BER of 10^{-5}.

Figures 6.18 and 6.19 show the BER vs. E_b/N_0 for 64QAM in the 4×4 and the 8×8 MIMO systems, respectively. The proposed detection with $\varepsilon_{TH} = \{0.16, 0.36, 0.64\}$ in Fig. 6.18 has a little improvement at a BER of 10^{-5} compared to LR-OSIC, respectively. As the same trend, the proposed detection as seen in Fig 6.19 can also provides the near-ML performance in the 8×8 MIMO system.

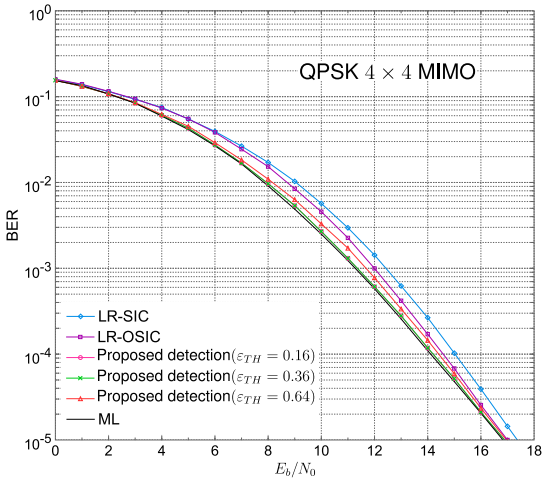

Figure 6.14: The E_b/N_0 vs. BER characteristics in the 4×4 MIMO: QPSK.

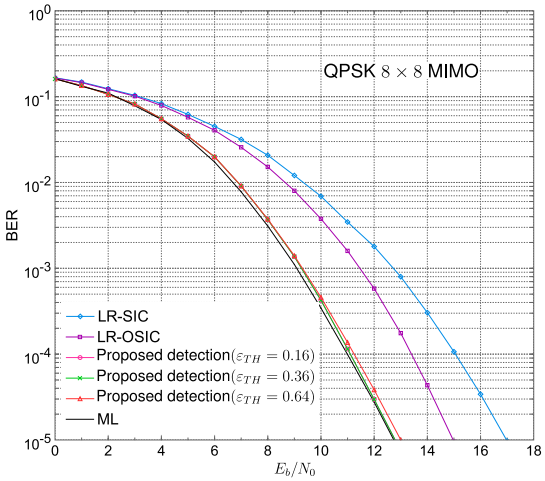

Figure 6.15: The E_b/N_0 vs. BER characteristics in the 8×8 MIMO: QPSK.

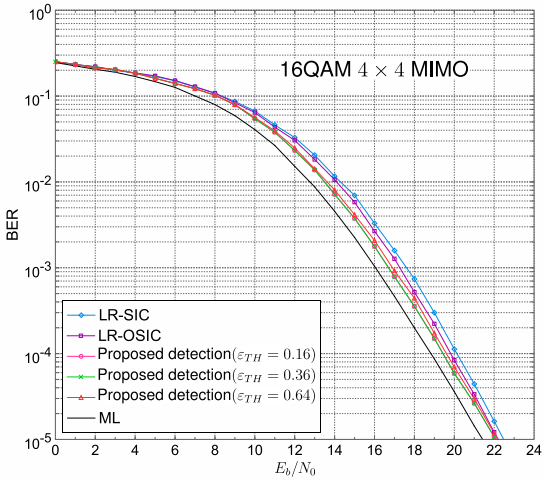

Figure 6.16: The E_b/N_0 vs. BER characteristics in the 4×4 MIMO: 16QAM.

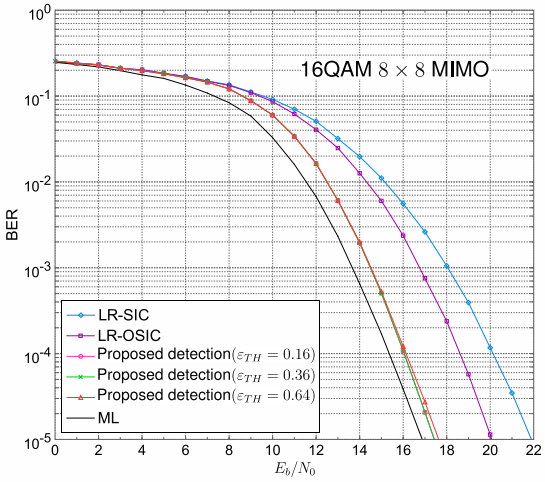

Figure 6.17: The E_b/N_0 vs. BER characteristics in the 8×8 MIMO: 16QAM.

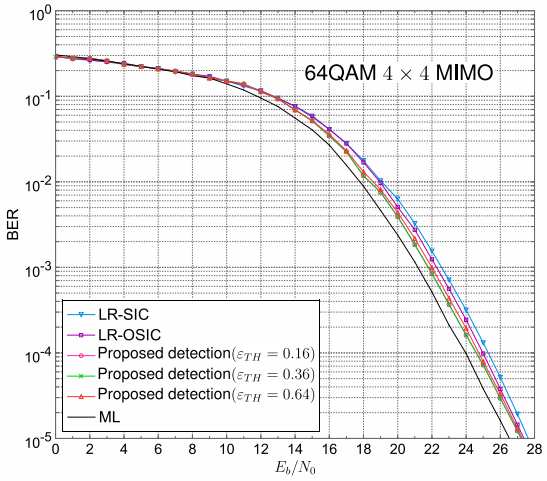

Figure 6.18: The E_b/N_0 vs. BER characteristics in the 4×4 MIMO: 64QAM.

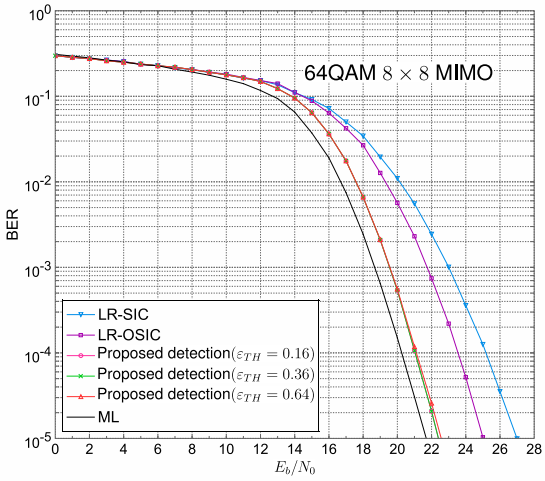

Figure 6.19: The E_b/N_0 vs. BER characteristics in the 8×8 MIMO: 64QAM.

Thus, the proposed detection has great improvement of BER performance compared to LR-OSIC and is effective with the same list candidates in the 8×8 MIMO system. Even for the high modulation order such as 64QAM, the proposed detection also requires the same complexity as the modulation order of QPSK and 16QAM.

6.4.3 Computational complexity

The flat fading channel is assumed that the data packet length is much shorter than the coherence time of the channel, treating the channel to be non-time varying during the packet duration. The LLL reduction and ordering operations of the channel matrix are performed at the beginning of the packet, which features the polynomial complexity. Hence we can apply them all over the packet and the above complexity can be negligible. We focus on the analysis of the computational complexity in the signal estimation stage.

We compared the complexity of the LR-SIC, the LR-OSIC and the proposed detection in the signal estimation, respectively. Without the ordering operations, the LR-SIC and the LR-OSIC have the same complexity in the signal estimation stage. The complexity for computing $\mathbf{y}'$ in (6.5) and $\hat{\mathbf{v}}$ in (6.6) is counted up

as $(8N_t^2 + 8N_tN_r - 2N_t)$ and $4N_t^2$ flops, respectively. The scaled and shifted operations in (6.8) requires $(4N_t + 4N_r)$ flops. In addition, the scaled back and the shifted back operations for the transmit signal is counted up as $4N_t$ flops . Hence, the total complexity of the LR-OSIC is $(20N_t^2 + 8N_tN_r + 4N_t + 4N_r)$ flops, which requires 480 flops for $N_t = N_r = 4$ and 1856 flops for $N_t = N_r = 8$.

We observed the probability of $\varepsilon_v \leq \varepsilon_{TH}$ for the proposed detection with $\varepsilon_{TH} = \{0.16, 0.36, 0.64\}$ in the 4×4 and the 8×8 MIMO systems, respectively, which implied the percentage of the estimate of the LR-OSIC detection to be the final estimate of the transmit signal without the list generation. The additional complexity for the list generation is $2N_t$ and $(\frac{16N_t^3 - N_t}{3} - 2N_t^2)$ flops for computing the candidates with $l = i$ and the rest symbols with $l < i$ in (6.12), respectively. And the optimal decision in (6.17) requires $8N_t$ flops for computing the path metric of the LR-OSIC and $(8N_t^2 + 4N_t)$ flops for that of the list candidates. The total extra complexity of the conditional list generation requires $(\frac{16N_t^3 + 41N_t}{3} + 6N_t^2)$ flops.

As seen in Figs. 6. 20 - 6. 25, the probability of $\varepsilon_v \leq \varepsilon_{TH}$ for the proposed detection with $\varepsilon_{TH} = 0.64$ is more than 95% corresponding to a BER below 10^{-3} for three modulations in the 4×4 MIMO system, which results in lower complexity of the conditional list generation. Therefore, the proposed detection with $\varepsilon_{TH} = 0.64$ has much better tradeoff between the BER performance and the complexity.

In the 8×8 MIMO system, since the proposed detection with $\varepsilon_{TH} = 0.36$ can achieve the near-ML performance, the percentages of $\varepsilon_v \leq \varepsilon_{TH}$ for QPSK, 16QAM and 64QAM are about 88%, 88% and 90% corresponding to the BER of 10^{-4}, and about 96%, 96% and 97% corresponding to the BER of 10^{-5}, respectively. Therefore, the conditional list detection requires very lower complexity at a BER below 10^{-4} and the proposed detection requires almost the same complexity of the LR-OSIC in the high E_b/N_0 region, which requires 1856 flops for $N_t = N_r = 8$ excluding the complexity of the LR operations and the ordering operations. It is noticeable that the same complexity of the proposed detection is required regardless the modulation order, which is more worthy for the high modulation order such as 64QAM.

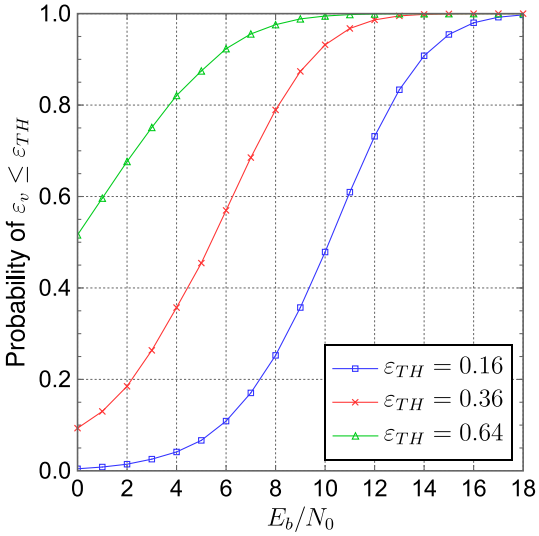

Figure 6.20: The E_b/N_0 vs. Probability of $\varepsilon_v \leq \varepsilon_{TH}$ for the proposed detection in the 4×4 MIMO: QPSK.

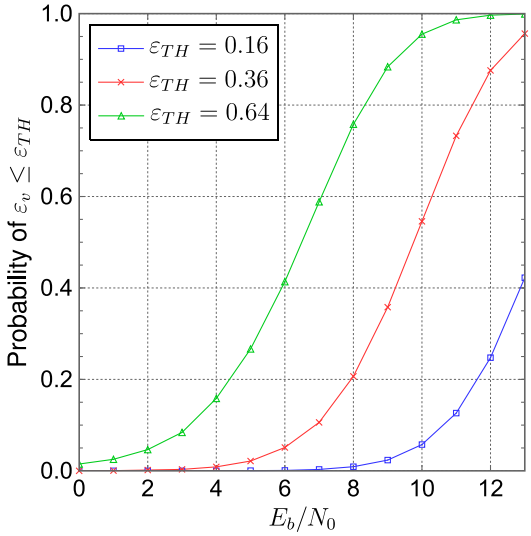

Figure 6.21: The E_b/N_0 vs. Probability of $\varepsilon_v \leq \varepsilon_{TH}$ for the proposed detection in the 8×8 MIMO: QPSK.

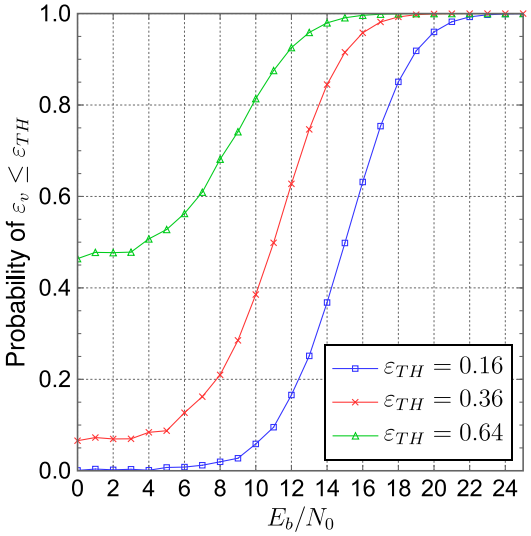

Figure 6.22: The E_b/N_0 vs. Probability of $\varepsilon_v \leq \varepsilon_{TH}$ for the proposed detection in the 4×4 MIMO: 16QAM.

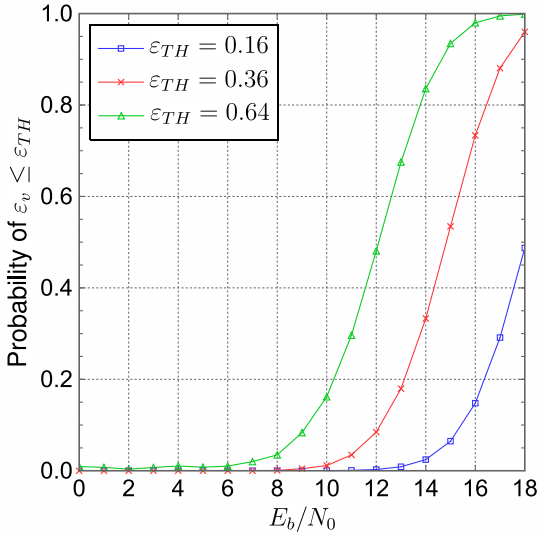

Figure 6.23: The E_b/N_0 vs. Probability of $\varepsilon_v \leq \varepsilon_{TH}$ for the proposed detection in the 8×8 MIMO: 16QAM.

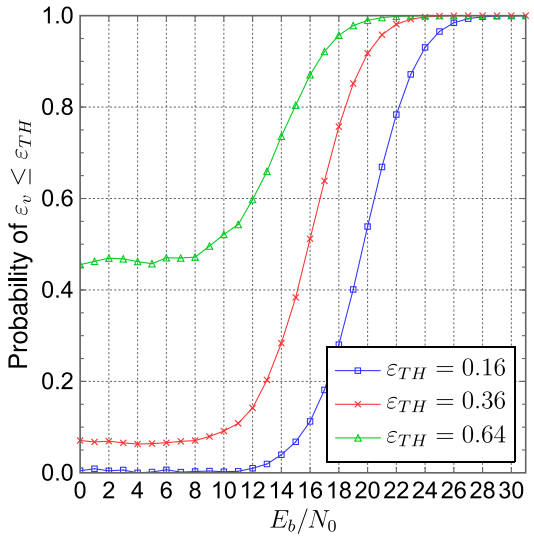

Figure 6.24: The E_b/N_0 vs. Probability of $\varepsilon_v \leq \varepsilon_{TH}$ for the proposed detection in the 4×4 MIMO: 64QAM.

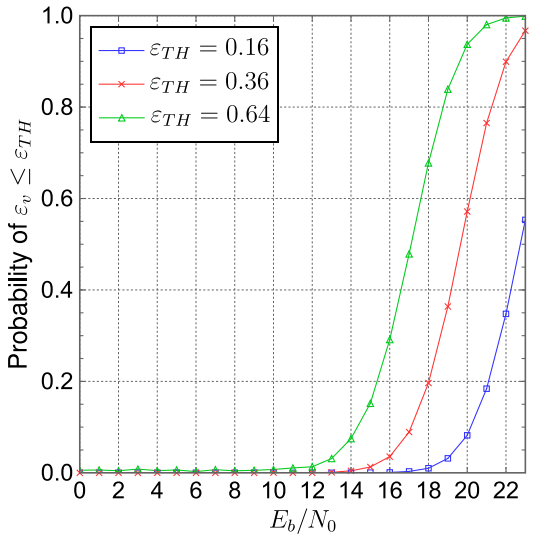

Figure 6.25: The E_b/N_0 vs. Probability of $\varepsilon_v \leq \varepsilon_{TH}$ for the proposed detection in the 8×8 MIMO: 64QAM.

6.5 Chapter summary

In this chapter, we proposed the OSIC with conditional list generation for lattice-reduction aided MIMO detection. The LR-OSIC was first introduced in order to obtain more reliable estimate in the LR domain. Then, we applied the mean squared error of the new signal vector to evaluate the channel condition and the reliability for the soft estimate of the LR-OSIC. The list tree was generated to update the soft estimate of the LR-OSIC in the condition of $\varepsilon_v > \varepsilon_{TH}$. Combining the LR algorithm with ordering method, the value of δ decreased and the more reliable symbol was prior to being detected. The conditional list detection further reduced the error propagation. The simulation results exhibited that the proposed detection can achieve the near-ML performance with almost the same complexity of the LR-OSIC in the high E_b/N_0 region in the 8×8 MIMO, especially for QPSK modulation. For the high modulation order, the proposed detection was also effective even in the large size MIMO.

Chapter 7

Discussions and future work

7.1 Contributions and discussions

As an essential part of the MIMO systems, different MIMO detection schemes have been well discussed over the past decade. In the fast developing wireless communication systems, since it is attractive to exploit multi-path propagation without the expense of high complexity, this thesis introduced our works in lattice reduction aided detection and its application in MIMO systems, especially towards the low complexity MIMO detection.

As described in chapter 1, there are many branches for the MIMO detections. SD and QRM-MLD belongs to the exhaustive tree search. The difference is that SD is depth-first algorithm and QRM-MLD is breadth-first algorithm. Furthermore, the LR technology is to look for a better lattice basis. The LR operations are performed on the channel matrix. Hence, we obtain much better decision boundary and more reliable signal estimation. In conclusion, we have the same objectives and do the researches on different fields of the MIMO detection.

First, we have reviewed and explained the ML and the linear detections, from where we gave the argument between the performance and the complexity. Next, we presented the technology of lattice reduction, combined with the linear, the SIC, the GS and the list detections. These detection schemes improved the performance with relatively low complexity. The numerical results exhibited that the BER curves in the small size MIMO systems approached that of ML detection with the complexity costs, such as more complicated computing in the signal

estimation stage in the LR-GS detection, ordering the detection sequence in the LR-OSIC detection, and the decision of the list candidates in the LR-List detection. Meanwhile, for the large size MIMO system, the improvements of the above conventional detections were not sufficient to approach the ML performance.

Our researches have been investigated in order to achieve the ultimate goal looking for a near-ML detection scheme on the performance together with low complexity. The objective is to solve three problems existed in MIMO detection methods as

- In order to design the effective detection scheme with very low complexity in the small size MIMO systems, we applied a novel adaptive tree search with variable path expansion to solve the problem, which was high complexity for the conventional QRM-MLD in particular for the large size MIMO system and the high modulation order. The adaptive tree search scheme was to adaptively control the candidates for each survived branch in the tree search. We adopted a path metric ratio function to evaluate the reliability for all the survived branches. To decrease the number of the low reliable candidates in each layer, a large amount of the computation for the path metric was avoided.

- Another detection method, improving the quantization scheme based on LR-GS detection in the signal estimation, can fix the problem in the conventional LRA detection using the rounding operation, which resulted in the less reliable signal estimation and led to the BER performance loss. In order to decrease the quantization errors in the quantization step in the LR-domain, we gave another quantization candidate according to the rounding integer. We used a simple tree search in order to rarely correct some quantization errors. The threshold function was defined by the minimum partial path metric for each entry of the signal vectors. Hence the BER performance of the proposed quantization scheme was improved by decreasing the quantization errors.

- The third detection scheme was paid attention on improving the BER performance in the large size MIMO system, to decrease the error propagation

of the property for the SIC detection due to degrading the performance. The LR-OSIC was first introduced to obtain more reliable estimate in the LR domain. We had investigated the distribution of MSE in the LR domain to evaluate the channel condition and the reliability for the soft estimate of the LR-OSIC. The list tree is generated to update the soft estimate of the LR-OSIC in the condition of $\varepsilon_v > \varepsilon_{TH}$. For the high modulation order, the proposed detection was also effective even in the large size MIMO. The complexity was same regardless of the modulation order.

7.2 Comparison of three proposed detections

In this thesis, we presented three proposed detection schemes: the adaptive tree search with variable path expansion detection (Chapter 4), the improved quantization scheme based on LR-GS detection (Chapter 5), and the conditional list based on LR-OSIC detection (Chapter 6) as proposed detection 1, proposed detection 2, and proposed detection 3, respectively.

We gave an example of 16QAM for the BER characteristics as seen in Figs. 7.1 and 7.2, respectively. The best BER performance was achieved by the proposed detection 1 in the 4×4 and 8×8 MIMO systems. In the small size MIMO system, the proposed detection 2 achieved almost same BER performance compared to the proposed detection 1, and the BER curve of the proposed detection 3 was about 0.5dB worse than that of the proposed detection 1 at the BER of 10^{-5}. In the large size MIMO system, the proposed detection 3 achieved almost the same BER performance as the ML detection. the BER curves of the proposed detections 2 and 3 were about 0.8dB and 0.4dB worse than that of the proposed detection 1 at the BER of 10^{-5}.

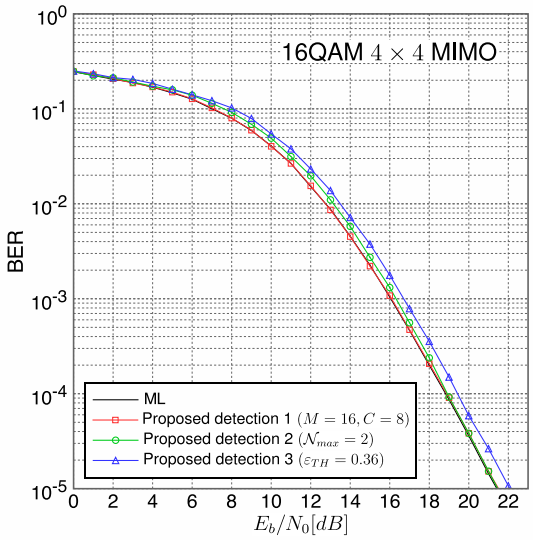

Figure 7.1: The comparison of BER characteristics using the three proposed detections in the 4×4 MIMO: 16QAM.

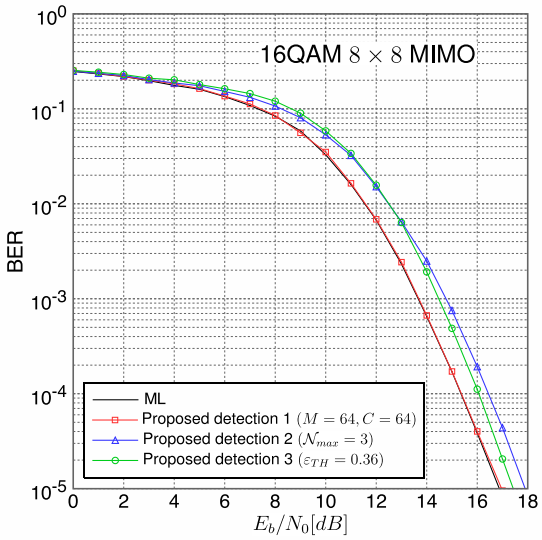

Figure 7.2: The comparison of BER characteristics using the three proposed detections in the 8×8 MIMO: 16QAM.

Next, we compared the computation complexity. If the slow fading channel was assumed that the data packet length is much shorter than the coherence time of the channel, we can treat the channel to be non-time varying during the packet duration. Since the LLL reduction, GSO procedure or ordering operations was performed at the beginning of the packet, we can apply them all over the packet. In this case, we can ignore the complexity of the LR operations, which required the complexity $O(x^3)$. The complexity of LR operations is as described in [39], [57]. The complexity of LR operation requires high complexity as the value of δ or the size of MIMO system increases. The LLL algorithm with $\delta = 0.95$ in proposed detection 2 requires higher complexity than that of LLL algorithm and ordering operations in proposed detection 3 in the large size MIMO system. Supposing some applications, we must treat the LR operations symbol by symbol, and hence the proposed detection 3 was suitable in the small size MIMO system, which required relatively low complexity in the signal estimation and the complexity $O(x^2)$ for the LR operations. In this thesis we focus on the complexity in the signal estimation. Hence, the proposed detections 2 and 3 required very low complexity in the signal estimation regardless of the modulation order, respectively.

Table 7.1: Comparison of three proposed detections

Size of MIMO	Proposed Detection	Complexity of Signal Estimation	BER Performance
4×4	1	Medium	Near-ML
	2	Low	Near-ML
	3	Low	Suboptimal ML
8×8	1	High	Near-ML
	2	Low	Suboptimal ML
	3	Low	Suboptimal ML

We made comparison of the BER performance and the complexity among three schemes as seen in Table 7.1. Note that near-ML is defined that the BER curve is close to the ML curve and suboptimal ML is about 0.5 dB worse than the BER curve of ML detection.

The proposed detection 1 was an exhaustive tree search, which was breadth-first algorithm. It required very low complexity to make the channel matrix to be upper triangular matrix, in order to reduce the complexity in the following computing of path metric. Hence the proposed detection 1 remarkably reduced the complexity of QRM-MLD in the small size MIMO system, especially for the high modulation order. The proposed detection 1 had a little reduction of complexity in the large size MIMO system. Considering the complexity, the proposed detection 1 was not suitable in the large size MIMO system or high modulation order.

The proposed detections 2 and 3 applied the LR technology. Using the LR operations of the channel matrix, the complexity in the signal estimation became same regardless of the modulation order, which was very worthy for the high modulation order. The proposed detection 2 achieved near-ML performance in the small size MIMO system, and required very low complexity in the signal estimation stage. The proposed detection 2 achieved suboptimal performance in the large size MIMO system. However, it required a little high complexity in the LR operation in order to achieve the near-ML performance. In addition, the proposed detection 3 was appropriate for the large size MIMO system and the

Table 7.2: Suitable applications of three proposed detections

Channel	Size of MIMO	Modulation Order	Proposed Detection
Fast fading	4×4	QPSK &16QAM 64QAM	1
	8×8	QPSK &16QAM	1
		64QAM	3
Slow fading	4×4	QPSK &16QAM 64QAM	2
	8×8	QPSK &16QAM 64QAM	3

high modulation order, i.e. the 8×8 MIMO system, due to less complexity for the LR operations and near-ML performance.

In conclusion, in the case of slow fading channel, we can ignore the complexity of LR operations. The proposed detections 2 and 3 with large improvement of BER performance were appreciate in high modulation order or/and large size MIMO system. Supposing in the fast fading channel, the proposed detection 1 with near-ML performance was more suitable to apply in the small size MIMO system and low modulation order. Since the LR operation of the proposed detections 2 and 3 requires very high complexity, it cannot be ignored in the signal estimation. We recommended the suitable applications for the proposed detection according to the size of MIMO system, the modulation order and the type of fading channel in the following table.

7.3 Future work

Despite the advances in MIMO research, there is a strong argument that the full benefits of spatially distributed transmission have only been initially explored. There is a growing movement to look at MIMO systems employing a very large number of transmit antennas (e.g., tens or hundreds of antennas). These systems are most often referred to as massive MIMO or hyper MIMO systems. Massive MIMO is still in its infancy because there are a number of unanswered technical

questions. The receiver must have a usable estimate of the channel conditions in order to reliably decode the transmitted signal. As well, a reliable estimate of the channel at the transmitter side is absolutely critical to facilitate advanced point-to-point MIMO techniques. It was even with very noisy channel estimation, adding more antennas at the transmitter.

On large MIMO systems,*large* means number of transmit and receive antennas of the order of tens to hundreds. Such large MIMO systems will be of immense interest because of the very high spectral efficiencies possible in such systems. For example, in a VBLAST system, increased number of transmit antennas means increased data rate without bandwidth increase. However, major bottlenecks in realizing such large MIMO systems include the lack of practical low-complexity detectors for such large systems, and the associated channel estimation issues. In the future research, we primarily focus on the second problem, i.e., low-complexity large MIMO detection. Specifically, we present a low-complexity detector for large MIMO systems that employ spatial multiplexing, and evaluate its performance without and with channel estimation errors.

As for future work, designing the suitable detection algorithms or schemes is an interesting research topic to achieve the better performances for the massive MIMO system. This could lead to interesting and useful applications to future wireless communications.

Appendix A

Weight matrices of MMSE

For MMSE estimation, we first derive the weight matrix. The optimum weight matrix $\mathbf{W}_{MMSE}$ in (2.33) is recalled as

$$\mathbf{W}_{MMSE} = \arg\min_{\mathbf{W}} E\left[\left\|\mathbf{s}^c - \mathbf{W}^{\mathrm{H}}\mathbf{y}^c\right\|^2\right] \tag{A.1}$$

Taking derivative of the argument of (A.1) with respect to $\mathbf{W}$, then equation it to be zero, we obtain the optimum weight matrix. The estimated signal $\tilde{\mathbf{s}}^{c(MMSE)}$ is obtained as

$$\tilde{\mathbf{s}}^{c(MMSE)} = \mathbf{W}_{MMSE}^{\mathrm{H}}\mathbf{y}^c \tag{A.2}$$

The argument of (A.1) is expressed as

$$\begin{aligned} A =& E\left[\left\|\mathbf{s}^c - \mathbf{W}^{\mathrm{H}}\mathbf{y}^c\right\|^2\right] \\ =& E\left[\left(\mathbf{s}^c - \mathbf{W}^{\mathrm{H}}\mathbf{y}^c\right)^{\mathrm{H}}\left(\mathbf{s}^c - \mathbf{W}^{\mathrm{H}}\mathbf{y}^c\right)\right] \\ =& E\left[\left(\mathbf{s}^{c\mathrm{H}} - \mathbf{y}^{c\mathrm{H}}\mathbf{W}\right)\left(\mathbf{s}^c - \mathbf{W}^{\mathrm{H}}\mathbf{y}^c\right)\right] \\ =& E\left[\mathbf{s}^{c\mathrm{H}}\mathbf{s}^c\right] - E\left[\mathbf{s}^{c\mathrm{H}}\mathbf{W}^{\mathrm{H}}\mathbf{y}^c\right] - E\left[\mathbf{y}^{c\mathrm{H}}\mathbf{W}\mathbf{s}^c\right] + \\ & E\left[\mathbf{y}^{c\mathrm{H}}\mathbf{W}\mathbf{W}^{\mathrm{H}}\mathbf{y}^c\right] \end{aligned} \tag{A.3}$$

Next, take derivative of A with respect to $\mathbf{W}$. In this derivation, we apply the following formulas:

$$\begin{aligned}\frac{\partial(\mathbf{a}^{\mathrm{T}}\mathbf{X}\mathbf{b})}{\partial\mathbf{X}} &= \mathbf{a}\mathbf{b}^{\mathrm{T}} \\ \frac{(\partial\mathbf{x}^{\mathrm{H}}\mathbf{B})}{\partial\mathbf{x}} &= 0\end{aligned} \tag{A.4}$$

Then, we have

$$\frac{\partial A}{\partial\mathbf{W}} = 0 - 0 - E\left[\mathbf{y}^{c*}\mathbf{s}^{c\mathrm{T}}\right] + E\left[\mathbf{y}^{c*}\left(\mathbf{W}^{\mathrm{H}}\mathbf{y}^{c}\right)^{\mathrm{T}}\right] \tag{A.5}$$

where

$$E\left[\mathbf{y}^{c*}\mathbf{s}^{c\mathrm{T}}\right] = \left(E\left[\mathbf{y}^{c}\mathbf{s}^{c\mathrm{H}}\right]\right)^{*} \tag{A.6}$$

and

$$E\left[\mathbf{y}^{c*}\left(\mathbf{W}^{\mathrm{H}}\mathbf{y}^{c}\right)^{\mathrm{T}}\right] = E\left[\mathbf{y}^{c*}\mathbf{y}^{c\mathrm{T}}\mathbf{W}^{*}\right] = \left(E\left[\mathbf{y}^{c}\mathbf{y}^{c\mathrm{H}}\right]\mathbf{W}\right)^{*} \tag{A.7}$$

Let $\frac{\partial A}{\partial\mathbf{W}} = 0$. Then $\mathbf{W}$ in (A.5) becomes the optimum weight matrix $\mathbf{W}_{MMSE}$, and it holds that

$$\left(E\left[\mathbf{y}^{c}\mathbf{y}^{c\mathrm{H}}\right]\mathbf{W}_{MMSE}\right)^{\mathrm{H}} = \left(E\left[\mathbf{y}^{c}\mathbf{s}^{c\mathrm{H}}\right]\right)^{\mathrm{H}} \tag{A.8}$$

Or

$$\mathbf{W}_{MMSE}^{\mathrm{H}}E\left[\mathbf{y}^{c}\mathbf{y}^{c\mathrm{H}}\right] = E\left[\mathbf{s}^{c}\mathbf{y}^{c\mathrm{H}}\right] \tag{A.9}$$

Finally, the optimum weight matrix is obtained as

$$\mathbf{W}_{MMSE}^{\mathrm{H}} = E\left[\mathbf{s}^{c}\mathbf{y}^{c\mathrm{H}}\right]\left(E\left[\mathbf{y}^{c}\mathbf{y}^{c\mathrm{H}}\right]\right)^{-1} \tag{A.10}$$

First, let us calculate $E\left[\mathbf{s}^{c}\mathbf{y}^{c\mathrm{H}}\right]$.

$$\begin{aligned}E\left[\mathbf{s}^{c}\mathbf{y}^{c\mathrm{H}}\right] &= E\left[\mathbf{s}^{c}\left(\mathbf{H}^{c}\mathbf{s}^{c} + \mathbf{z}^{c}\right)^{\mathrm{H}}\right] \\ &= E\left[\mathbf{s}^{c}\left(\mathbf{s}^{c\mathrm{H}}\mathbf{H}^{c\mathrm{H}} + \mathbf{z}^{c\mathrm{H}}\right)\right] \\ &= E\left[\mathbf{s}^{c}\mathbf{s}^{c\mathrm{H}}\right]\mathbf{H}^{c\mathrm{H}}\end{aligned} \tag{A.11}$$

where

$$
\begin{aligned}
E\left[\mathbf{s}^c\mathbf{s}^{c\mathrm{H}}\right] &= E\left\{\begin{bmatrix} s_1^c \\ \vdots \\ s_i^c \\ \vdots \\ s_{N_t}^c \end{bmatrix}\begin{bmatrix} s_1^{c*} & \dots & s_i^{c*} & \dots & s_{N_t}^{c*} \end{bmatrix}\right\} \\
&= E\left\{\begin{bmatrix} |s_1^c|^2 & \dots & s_1^c s_i^{c*} & \dots & s_1^c s_{N_t}^{c*} \\ \vdots & \ddots & \vdots & & \vdots \\ s_i^c s_1^{c*} & \dots & |s_i^c|^2 & \dots & s_i^c s_{N_t}^{c*} \\ \vdots & & \vdots & \ddots & \vdots \\ s_{N_t}^c s_1^{c*} & \dots & s_{N_t}^c s_i^{c*} & \dots & |s_{N_t}^c|^2 \end{bmatrix}\right\} \\
&= E_s\mathbf{I}_{N_t}
\end{aligned}
\tag{A.12}
$$

where $E_s = \frac{E[\|\mathbf{s}\|^2]}{N_t}$. Then, Eq.(A.11) yields

$$
E\left[\mathbf{s}^c\mathbf{y}^{c\mathrm{H}}\right] = E\left[\mathbf{s}^c\mathbf{s}^{c\mathrm{H}}\right]\mathbf{H}^{c\mathrm{H}} = E_s\mathbf{H}^{c\mathrm{H}} \tag{A.13}
$$

Next, we derive how to calculate $E[\mathbf{y}^c\mathbf{y}^{c\mathrm{H}}]$ using (A.12) as

$$
\begin{aligned}
E\left[\mathbf{y}^c\mathbf{y}^{c\mathrm{H}}\right] &= E\left[\left(\mathbf{H}^c\mathbf{s}^c + \mathbf{z}^c\right)\left(\mathbf{H}^c\mathbf{s}^c + \mathbf{z}^c\right)^{\mathrm{H}}\right] \\
&= E\left[\left(\mathbf{H}^c\mathbf{s}^c + \mathbf{z}^c\right)\left(\mathbf{s}^{c\mathrm{H}}\mathbf{H}^{c\mathrm{H}} + \mathbf{z}^{c\mathrm{H}}\right)\right] \\
&= \mathbf{H}^c E\left[\mathbf{s}^c\mathbf{s}^{c\mathrm{H}}\right]\mathbf{H}^{c\mathrm{H}} + E\left[\mathbf{z}^c\mathbf{z}^{c\mathrm{H}}\right] \\
&= E_s\mathbf{H}^c\mathbf{H}^{c\mathrm{H}} + N_0\mathbf{I}_{N_r}
\end{aligned}
\tag{A.14}
$$

Substituting (A.13) and (A.14) into (A.10), we have

$$
\begin{aligned}
\mathbf{W}_{MMSE}^{\mathrm{H}} &= E\left[\mathbf{s}^c\mathbf{y}^{c\mathrm{H}}\right]\left(E\left[\mathbf{y}^c\mathbf{y}^{c\mathrm{H}}\right]\right)^{-1} \\
&= E_s\mathbf{H}^{c\mathrm{H}}\left(E_s\mathbf{H}^c\mathbf{H}^{c\mathrm{H}} + N_0\mathbf{I}_{N_r}\right)^{-1} \\
&= \mathbf{H}^{c\mathrm{H}}\left(\mathbf{H}^c\mathbf{H}^{c\mathrm{H}} + \gamma^{-1}\mathbf{I}_{N_r}\right)^{-1}
\end{aligned}
\tag{A.15}
$$

where γ is defined as $\gamma \triangleq \frac{E_s}{N_0}$. After that, we derive

$$\begin{aligned}\mathbf{H}^{c\mathrm{H}}\Big(\mathbf{H}^{c}\mathbf{H}^{c\mathrm{H}}+\gamma^{-1}\mathbf{I}_{N_r}\Big) &= \mathbf{H}^{c\mathrm{H}}\mathbf{H}^{c}\mathbf{H}^{c\mathrm{H}}+\gamma^{-1}\mathbf{H}^{c\mathrm{H}} \\ &= \Big(\mathbf{H}^{c\mathrm{H}}\mathbf{H}^{c}+\gamma^{-1}\mathbf{I}_{N_t}\Big)\mathbf{H}^{c\mathrm{H}}\end{aligned} \tag{A.16}$$

Then, multiplying the both sides of (A.16) from the right hand by $\Big(\mathbf{H}^{c}\mathbf{H}^{c\mathrm{H}}+\gamma^{-1}\mathbf{I}_{N_r}\Big)^{-1}$ and from the left hand by $\Big(\mathbf{H}^{c\mathrm{H}}\mathbf{H}^{c}+\gamma^{-1}\mathbf{I}_{N_t}\Big)^{-1}$, Eq. (A.16) becomes that

$$\begin{aligned}&\Big(\mathbf{H}^{c\mathrm{H}}\mathbf{H}^{c}+\gamma^{-1}\mathbf{I}_{N_t}\Big)^{-1}\mathbf{H}^{c\mathrm{H}}\Big(\mathbf{H}^{c}\mathbf{H}^{c\mathrm{H}}+\gamma^{-1}\mathbf{I}_{N_r}\Big)\Big(\mathbf{H}^{c}\mathbf{H}^{c\mathrm{H}}+\gamma^{-1}\mathbf{I}_{N_r}\Big)^{-1} \\ =\ &\Big(\mathbf{H}^{c\mathrm{H}}\mathbf{H}^{c}+\gamma^{-1}\mathbf{I}_{N_t}\Big)^{-1}\Big(\mathbf{H}^{c\mathrm{H}}\mathbf{H}^{c}+\gamma^{-1}\mathbf{I}_{N_t}\Big)\mathbf{H}^{c\mathrm{H}}\Big(\mathbf{H}^{c}\mathbf{H}^{c\mathrm{H}}+\gamma^{-1}\mathbf{I}_{N_r}\Big)^{-1}\end{aligned} \tag{A.17}$$

Finally, we can obtain that

$$\Big(\mathbf{H}^{c\mathrm{H}}\mathbf{H}^{c}+\gamma^{-1}\mathbf{I}_{N_t}\Big)^{-1}\mathbf{H}^{c\mathrm{H}} = \mathbf{H}^{c\mathrm{H}}\Big(\mathbf{H}^{c}\mathbf{H}^{c\mathrm{H}}+\gamma^{-1}\mathbf{I}_{N_r}\Big)^{-1} \tag{A.18}$$

$\mathbf{W}^{\mathrm{H}}_{MMSE}$ in (A.15) is reformulated using (A.18) such that

$$\mathbf{W}^{\mathrm{H}}_{MMSE} = \Big(\mathbf{H}^{c\mathrm{H}}\mathbf{H}^{c}+\gamma^{-1}\mathbf{I}_{N_t}\Big)^{-1}\mathbf{H}^{c\mathrm{H}} \tag{A.19}$$

Using (A.19), the soft estimate of the transmit signal vector for the MMSE detection is given by

$$\begin{aligned}\tilde{\mathbf{s}}^{c(MMSE)} &= \mathbf{W}^{\mathrm{H}}_{MMSE}\mathbf{y}^{c} \\ &= \left(\mathbf{H}^{c\mathrm{H}}\mathbf{H}^{c}+\gamma^{-1}\mathbf{I}_{N_t}\right)^{-1}\mathbf{H}^{c\mathrm{H}}\mathbf{y}^{c}\end{aligned} \tag{A.20}$$

Appendix B

MMSE estimation of signal vector v

In [34], Hassibi proposed an MMSE detector with the extended matrix form as

$$\bar{\mathbf{y}}^c \triangleq \begin{bmatrix} \mathbf{y}^c \\ \mathbf{0}_{N_t} \end{bmatrix},\ \bar{\mathbf{H}}^c \triangleq \begin{bmatrix} \mathbf{H}^c \\ \sqrt{\gamma^{-1}}\mathbf{I}_{N_t} \end{bmatrix},\ \bar{\mathbf{z}}^c \triangleq \begin{bmatrix} \mathbf{z}^c \\ -\sqrt{\gamma^{-1}}\mathbf{s}^c \end{bmatrix} \tag{B.1}$$

where $\gamma = E_s/N_0$ with $E_s = E[\|\mathbf{s}^c\|^2]/N_t$. The LLL algorithm transforms the channel matrix $\bar{\mathbf{H}}$ and the unity matrix $\mathbf{I}_{N_t}$ into the reduced matrix $\bar{\mathbf{H}}'$ and the transformation matrix $\mathbf{T}$, respectively.

Recall the shifted and scaled receive signal in (3.22) as

$$\begin{aligned} \bar{\mathbf{y}}^{c\mathcal{S}} &= \bar{\mathbf{H}}^c \left(\frac{\mathbf{s}^c}{2} + \frac{K-1}{2}(1+j)\mathbf{1}_{N_t} \right) + \frac{\bar{\mathbf{z}}^c}{2} \\ &= \left(\bar{\mathbf{H}}\mathbf{T}^c\right) \left(\mathbf{T}^{c-1} \left(\frac{\mathbf{s}^c}{2} + \frac{K-1}{2}(1+j)\mathbf{1}_{N_t} \right) \right) + \frac{\bar{\mathbf{z}}^c}{2} \\ &\equiv \bar{\mathbf{H}}^{c\prime}\mathbf{v}^c + \frac{\bar{\mathbf{z}}^c}{2} \end{aligned} \tag{B.2}$$

where $\bar{\mathbf{H}}^{c\prime} = \bar{\mathbf{H}}\mathbf{T}^c$, and the new signal vector in the LR domain $\mathbf{v}^c$ is defined as $\mathbf{v}^c \triangleq \mathbf{T}^{c-1}\left(\frac{\mathbf{s}^c}{2} + \frac{K-1}{2}(1+j)\mathbf{1}_{N_t}\right)$. The scaled and shifted vector of $\mathbf{s}^c$ is defined as

$$\mathbf{s}^{c\mathcal{S}} = \mathcal{S}[\mathbf{s}^c] \triangleq \frac{\mathbf{s}^c}{2} + \frac{K-1}{2}(1+j)\mathbf{1}_{N_t} \tag{B.3}$$

Therefore, Eq. (B.2) or (3.22) can be extended as

$$\begin{aligned}
\bar{\mathbf{y}}^{c\mathcal{S}} \triangleq \begin{bmatrix} \mathbf{y}^{c\mathcal{S}} \\ \mathbf{0}_{N_t} \end{bmatrix} &= \left(\bar{\mathbf{H}}\mathbf{T}^c\right)\mathbf{v}^c + \frac{\bar{\mathbf{z}}^c}{2} \\
&= \left(\underbrace{\begin{bmatrix} \mathbf{H}^c \\ \sqrt{\gamma^{-1}}\mathbf{I}_{N_t} \end{bmatrix}}_{\bar{\mathbf{H}}} \mathbf{T}^c \right)\mathbf{v}^c + \frac{\bar{\mathbf{z}}^c}{2} \\
&= \begin{bmatrix} \mathbf{H}^c\mathbf{T}^c \\ \sqrt{\gamma^{-1}}\mathbf{T}^c \end{bmatrix}\mathbf{v}^c + \frac{\bar{\mathbf{z}}^c}{2} \\
&= \underbrace{\begin{bmatrix} \mathbf{H}^{c\prime} \\ \sqrt{\gamma^{-1}}\mathbf{T}^c \end{bmatrix}}_{\bar{\mathbf{H}}'}\mathbf{v}^c + \frac{\bar{\mathbf{z}}^c}{2}
\end{aligned} \tag{B.4}$$

where $\mathbf{y}^{c\mathcal{S}}$ denotes the shifting and scaling of the original receive signal.

According to (B.4), Eq. (3.24) can be derived as

$$\begin{aligned}
\tilde{\mathbf{v}}^{c(LR-MMSE)} &= \bar{\mathbf{H}}^{c\prime\dagger}\bar{\mathbf{y}}^{c\mathcal{S}} \\
&\equiv \left(\bar{\mathbf{H}}^{c\prime\mathrm{H}}\bar{\mathbf{H}}^{c\prime}\right)^{-1}\bar{\mathbf{H}}^{c\prime\mathrm{H}}\bar{\mathbf{y}}^{c\mathcal{S}} \\
&= \left(\begin{bmatrix} \mathbf{H}^{c\prime\mathrm{H}} & \sqrt{\gamma^{-1}}\mathbf{T}^{c\mathrm{H}} \end{bmatrix} \begin{bmatrix} \mathbf{H}^{c\prime} \\ \sqrt{\gamma^{-1}}\mathbf{T}^c \end{bmatrix} \right)^{-1} \begin{bmatrix} \mathbf{H}^{c\prime\mathrm{H}} & \sqrt{\gamma^{-1}}\mathbf{T}^{c\mathrm{H}} \end{bmatrix} \begin{bmatrix} \mathbf{y}^{c\mathcal{S}} \\ \mathbf{0}_{N_t} \end{bmatrix} \\
&= \left(\mathbf{H}^{c\prime\mathrm{H}}\mathbf{H}^{c\prime} + \gamma^{-1}\mathbf{T}^{c\mathrm{H}}\mathbf{T}^c\right)^{-1}\mathbf{H}^{c\prime\mathrm{H}}\mathbf{y}^{c\mathcal{S}}
\end{aligned} \tag{B.5}$$

References

[1] D. Tse and P. Vishwanath, **"Fundamentals of wireless communications,"** *Cambridge University Press*, 2005. 1, 10

[2] D. Tse and P. Vishwanath, **"Implementable wireless access for B3G networks. I. MIMO mimo channel measurement, analysis, and modeling [Topics in Radio Communications],"** *IEEE Commun.*, vol. 45, no. 3, pp. 85-92, Mar. 2007.

[3] P. W. Wolniansky, G. J. Foschini, G. D. Golden, and R. Valenzuela, **"V-BLAST: an architecture for realizing very high data rates over the rich-scattering wireless channel,"** in *Proc. Int. Symposium on Signals, Systems, and Electronics. Conference Proceedings*, pp. 295-300 , Oct. 1998.

[4] G.J. Foschini and M.J. Gans, **"On Limits of Wireless Communications in a Fading Environment when Using Multiple Antennas,"** *Wireless Personal Communications*, pp. 295-300, Oct. 1998.

[5] P. W. Wolniansky, G. J. Foschini, G. D. Golden, and R. Valenzuela, **"Diversity and multiplexing: a fundamental tradeoff in multiple-antenna channels,"** *IEEE Trans. on Information Theory*, vol. 49, no. 5, pp. 1073-1096, 2003.

[6] L. Zheng and D. N. C. Tse, **"Diversity and multiplexing: a fundamental tradeoff in multiple-antenna channels,"** *IEEE Trans. on Information Theory*, Vol. 49, No. 5, pp. 1073-1096, 2003. 10

[7] G. J. Foshini, **"Layered space-time architecture for wireless communication in the fading environment when using multiple antennas,"** *Bell Labs Tech. J.*, vol. 1, no. 2, pp. 41-59, Autumn 1996.

[8] A. J. Paulraj, D. A. Gore, R. U. Nabar, and H. Bölcskei, **"An overview of MIMO communications-A key to gigabit wireless,"** *Proc. IEEE*, vol. 92, no. 2, pp. 198-218, Feb. 2004.

[9] G. D. Golden, G. J. Foshini, R. A. Valenzuela, and P. W. Wolniansky, **"Detection algorithm and initial laboratory results using V-BLAST space-time communication architecture,"** *Electron. letter*, vol. 35, no. 1, pp. 14-16, Jan. 1999. 3

[10] D. A. Basnayaka, P. J. Smith, and P. A. Martin, **"Performance Analysis of Macro diversity MIMO Systems with MMSE and ZF Receivers in Flat Rayleigh Fading,"** *IEEE Trans. Wirel. Commun.*, vol. 12, no. 5, pp. 2240-2251, May 2013. 3

[11] C. Windpassinger, L. Lampe, R. F. H. Fischer, and T. Hehn, **"A performance study of MIMO detectors,"** *IEEE Trans. Commun.*, vol.5, pp. 2004-2008, Aug. 2006. 1, 2, 5, 16

[12] L.G. Barbero and J.S. Thompson, **"Fixing the complexity of the sphere decoder for MIMO detection,"** *IEEE Trans. Commun.*, vol.7, pp. 2131-2142, June 2008.

[13] S. Lei, C. Xiong, X. Zhang, and D. C. Yang, **"Adaptive control of surviving branches for fixed-complexity sphere decoder,"** in *Proc. IEEE VTC2010 Spring*, Taipei, Taiwan, May 2010.

[14] L. Xing, **"The expected complexity of sphere decoding algorithm in spatial correlated MIMO channels,"** in *Proc. IEEE Int. Symposium on Information Theory (ISIT2009)*, pp. 2043-2047, Seoul, Korea, Jun. 2009.

[15] L.G. Barbero, T. Ratnarajah, and C. Cowan, **"A low-complexity soft-MIMO detector based on the fixed-complexity sphere decoder,"** in *IEEE Int. Conf. on Acoustics, Speech and Signal Processing*, pp. 2669-2672, Las Vegas, Nevada, U.S.A., Mar. 2008.

[16] B. Hassibi and V. Haris, **"A low-complexity soft-MIMO detector based on the fixed-complexity sphere decoder,"** *IEEE Transactions on Signal Processing*, vol.53, no. 8, pp. 2806-2818, Aug 2005. 5

[17] B. Kim and K. Choi, **"A very low complexity QRD-M algorithm based on limited tree search for MIMO systems,"** in *Proc. IEEE VTC2008 Spring*, pp. 1246-1250, May 2008. 5, 21, 87, 98

[18] L. Liu, J. Wang, D. Yan, B. Wang, and P. Xu, **"Joint maximum likelihood and QRD-M detection algorithm for MIMO system,"** in *Int. Colloquium on Computing, Communication, Control, and Management*, pp. 291-294, Sanya, China, Aug. 2009.

[19] H. Kawai, K. Higuchi, N. Maeda, and M. Sawahashi, **"Adaptive control of surviving symbol replica candidates in QRM-MLD for OFDM MIMO multiplexing,"** *IEEE J. on Sel. Areas in Commun.*, vol. 24, no. 6, pp. 1130-1140, June 2006. 23

[20] K.J. Kim, J. Yue, R.A. Iltis, and J.D. Gibson, **"A QRD-M/Kalman filter-based detection and channel estimation algorithm for MIMO-OFDM systems,"** *IEEE Trans. Wireless Commun.*, vol. 4, no. 2, pp. 710-721, March 2005. 21

[21] H. Kawai, K. Higuchi, N. Maeda, M. Sawahashi, T. Ito, Y. Kakura, A. Ushirokawa, and H. Seki, **"Likelihood function for QRM-MLD suitable for soft-decision turbo decoding and its performance for OFCDM MIMO multiplexing in multipath fading channel,"** *IEICE Trans. Commun.*, vol. E88-B, no. 1, pp. 47-57, Jan. 2005.

[22] S. Sun, Y. Dai, Z. Lei, K. Higuchi, and H. Kawai, **"Pseudo-inverse MMSE based QRD-M algorithm for MIMO OFDM,"** in *Proc. IEEE VTC2006-Spring*, pp. 1545-1549, Melbourne, Australia, May 2006. 87

[23] W. H. Chin, **"QRD based tree search data detection for MIMO communication systems,"** in *Proc. IEEE VTC2005 Spring*, vol. 3, pp: 1624-1627, May 2005. 6, 87, 98

[24] X. Dai, **"Low Complexity Maximum-Likelihood Based QRD-M for MIMO Systems with S-QAM or APSK,"** in *Proc. IEEE Int. Conf. on Commun. (ICC2010)*, pp: 1-6, May 2010.

[25] H. Matsuda, K.Honjo, and T.Ohtsuk, **"Signal detection scheme combining MMSE V-BLAST and variable K-best algorithms based on minimum branch metric,"** in *Proc. IEEE VTC2005-fall*, pp. 19-23, Sep. 2005.

[26] B. Kim and K. Choi, **"SNR measurement free adaptive K-Best algorithm for MIMO systems,"** in *Proc. IEEE WCNC 2008*, pp: 628-633, Apr. 2008.

[27] J. Pons and P. Duvaut, **"New approaches for lowering path expansion complexity of K-best MIMO detection algorithms,"** in *Proc. IEEE ICC2009*, Dresden, Germany, June 2009. 5

[28] E. Agrell, T. Eriksson, A. Vardy, and K. Zeger, **"Closest point search in lattices,"** *IEEE Transactions on Information Theory*, vol. 48, pp. 2201-2214, Aug. 2002. 5, 27

[29] L. Cong, **"On the Proximity Factors of Lattice,"** *IEEE Trans. on Information Theory*, vol. 59, no. 6, pp. 2795-2808, 2011.

[30] X. Ma and W. Zhang, **"Performance analysis for MIMO system with lattice-reduction aided linear equalization,"** *IEEE Trans. Commun.*, vol.56, pp. 309-318, Feb. 2008. 27, 34

[31] I. Berenguer and X. Wang, **"MIMO Antenna Selection With Lattice-Reduction-Aided Linear Receivers,"** *IEEE Transactions on Vehicular Technology*, vol. 53, no. 5, pp. 1289-1302, Sep. 2004.

[32] Y. H. Gan, C. Ling, and W. H. Mow, **"Complex Lattice Reduction Algorithm for Low-Complexity Full-Diversity MIMO Detection,"** *IEEE Trans. on Signal Processing*, vol. 57, no. 7, pp. 2701-2710, Jul. 2009.

[33] X. Wang, Z. He, K. Niu, W. Wu, and X. Zhang, **"An improved detection based on lattice reduction in MIMO systems,"** in *Proc. IEEE Symposiumn Personal, Indoor, Mobile and Radio Commun. (PIMRC06)*, Helsinki, Finland, Sep. 2006.

[34] H. Hassibi, **"An efficient square-root algorithm for BLAST,"** in *Proc. IEEE Int. Conf. on Acoustic, Speech, Signal Processing*, vol. 2, pp. II737-II740, Istanbul, Turkey, Jun. 2000. 34, 139

[35] D. Wübben, R. Böhnke, V. Kuhn, and K. D. Kammeyer, **"MMSE-based lattice-reduction for near-ML detection of MIMO systems,"** in *Int. ITG Workshop on Smart Antennas (WSA)*, Munich, Germany, Mar. 2004. 5

[36] A. K. Lenstra, H. W. Lenstra, and L. Lovász, **"Factoring polynomials with rational coefficients,"** *Mathematische Annalen*, Vol. 261, No. 4, pp. 515-534, Springer Berlin/Heidelberg, Dec. 1982. 5

[37] C. Windpassinger and R. F. H. Fischer, **"Low-complexity near-maximum-likelihood detection and precoding for MIMO systems using lattice reduction,"** in *Proc. IEEE Inform. Theory Workshop*, pp. 345-348, France, April 2003.

[38] C. Windpassinger and R. F. H. Fischer, **"Pre-Processed Recursive Lattice Reduction for Complexity Reduction in Spatially and Temporally Correlated MIMO Channels,"** *IEICE Transactions on Communications*, Vol. E92-B, No. 4, pp. 1392-1396, 2009.

[39] T. Fujino, **"Gram-Schmidt combined LLL lattice-reduction aided detection in MIMO systems,"** *REV J. on Electron. and Commun.*, vol. 1, no. 2, pp. 106-114, April-June, 2011. 38, 59, 86, 130

[40] T. Fujino, S. Wakazono, and Y. Sasaki, **"A Gram-Schmidt based lattice-reduction aided MMSE detection in MIMO systems,"** in *Proc. IEEE Global Communications Conf. (Globecom'09)*, Honolulu, USA, Dec. 2009.

[41] C. M. Kinoshita, W. Hou, Y. Sasaki, and T. Fujino, **"A low complexity lattice reduction aided detection based on Gram-Schmidt,"** in *Proc. IEEE Signal Processing and Information Technology (ISSPIT10)*, Luxor, Egypt, Dec. 2010. 38

[42] D. Wübben, R. Böhnke, V. Kuhn, and K. D. Kammeyer, **"MMSE extension of V-BLAST based on sorted QR decomposition,"** in *Proc. IEEE Int. Vehicular Technology Conf. VTC 2003-Fall* , vol. 1, PP. 508-512, Oct. 2003.

[43] D. Wübben, R. Böhnke, V. Kuhn, and K. D. Kammeyer, **"Near-maximum-likelihood detection of MIMO systems using MMSE-based lattice reduction,"** in *Proc. IEEE Int. Conf. on Commu. (ICC2003)* , vol. 2, PP. 798-802, Jun. 2004.

[44] D. Wübben, R. Böhnke, V. Kuhn, and K. D. Kammeyer, **"A New Lattice Reduction Algorithm for LR-Aided MIMO Linear Detection,"** *IEEE Trans. on Wireless Commun.*, vol. 10, no. 8, PP. 2417-2422, Aug. 2011. 27

[45] K. Lee, J. Chun, and L. Hanzo, **"Optimal Lattice-Reduction Aided Successive Interference Cancellation for MIMO Systems,"** newblock *IEEE Trans. on Wireless Commun.*, vol. 6(7). pp. 2438-2443, 2007. 27, 107

[46] T. Yamamoto and T. Fujino, **"An improved lattice-reduction aided MMSE with successive interference cancellation,"** in *Proc. IEEE Conf. on Advanced Technologies for Commun. (ATC2008)*, pp. 45-49, Hanoi, Vietnam, Oct. 2008. 107

[47] J. Choi and H. Nguyen, **"SIC-Based Detection With List and Lattice Reduction for MIMO Channels,"** *IEEE Trans. on Vehicular Technology*, vol. 58, no. 7, pp. 3786-3790, Sep. 2009. 27, 50, 108

[48] Z. Lei, Y. Dai, and S. Sun, **"Near optimal list MIMO detection,"** in *Proc. IEEE Conf. on Personal, Indoor and Mobile Radio Communications (PIMRC)*, vol. 4, pp. 2441-2446, Berlin, Germany, Sep. 2005.

[49] T. Shimokawa and T. Fujino, **"Iterative lattice reduction aided MMSE list detection in MIMO systems,"** in *Proc. IEEE Conf. on Advanced Technologies for Commun. (ATC2008)*, pp. 50-54, Hanoi, Vietnam, Oct. 2008. 27, 50

[50] L. Bai and J. Choi, **"Partial MAP-Based List Detection for MIMO Systems,"** *IEEE Transactions on Vehicular Technology*, vol.58, no. 5, pp. 2544-2548, 2009.

[51] J. Lee, B. Shim, and K. Insung, **"Soft-Input Soft-Output List Sphere Detection with a Probabilistic Radius Tightening,"** *IEEE Trans. on Wireless Commun.*, vol.11, no. 8, pp. 2848-2857, Aug. 2012.

[52] T.M. Aulin, **"Breadth-first maximum likelihood sequence detection: basics,"** *IEEE Trans. on Wireless Commun.*, vol.47, no. 2, pp. 208-216, 1999.

[53] T.M. Aulin, **"Breadth-first maximum-likelihood sequence detection: geometry,"** *IEEE Trans. on Wireless Commun.*, vol.51, no. 12, pp. 2071-2080, Dec. 2003.

[54] M. Mohammad, C. Ravishankar, and C. Barnett, **"A comparison between the M-algorithm and the list Viterbi algorithm,"** in *Proc. IEEE Military Communications Conference (MILCOM2008)*, pp. 1-5, San Diego, USA, Nov. 2008.

[55] T. Nozoe, H. Negishi, T. Shimokawa, and T. Fujino, **"An improved lattice-reduction aided MMSE detection with SIC and QRM**

in MIMO systems," in *Proc. IEEE Int. Symposium on Signal Processing and Information Technology*, pp. 293-297, Luxor, Egypt, Dec. 2010.

[56] G. H. Golub and C. F. V. Loan, **"Matrix Computations,"** *3rd ed. Baltimore, MD: John Hopkins University Press*, 1996. 21, 45

[57] Phong Q. Nguyen and Brigitte Ballée, **"The LLL Algorithm: Survey and Applications,"** *Springer Heidelberg Dordrecht London New York*, 2010. 130

Publications

List of Publications Directly Related to The Dissertation

Journal Papers

1. Wei Hou, Tadashi Fujino, Toshiharu Kojima, **"Adaptive Tree Search Detection with Variable Path Expansion Based on Gram-Schmidt Orthogonalization in MIMO Systems",** Cyber Journals: Multidisciplinary Journals in Science and Technology, Journal of Selected Areas in Telecommunications(JAST), July Edition, 2012. **(Related to Chapter-4) (Published)**

2. Wei Hou, Tadashi Fujino, Toshiharu Kojima, **"An Improved Quantization Scheme for Lattice-Reduction Aided MIMO Detection Based on Gram-Schmidt Orthogonalization",** IEICE Trans. on Fundamentals of Electronics, Communications and Computer Sciences, vol. E96-A, no.12, pp. 2405-2414, Dec. 2013.**(Related to Chapter-5) (Published)**

Letter Papers

3. Wei Hou, Tadashi Fujino, Toshiharu Kojima, **"Quantization Error Reduction for MIMO Detection Based on Orthogonal Lattices",** IEICE Communications Express (ComEX), vol. 2 no. 2, pp. 42-48, Feb. 2013. **(Published)**

4. Wei Hou, Tadashi Fujino, Toshiharu Kojima, **"Low complexity MIMO detection using OSIC with conditional list generation",** IEICE Communications Express (ComEX), vol. 2 no. 10, pp. 447-452, Oct. 2013. **(Related to Chapter-6) (Published)**

International Conference Papers

5. Wei Hou, Tadashi Fujino, Toshiharu Kojima, **"Efficient Quantization Scheme for Lattice-Reduction Aided MIMO Detection"** , Proc. IEEE International Conference on Advanced Technologies for Communications (IEEE ATC'13), Ho Chi Minh City, Vietnam, Oct. 16-18 2013.

6. Wei Hou, Tadashi Fujino, Toshiharu Kojima, **"Adaptive Candidate Selection Scheme in QRM-MLD Algorithm for MIMO Detection"** , Proc. IEEE International Conference on Wireless and Mobile Computing, Networking and Communications (IEEE WiMob'12), Barcelona, Spain, Oct. 08-10 2012.

7. Wei Hou, Tadashi Fujino, Toshiharu Kojima, **"MIMO System and Its Detection for Wireless Communication"** , Proc. International World Congress of Emerging Infotech-2012 (WCEIT-2012), Dalian, China, Aug. 28-30 2012.

8. Wei Hou, Hidekazu Negishi, Tadashi Fujino, **"A List Detection with partial SIC based on Reciprocal Lattice-Reduction in MIMO Systems"** , Proc. IEEE International Symposium on Signal Processing and Information Technology (IEEE ISSPIT'10), Luxor, Egypt, Dec. 15-18 2010.

9. Wei Hou, Tadashi Fujino, **"Low-complexity MIMO Data Detection Using Dual Lattice-Basis Reduction"** , Proc. IEEE International Conference on Signal Processing (IEEE ICSP'10), Beijing, China, Oct. 24-28 2010.

10. Hidekazu Negishi, Wei Hou, Tadashi Fujino, **"An MMSE Detector Applying Reciprocal-Lattice Reduction in MIMO Systems"** , Proc.

IEEE International Conference on Advanced Technologies for Communications (IEEE ATC'10), Ho Chi Minh City, Vietnam, Oct. 20-22 2010.

11. Hidekazu Negishi, Wei Hou, Tadashi Fujino, **"MMSE Detector Using Forward and Backward Reciprocal-Lattice Reduction in MIMO Systems"** , Proc. IEEE International Symposium on Signal Processing and Information Technology (IEEE ISSPIT'10), Luxor, Egypt, Dec. 15-18 2010.

12. Caio Masakazu Kinoshita, Wei Hou, Tadashi Fujino, **"A Low Complexity Lattice Reduction Aided Detection Based on Gram-Schmidt"** , Proc. IEEE International Symposium on Signal Processing and Information Technology (IEEE ISSPIT'10), Luxor, Egypt, Dec. 15-18 2010.

Domestic Conference Papers

13. Wei Hou, Tadashi Fujino, Toshiharu Kojima, **"Improved SIC Based on Lattice Reduction and Gram-Schmidt Procedure in MIMO Systems",** IEICE General Conference 2013, Gifu, Japan, Mar. 19-22 2013.